UILU ENG 79 4012

IMPROVING THE PERFORMANCE AND FUEL CONSUMPTION OF DUAL CHAMBER STRATIFIED CHARGE SPARK IGNITION ENGINES

S. C. Sorenson, S. S. Pan, J. J. Bruckbauer, and
G. R. Gehrke
Department of Mechanical and Industrial Engineering
University of Illinois at Urbana-Champaign
Urbana, IL 61801

Final Technical Report for

Research Performed under

Grant No. US ERDA 77-2-02-4493

U. S. Department of Energy
Washington, D.C.

September 1979

DISCLAIMER

INTRODUCTION

This report is the final report on the project entitled "Improving the Performance and Fuel Consumption of Dual Chamber Stratified Charge Spark Ignition Engines." The final year of the project was supported by the Department of Energy (ERDA) under Grant US ERDA EC-77-2-02-4493. The final year was a continuation of earlier support under the NSF RANN program and initial funding was supplied under NSF Grant NSF AER 74-20702. A final report of the work under NSF sponsorship has been sent to NSF and is also available from the University of Illinois under Report No. UILU ENG 77-4012.

The current report is based primarily on the graduate dissertations of two former University of Illinois graduate students. Dr. Samuel S. Pan wrote his doctoral disdertation on the theoretical model for the combustion process in the DCSC engine, and Mr. James Bruckbauer completed his Master of Science degree with the experimental study of the performance of the DCSC engine as a thesis topic. Mr. Glenn Gehrke also assisted in the completion of the experimental studies.

SUMMARY

The project described herein involves a combined experimental and theoretical investigation of the nature of the combustion processes in a dual chamber stratified charge spark ignition engine. From earlier work [1 2]*, it was apparent that the problem of understanding the mixing process in the main chamber gases is essential in determining and improving the operating characteristics of the engine, particularly in the area of nitric oxide emissions. Consequently, the efforts of this current work were concentrated in this area. The experimental investigation was conducted on a specially constructed single cylinder engine which has been described elsewhere [1,2]. This engine was used to both conduct experiments to study mixing effects and to obtain experimental data for the validation of the computer model which was constructed in the theoretical portion of the study. The details of these studies are contained in the following sections of the report. The significant results of the studies will be summarized here.

In an effort to gain more insight into the experimentally occurring mixing processes, a new fuel injection system was constructed for the main chamber intake port. It utilized an electronically controlled injector with a variable start of injection. The fuel air ratio was controlled by varying the duration of the injector nozzle opening. Other studies have indicated that port injection can have beneficial effects in extending the lean limits of combustion and introducing further charge stratification [3]. Studies were conducted on the effect of fuel injection timing on performance and emissions using the combination of orifice size and prechamber to main chamber flow rate ratio

*Numbers in brackets refer to entries in REFERENCES FOR SUMMARY, p. S.7.

which gave the best overall compromise between emissions and performance. In general, fuel injection gave slightly higher oxides of nitrogen, but considerably lower hydrocarbon and carbon monoxide emissions than the carbureted form of the engine. It was also found that fuel injection into the main chamber intake port starting at top dead center gave the lowest emissions at equivalent power levels. Injection at 110 degrees after top dead center also gave lower nitric oxide and hydrocarbon emissions but slightly higher carbon monoxide emissions. Emissions of hydrocarbons and carbon monoxide were higher with injection at 60 degrees after top dead center and at bottom dead center while nitric oxide emissions remained about the same. Injection duration, which was a function of the fuel air ratio, was on the order of 70 crank angle degrees.

The differences in emissions with changes in injection timing indicated that there were inhomogeneities in the main chamber charge at the time of combustion. In an effort to improve the degree of mixing in the main chamber, a series of experiments was conducted in which the shape of the main chamber intake port was modified in order to impart a swirling motion to the main chamber intake charge. These experiments indicated a substantial increase in the power output from the engine which is thought to be due to the increase in combustion rate which resulted from the increased turbulence created by the intake port obstruction. Consequently, nitric oxide emissions also increased. The data indicate, however, that at equivalent power levels, the nitric oxide emissions are approximately 30 percent lower with swirl in the main chamber than without swirl. This effect is felt to be due to the

reduction of the zone of intermediate stoichiometry which exists between the prechamber gases and the main chamber gases. The swirl improves the mixing on the intake stroke, giving a more homogeneous main chamber mixture, a smaller zone with slightly lean stoichiometry, and consequently lower nitric oxide emissions at equivalent power levels. This conclusion has been substantiated by studies with the computer simulation.

The second portion of the study was the development of a computer simulation of the combustion process. The technique chosen was to construct a one-dimensional flame with time and spatially dependent cross sectional area and to calculate the flame propagation process by the numerical integration of the conservation equations for mass, momentum, and energy. Experimentally determined ignition delays were used to determine the start of combustion, i.e., the establishment of a developed flame. An empirical turbulent diffusivity model was used along with simple second order Arrhenius type kinetics for the oxidation of the fuel. Simple Zeldovich kinetics were used for the nitric oxide kinetics, assuming equilibrium atomic oxygen and steady state nitrogen atom concentrations. A modified version of the Woschni heat transfer correlation was used for heat transfer calculation. While it is well recognized that under some conditions the combustion is strongly influenced by a jet issuing from the prechamber, our photographic studies have indicated that the combustion in the DCSC engine can often be characterized by a spherical or one-dimensional flame. The results of the combined experimental and theoretical study indicate that the one-dimensional model can ineed be used to quantitatively study the effects of non-uniform mixtures on the behavioral trends of nitric oxide emissions and performance.

One of the prime objectives of the model use was the investigation of the effects of main chamber mixing on the performance and emissions. Our previous work had indicated that the use of a perfect mixing model for the main chamber gases at the time of combustion was inadequate with respect to explaining the effects of variations in the percent flow through the prechamber and effects of variations in the prechamber air fuel ratio. A simple mixing model was developed in which it is assumed that at bottom dead center at the end of the intake stroke, 50 percent of the main chamber gases have perfectly mixed with the overfill from the prechamber.

The remainder of the main chamber gases are assumed to be unmixed with respect to the prechamber overfill gases, i.e., they remain at the composition of the main chamber intake gases. It is also assumed that no further mixing occurs on the compression stroke and that only gases at the composition of the intermediate zone enter the prechamber on the compression stroke. This simplified model was successful in calculating the effects of variations in prechamber fuel air ratio and prechamber to main chamber flow rate ratio on the emissions of nitric oxide and the engine pressure time history. The use of a model which assumes perfect mixing in the main chamber cannot predict this effect since, under the variations in the flow rate and air fuel parameters in the experimental study, the perfect main chamber mixing model predicts the same fuel air ratio in the main chamber. This is inadeuate to explain the observed experimental results. The mixing model also predicted that an increase in the degree of mixing in the main chamber at the time of combustion should also reduce the nitric oxide due to the reduction of the zone of intermediate stoichiometry which is assumed to exist at the output of

the prechamber. This conclusion was borne out by the experimental studies.

A slightly more complicated mixing model which allowed for additional mixing between the prechamber and main chamber gases on the compression stroke was also tried but gave results which were not substantially different from the previous mixing model. It is realized that the assumption of 50 percent mixing at the end of the intake stroke is arbitrary but there is no currently available information on the nature of the mixing process in DCSC engines.

The general conclusions of the study are as follows:

1. The degree of charge homogeneity in the main chamber at the time of combustion is very important in determining the nitric oxide emissions of the dual chamber stratified charge spark ignition engine (DCSC).
2. A degree of swirl in the intake charge is beneficial in improving the performance of the DCSC engine in that higher power was attained at a given level of nitric oxide emission with the engine utilizing swirl as opposed to the engine without swirl. Hydrocarbon and carbon monoxide emissions were also reduced with the use of swirl and the combustion rate was increased due to the added turbulence.
3. The use of timed fuel injection in the main chamber intake system significantly reduces hydrocarbon and carbon monoxide emissions, with an insignificant effect on nitric oxide emission and power. Injection starting at top dead center on the intake stroke proved to have the lowest overall emissions for a given power level.

4. The ratio of the prechamber fuel flow to the total fuel flow to the engine is more significant than the ratio of prechamber air flow to total air flow in determining performance characteristics.
5. A one-dimensional combustion model can be used to accurately predict trends in engine operation conditions and nitric oxide emissions even though the actual flame in the engine is not completely one-dimensional.
6. A simple model for mixing of the main chamber and prechamber intake gases at the start of compression proved adequate to explain the effects of swirl, ignition timing, overall fuel air ratio, volumetric efficiency, and variations in prechamber air fuel ratio and fuel rate percentage on engine power and nitric oxide emissions.

REFERENCES

1. Sorenson, S. C., "Improving the Performance and Fuel Consumption of Dual Chamber Stratified Charge Spark Ignition Engines," Final Report for Grant NSF AER 74-20702, UILU ENG 77 4012, University of Ill. at Urbana-Champaign, Dept. of Mech. and Ind. Engr., May 1977.

2. Hull, W. L., and S. C. Sorenson, "Research on a Dual-Chamber Stratified Charge Engine," SAE Paper 780488, G. Edwin Burks Lecture, Earthmoving Industry Conference, Peoria, Ill., 11 April 1978.

3. Peters, B. D., and A. A. Quader, "'Wetting' the Appetite of Spark Ignition Engine for Lean Combustion," SAE Paper 780234, 1978.

SECTION I

Section I is based on the Ph.D. Dissertation entitled "Combustion Simulation of a Dual Chamber Stratified Charge Spark Ignition Engine," by Samuel S. Pan, Department of Mechanical and Industrial Engineering, University of Illinois at Urbana-Champaign, January 1979.

ABSTRACT

A one-dimensional mathematical model for the simulation of the combustion process in a dual chamber stratified charge spark ignition engine has been developed. The model includes the submodels of ignition, mixing, chemical kinetics, heat transfer, turbulent diffusivity, and NO formation. A superimposed Gaussian distribution function for the temperature and species is used for the ignition simulation. Three mixing zones: the perfectly mixed prechamber, and a perfectly mixed and an unmixed zone in the main chamber, are assumed for the mixing model. An empirical rate equation assuming a reaction which is first order in fuel and first order in oxygen with an empirical pressure correction is used for the chemical kinetic model. The heat loss is calculated through a modification of Woschni's equation. Turbulence phenomena are simulated by a simple mixing length theory with an empirical effect of throat diameter change. The simple Zeldovich mechanism is used for the NO calculation. Studies are made on the basic parameters, such as the turbulence level, the preexponential constant, the heat transfer, the mixing percentage, the total air fuel ratio, the prechamber intake air fuel ratio, the prechamber intake mass flow ratio, the volumetric efficiency, the throat diameter, and the spark location and timing. The calculated results correlate well with the experimental data. All the predicted trends agree with the experimental trends over the range of the engine conditions investigated. The model will be useful for the improvement of the performance and the design of the dual chamber stratified charge spark ignition engines.

TABLE OF CONTENTS

APPENDICES Page

NOMENCLATURE

A	--area, in^2
AF	--air-fuel ratio
a	--reaction order for the fuel
a0	--constant coefficient for least square fitting
a1	--constant coefficient for least square fitting
a2	--constant coefficient for least square fitting
B	-- bore size
B1	--constant coefficient for the geometry function
B2	--constant coefficient for the geometry function
B3	--constant coefficient for the geometry function
B4	--constant coefficient for the geometry function
B5	--constant coefficient for the geometry function
b	--reaction order for the oxygen
$C\ell$	--average combustion chamber clearance, in
$C\ell_1$	--main chamber maximum clearance, in
$C\ell_2$	--main chamber minimum clearance, in
C_p	--the specific heat at constant pressure, in-lbf/lbm °R
C_s	--constant coefficient for diameter correction in turbulent model
C_v	--the specific heat at constant volume, in-lbf/lbm °R
D(x)	--function of chord in the main chamber, in
d	--diameters, in
E	--activation energy, Kcal/gm mole
e	--specific energy, in-lbf/lbm
FR	--prechamber intake mass flow ratio

f --residual fraction

f_T --coefficient for temperature in restricted time step control

f_ε --coefficient for species in restricted time step control

H(x) --function of clearance height, in

h --heat transfer coefficient, in-lbf/in^2 °R sec

hr --heat of reaction, in-lbf/lbm mole

I --internal grid point

K2 --second order chemical kinetic rate constant

k0 --equilibrium constant

k1 --reaction rate constant

k2 --reaction rate constant

k3 --reaction rate constant

k4 --reaction rate constant

L --spatial length, in

Lx --mixing length, in

M --molecular weight, lbm/lbm mole

M.C. --main chamber

m --mass, lbm

m1 --mass in the lean zone of main chamber, lbm

m2 --mass in the intermediate zone of main chamber, lbm

m2,3 --mixing mass from the intermediate zone to the prechamber, lbm

Nu --Nusselt number

n --number of moles, mole

n_p --number of moles of the product, mole

n_R --number of moles of the reactant, mole

P --gas pressure, psi

P.C. --prechamber

$\tilde{P}$ --perimeter, in

PM2 --mixing percentage

Pr --Prandtl number

Q --heat transfer, in-lbf

R --gas constant, in-lbf/lbm °R

RC --crank arm length, in

Re --Reynolds number

Ro --universal gas constant, in-lbf/lbm mole °R

S --least square

T --gas temperature, °R

t --time, sec

U --overall heat transfer coefficient, in-lbf/in^2 °R sec

u --gas velocity, in/sec

u' --turbulent intensity, in/sec

u_p --mean piston speed, in/sec

V --volume, in^3

V_c --combustion chamber volume, in^3

V_d --piston displacement, in^3

X --percentage of prechamber intake mass overflow into main chamber

x --spatial variable, in

Y --percentage of reverse-flow from main chamber into prechamber

y(t) --function of piston distance from TDC, in

Z --preexponential constant, in^3/lbm mole sec

Greek Symbols

α --turbulent diffusivity, in^2/sec

β --correction power for pressure

γ --correlation power for the effect of throat diameter

ε --mass fraction of species

ηv --volumetric efficiency

Θ --crank angle

μ --gas viscosity, lbm/in sec

ν --stoichiometric coefficient

ρ --gas density, lbm/in^3

Φ --equivalence ratio

ω --angular frequency, 1/sec

Subscripts

a --air

chem. --chemical reaction

cond. --heat conduction

conv. --heat convection

f --fuel

g --gas

gen. --generated

H --high value

i --intake value or internal grid point

id --ignition delay

in --inflow

L --low value

M	--middle value
m	--main chamber
n	--normalized value
o	--initial value
oi	--orifice inlet
oo	--orifice outlet
out	--outflow
p	--prechamber
R	--residual
r	--reference
s	--spark time
st	--stoichiometric
store	--in the system
T	--total
t	--partial total
th	--throat
w	--wall
ϕ	--bottom dead center
1	--fuel
2	--oxygen
3	--product
4	--nitric oxide
5	--nitrogen
$+\frac{1}{2}$	--advance half grid size
$-\frac{1}{2}$	--retard half grid size

Superscripts

n --time step

- --average value

• --time rate

Notations

[ ] --concentration

| | --absolute value

LIST OF TABLES

LIST OF FIGURES

Figures

CHAPTER I

INTRODUCTION

Since the development of high speed digital computers, a large amount of engine modeling work has been accomplished through the numerical simulation technique. The cost and time invested for the research and development of the engine modeling have been reduced significantly. Once the simulation model is developed, it can be used for a thorough investigation of the basic design parameters. It is too costly and tedious to work on the engine experimentally. Computer simulation thus becomes more and more an important tool for the research and development of the engine design (Boni 1975).

The engine simulation models usually can be classified into two categories: the zero-dimensional and the multi-dimensional.

In the first category, which has been the most popular because of its simplicity, the combustion chamber is divided into burned and unburned zones. With only time taken as a dependent variable, the first law of thermodynamics is applied to the combustion zones individually. The system is described by a set of ordinary differential equations. The results are obtained by solving the ordinary differential equations. It uses experimental data, like pressure time history, to correlate a proper burning rate. The correlation between the numerical results and the experimental data are satisfied. However, there is no information about the spatial variation of the dependent variables. For instance, the propagation of the flame can

not be described through this type of model. Although it has been very useful for the engine research and development, the information from the prediction of the model is limited.

In the second category which includes one, two, or three dimensional models, the spatial variation is considered. Basic physical laws are applied through the conservation of mass, momentum and energy to the whole system. In addition to the time dependence, the independent variables also may involve one, two, or three space variables. The system is described by a set of partial differential equations. The numerical technique required is more complicated and demanding, but more information is predicted. The propagation of the flame, and the aerodynamic structure of the fluid are well described through the multi-dimensional models. Obviously, more effort and cost have to be paid off. A literature review of engine modeling is discussed in the next chapter.

The nature of this research is a one-dimensional model for a dual chamber stratified charge (DCSC) spark ignition engine. The main assumptions are: one phase, one dimensional, overall one step second order chemical kinetics, equal turbulent diffusivity for mass, momentum and energy, and the simple Zeldovich mechanism for NO emission. Seven non-linear unsteady state partial differential equations are solved by the MacCormack predictor-corrector technique. The Courtant-Friedrich-Levy (CFL) stability criterion is obeyed for the maximum time step size. Because of the non-stoichiometric combustion in the DCSC model, a restrictive time step control is also applied.

Many ad hoc sub models, such as the mixing model, the second order chemical kinetics, the heat transfer, the turbulent diffusivity, the simple Zeldovich mechanism, the Gaussian ignition profile, and the geometry functions, are used. The predictions of the simulation model are compared with experimental data. Basic studies are made for the geometrical parameters, the operational parameters, and the combustion parameters. The detail of the model development and its results are discussed in the following chapters.

CHAPTER II

LITERATURE REVIEW

A. History, Research And Development

Due to the fossil fuel shortage problems, ways to use fuel economically have become the main concern in every energy utilization facility. This has a strong impact on the automobile industry. Much research effort has been concentrated on fuel economy design. To design more efficient power plants is one of the approaches. Meanwhile, the exhaust emission control has also been forced by the government legislation to be applied in the newer model vehicles. The DCSC spark ignition engine is one of the prospective power plants which has both the advantages of fuel economy and lower emission.

The concept of the DCSC engine was invented by Sir Harry R. Ricardo in 1918. Since then, there have been many patents of DCSC engine which have been issued (Turkish 1974). Roessler and Muaszew (1975) described most of the research and development work of automobile manufacturers, engine manufacturers and research institutes as well as listing all the patents which have been granted in the United States.

The engine manufacturing industry showed little interest in the early years. However, the interest of the DCSC engine was renewed recently due to the advantage of its low emissions and fuel economy. Many groups have been investigating the possible application of this prospective engine on the light duty vehicles.

Honda Motor Company was the most successful one in the research and development of DCSC engines. Their Compound Vortex Controlled Combustion (CVCC) engine (Date, et al., 1974; Yagi, et al., 1976) has been built in the Civic model since 1975. Not only did it pass 1975 U.S. federal emission standards but also it has the same or better fuel economy compared to the conventional engines. Other industry groups, such as Ford Motor Company (Purins 1974), General Motors Corporation (Davis, et al., 1974; Krieger, et al., 1976), Eaton Corporation (Turkish 1974), Volkswagenverk AG (Brandstetter 1975, 1976), have also done substantial research and development work on the DCSC engine.

B. Physical Description Of The Dual Chamber Engine

The dual chamber engine consists of a prechamber and a main chamber connected by an orifice as shown in Figure 1. The spark plug is located in the prechamber. During the intake process, a rich mixture is supplied to the prechamber, and a lean mixture is supplied to the main chamber. Some extra rich mixture of the prechamber overflows into the main chamber and mixes with the lean mixture there. During the compression process, some lean mixture of the main chamber flows back into the prechamber and dilutes the rich mixture in the prechamber. This mixing effect can be seen clearly on the air-fuel ratio versus crank angle diagram as given in Figure 2. During the intake period, the air fuel ratio in the prechamber stays constant, and the air fuel ratio in the main chamber is enriched by the over-flow rich mixture from the prechamber. During the compression period, the air-fuel

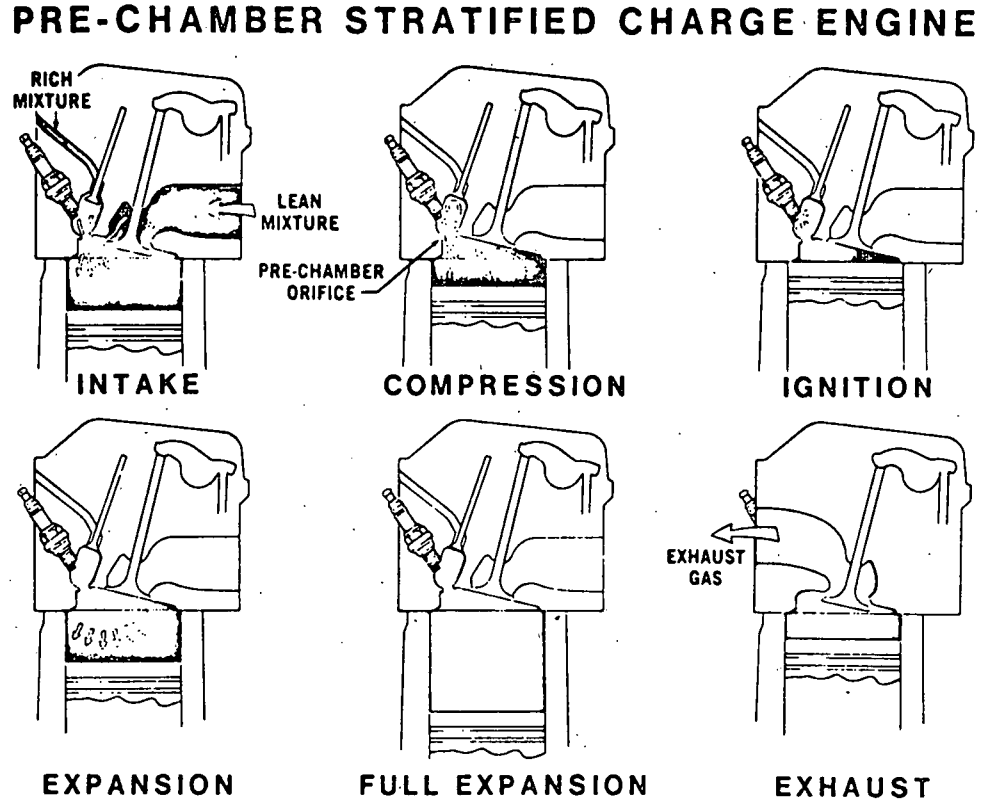

Figure 1. Prechamber Stratified Charge Engine (Purins 1974)

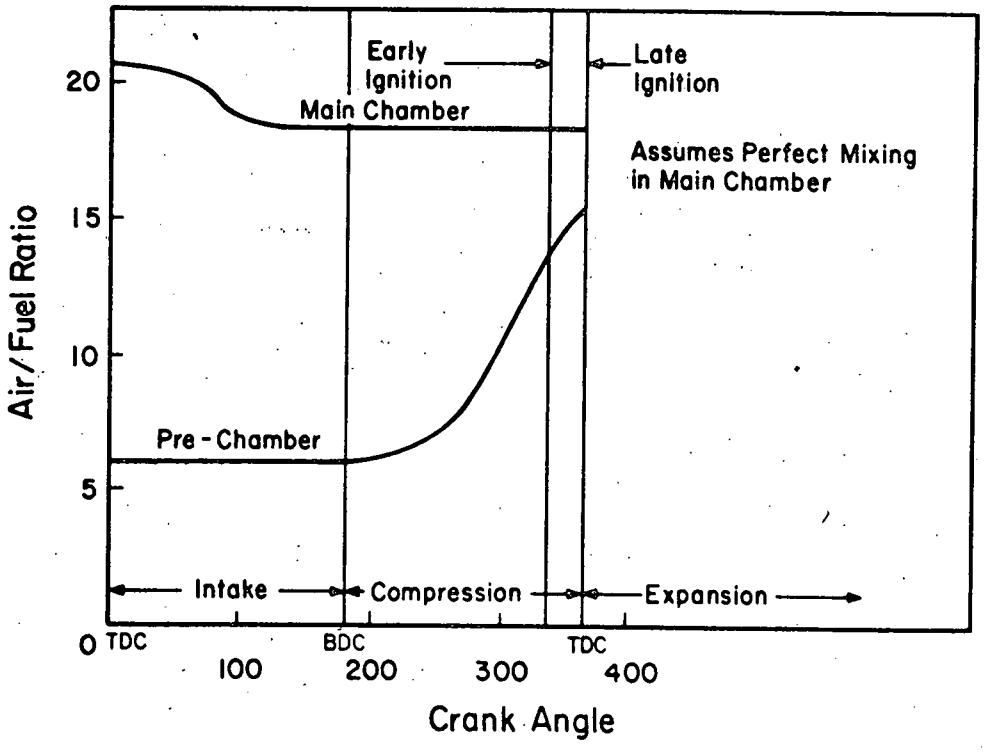

Figure 2. Combustion Chamber A/F VS. Crank Angle (Purins 1974)

ratio in the main chamber stays constant, the air-fuel ratio in the prechamber is diluted by the back-flow lean mixture from the main chamber. An ignitable mixture is formed near the spark plug at the time of ignition. The rich mixture in the prechamber is burned first. A rapid pressure rise is induced in the prechamber. The burning flame propagates through the orifice as a strong jet into the main chamber. This flame jet ignites the lean mixture in the main chamber. The DCSC engine is therefore named as the "jet ignition engine." The stratified charge and the two-staged combustion are the unique characteristics of the dual chamber combustion.

C. Advantages And Disadvantages

According to the emission characteristic curves as Figure 3 illustrated, the lean mixture burning produces the least emission. With conventional spark ignition engines, the air-fuel ratio has a lean limit around 19 to 1 because of the ignitability; and even if the lean mixture is ignited, the combustion rate is slow and thus the efficiency is low. The DCSC engine eases both problems. The rich mixture which is supplied to the prechamber assures positive ignition at the time of spark. The jet induced through the connecting orifice generates substantial turbulence for both better mixing and more efficient burning in the combustion chambers. Through two-staged combustion in the DCSC engine, the overall air-fuel ratio can be extended beyond the conventional lean limit. This capability of efficient burning of the lean mixture is the way to achieve better fuel economy.

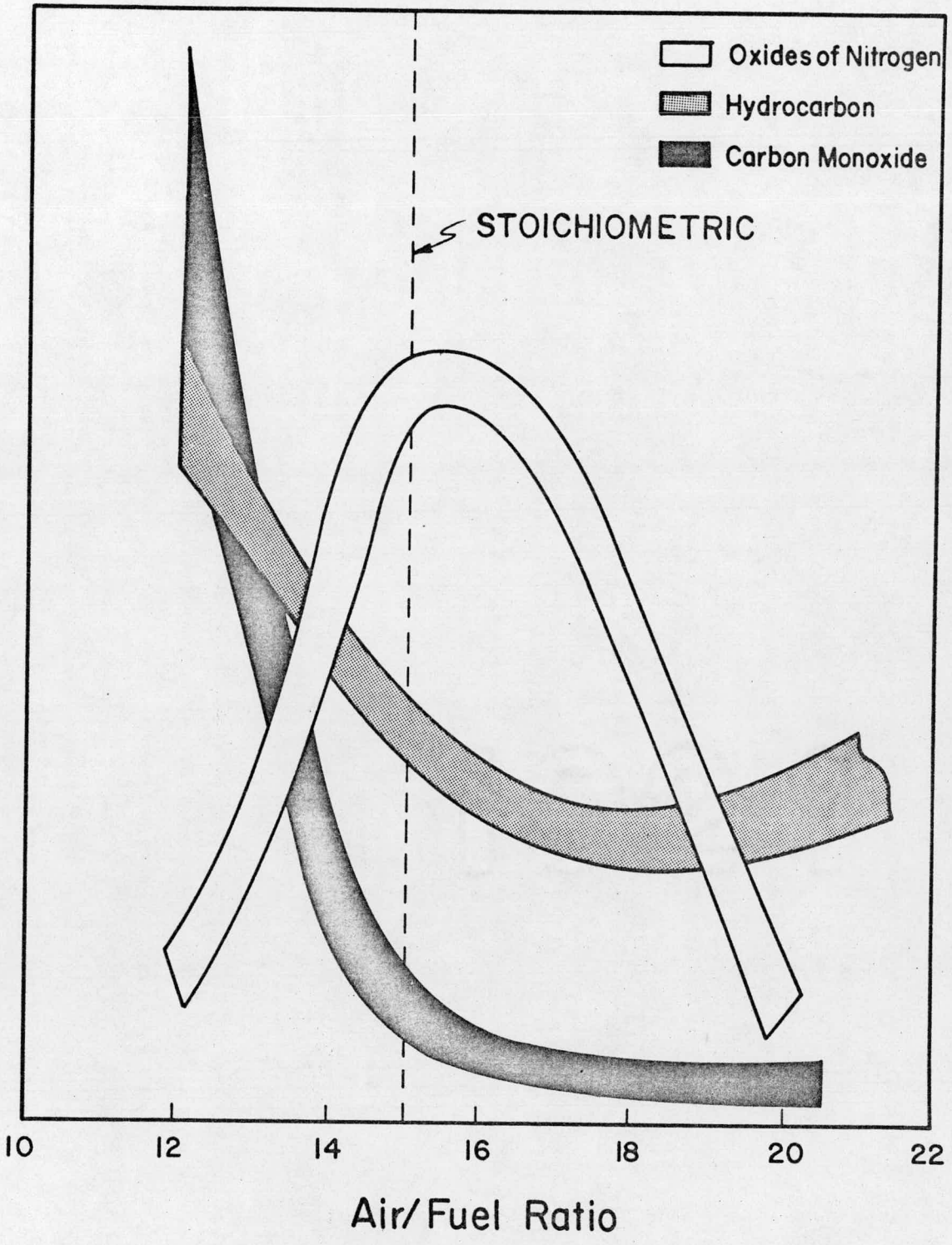

Figure 3. Emission Concentration Relationship To A/F Ratio

Due to the charge stratification, the peak temperature in the main chamber is lower, and therefore it produces a much less NO emission. The relative high average temperature in the later part of the combustion and ample oxygen availability also promote more complete oxidation of HC and CO. Less power output and more heat loss are the disadvantages.

D. Engine Modeling

The combustion in the internal combustion engine is an unsteady state, three dimensional, and sometimes two phase phenomena. Bracco (1974, 1977) gave an excellent review on modeling combustion within the internal combustion engine. For simplication simulation models are made with varying assumptions. The less restraints applies to the model, the more information it can predict, and the closer it should be able to simulate to the real case; however, more efforts need to be invested.

It is too complex and too costly to work on a three-dimensional model at the present stage. The Princeton group and other researchers have been working on two-dimensional, two-phase, unsteady state models (Bracco 1977; Boni 1975, etc.). This will be the most detailed model which has ever been investigated.

One-dimensional models are the next most informative ones. Sirignano (1971) presented an uniform charge reciprocating engine. Bracco and Sirignano (1972) examined an uniform charge, rotary engine. Bracco (1973) also investigated a model for a direct injection,

stratified charge rotary engine. A carbureted stratified charge, reciprocating engine was presented by Rosentweig-Bellan and Sirignano (1973). Boni, et al., (1976) developed a one-dimensional model for a divided chamber, stratified charge engine, as did Dwyer, et al., (1976) for a prechamber of a stratified charge engine. Sorenson (1978) has simulated turbulent combustion in a single constant volume chamber.

Zero dimensional models are the most popular ones because of their simplicity. Only time is taken as the independent variable. The system is modeled by ordinary differential equations instead of partial differential equations. The information predicted is hence less than the higher dimensional models. Hires (1975) investigated the performance and emissions from a jet ignition stratified charge engine. A model of a three-value stratified charge engine with a small prechamber was presented by Davis, et al., (1974). Asanuma, et al., (1978) had a complete zero-dimensional simulation cycle for the three-value stratified charge engine.

Although Davis, et al., Hires, and Asanuma, et al., have worked on the DCSC engine, the spatial information was absent. Both Dwyer and Bellan and Sirignano have investigated a stratified charge engine for a single chamber. Only Boni, et al., did one-dimensional simulation on a DCSC engine, but the model was not compared with any experimental data. One of the objectives of this research is to compare and correlate the simulation model with the experimental data.

CHAPTER III

OBJECTIVES

(1) to develop a one-dimensional simulation model for the combustion process in a DCSC spark ignition engine.

The simulation model covers the duration from the initiation of the flame by the spark to the completion of the combustion.

(2) to compare the predicted values with the experimental data.

The experimental data, such as the pressure-time diagram, the NO emission, will be used for the correlation between the simulation model and the test engine.

(3) to use the developed model to do a basic parameter study.

(a) total air-fuel ratio.

(b) prechamber intake air-fuel ratio and prechamber intake mass flow ratio.

(c) volumetric efficiency.

(d) throat diameter.

(e) spark timing.

CHAPTER IV

MODEL DEVELOPMENT

A. Assumptions

1. One-Dimensional System

Only one spatial independent variable is involved (Figure 4-6). The flame starts in the prechamber, passes through the orifice, and propagates into the main chamber. It is assumed that all the properties are uniform along the direction perpendicular to the spatial axis. The cross section area perpendicular to the spatial axis is taken as the burning area of the flame. It is assumed that the flame has a very fast lateral expansion rate, and therefore, it has the same burning area as the expansion area at the outlet of the orifice when the flame reaches the main chamber.

2. All Fuel Vaporized

It is a one-phase flow and premixed system. All fuel is vaporized and mixed with the air and the residual before the initiation of the combustion.

3. All Substances Assumed To Be Ideal Gases

All the gases obey the perfect gas law.

4. All Gases Mixed At The Start Of Combustion

Two types of mixing model have been assumed.

a) Complete mixing model

All fuel, air and residuals are completely mixed in the main chamber as well as in the prechamber at any time before spark ignition. This model was used at the beginning of the research for its simplicity.

b) Three-mixing-zones model

The complete mixing model is good in the prechamber for its relatively small volume. In the main chamber, because of the relatively large volume and the time dependent volume change, complete mixing becomes a questionable assumption. It has been confirmed (Date, et al., 1974; Krieger, et al., 1976) that during the intake period, the overflow rich mixture from the prechamber mixes with the lean mixture of the main chamber near the orifice outlet. During the compression period, only the portion near the orifice outlet of the main chamber flows back into the prechamber and dilutes the rich mixture in the prechamber. The mixture at the boundary of the main chamber probably neither mixes with the overflow rich mixture from the prechamber nor flows back into the prechamber, but remains at the intake air-fuel ratio condition all the time. The model is thus modified that there are three mixing zones: the prechamber rich zone, the main chamber intermediate zone, and the main chamber lean zone. Only the mixture in the prechamber rich zone mixes with the mixture in the main chamber intermediate zone. The main chamber lean zone is assumed to have the intake air-fuel ratio throughout the intake and the compression processes. The detail of this three-mixing-zones model appears in the Appendix J.

5. Fuel Chemistry Described By A Single Step Reaction

For the purpose of simplification, ethylene C_2H_4 was used for the fuel. The products consists of carbon dioxide and the water vapor for the stoichiometric combustion,

$$C_2H_4 + 3O_2 + 3 \times 3.764\ N_2 \rightarrow 2CO_2 + 2H_2O + 3 \times 3.764\ N_2 \ . \qquad \text{(IV.1)}$$

6. Identical Molecular Weight For All Gases

The average molecular weight for the mixture which has been calculated in Appendix G is 28.85. For the purpose of simplification, all the gases have identical molecular weight as the average value. By this assumption, the mole fraction is identical to the mass fraction.

7. Inviscid Flow

The fluid flow is assumed frictionless. Since the turbulence level is high in the dual chamber flow system, the viscous effect is relatively small.

8. Overall One Step Second Order Chemical Kinetics

$$A + B \rightarrow C \qquad \text{(IV.2)}$$

$$\frac{d[A]}{dt} = -K2\ [A]^a[b]^b \qquad \text{(IV.3)}$$

An empirical chemical kinetic model similar to that of the Princeton group (Sirignano 1971; Bracco, et al., 1972) was used. The assumption is made arbitrarily that $a = b = 1$. An empirical term P^β is added to correlate the effect of pressure. The empirical expression for the model is,

$$\frac{d[A]}{dt} = -ZP^{\beta}\,[A]^{a}[B]^{b}\exp(-E/RT) \qquad [\text{lbm-mole/in}^3\ \text{sec}] \quad \text{(IV.4)}$$

9. Heat Loss Modeled By An Overall Heat Transfer Coefficient

$$\dot{Q} = -\,U\tilde{P}\Delta x\,(T_g - T_w) \qquad [\text{in-lbf/sec}] \quad \text{(IV.5)}$$

The overall heat transfer coefficient U is estimated through Woschni's heat transfer equation (1967). The equation derivation and its units conversion are given in Appendix E.

10. Turbulent Effects Modeled By A Turbulent Diffusivity Which Is The Same For The Mass, Momentum And Energy Diffusion

The model of the turbulent diffusivity is similar to the Princeton models (Sirignano, Bracco, et al.). The turbulent Lewis number, Prandtl number and Schmidt number were assumed to be one. Therefore, the turbulent diffusivity is the same for the mass, momentum and energy diffusion. For the dual chamber system, it was modeled by a simple mixing length theory,

$$\alpha = c\ Lx\ u' \qquad [\text{in}^2/\text{sec}] \quad \text{(IV.6)}$$

where $c = C_s\,(\frac{d_r}{d_{th}})^{\gamma}$

$$Lx = (y + C\ell) \qquad [\text{in}]$$

$$u' \propto u_{pn} + |u| \qquad [\text{in/sec}]$$

$$u_{pn} = u_p^{\,2}/u_{pr} \qquad [\text{in/sec}].$$

Mainly, the model consists of three elements, the correlation constant, the mixing length, and the turbulent intensity: (1) The correlation constant c correlates the effect of throat diameter. The ratio of throat diameter raised to the power γ simulates the change of turbulence caused by the change of the orifice size. The values of constant C_s and γ are determined by comparison with the experimental data to give correct burning rate. (2) The instantaneous chamber height is used for the mixing length. (3) The turbulent intensity is modeled by two parts. The first part is due to the piston speed. Through turbulent flame speed analysis (Sorenson 1978), the turbulent flame speed is proportional to the square root of the turbulent diffusivity. The turbulent flame speed is also proportional to the engine speed. It is assumed that the turbulent diffusivity is proportional to the turbulent intensity. The turbulent diffusivity is therefore proportional to the square of the engine speed. The literature data (Semenov 1958; and Lancaster 1976) showed this relationship. In Lancaster's investigation, it was felt that his shrouded nonstationary data is more relevant to the dual chamber flow system because its mean velocity is better defined. This particular set of data does show the quadratic relationship between the turbulent intensity and the engine speed. For consistency of units, the square of the mean piston speed has been normalized by dividing a reference mean piston speed. The second part of the characteristic velocity is due to the absolute value of the local gas velocity. Obviously, the higher the gas velocity is induced, the more the turbulence is generated.

11. Simple Zeldovich Mechanism For NO Formation

Newhall and Shahed (1967) used a simple Zeldovich mechanism for NO formation

$$O + N_2 \underset{k4}{\overset{k1}{\rightleftharpoons}} NO + N \qquad \text{(IV.7)}$$

$$N + O_2 \underset{k3}{\overset{k2}{\rightleftharpoons}} NO + O \qquad \text{(IV.8)}$$

The steady state for nitrogen atom concentration [N] and the equilibrium state for oxygen concentration [O_2] and oxygen atom concentration [O] were assumed. The detail of the model development and the specific reaction constants are presented in Appendix C.

B. Mathematical Formulation

When applying the basic physical laws to the simplified geometry, the system is described by the conservation equations for the mass, momentum, energy, and the species. Since it is a one-dimensional, time dependent model, these conservation equations are partial differential equations. The details of the derivation of the conservation equations are presented in Appendix A. The initial conditions are the initial values at the time of spark. The boundary conditions are the boundary values at the two end walls.

1. Equations

a) Conservation of mass

$$\frac{\partial}{\partial t}(\rho A) + \frac{\partial}{\partial x}(\rho A u) = 0 \qquad \text{(IV.9)}$$

b) Conservation of momentum

$$\frac{\partial u}{\partial t} + u \frac{\partial u}{\partial x} = - \frac{1}{\rho} \frac{\partial P}{\partial x} + \frac{1}{\rho A} \frac{\partial}{\partial x} (\rho A \alpha \frac{\partial u}{\partial x}) \qquad \text{(IV.10)}$$

c) Conservation of energy

$$\frac{\partial}{\partial t} (C_v T) + u \frac{\partial}{\partial x} (C_v T) + \frac{u}{\rho A} \frac{\partial}{\partial x} (\rho \alpha A \frac{\partial u}{\partial x}) + \frac{uP}{\rho A} \frac{\partial A}{\partial x} + \frac{P}{\rho} \frac{\partial u}{\partial x}$$

$$= \frac{1}{\rho A} \frac{\partial}{\partial x} (\rho A C_p \alpha \frac{\partial T}{\partial x}) - \frac{U\tilde{P}}{\rho A} (T_g - T_w)$$

$$+ hrZ \frac{\varepsilon_1 \varepsilon_2 \rho}{M^2} e^{-E/RoT} - \frac{P}{\rho A} \frac{\partial A}{\partial t} \qquad \text{(IV.11)}$$

d) Conservation of mass for species

$$\frac{\partial \varepsilon_i}{\partial t} + u \frac{\partial \varepsilon_i}{\partial x} = \frac{1}{\rho A} \frac{\partial}{\partial x} (\rho A \alpha \frac{\partial \varepsilon_i}{\partial x}) + \gamma_i Z P^{-\beta} \frac{\varepsilon_1 \varepsilon_2 \rho}{M} e^{-E/RoT} \qquad \text{(IV.12)}$$

e) Equation of state

$$P = \frac{\rho RoT}{M} \qquad \text{(IV.13)}$$

2. Initial Conditions

a) $\varepsilon_1(o, x) = \varepsilon_{1o}$

b) $\varepsilon_2(o, x) = \varepsilon_{2o}$

c) $\varepsilon_3(o, x) = \varepsilon_{3o}$

d) $\varepsilon_4(o, x) = \varepsilon_{4o}$

e) $\varepsilon_5(o, x) = 1 - \varepsilon_{1o} - \varepsilon_{2o} - \varepsilon_{3o} - \varepsilon_{4o}$

f) $P(o, x) = P_o$

g) $\rho(o, x) = \rho_o$

h) $T(o, x_s) = T_s$

i) $u(o, x) = 0$

The initial values of the mass fraction of the species were calculated through the mixing model subroutine. The initial value of gas pressure was obtained from the engine pressure data at ignition. The initial total intake mass was calculated from the total mass flow rate, the residual fraction and the engine speed, as follows:

$$m_T = 2\,\dot{m}_T/[(1 - f) \times rpm \times 60] \qquad [lbm] \qquad (IV.14)$$

The initial total volume was obtained from the geometry function. The initial density and temperature were then calculated through the equation of state. The initial spark temperature was estimated through the ignition subroutine.

3. Boundary Conditions

a) $u(t, o) = u(t, L) = 0$

b) $\frac{\partial \rho}{\partial x}(t, o) = \frac{\partial \rho}{\partial s}(t, L) = 0$

c) $\frac{\partial P}{\partial x}(t, o) = \frac{\partial P}{\partial x}(t, L) = 0$

d) $\frac{\partial T}{\partial x}(t, o) = \frac{\partial T}{\partial x}(t, L) = 0$

e) $\frac{\partial \varepsilon_1}{\partial x}(t, o) = \frac{\partial \varepsilon_1}{\partial x}(t, L) = 0$

f) $\frac{\partial \varepsilon_2}{\partial x}(t, o) = \frac{\partial \varepsilon_2}{\partial x}(t, L) = 0$

$$g)\ \frac{\partial \varepsilon_3}{\partial x}(t, o) = \frac{\partial \varepsilon_3}{\partial x}(t, L) = 0$$

$$h)\ \frac{\partial \varepsilon_4}{\partial x}(t, o) = \frac{\partial \varepsilon_4}{\partial x}(t, L) = 0$$

$$i)\ \frac{\partial \varepsilon_5}{\partial x}(t, o) = \frac{\partial \varepsilon_5}{\partial x}(t, L) = 0$$

The gas velocity was zero at the end walls. It was also assumed that the density, the pressure, the temperature and the mass fraction of the species have zero gradient at the boundaries.

C. Numerical Method

Totally, there are seven non-linear partial differential equations with unknown dependent variables ρ, u, T, ε_1, ε_2, ε_3, and ε_4. The inclusion of the momentum equation results in a set of equations that are both hyperbolic and parabolic in nature. All the differential equations have been written in time derivatives of the dependent variables. The details of this derivation are given in Appendix A. The MacCormack predictor-corrector technique (Dwyer, et al., 1974) is used to integrate these temporal derivatives.

1. The Numerical Integration Technique

a) Predictor

$$\overline{Y_i^{n+1}} = Y_i^n + \left(\frac{dY}{dt}\right)_i^n \Delta t \qquad \text{(IV.15)}$$

Euler's method is used first to predict a value at one time step advance. Y represents all the dependent variables.

b) Corrector

$$Y_i^{n+1} = \tfrac{1}{2}[Y_i^n + \overline{Y_i^{n+1}} + \overline{(\frac{dY}{dt})_i^{n+1}}\Delta t] \qquad \text{(IV.16)}$$

The improved Euler method is then used to correct the predictor at one time step advance. This predictor-corrector technique gives second order accuracy. The standard forward difference, central difference and backward difference schemes are used for the spatial derivatives. The forward difference is used for the first order spatial derivatives in the predictor.

$$(\frac{dY}{dx})_i^n = \frac{Y_{i+1}^n - Y_i^n}{\Delta x} \qquad \text{(IV.17)}$$

The backward difference is used for the first order spatial derivatives in the corrector

$$(\frac{dY}{dx})_i^{n+1} = \frac{Y_i^{n+1} - Y_{i-1}^{n+1}}{\Delta x} \qquad \text{(IV.18)}$$

The central difference is used for the second order spatial derivatives in both the predictor and the corrector

$$(\frac{d^2Y}{dx^2})_i^n = \frac{Y_{i+1}^n - 2Y_i^n + Y_{i-1}^n}{\Delta x} \qquad \text{(IV.19)}$$

$$(\frac{d^2Y}{dx^2})_i^{n+1} = -\frac{Y_{i+1}^{n+1} - 2Y_i^{n+1} + Y_{i-1}^{n+1}}{\Delta x^2} \qquad \text{(IV.20)}$$

Appendix B gives all the equations in finite difference form for both the predictor and corrector.

2. The Stability Criteria

a) The maximum time step

For the calculations in wave dynamics, the Courtant-Friedrich-Levy (CFL) stability criterion must be obeyed (Warming, et al., 1973),

$$\Delta t \leq \frac{\Delta x}{|u| + c} \tag{IV.21}$$

where c = local acoustic velocity [in/sec]

The time step size calculated from CFL condition is used as the maximum time step allowed.

b) The restricted time step

It is found that for stratified charge chemical reaction system, more step size restrictions are needed for a stable calculation.

(1) The temperature rise at any location during any one time step is limited to only one percent increase. This restriction is to prevent the instability caused by the overshoot in regions of rapid temperature rise. The restricted time step is calculated as following:

$$\frac{\partial T}{\partial t} \Delta t = f_T \, T \tag{IV.22}$$

$$\Delta t = f_T \frac{T}{\frac{\partial T}{\partial t}} \tag{IV.23}$$

where $f_T = 0.01$

(2) No species concentration is allowed to become negative, otherwise, it violates physical laws. Also, the negative values will change the sign of the reaction rate term and cause instability. This restriction is quite severe in the stratified charge combustion system due to its non-stoichiometric chemical reaction. The restricted time step is calculated as follows:

$$\left|\frac{\partial \varepsilon_i}{\partial t}\right| \Delta t = f_\varepsilon \varepsilon_i \tag{IV.24}$$

$$\Delta t = f_\varepsilon \frac{\varepsilon_i}{\left|\frac{\partial \varepsilon_i}{\partial t}\right|} \tag{IV.25}$$

where $f_\varepsilon = 0.7$

(3) A minimum time step is set as a bound. If any of the species concentration becomes very small, the time step will become extremely small as the second step size criterion takes effect. As the concentration approaches zero, the number of integrations becomes infinitely large. To prevent this occurrence, the derivative of any species of which the concentration is less than 10^{-6} is set to zero. Because of its negligible concentration, the energy release and mass concentration are not significantly affected. This restriction is used only when the derivative of species concentration is negative. If this restriction is applied, a minimum time step of 10^{-7} is assigned.

The complete flow chart of the restricted time step control is shown on Figure 44. Generally, the maximum time step from CFL condition is used, but when the restricted time step becomes smaller, the restricted time step is applied.

3. Computer Programming

For more generality and better programming, the simulation model has been developed into one main program, thirteen subroutines, three subfunctions and one common data block. The program is written in FORTRAN IV, and run on the IBM 360/75 digital computer of University of Illinois at Urbana-Champaign. The average CPU time for a complete calculation is around 20 minutes. The flow chart of the main program, the description of each subroutine, and the complete program appears in Appendix K.

D. Model Development

1. Model Geometry

The development of model geometry has two stages.

a) The simplified geometry

Initially a simplified geometry was assumed consisting of a cylindrical prechamber and cylindrical main chamber connected by a cylindrical orifice as shown in Figure 4.

b) The modified geometry

In the second stage, some modifications of the geometry are made:

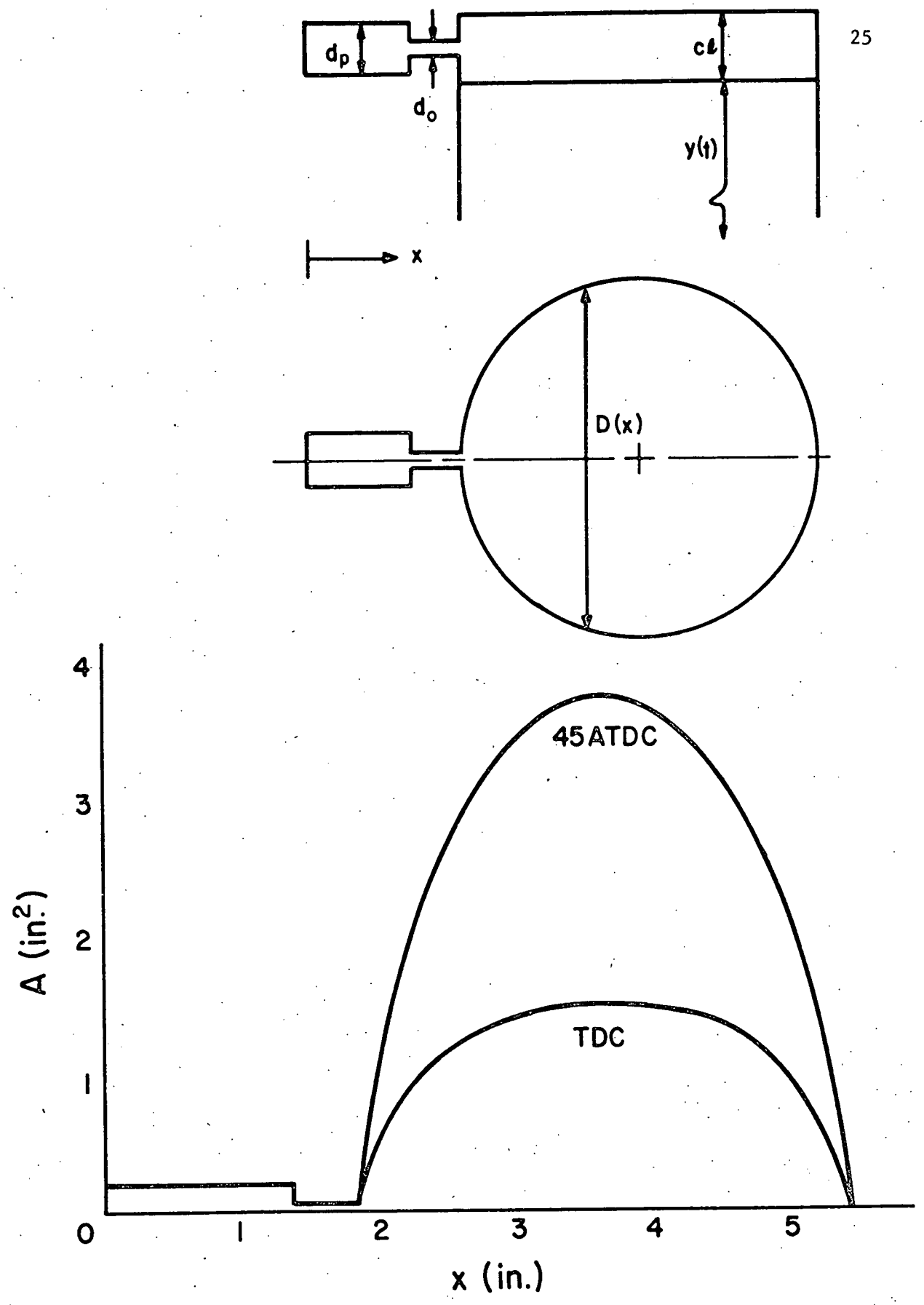

Figure 4. Cylindrical Combustion Chamber And Its Area Function

(1) Due to the discontinuity by the sudden area change at the inlet and the outlet of the orifice, numerical instability was encountered. The cylindrical orifice was then modified to a nozzle shape as illustrated in Figure 5. This continuous smooth area change through the orifice solved the instability problem and gave much better numerical accuracy. Physically, the characteristic of a fluid flow interaction between the two chambers is also better described by a nozzle passage.

(2) To match the test engine geometry, the shape of the main chamber was modified from a cylinder to a wedge as shown in Figure 6. The effect of the main chamber shape on calculated pressure time history is shown in Figure 7. The original simplified cylindrical main chamber has a clearance height of 0.4104 inches. When the clearance height near the orifice outlet is increased, the clearance height at the end wall needs to be decreased in order to keep the same main chamber volume. The change of the main chamber from the cylindrical shape to a wedge shape changes the mass distribution. More mass is burned earlier and a faster pressure rise is encountered. The wedge shaped main chamber with a maximum clearance of 0.8074 inches was used for the simulation model.

(3) Figure 8 illustrates the effect of the spark location on the calculated pressure time history. The spark was

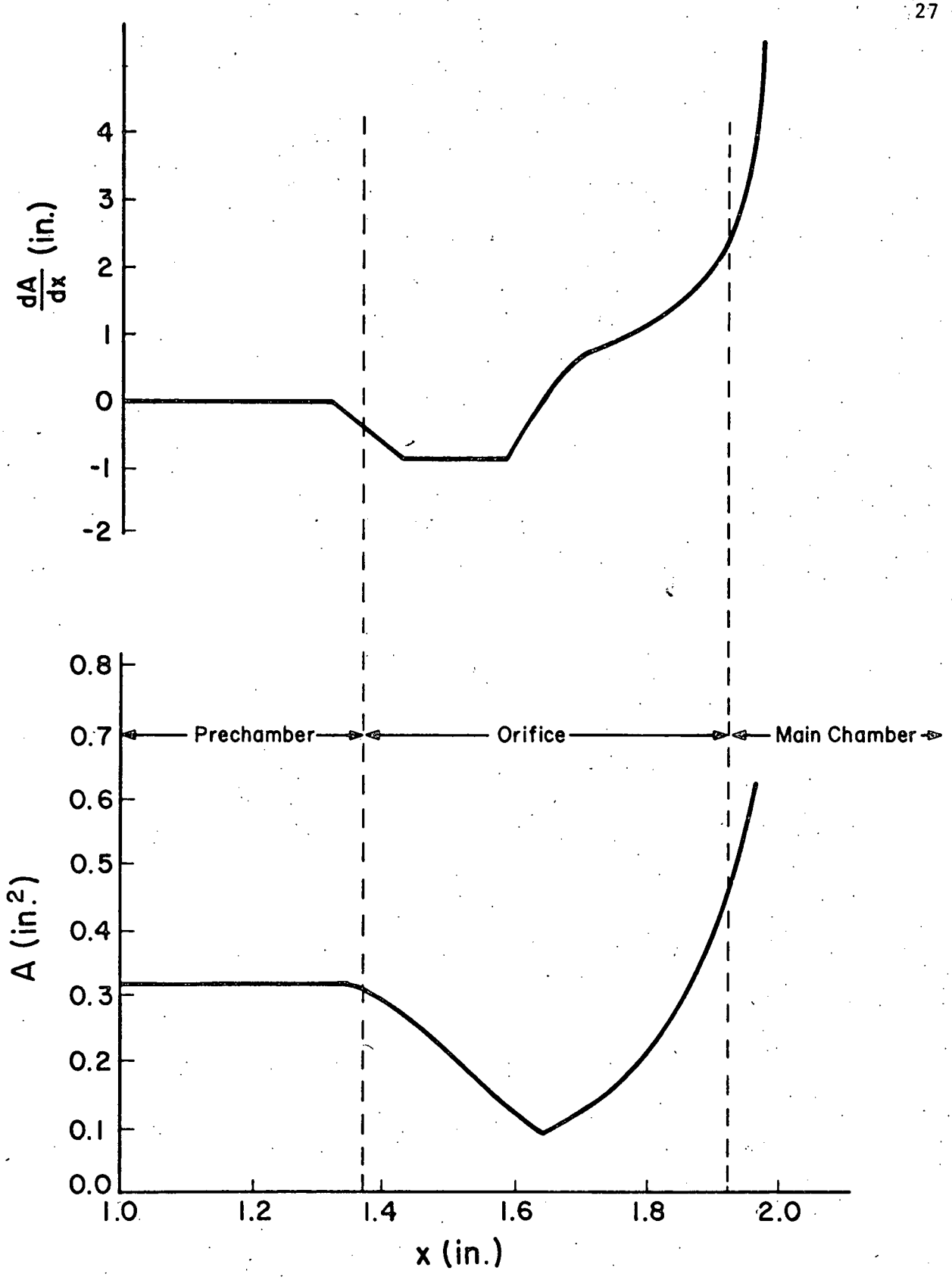

Figure 5. Area Functions Of A Nozzle Shape Orifice

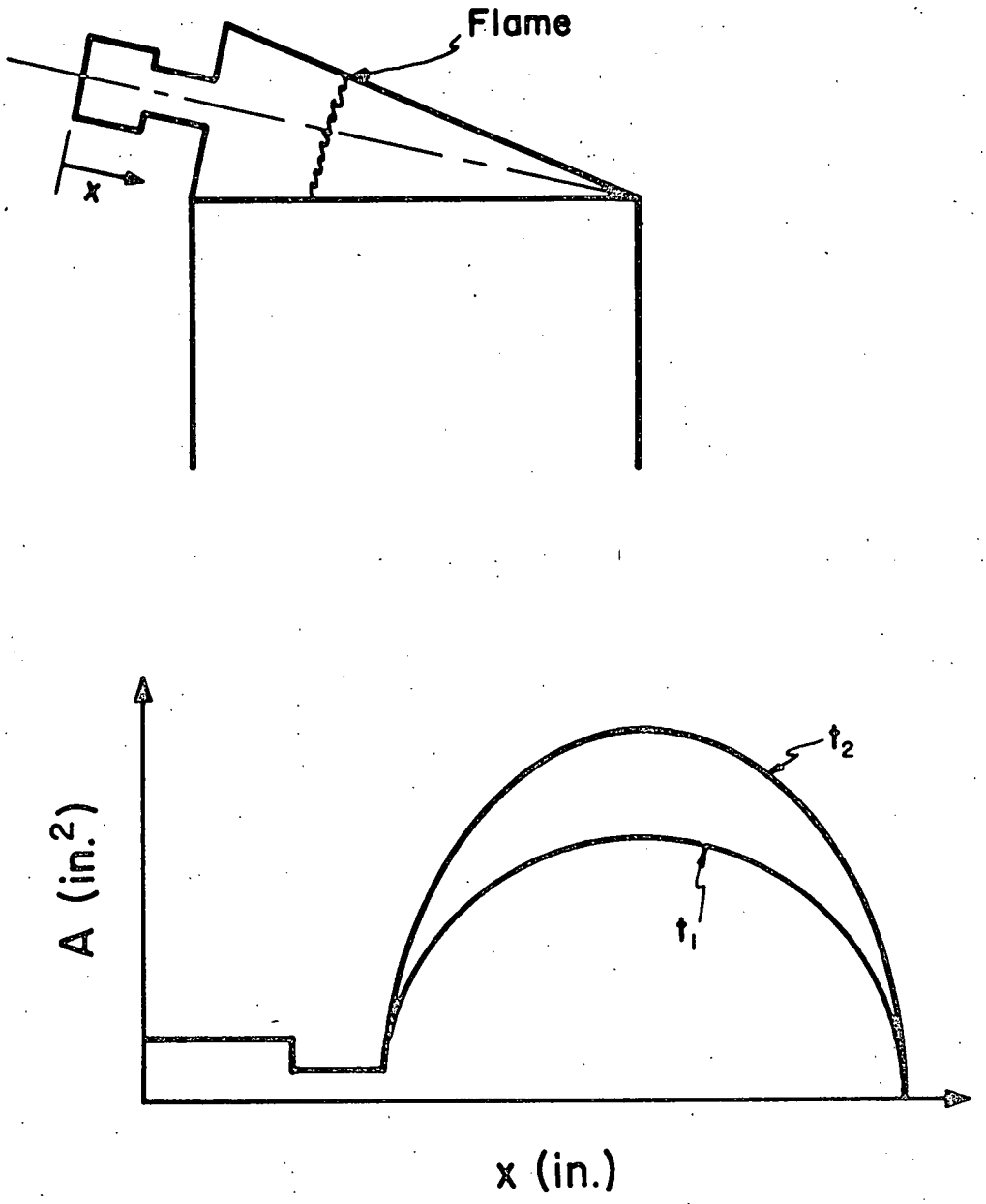

Figure 6. Wedged Combustion Chamber And Its Area Function

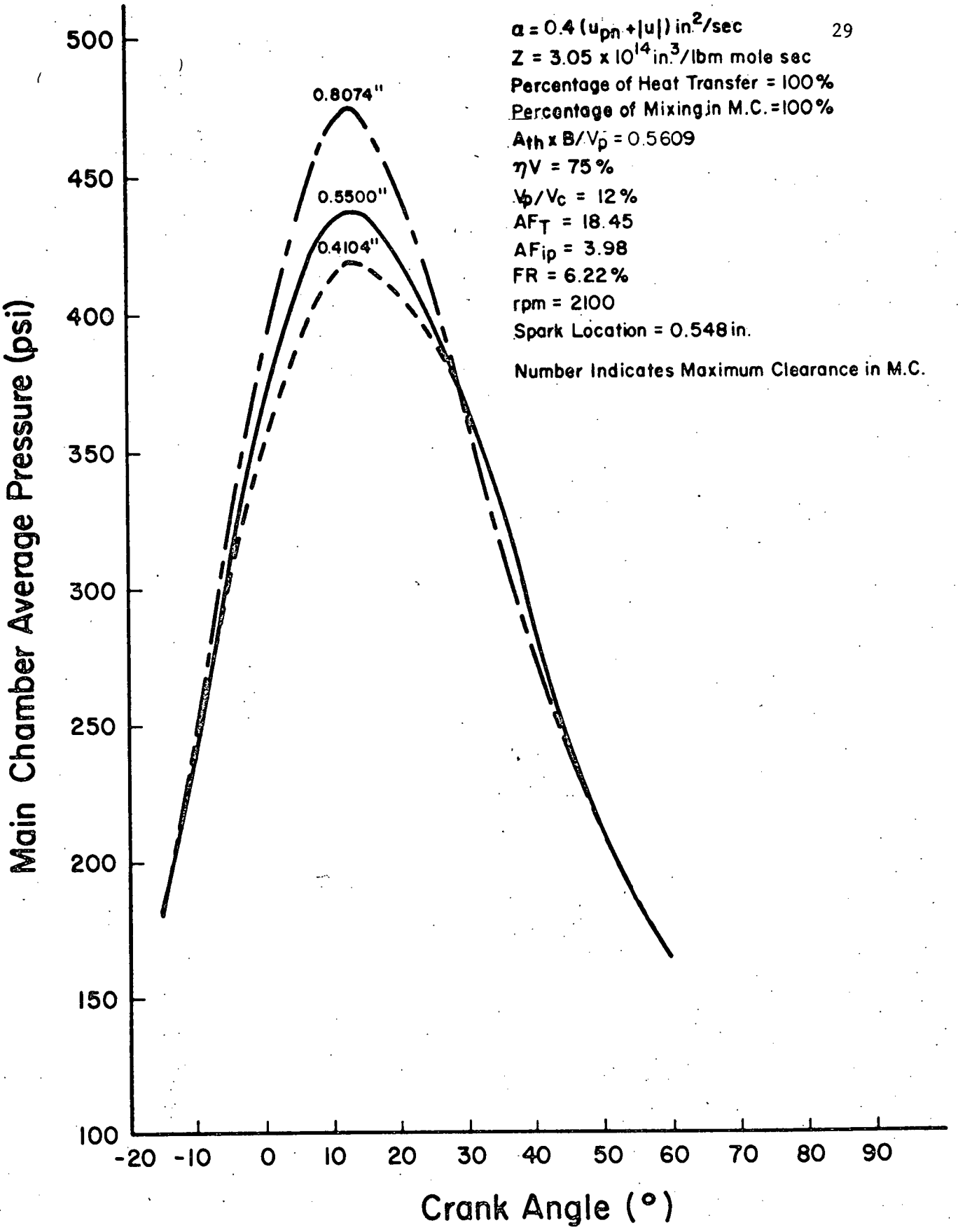

Figure 7. Effect Of Main Chamber Shape On Pressure Time History

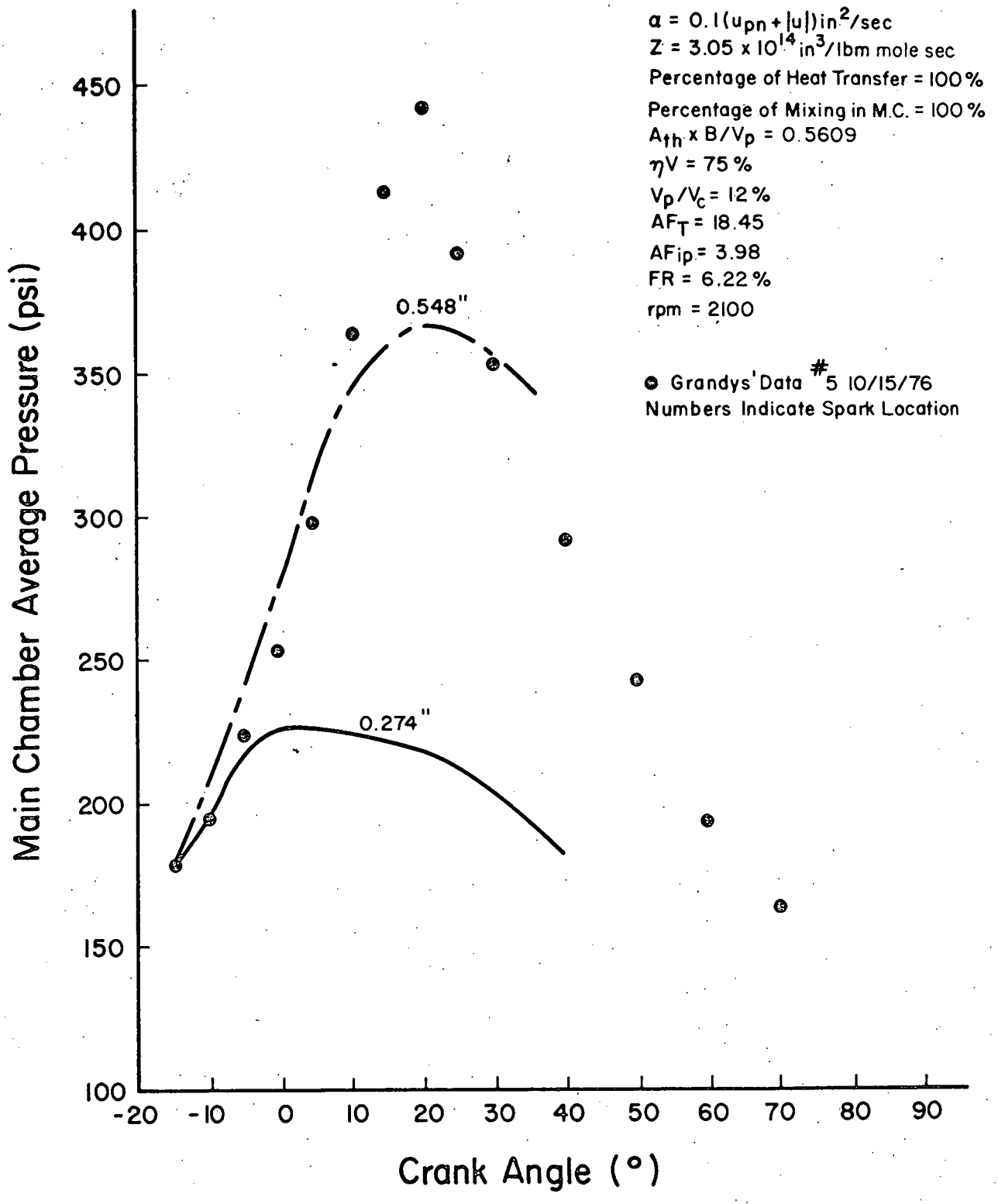

Figure 8. Effect of Spark Location On Pressure Time History

originally set at 0.274 inches near the end wall of the prechamber. When the spark location was moved out from the end wall, the power output was increased. This is due to the flame traveling in both directions when the spark is out in the chamber, instead of only one direction when the spark is located at the end wall. According to the conventional theory of the chamber design (Obert, 1973), if the ignition starts in the middle of the chamber, it takes half the time for the flame to travel across the chamber than if the ignition starts at either end. In the engine case, although the spark is located at end wall of the prechamber, the origin of the spatial axis was set at the prechamber intake value. It was believed that the test engine had the similar case as the later version, where the spark located in the middle of the prechamber. A distance of 0.548 inches from the origin was chosen for the spark location to simulate the distance from the prechamber intake valve to the spark plug in the test engine. The prechamber has the same cylindrical shape as before. The detail of the geometry function for the dual chamber model is given in Appendix I.

2. Model Parameter Study

The basic parameters for the combustion model are: the turbulent diffusivity α, the preexponential constant Z, the activation energy E, the overall heat transfer coefficient U, and the mixing percentage PM2.

A constant value of 30 Kcal/gm mole was used for the activation energy (Sirignano and Bracco, 1972). The sensitivity of the other parameters has been studied. The following base values were used for this purpose:

$$\alpha = 0.1\ (u_{pn} + |u|) \qquad [in^2/sec]$$

$$Z = 3.05 \times 10^{14} \qquad [in^3/lbm\ mole\ sec]$$

Percentage of heat transfer of Woschni's model = 100%

Percentage of mixing in main chamber = 100%

a) Turbulent diffusivity

It is known that the higher the turbulence level, the better the mixing, the faster the burning rate, and the higher the power output. The calculation agrees with this trend. Figure 9 and Figure 10 give the effect of the turbulent diffusivity on the calculated pressure time history and mass fraction burned. The data of the mass fraction burned was estimated from the photographs of the engine combustion (Hull and Sorenson, 1978). The mass fraction burned curve was calculated through the empirical equation (Miller, et al., 1954),

$$\text{Mass fraction burned} = \tfrac{1}{2}[1 - \cos(\frac{\Theta-\Theta_o}{\Delta\Theta_c} \cdot \pi)] \qquad \text{(IV.26)}$$

where Θ_o = initial angle of combustion

$\Delta\Theta_c$ = crank angle duration for combustion.

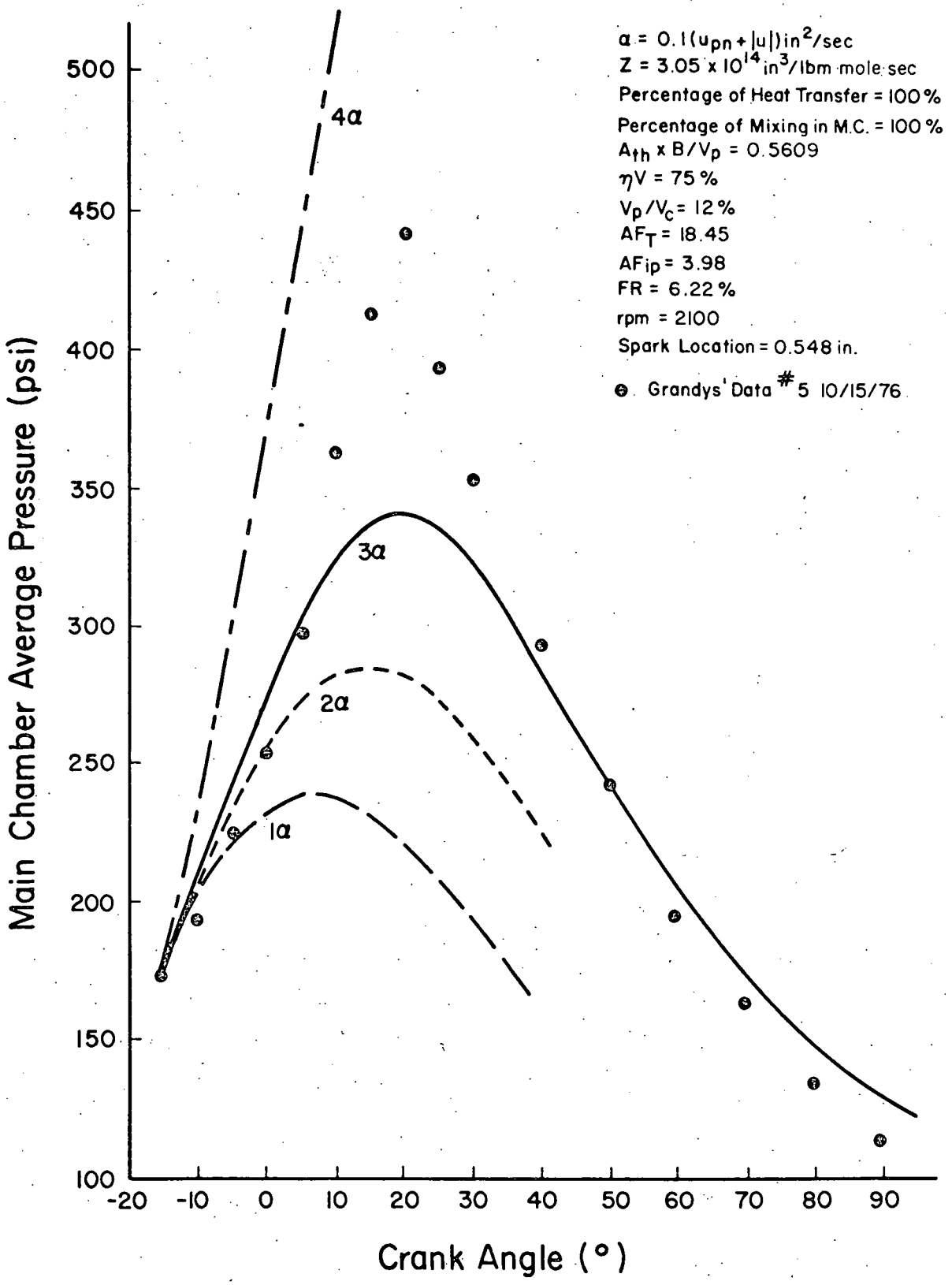

Figure 9. Effect Of Turbulent Diffusivity On Pressure Time History

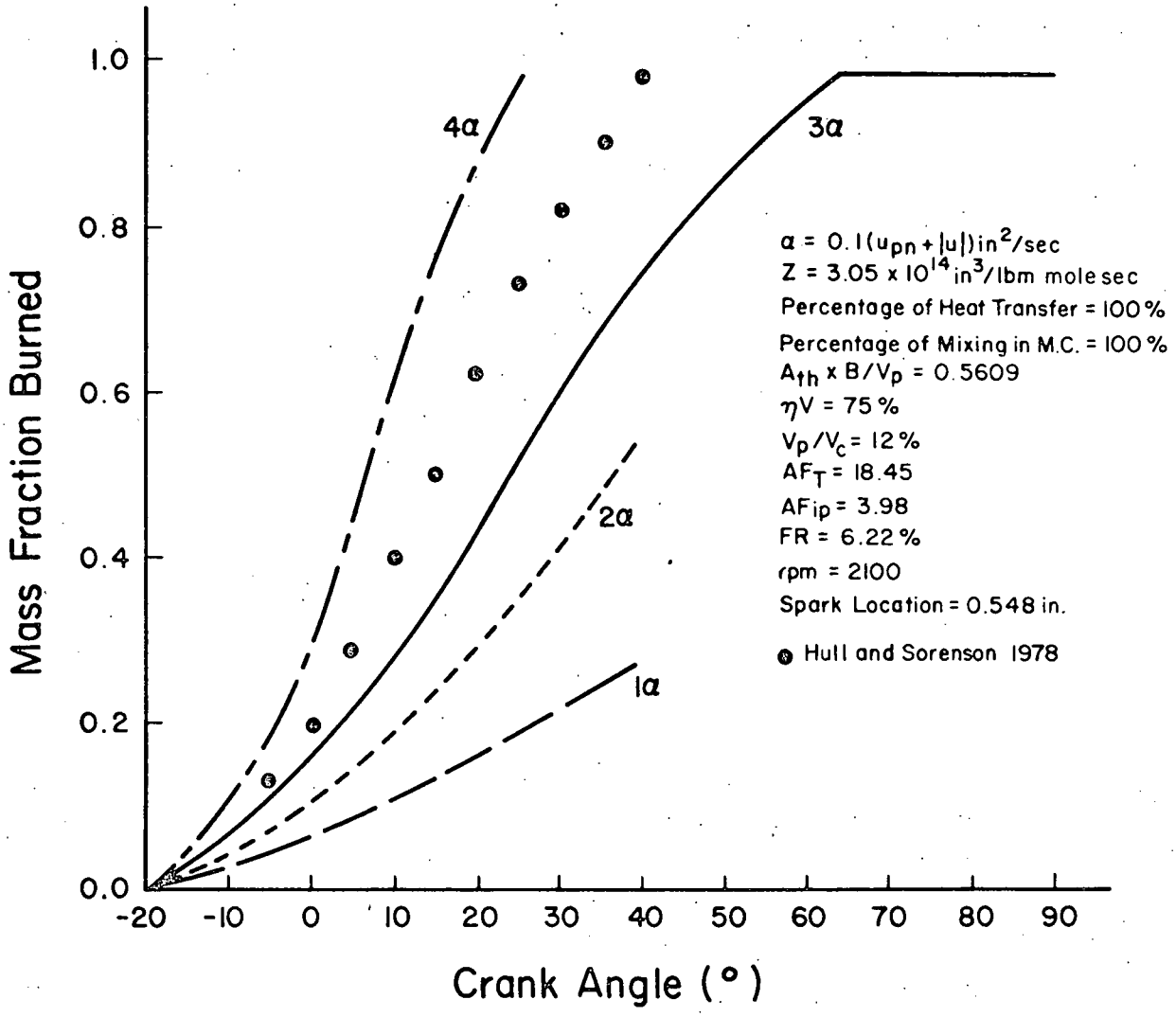

Figure 10. Effect Of Turbulent Diffusivity On Mass Fraction Burned

The effect of the turbulent diffusivity on NO production is given in Figure 11. It can be seen that the optimum value for this condition is between 3 and 4 times the baseline value from Figures 9, 10 and 11.

b) Preexponential constant

The effect of the preexponential constant on pressure and mass fraction burned is shown in Figure 12 and Figure 13. It can be seen that this preexponential constant plays an important role in the chemical kinetics. From the investigation of turbulent combustion modeling (Sorenson 1977), the flame speed is proportional to the square root of the product of the preexponential constant and the turbulent diffusivity. With the proper combination of the preexponential constant and the turbulent diffusivity, the correct burning rate can be correlated to the engine data.

c) Heat transfer

The effect of heat transfer on the calculated pressure time history and the NO production appears in Figure 14 and Figure 15 respectively. Comparing Figure 14 and Figure 9, the calculated pressure time history for the base diffusivity without heat transfer is about the same as that for 3 times the base diffusivity with heat transfer. Since the heat transfer affects the burning rate and the peak temperature, it plays an important role for both the power output and NO production.

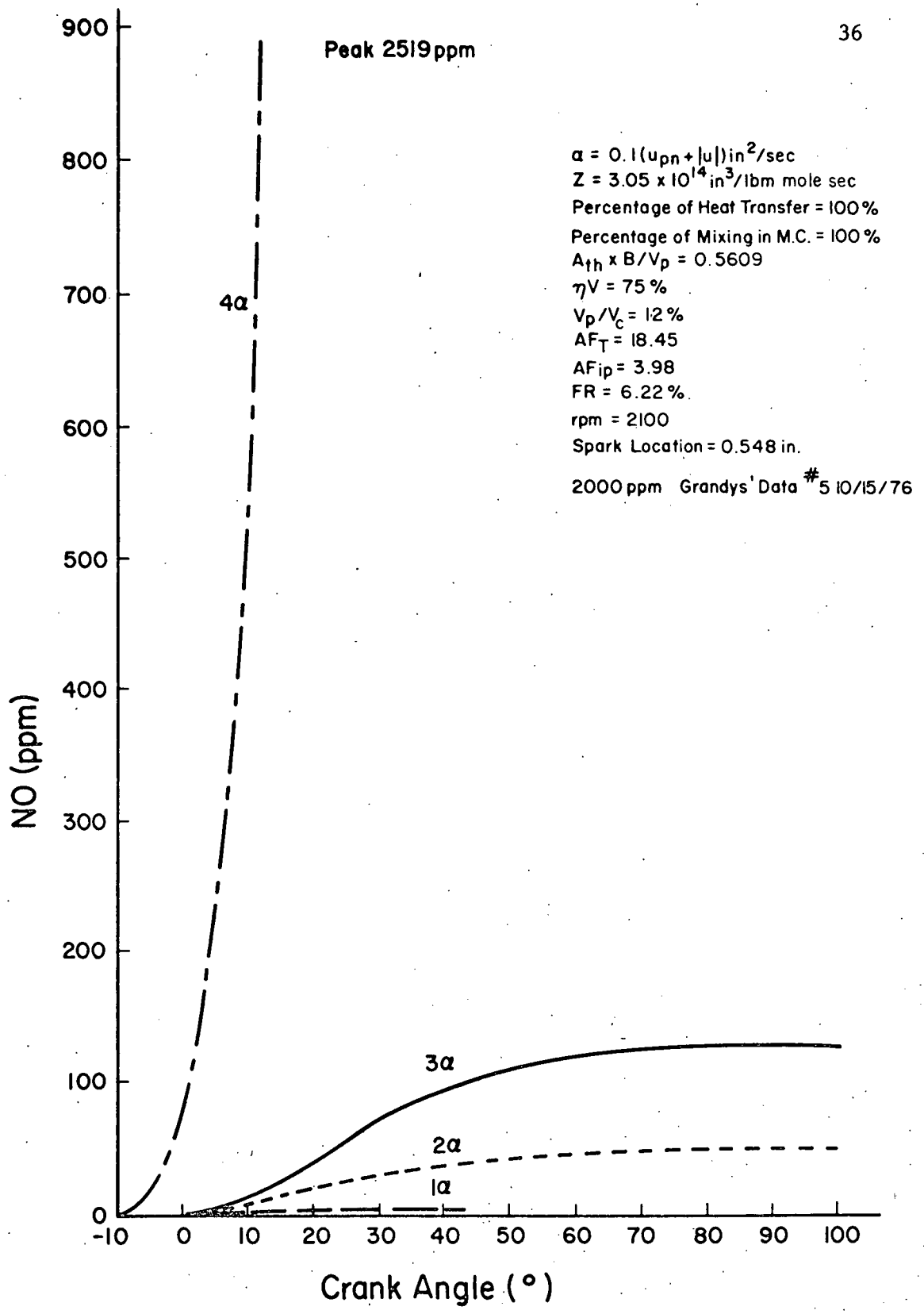

Figure 11. Effect Of Turbulent Diffusivity On NO Production

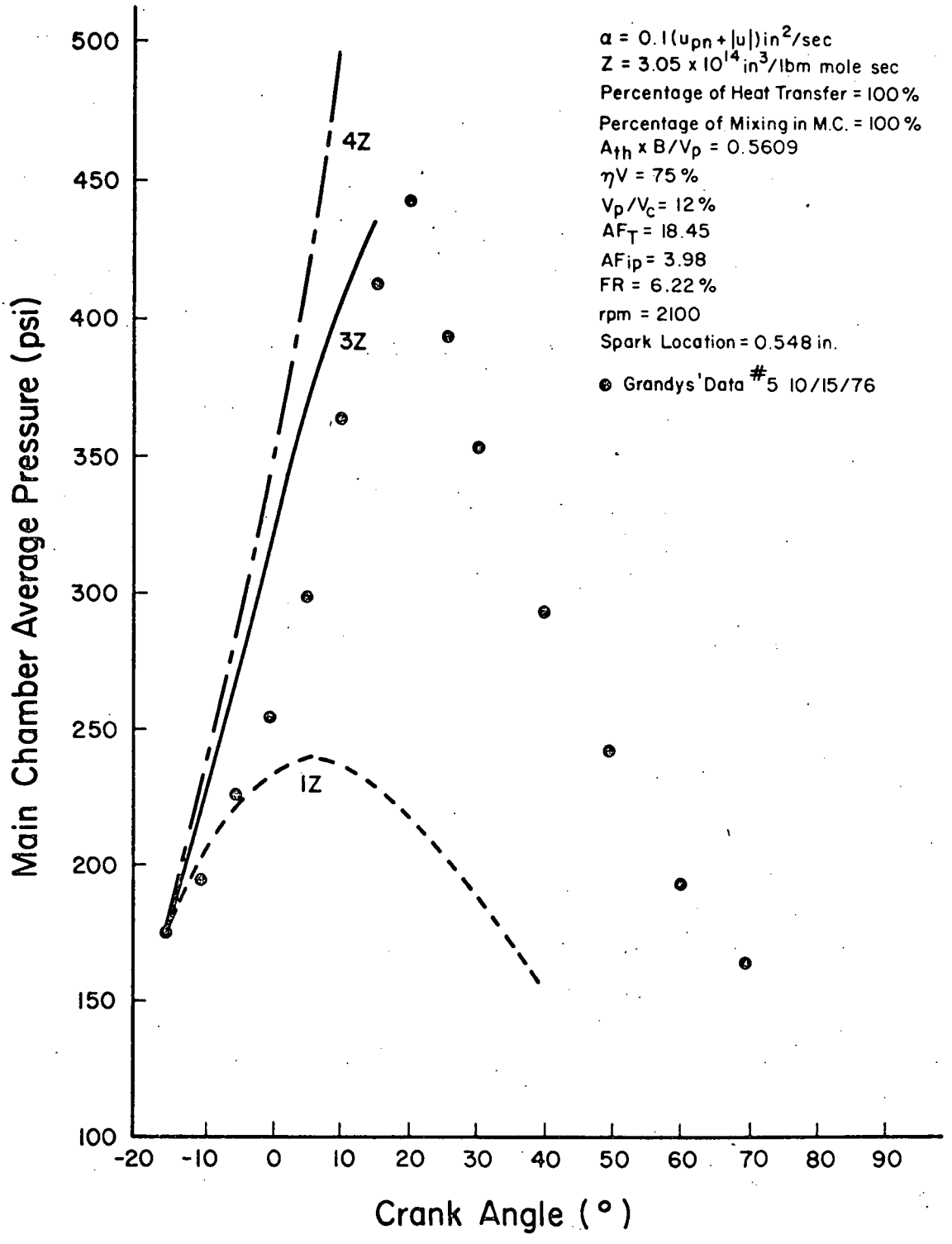

Figure 12. Effect Of Preexponential Constant On Pressure Time History

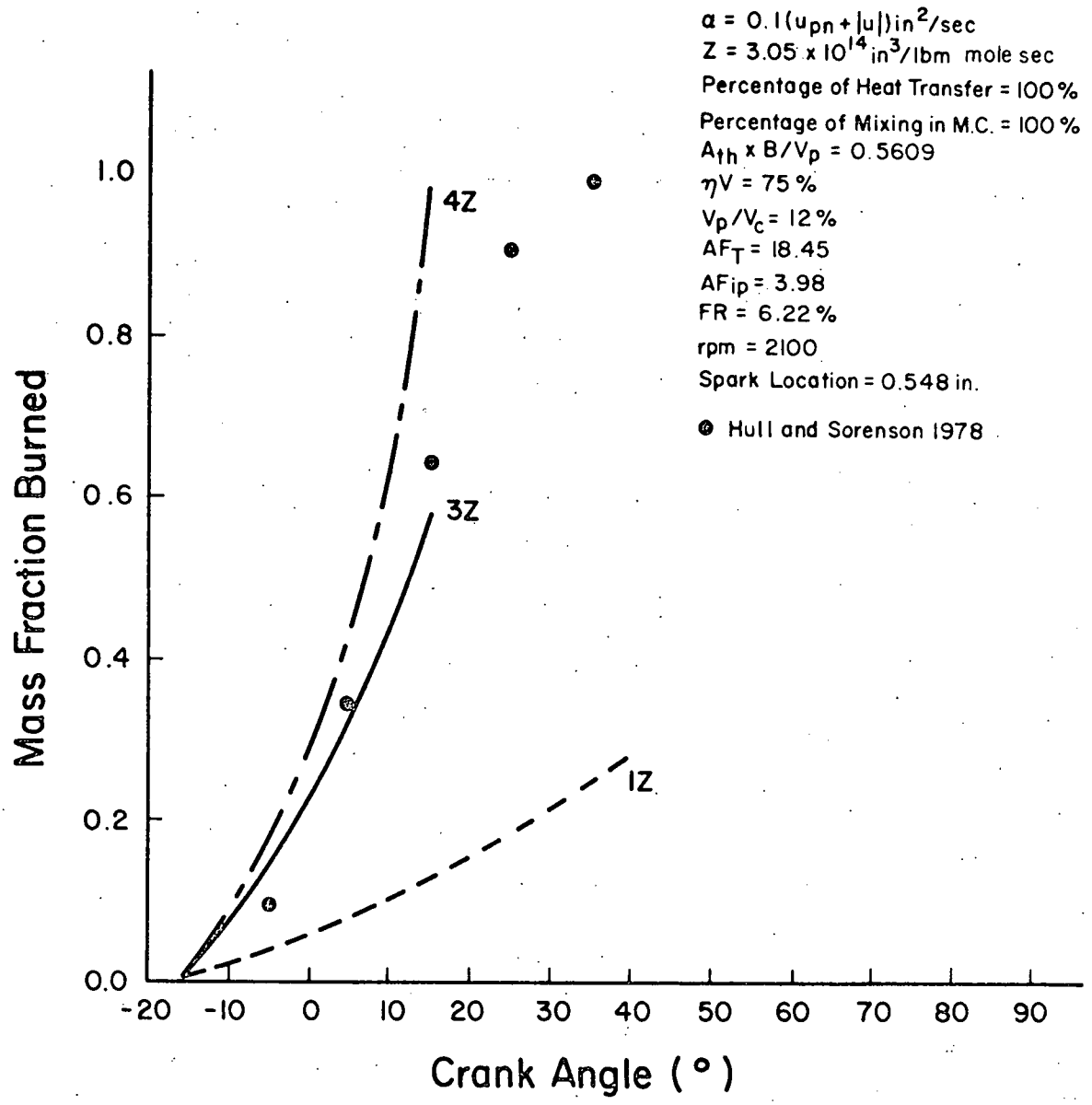

Figure 13. Effect of Preexponential Constant On Mass Fraction Burned

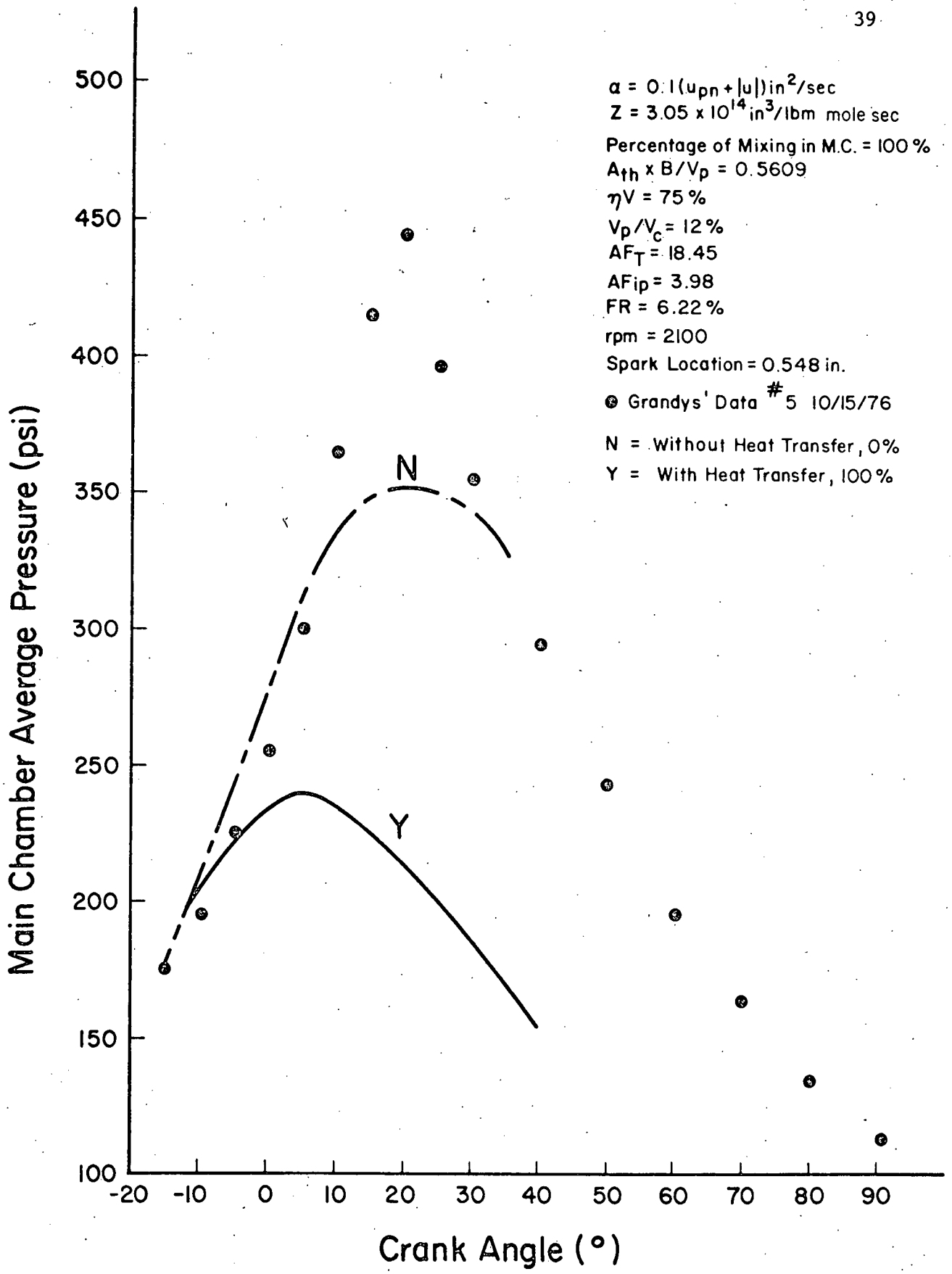

Figure 14. Effect Of Heat Transfer On Pressure Time History

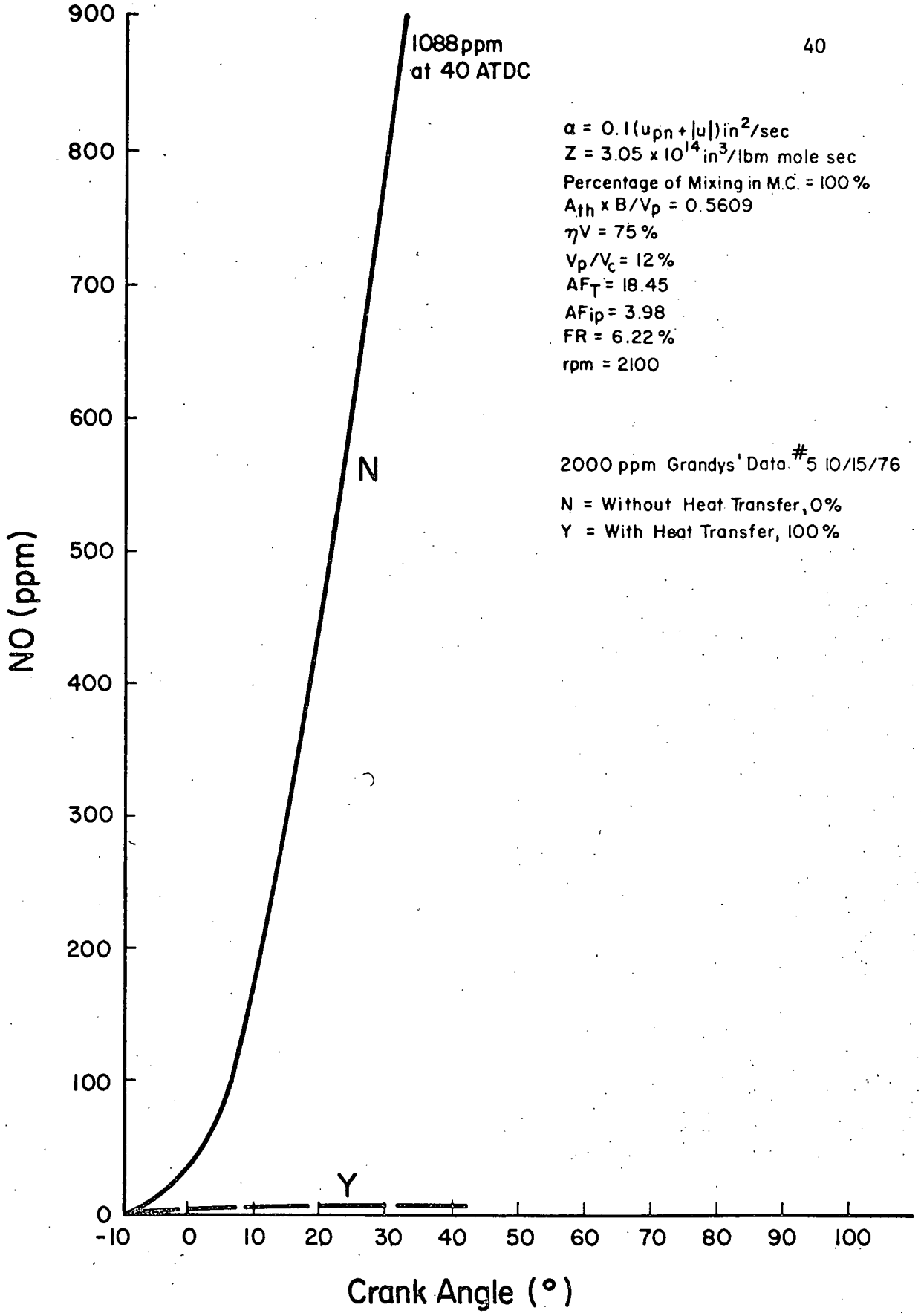

Figure 15. Effect Of Heat Transfer On NO Production

d) Mixing percentage

The effect of the mixing percentage on the calculated pressure time history and the mass fraction burned is given in Figure 16 and Figure 17. The less the mixing percentage, the richer the mixtures are in the intermediate zone and the prechamber, and the faster the burning rate will be in the first part of the combustion. The effect of the mixing percentage on the prechamber equivalence ratio at spark is shown in Figure 18. It agrees with the expected trend. The effect of the mixing percentage on the NO production appears in Figure 19. The less the mixing percentage, the more the NO production. It is known that the main source of the NO formation is in the intermediate zone. The peak values of NO formation occur at slightly leaner than the stoichiometric. The lower mixing percentage gives an environment that encourages the NO formation.

3. Numerical Parameters

In order to investigate the effect of the spatial grid size on numerical accuracy, test calculations were made with 20, 40, 60, 80, and 100 spatial grid points. It was found that the calculated results converged when the number of internal grid points was beyond 80. At the completion of the calculation of the 80 points, the mass conservation has an error of 2%. The effect of the grid size between 80 points and 100 points appears in Figure 20. The grid size of 6.85×10^{-2} inches was used for the model's calculations.

The maximum time step calculated from the CFL condition assuming a grid size of 6.85×10^{-2} inches, a maximum gas velocity of

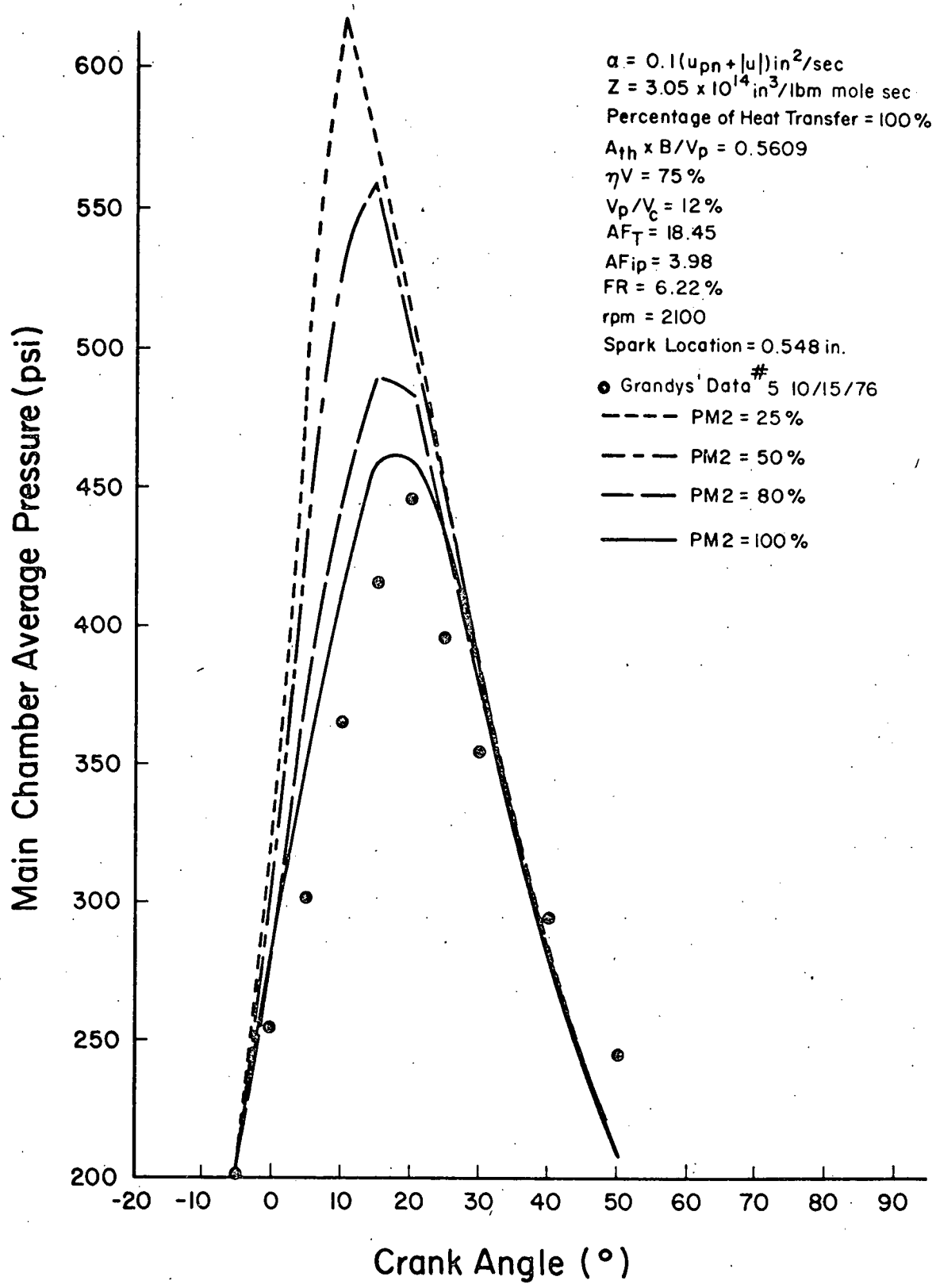

Figure 16. Effect Of Mixing Percentage On Pressure Time History

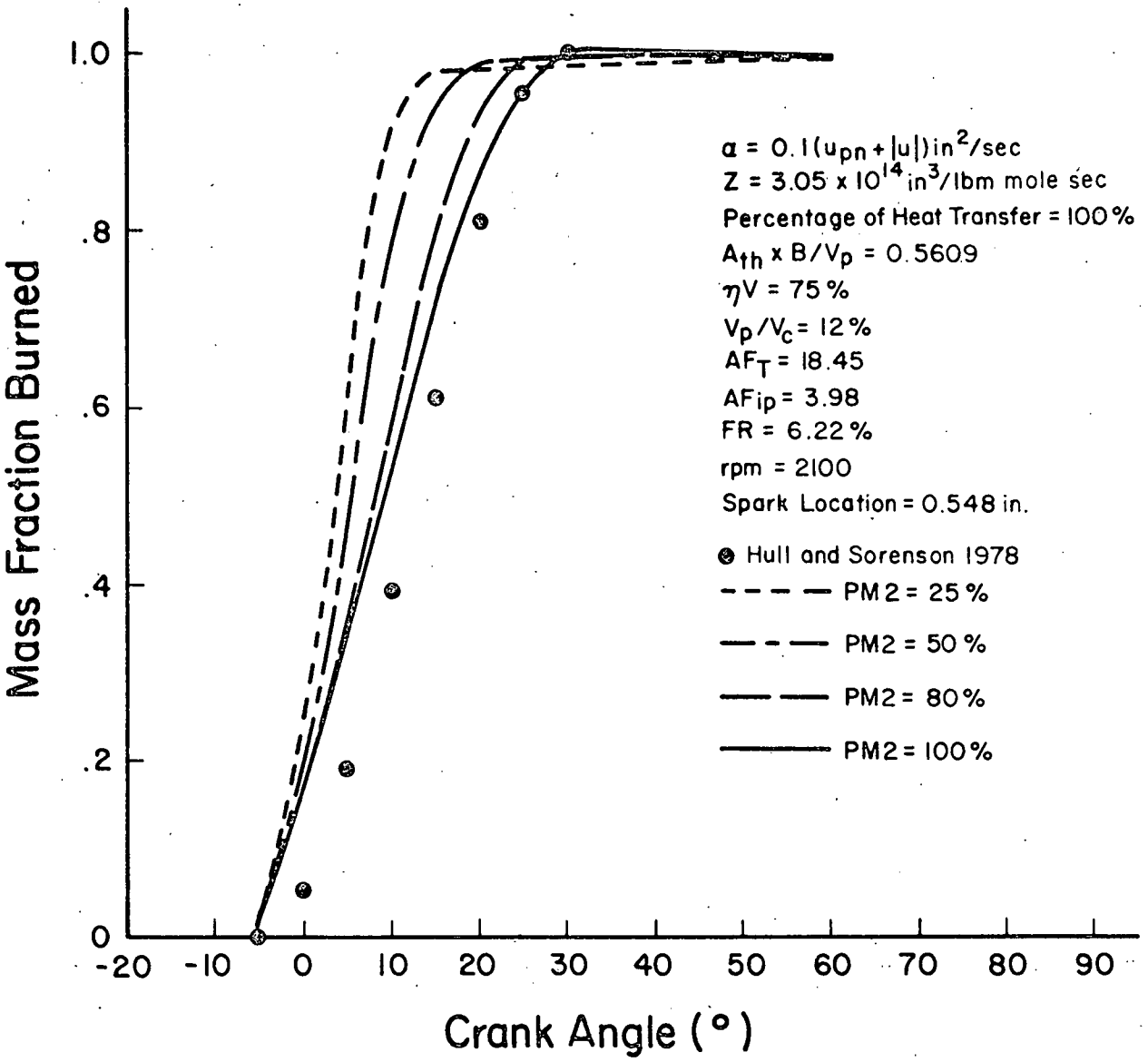

Figure 17. Effect Of Mixing Percentage On Mass Fraction Burned

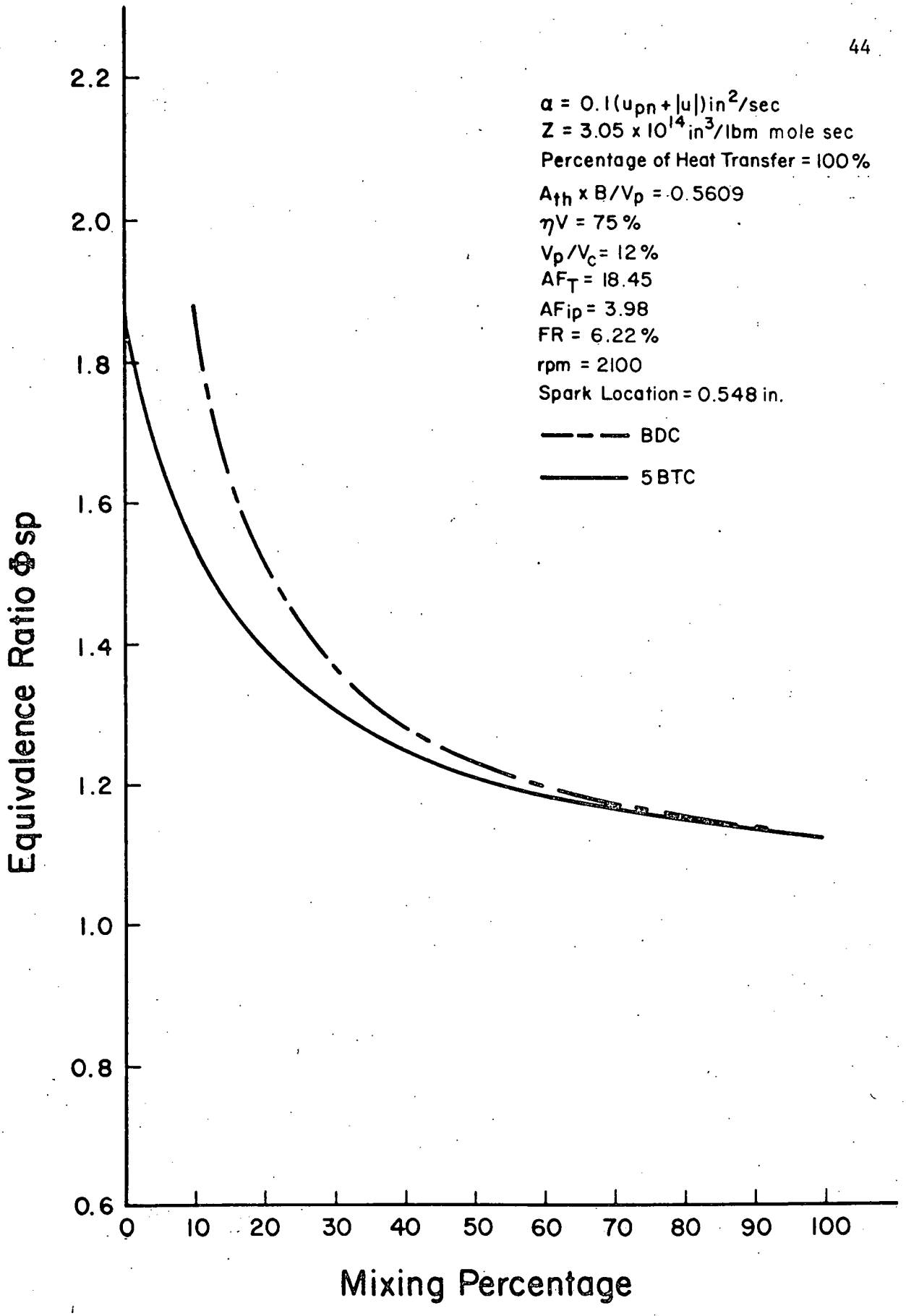

Figure 18. Effect Of Mixing Percentage On Prechamber Equivalence Ratio At Spark Time

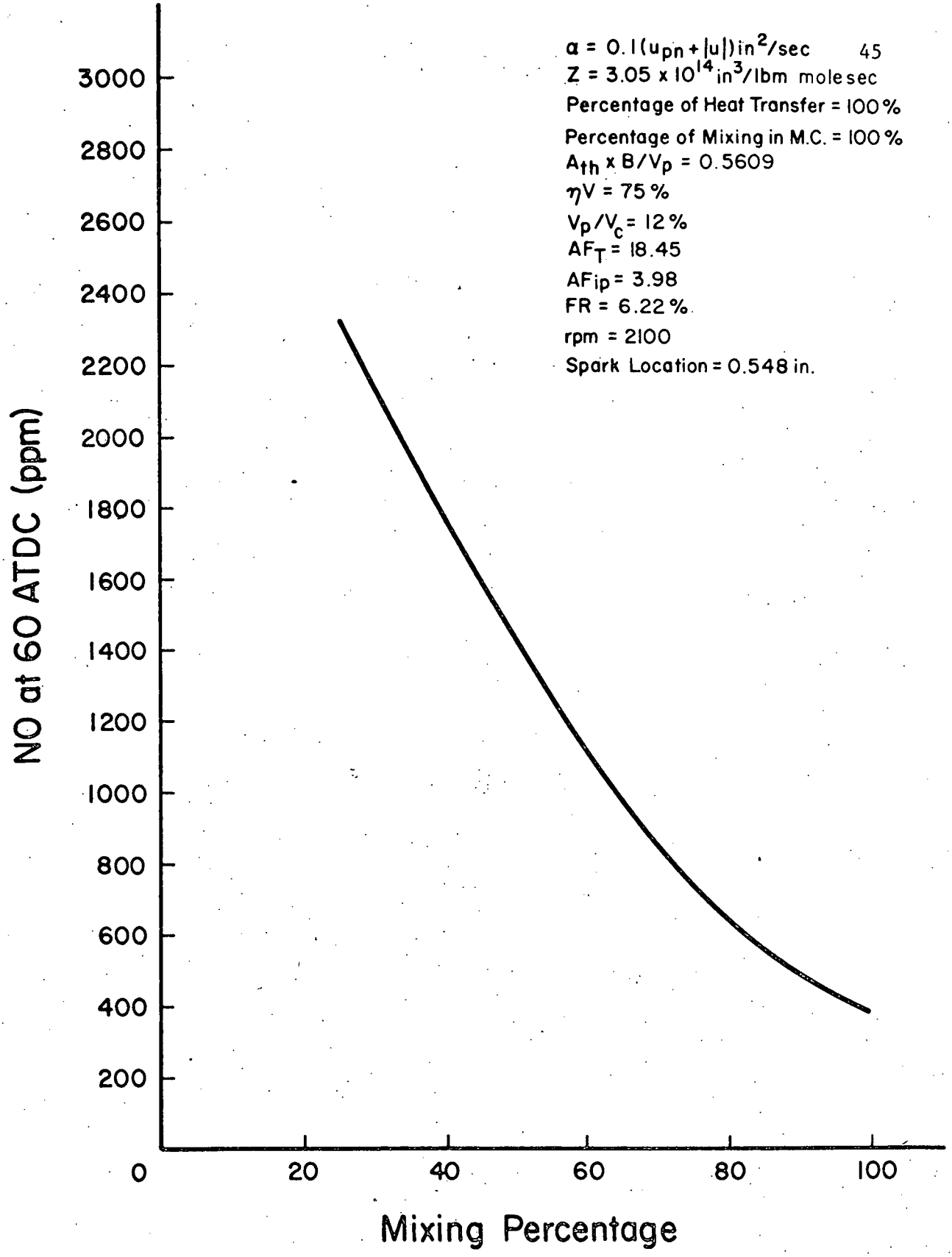

Figure 19. Effect Of Mixing Percentage On NO Production

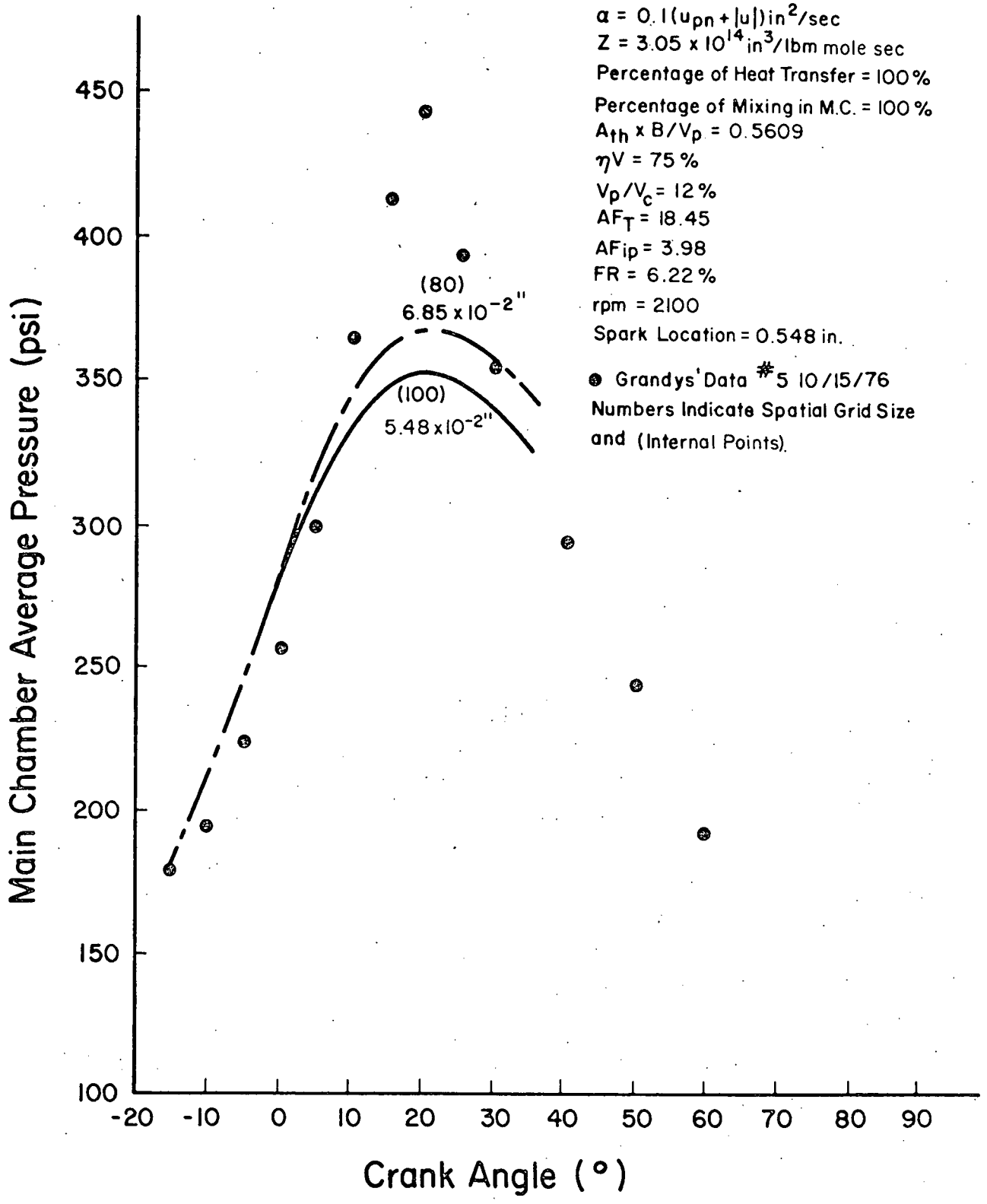

Figure 20. The Convergence Character Of Spatial Grid Size

3000 in/sec, and a maximum gas temperature of 5200°R is 1.5×10^{-6} sec. When setting the time derivative equal to zero and the mass fraction of fuel and/or oxygen becoming less than 1×10^{-6}, the minimum time step size is 1×10^{-7}. The maximum percentage of temperature rise at each point is restricted to 1%. The maximum percentage for the consumption of fuel and/or oxygen during one predictor time step is restricted to 70%. The minimum value for the mass fraction of the fuel and/or oxygen for setting the time derivation equal to zero is 1×10^{-6}.

4. Basic Correlation Runs

Four sets of data with variations of the throat diameter and the volumetric efficiency have been chosen for the basic correlation: (1) small orifice with part throttle, (2) small orifice with wide open throttle, (3) large orifice with part throttle, and (4) large orifice with wide open throttle. The basic parameters have been correlated according to the experimental data of the pressure-time diagram. The conditions for these runs are listed as No. 1 - No. 4 in Table 3. The correlation between the calculated results and the experimental data for the pressure time history are illustrated in Figures 21, 34, and 36.

a) Turbulent diffusivity

Equation IV.6 is used as the final model of the turbulent diffusivity. The correction power γ for the correlation of the effect of the throat diameter is 2. The constant coefficient C_s has a value

of 0.7. The turbulent diffusivity calculated through the model has a value of approximately 50 in^2/sec, which is in the same order of magnitude as one would estimate Lancaster's shrouded nonstationary data for a single chamber CFR engine (1976).

b) Preexponential constant

Equation IV.4 is used as the chemical kinetic model. The correlation with both the part throttle and the wide open throttle data gives β a value of 2 for the correction of pressure. By using the final turbulence diffusivity model and the chemical kinetic model, the preexponential constant has a value of $6.3 \times 10^{-17} in^3/lbm\ sec$ to give the optimum burning rate for all the basic runs.

c) Mixing percentage

The three-mixing zones model is used. Fifty percent mixing in the main chamber at the spark time is arbitrarily assumed.

d) Heat transfer

During the course of correlation, it was found that: (1) the calculated NO is much lower than the data, (2) the calculated burning rate during the expansion period is too slow compared to the data. Three modifications have been investigated:

(1) using mean gas temperature instead of local gas temperature in the equation IV.5.

It was found that the heat loss through this calculation is less than before. This method of application is more consistent with the original development of Woschni's

equation. The value of NO production is increased by a value of approximately 70% by this modification.

(2) assuming adiabatic condition for the main chamber lean zone.

It is assumed that the slow burning rate at the expansion period may be due to the over-estimated heat transfer rate during that time. Some evidence for this may be seen by comparing predicted heat transfer rates with those measured by Oberbye, et al., (1961). The adiabatic condition is assumed for the main chamber lean zone only. The correlation of both the pressure time history and NO production is improved over the original version.

(3) assuming fifty percent of the heat transfer calculated from the Woschni's equation as used in version (1).

It is felt that the heat transfer calculated from the Woschni's equation is overestimated, since his model was developed from the diesel engine data. Thirty to forty percent of the heat is transferred by radiation in a diesel engine (Ebersole, et al., 1963) which is not the case for the SI engine. Fifty percent of the heat transfer calculation from the Woschni's equation is chosen for the investigation. Again the correlation of both the pressure time history and NO production are improved.

For consistency of both the physical model which has heat transfer throughout the chamber and Woschni's model, the modification of version (3) is used for the final heat transfer model.

CHAPTER V

RESULTS

The experimental work was done on a single cylinder Briggs and Stratton overhead valve engine by Mr. Kenneth W. Grandys (1977) in the IC engine laboratory of the University of Illinois at Urbana-Champaign. Premixed propane and air were supplied to the prechamber, and premixed isooctane and air were supplied to the main chamber. The experiments were conducted at a constant engine speed of 2100 rpm and at either a partial throttle volumetric efficiency of 46% or an open throttle volumetric efficiency of 77%. Two nozzle sizes were studied: orifice diameter of 0.332 inches, and 0.437 inches. The prechamber volume included the volume within the 0.548 inch long nozzle. Three groups of prechamber air-fuel ratios and mass flow ratios were selected for the engine tests. Group A had a nominal prechamber air-fuel ratio of 7, and a prechamber mass flow ratio of 10%. Group B had a nominal prechamber air-fuel ratio of 4, and a prechamber mass flow ratio of 10%. Group C had a reduced prechamber mass flow ratio of 5%, and prechamber air-fuel ratio of 4. The operating conditions are listed in Table 1.

The pressure data was monitored by a Kistler model 602H pressure transducer in each chamber. The pressure signals and crank angle information from a magnetic pickup were displayed on an oscilloscope. The pressure-time data for each condition was recorded on a Polaroid oscilloscope camera. Since the pressure-time diagram indicates

Table 1. Operating Conditions Of Prechamber Engine

speed		2100 rpm
displacement		32.4 in^3
compression ratio		7.98
spark timing		10 - 31° BTC
coolant temperature		110° - 138°F (120°)
volumetric efficiency	part throttle	44.0 - 48.0 (45.8)
	open throttle	75.2 - 78.5 (76.8)
AF_T		15.84 - 24.12
throat diameter	small	0.332 in
	large	0.437 in
A_{th}/V_p	small	0.15748 in^{-1}
	large	0.25400 in^{-1}
V_p/V_c	small	11.9%
	large	12.7%

Note: Average range values shown in parentheses.

both the power output and combustion rate, this will be the basic data for the comparison.

The NO concentration was measured by a Beckman 315-A NDIR detector in terms of parts per million (ppm). For the comparison with the calculation results, the mass of NO formed per mass of fuel supplied to the engine was calculated:

$$NO = 1.44 \times 10^{-3} \frac{INO \times IHP}{\dot{m}_T \times \frac{FA}{1 + FA}} \qquad [Gm\ NO/gm\ fuel] \qquad (V.1)$$

where INO = indicated nitric oxide [gm/hp-hr]

IHP = indicated horsepower [hp]

The experimental data were recorded in Grandys' thesis (1977).

A. Typical Results

A typical printout of the constant parameters for a condition of large orifice with wide open throttle is given in Table 2.

1. Pressure-Time Diagram

A typical calculated pressure-time diagram for a condition of large orifice at wide open throttle is illustrated in Figure 21. The agreement between the calculated result and the experimental data is excellent.

2. Temperature Profile

The calculated temperature profile as a function of distance and time appears in Figure 22. The ignition process can be seen as a temperature spike in the prechamber at 10 BTC. The flame propagating

Table 2. Constant Parameter of Simulation Model

***** DUAL CHAMBER COMBUSTION MODEL PARAMETERS *****

***** GEOMETRICAL PARAMETERS *****

VPDVC =	12.6171	%	ATH*BORE/VP =	0.9047		VD =	32.4000	CBIN
VP =	0.5905	CBIN	VM =	4.0896	CBIN	VC =	4.6801	CBIN
AP =	0.3266	SQIN	ATH =	0.1500	SQIN	APS =	9.9650	SQIN
DIAP =	0.6448	IN	DIAT =	0.4370	IN	BORE =	3.5620	IN
XLC =	5.4800	IN	XLR =	6.4400	IN	S =	3.2514	IN
XCI =	1.3700	IN	XLO =	0.5480	IN	XOO =	1.9180	IN
CLL =	0.4037	IN	CLR =	0.0067	IN	CL =	0.4104	IN
CR =	7.9229							

***** OPERATIONAL PARAMETERS *****

FR =	9.3800	%	TIMSC =	10.0000	BTC	RPM =	2100.0000	
XSP =	0.5480	IN	AP ST =	14.2920		SM10 =	6.35569D-05	LBM
TSH =	4192.4881	R	TW =	900.0000	R	SMTO =	1.20433D-03	LBM
FP =	0.0088		FM =	0.0612		FT =	0.0700	
PHIP =	3.5259		PHIM =	0.6056		PHIT =	0.8343	
PHOP =	3.5259		PHOM2 =	0.9492		PHOM1	0.6056	
PHSP =	1.2516		PHSM2 =	0.9492		PHSM1 =	0.6056	
US P.C. =	0.0	IN/SEC	US M.C. =	0.0	IN/SEC			
PS P.C. =	180.0000	PSI	PS M.C. =	180.0000	PSI			
TS P.C. =	1161.7806	R	TS M.C. =	1161.7806	R			

***** COMBUSTION PARAMETERS *****

RR =	642.63	LBF-IN/LBM-R	EDR =	27193.00 R
Z =	6.30000D 17	CBIN/LBM-SEC	GR =	386.00 LBM-IN/LBF-SQSEC
HR =	1.71785D 08	LBF-IN/LBM	AMW =	28.85 LBM/LBMOLE
K4 =	50	%	CS =	4.0403D-01

***** NUMERICAL PARAMETERS *****

N =	81		NP =	29		NM =	52	
NOI =	21		NTH =	25		NOO =	29	
M2 =	47		POM2 =	53.8835	%	PSM2 =	48.5239	%
EPC =	70.00	%	EMIN =	1.00000D-06		TPC =	1.00	%
DLTMAX =	1.50000D-06	SEC	DLTMIN =	1.00000D-07	SEC	DELX =	6.85000D-02	IN

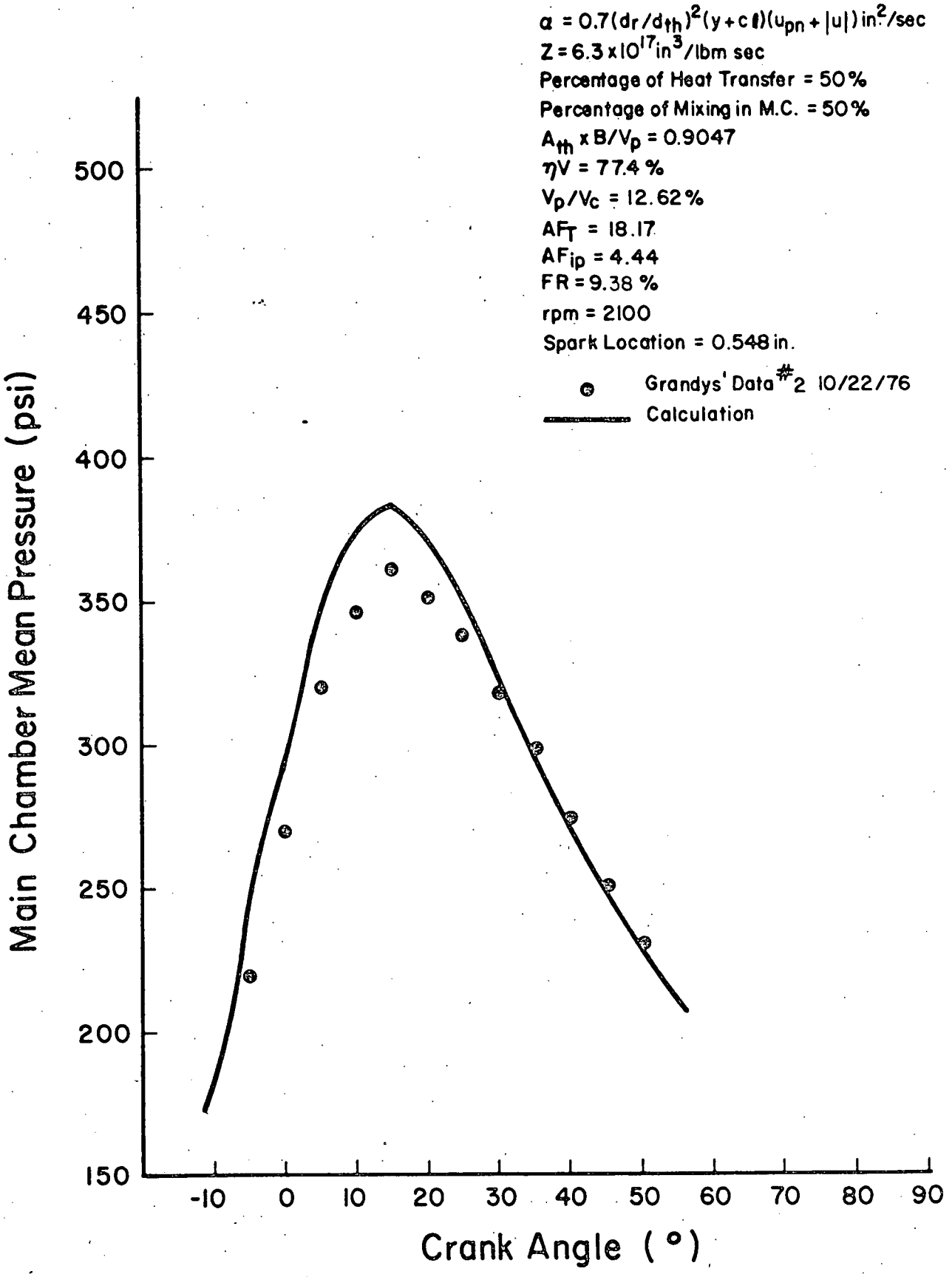

Figure 21. Typical Pressure-Time Diagram

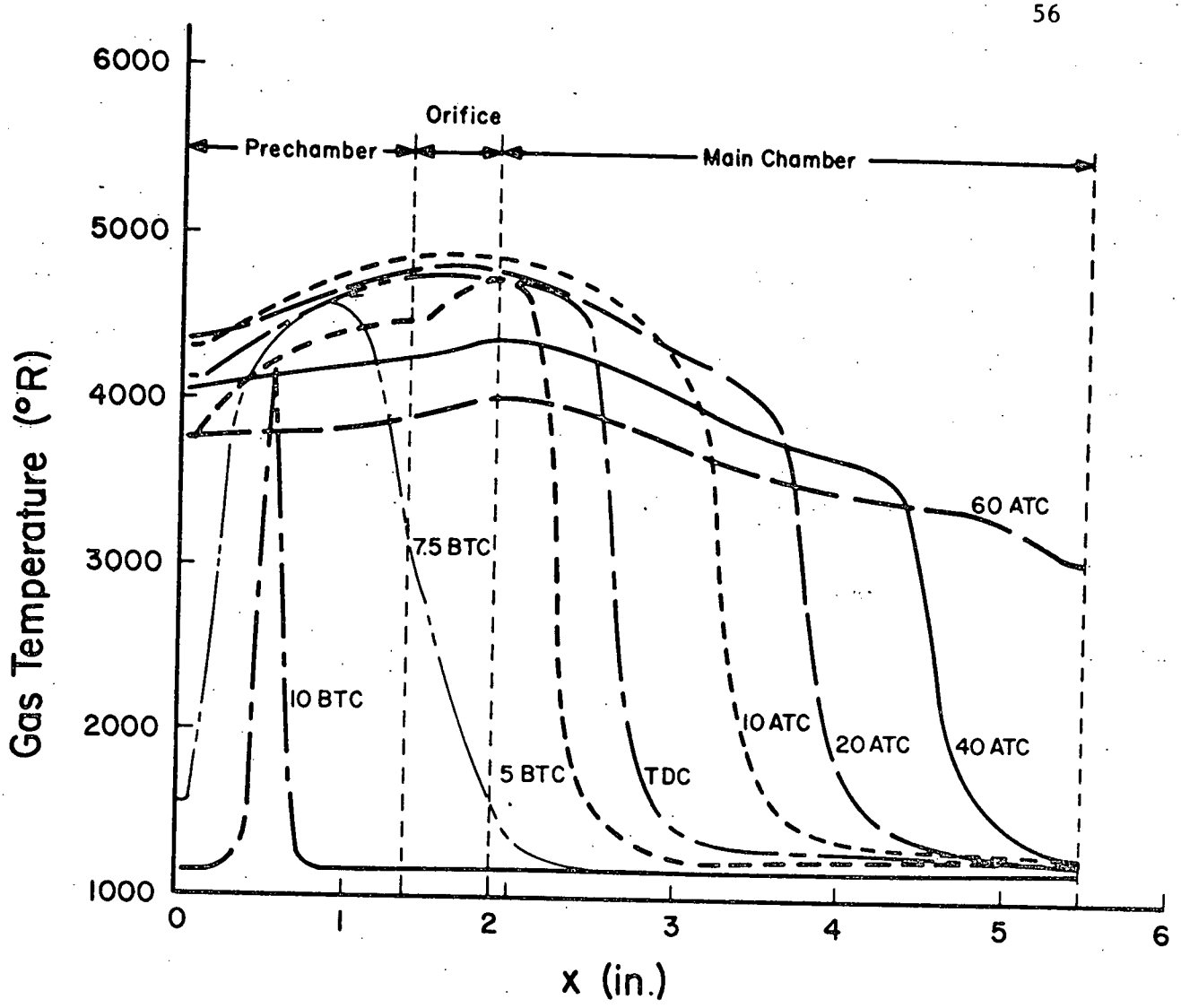

$\alpha = 0.7(d_r/d_{th})^2(y + c\ell)(u_{pn} + |u|)\ in^2/sec$
$Z = 6.3 \times 10^{17}\ in^3/lbm\ sec$
Percentage of Heat Transfer = 50%
Percentage of Mixing in M.C. = 50%
$A_{th} \times B/V_p = 0.9047$
$\eta V = 77.4\ \%$
$V_p/V_c = 12.62\ \%$
$AF_T = 18.17$
$AF_{ip} = 4.44$
FR = 9.38 %
rpm = 2100
Spark Location = 0.548 in.

Figure 22. Typical Temperature Profile

initially in two directions can be seen at 7.5 BTC. The flame speed is accelerated until it passes through the orifice with maximum speed at 5 BTC, and then slows down in the main chamber. The peak temperature at the orifice exit is due to the stoichiometric combustion condition. The drop in temperature at 60 ATC is due to both the expansion and the heat loss.

3. Velocity Profile

The calculated velocity profile as a function of distance and time is given in Figure 23. Comparing with Figure 22, flow out of the prechamber is observed when the flame is in the prechamber at 7.5 BTC, and reverse flow is observed when the flame is in the main chamber after 5 BTC. The flow becomes forward again at 40 ATC due to the expansion effect.

4. Equivalence Ratio Profile

Figure 24 gives the calculated equivalence ratio profile as a function of distance and time. Three-mixing zones at the spark time can be seen on this figure. The diffusion is observed in both directions. The stoichiometric condition in the intermediate zone in the main chamber is observed.

5. Fuel, Oxygen, and Product Mass Fraction Profile

Figure 25 gives the calculated mass fraction profile of fuel, oxygen, and product as a function of distance at two different times. The ignition profiles for the species can be seen clearly at 10 BTC.

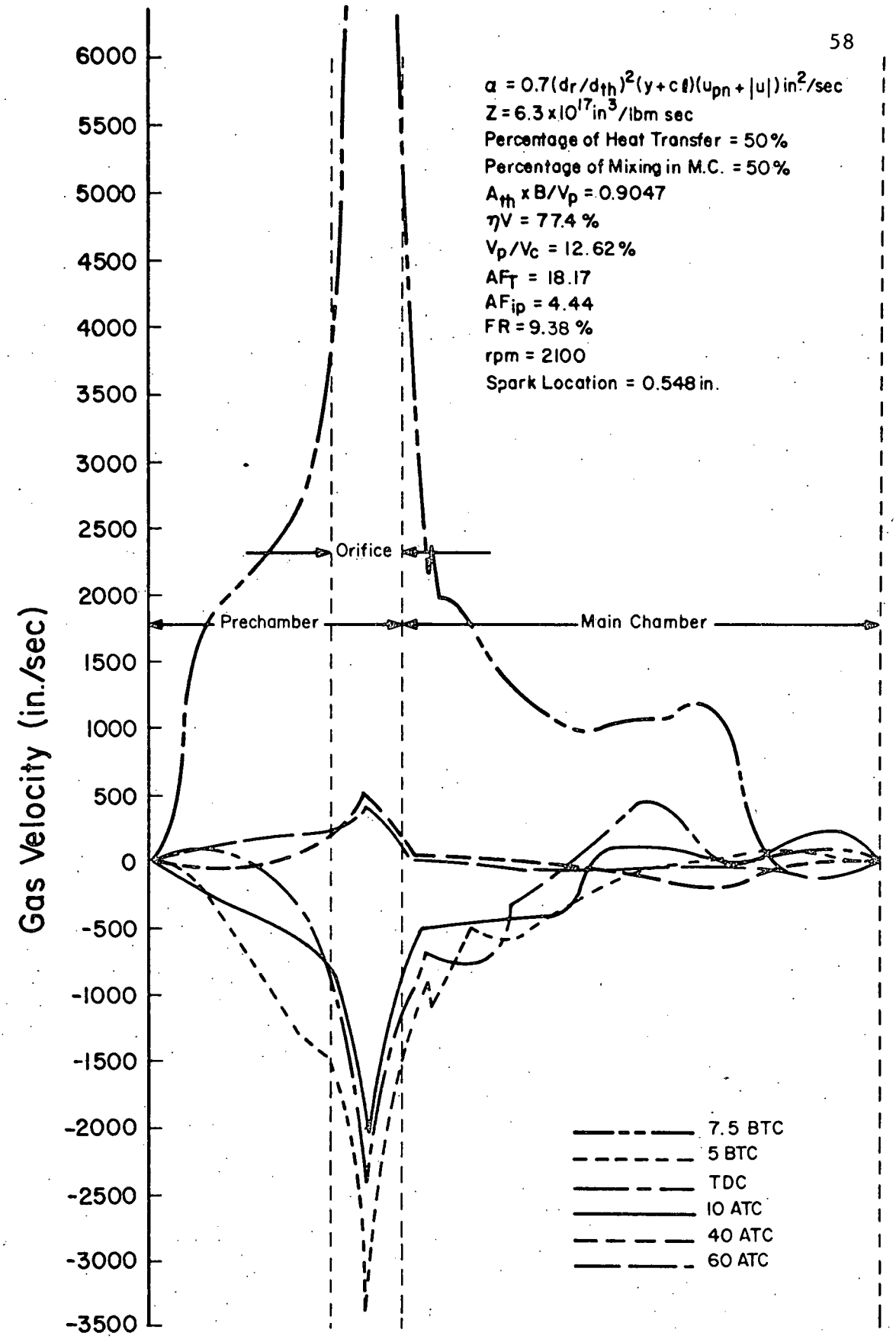

Figure 23. Typical Velocity Profile

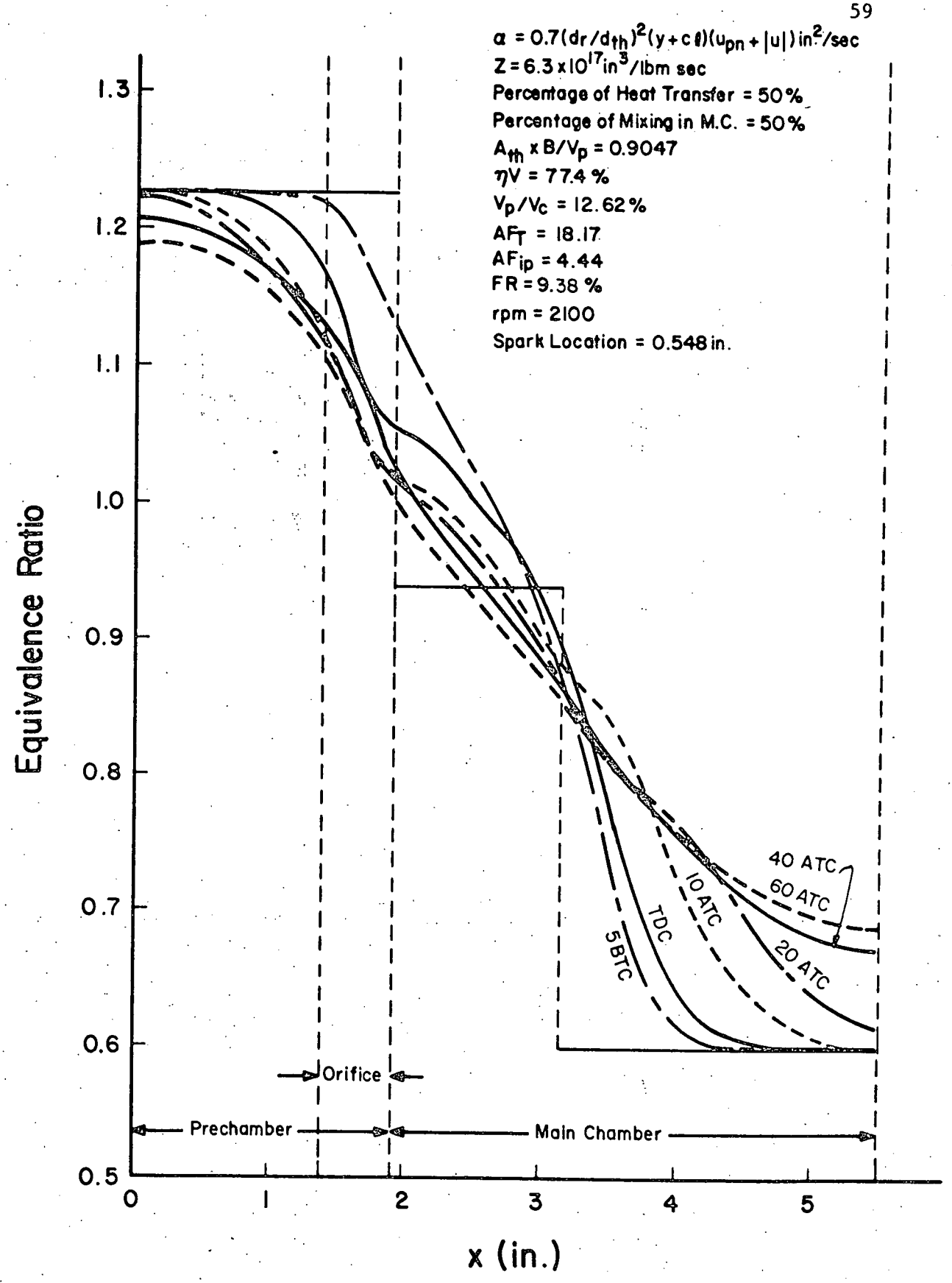

Figure 24. Typical Equivalence Ratio Profile

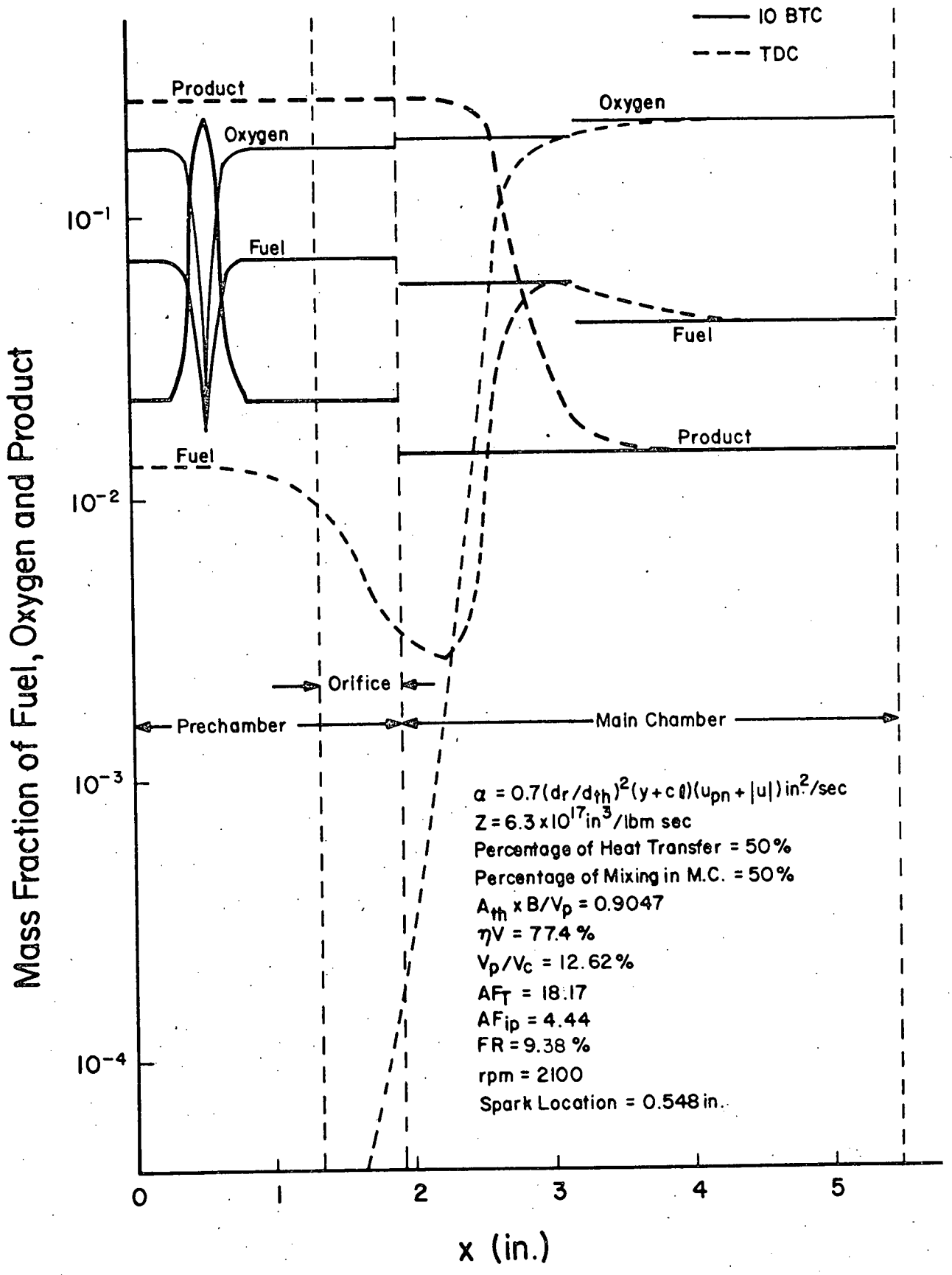

Figure 25. Typical Mass Fraction Profiles of Fuel, Oxygen, And Product

At TDC, the oxygen is almost consumed in the prechamber; some fuel is consumed in the combustion zone and some fuel remains unburned in both prechamber and the main chamber. The burned and unburned zones can be easily divided by the product profile at TDC.

6. Nitric Oxide Mass Fraction Profile

The calculated mass fraction of NO profile as a function of distance and time is illustrated in Figure 26. By comparing with Figure 24, converting the spatial scale to the equivalence ratio scale, the standard bell shape of the NO formation is clearly shown and the peaks occur for equivalence ratios slightly leaner than the stoichiometric. The main contribution of NO is in the intermediate mixing zone. The expansion effect is observed at 60 ATC.

B. Parameter Study

Table 3 lists the conditions of all the simulation runs for the parameter study. The number one run was chosen as the baseline run.

1. Total Air-Fuel Ratio

The effect of AF_T on pressure time history is given in Figure 27. When AF_T increases, the power output decreases. The spark timing needs to be advanced in order to give a similar power output when the overall leaner mixture is burned. The effect of AF_T on NO production is shown in Figure 28. Both the experiment and the calculation illustrate the trend of a reduction in the NO production when the overall air-fuel ratio increases. The magnitude of change correlates well

Table 3. Initial Conditions For Parameter Study

No.	$A_{th} \times B/V_p$	ηv (%)	$\dot{m}t$ (lbm/hr)	AF_T	AF_{ip}	FR (%)	θs (°CA BTC)	θid (°CA)	θo (°CA BTC)	Po (psi)	Data Date
1	.5609	45	40.168	17.78	4.24	9.39	15	4	11	120	#3 9/27/76
2	.5609	77	69.571	17.45	4.47	9.59	10	5	5	200	#3 10/13/76
3	.9047	45	40.913	19.41	4.31	9.34	24	9	15	115	#2 10/18/76
4	.9047	77	70.778	18.17	4.44	9.38	27	17	10	180	#2 10/22/76
5	.5609	45	39.935	20.77	4.30	9.42	20	7.5	12.5	120	#3 9/22/76
6	.5609	46	40.918	23.66	4.31	9.34	27	9.5	17.5	115	#3 9/17/76
7	.5609	45	40.196	17.81	4.34	9.43	13	3	10	120	#4 9/27/76
8	.5609	45	40.809	21.21	4.37	9.34	20	7.5	12.5	125	#5 9/17/76
9	.5609	45	40.820	21.08	4.37	9.33	26	8.5	17.5	115	#6 9/17/76
10	.5609	45	40.820	21.08	4.37	9.33	15	7.5	7.5	130	#7 9/17/76
11	.5609	45	40.110	20.10	7.28	9.50	15	12.5	2.5	130	#2 10/3/76
12	.5609	45	39.996	20.10	4.30	9.40	17	4.5	12.5	115	#6 9/22/76
13	.5609	45	42.652	20.08	4.36	4.90	23	8	15	120	#7 9/27/76
14	.9047	75	68.152	19.53	7.01	9.64	28	18	10	195	#1 10/25/76
15	.9047	76	70.174	19.76	4.44	9.46	30	20	10	195	#3 10/22/76
16	.9047	77	68.532	19.78	4.44	4.92	30	25	5	200	#6 10/20/76

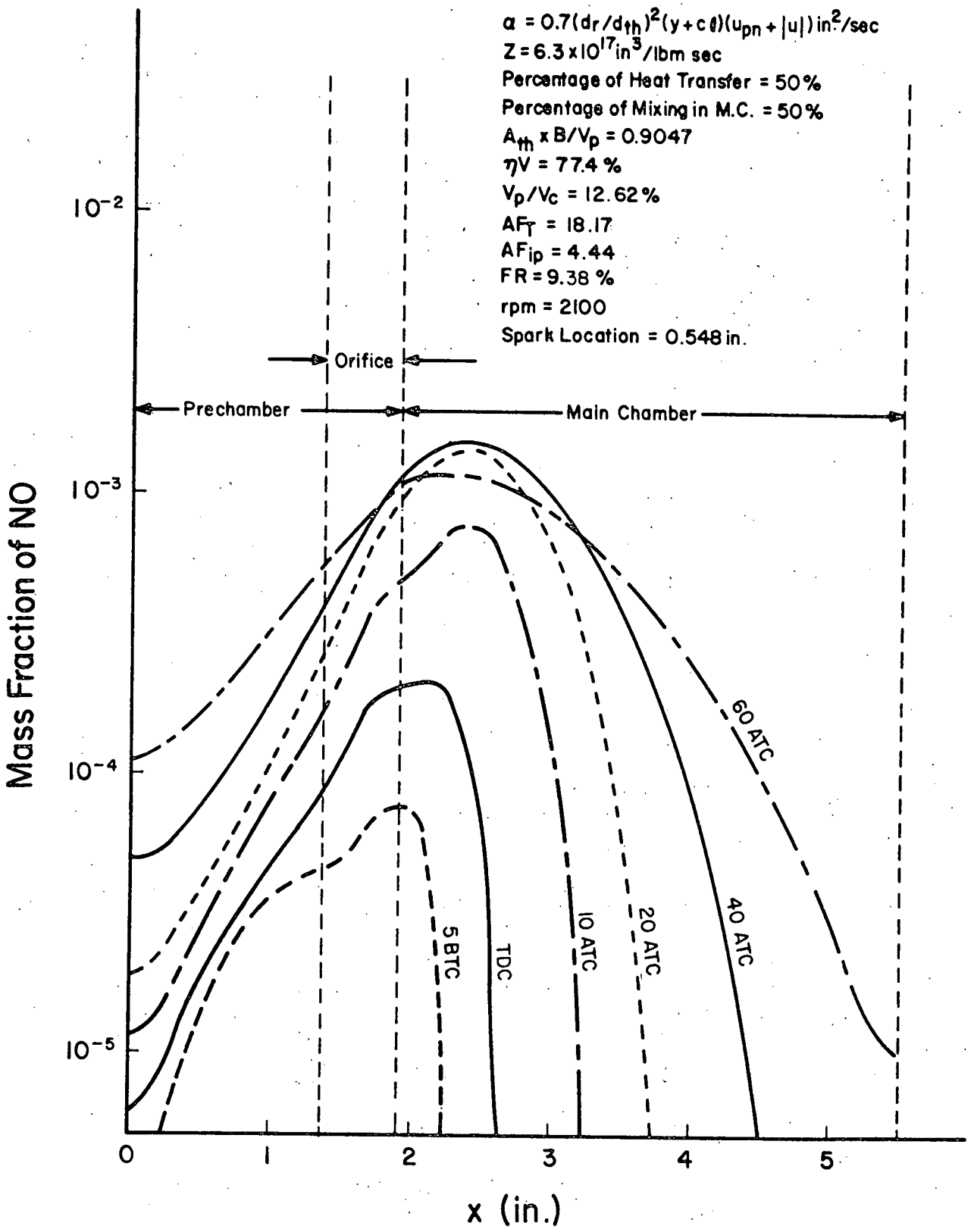

Figure 26. Typical Mass Fraction Profile Of NO Formation

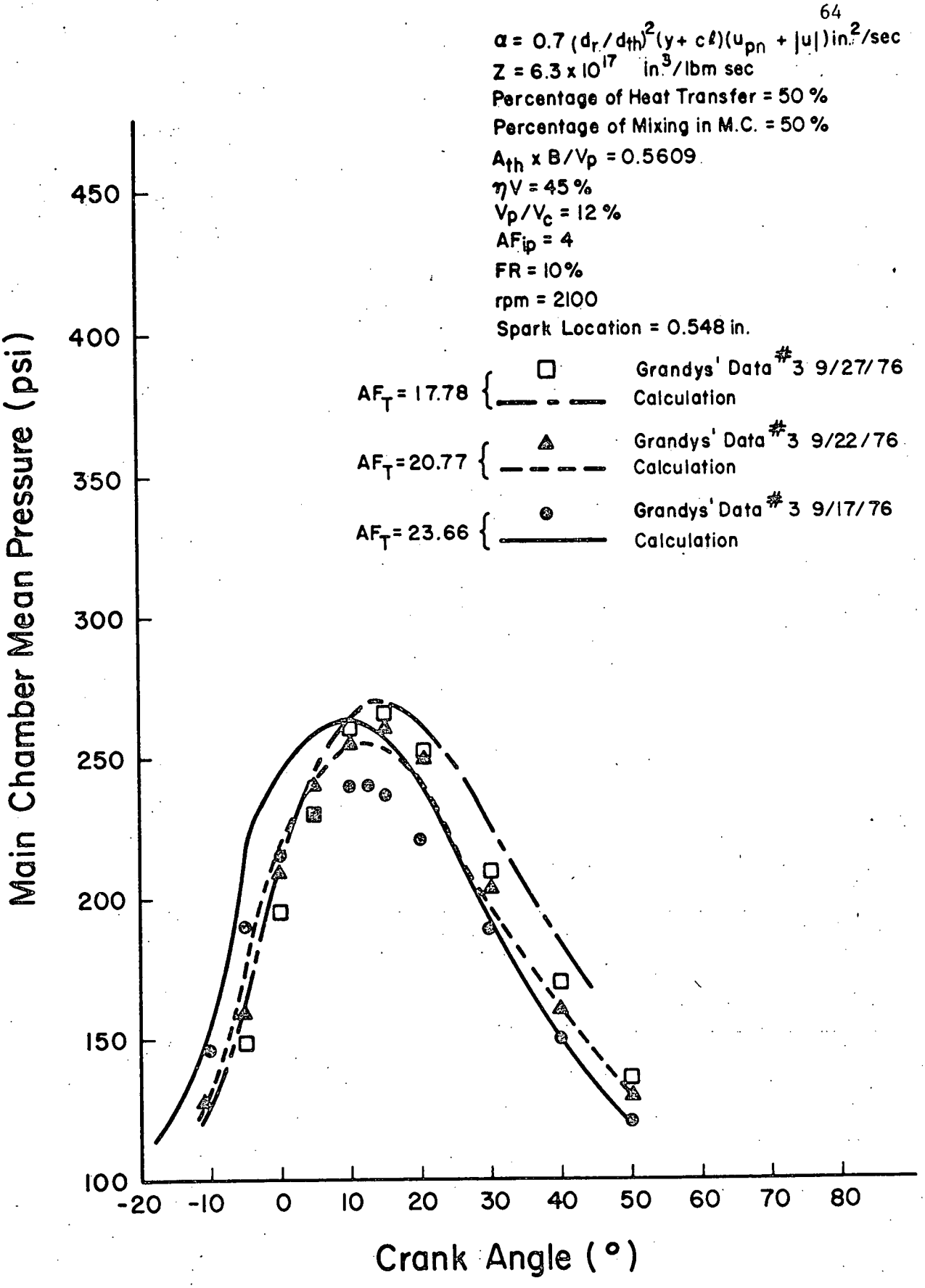

Figure 27. Effect Of AF_T On Pressure Time History

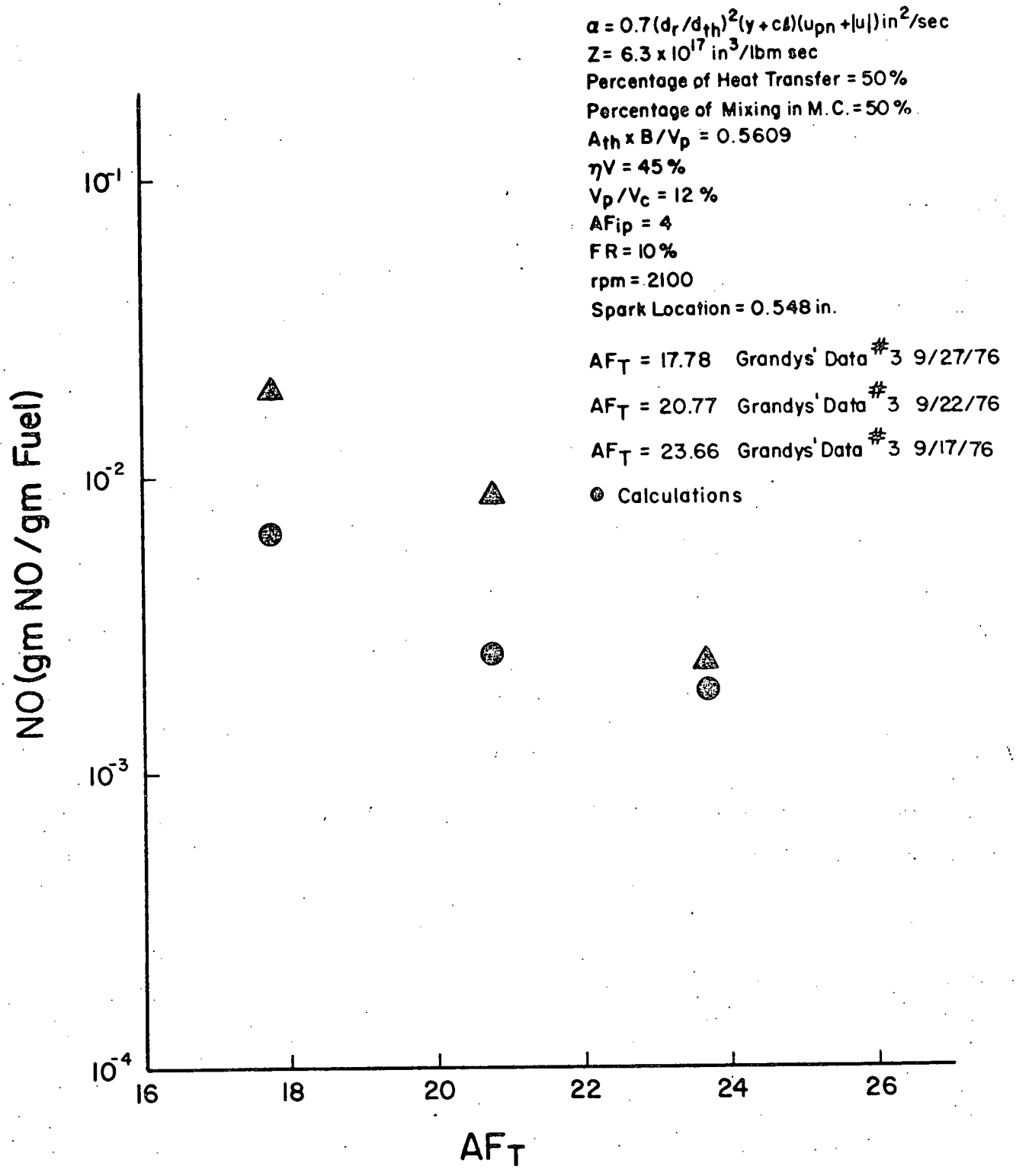

Figure 28. Effect Of AF_T On NO Production

for AF_T of 17.78 and 20.77. This correlation is changed at the AF_T of 23.66. The effect of AF_T on combustion duration is shown in Figure 29. This agrees with the expected trend that the combustion rate is slower when a leaner mixture is burned.

2. Prechamber Intake Air Fuel Ratio And Mass Flow Ratio

The effect of prechamber intake air-fuel ratio and mass flow ratio with large orifice at wide open throttle on calculated pressure time history is shown in Figure 30. Both the experiment and calculation show that when either reducing the prechamber intake mixture strength or the prechamber intake mass flow ratio, the power output is decreased. The effect of this group parameter on calculated NO production correlates very well with the experimental data except the C group as illustrated in Figure 31. Both the data and the calculation have the trend of NO production in the order of group B, A, and C. Another set of the effect of prechamber fuel group parameter with a small orifice at part throttle on the calculated pressure time history and the NO production is shown in Figures 32 and 33 respectively. The correlation of NO production is not as good as the previous set. The trend of NO production in the order of B, C, and A agrees between the data and the calculation.

3. Volumetric Efficiency

The effect of volumetric efficiency on pressure time history is illustrated in Figure 34. This effect is simulated by the correction parameter on pressure in the chemical kinetic rate equation. The

$\alpha = 0.7(d_r/d_{th})^2(y+c_s)(u_{pn}+|u|)\ in^2/sec$
$Z = 6.3 \times 10^{17}\ in.^3/lbm\ sec$
Percentage of Heat Transfer = 50 %
Percentage of Mixing in M.C. = 50 %
$A_{th} \times B/V_p = 0.5609$
$\eta V = 45\%$
$V_p/V_c = 12\%$
AFip = 4
FR = 10 %
rpm = 2100
Spark Location = 0.548 in.

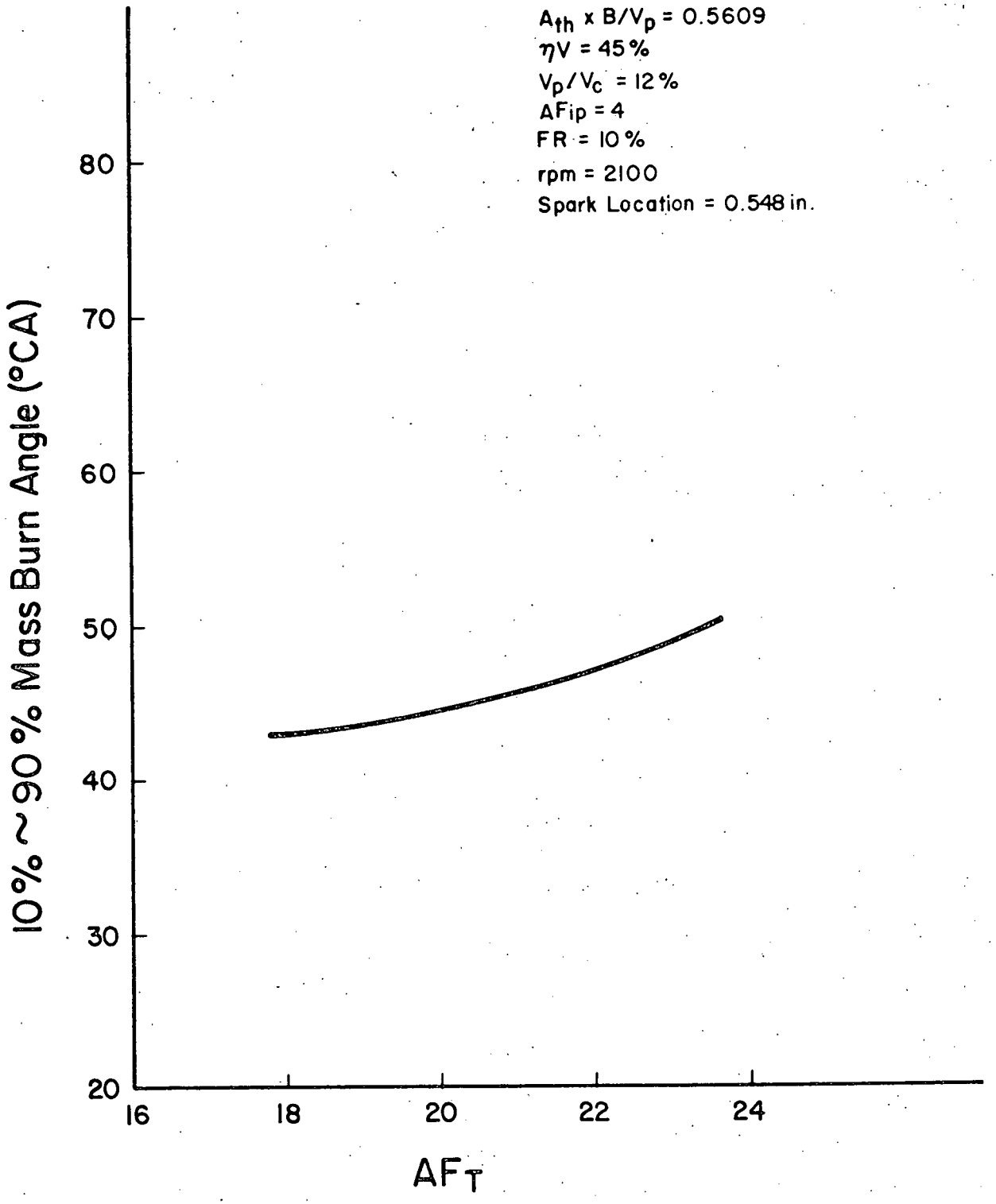

Figure 29. Effect Of AF_T On Combustion Duration

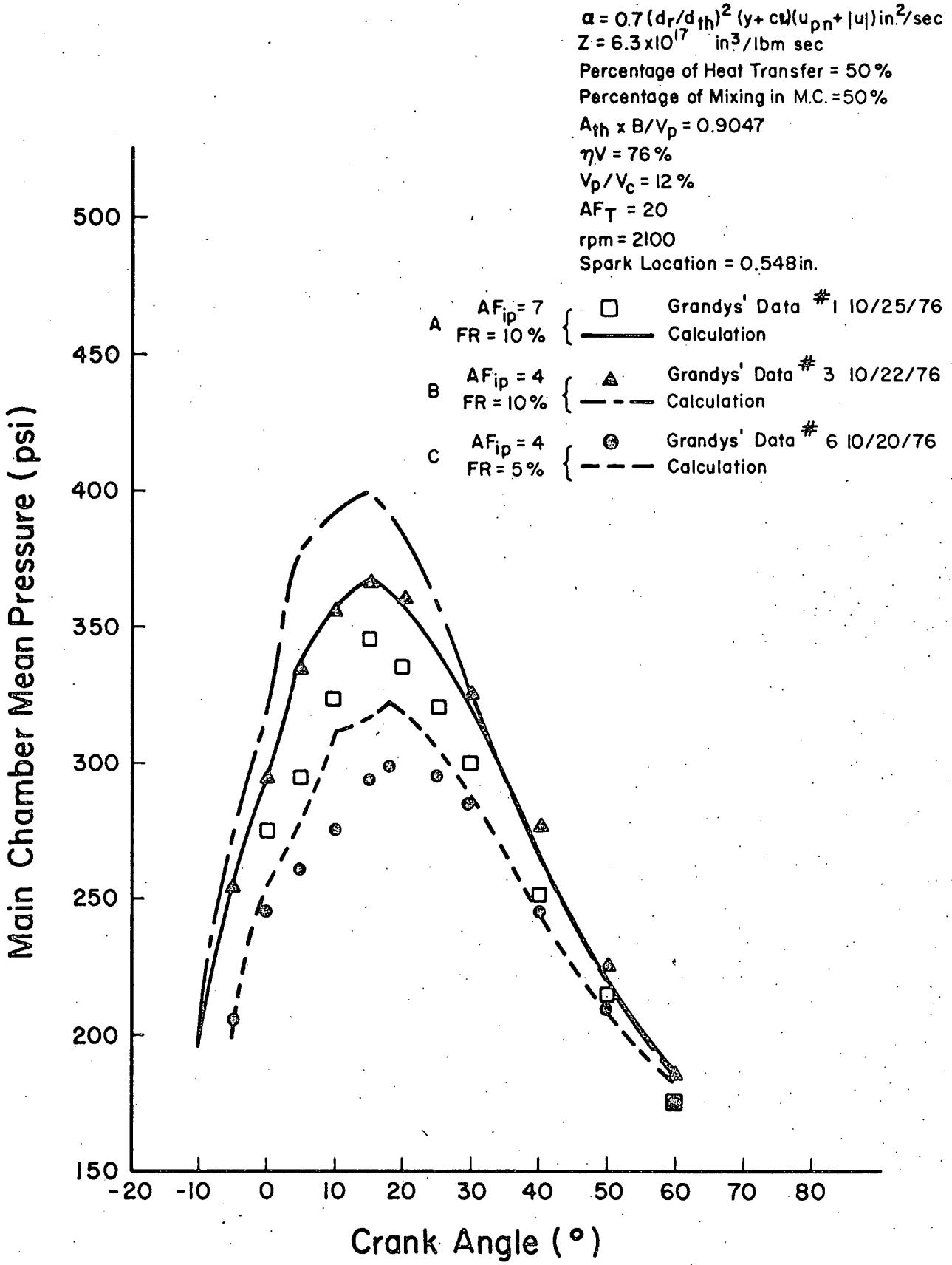

Figure 30. Effect Of Prechamber Fuel Group On Pressure Time History Of Large Orifice At Open Throttle

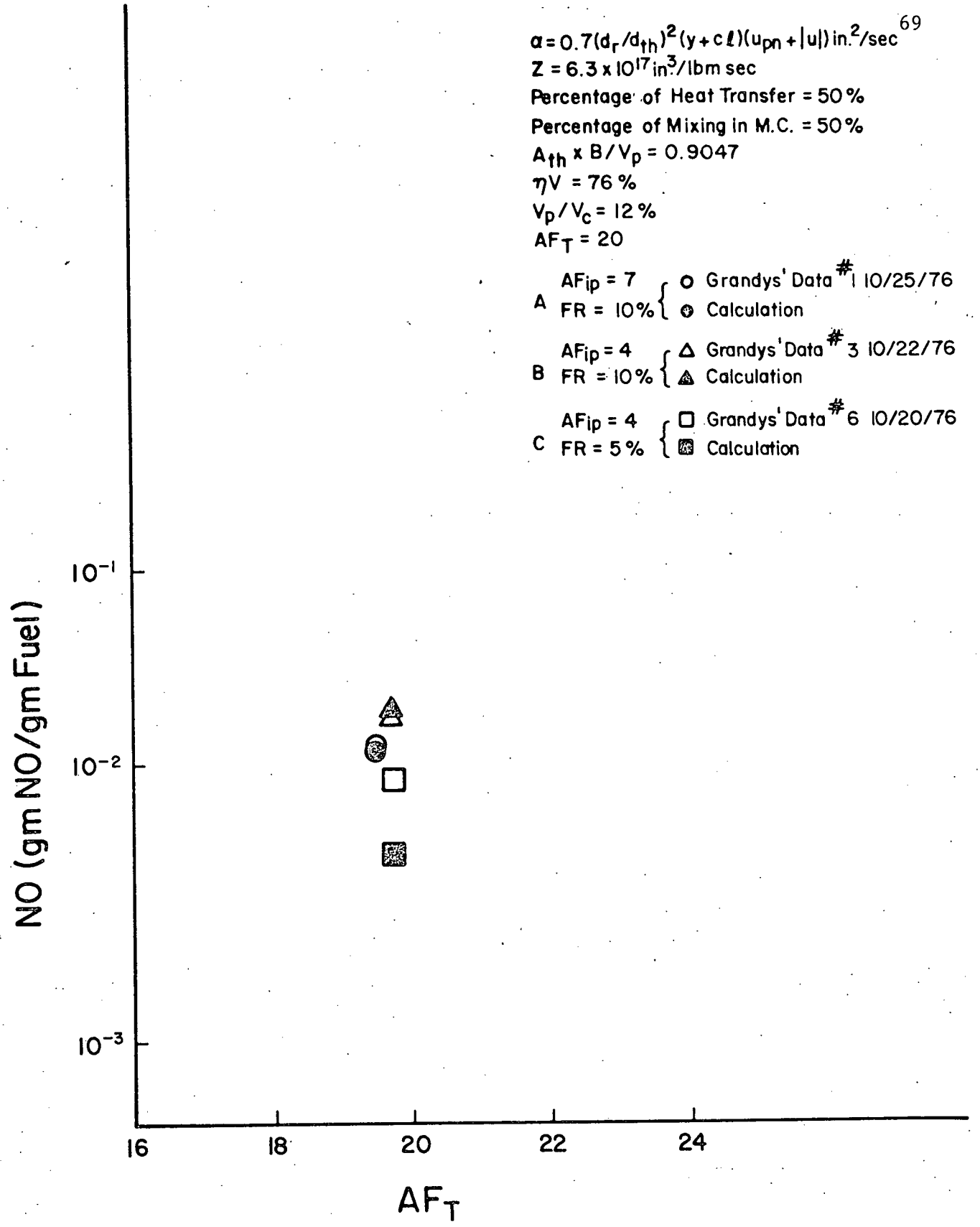

Figure 31. Effect Of Prechamber Fuel Group On NO Production Of Large Orifice At Open Throttle

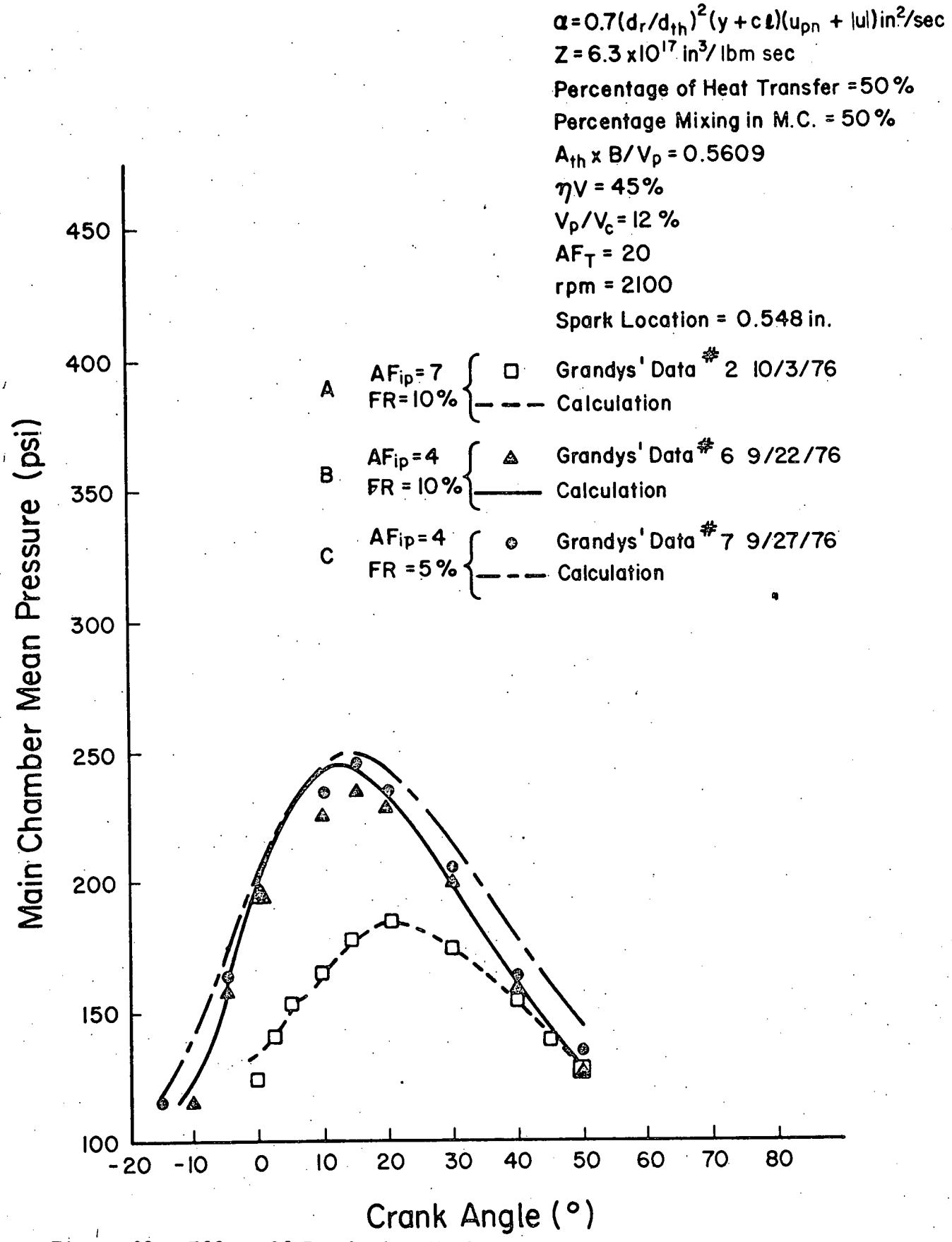

Figure 32. Effect Of Prechamber Fuel Group On Pressure Time History Of Small Orifice At Part Throttle

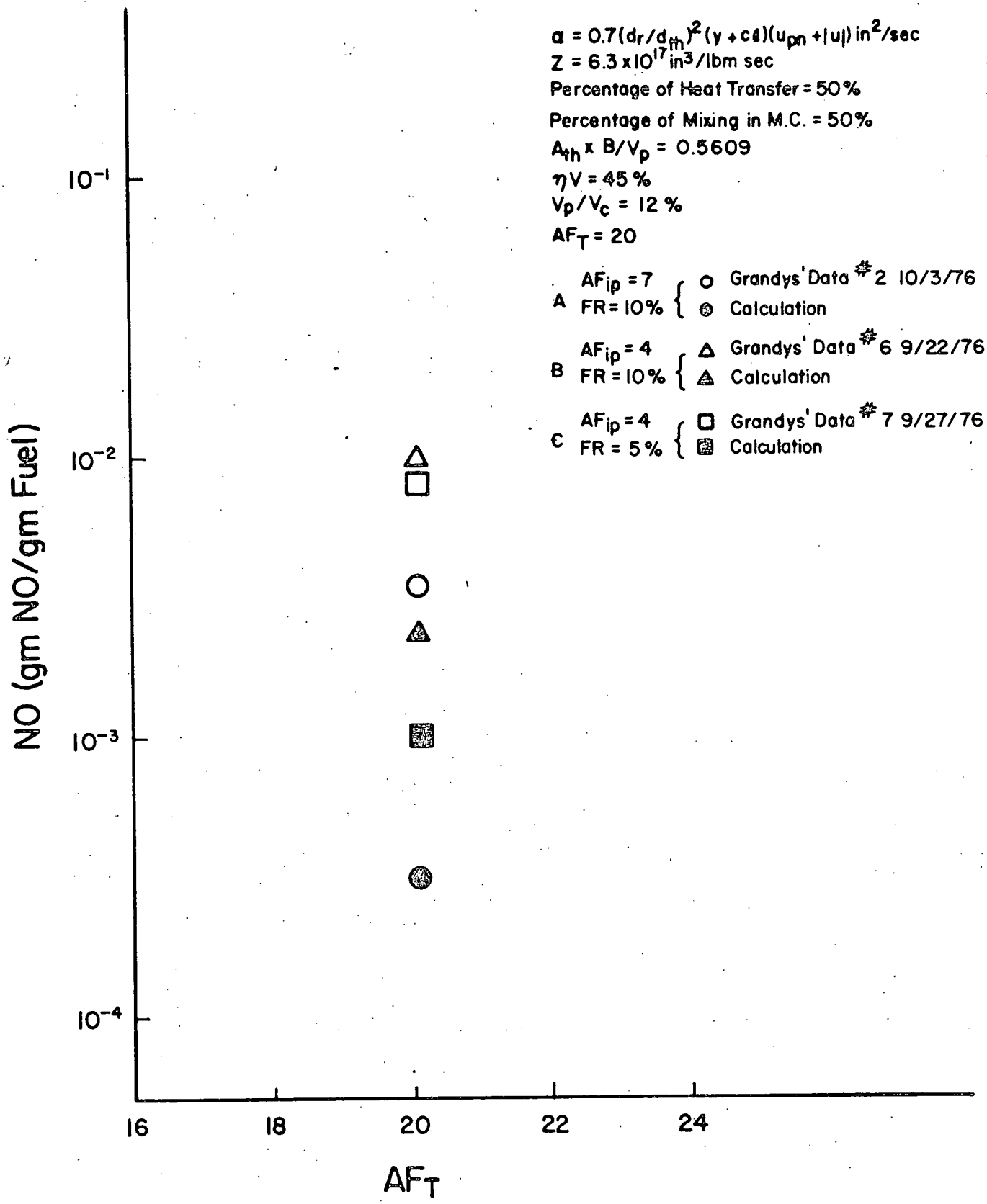

Figure 33. Effect Of Prechamber Fuel Group On NO Production Of Small Orifice At Part Throttle

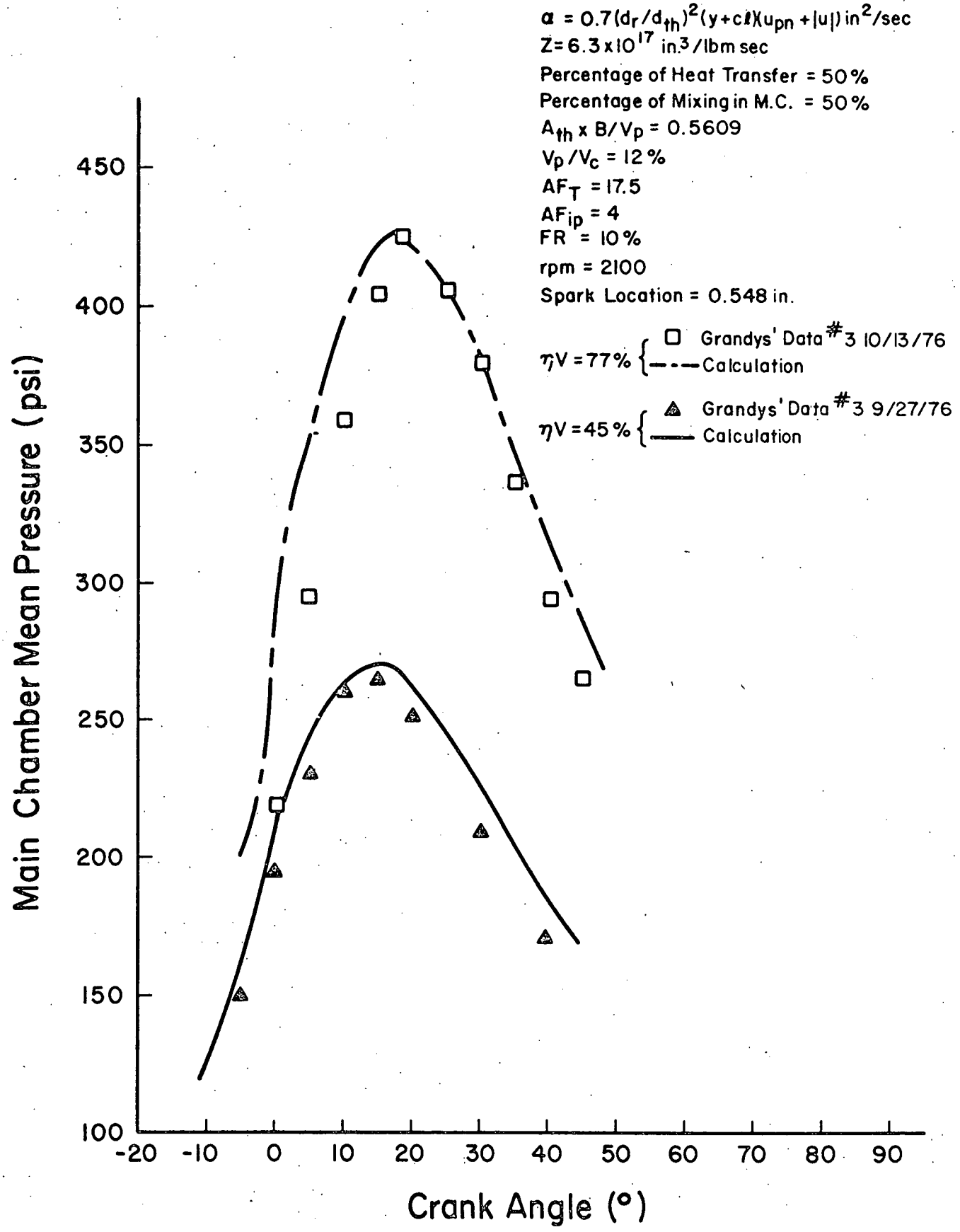

Figure 34. Effect Of Volumetric Efficiency On Pressure Time History

correlation between the calculation and the data is excellent. Figure 35 gives the effect of volumetric efficiency on NO production. Both the trend and the magnitude of change agree well between the calculation and the data.

4. Throat Diameter

Figure 36 illustrates the effect of the throat diameter on the pressure time history. A correction factor for the turbulence level due to the change of the throat diameter was built in the turbulent diffusivity model. The correlation between the calculation and the data for the effect of the throat diameter is good. The smaller the throat diameter, the stronger the flame jet from the prechamber, the higher the turbulence level, and the faster the burning rate. The effect of the throat diameter on the NO production at different AF_T is shown in Figure 37. Both trend and the magnitude of change agree between the calculation and the data.

5. Spark Timing

The effect of the spark timing on the calculated pressure time history is given in Figure 38. When the spark is advanced, the power increases; the spark retarded, the power decreases. Both the data and the calculation demonstrate this characteristic. The effect of spark timing on NO production is shown in Figure 39. The correlation between the calculation and the data is good. When advancing the spark, increasing the residence time at high temperature, it increases the NO production; retarding the spark, decreasing the residence time at high

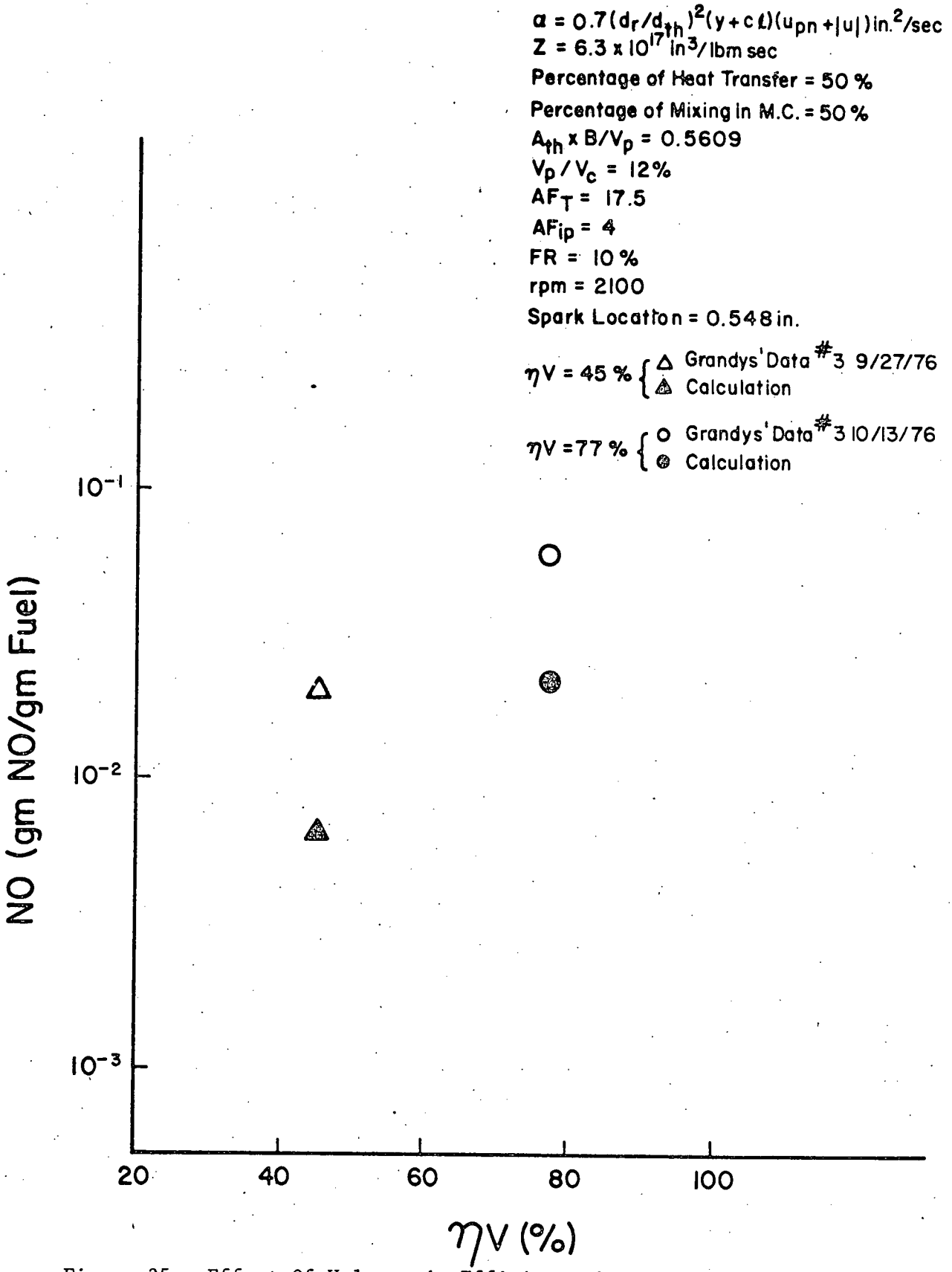

Figure 35. Effect Of Volumetric Efficiency On NO Production

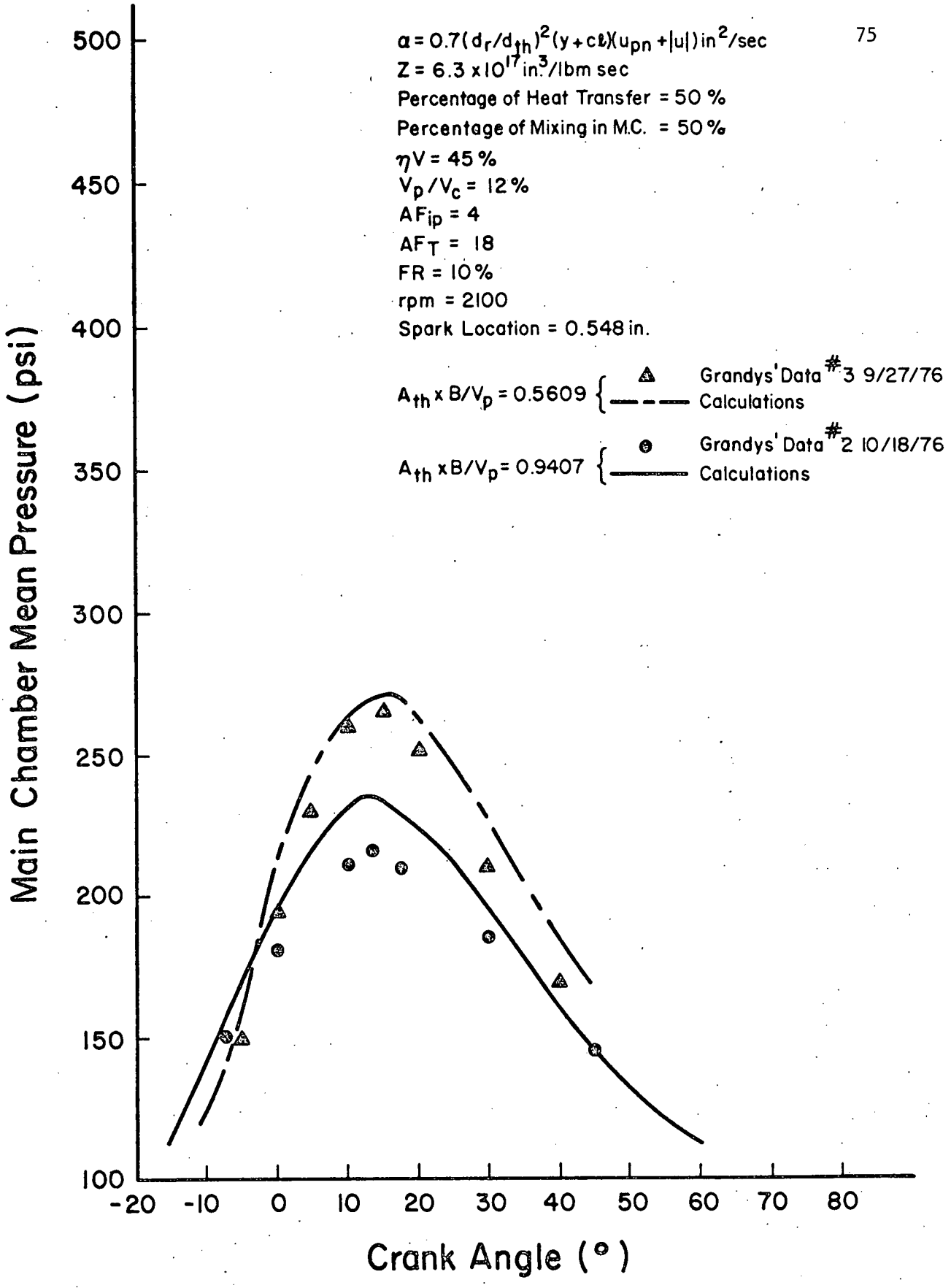

Figure 36. Effect Of Throat Diameter On Pressure Time History

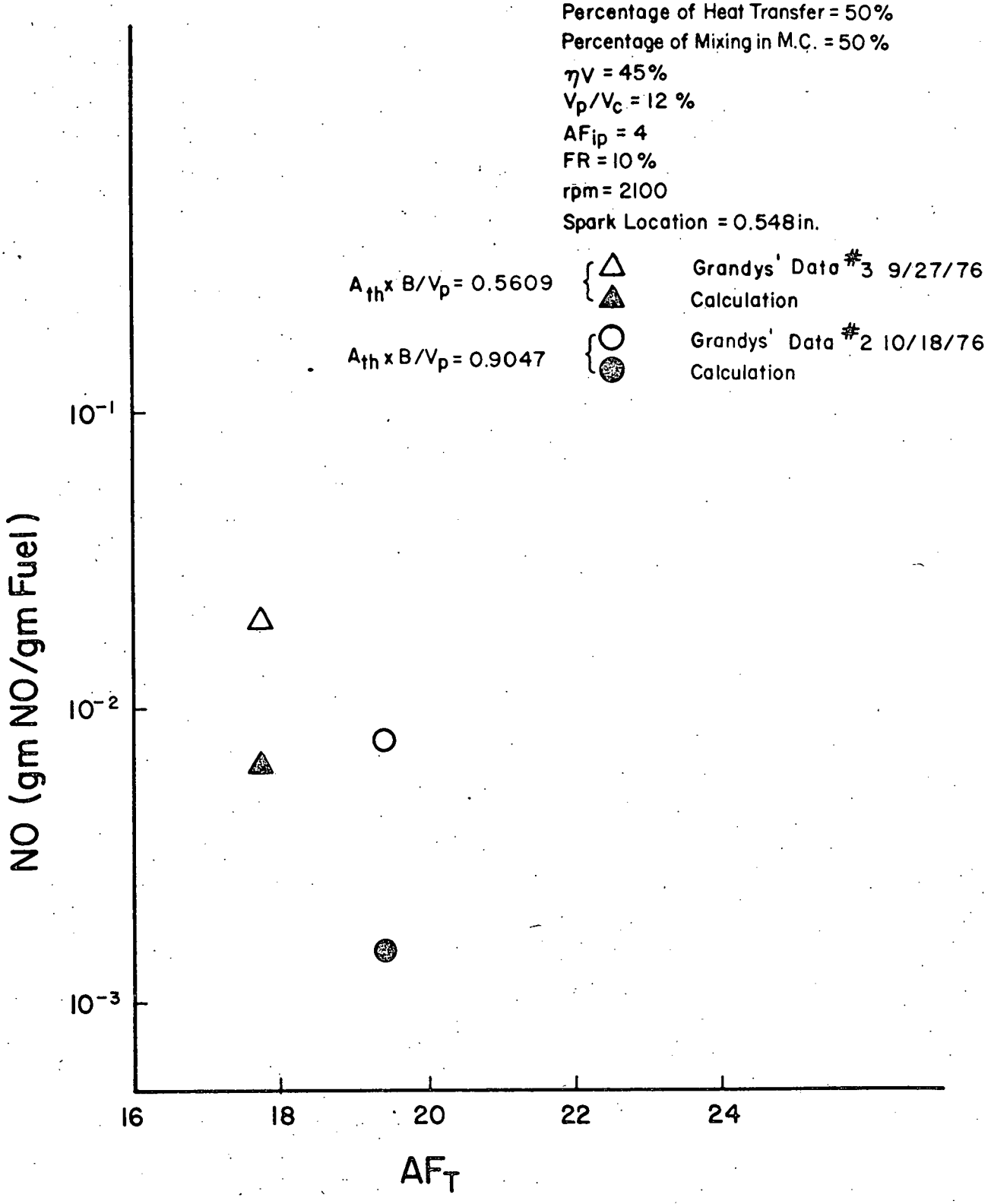

Figure 37. Effect Of Throat Diameter On NO Production

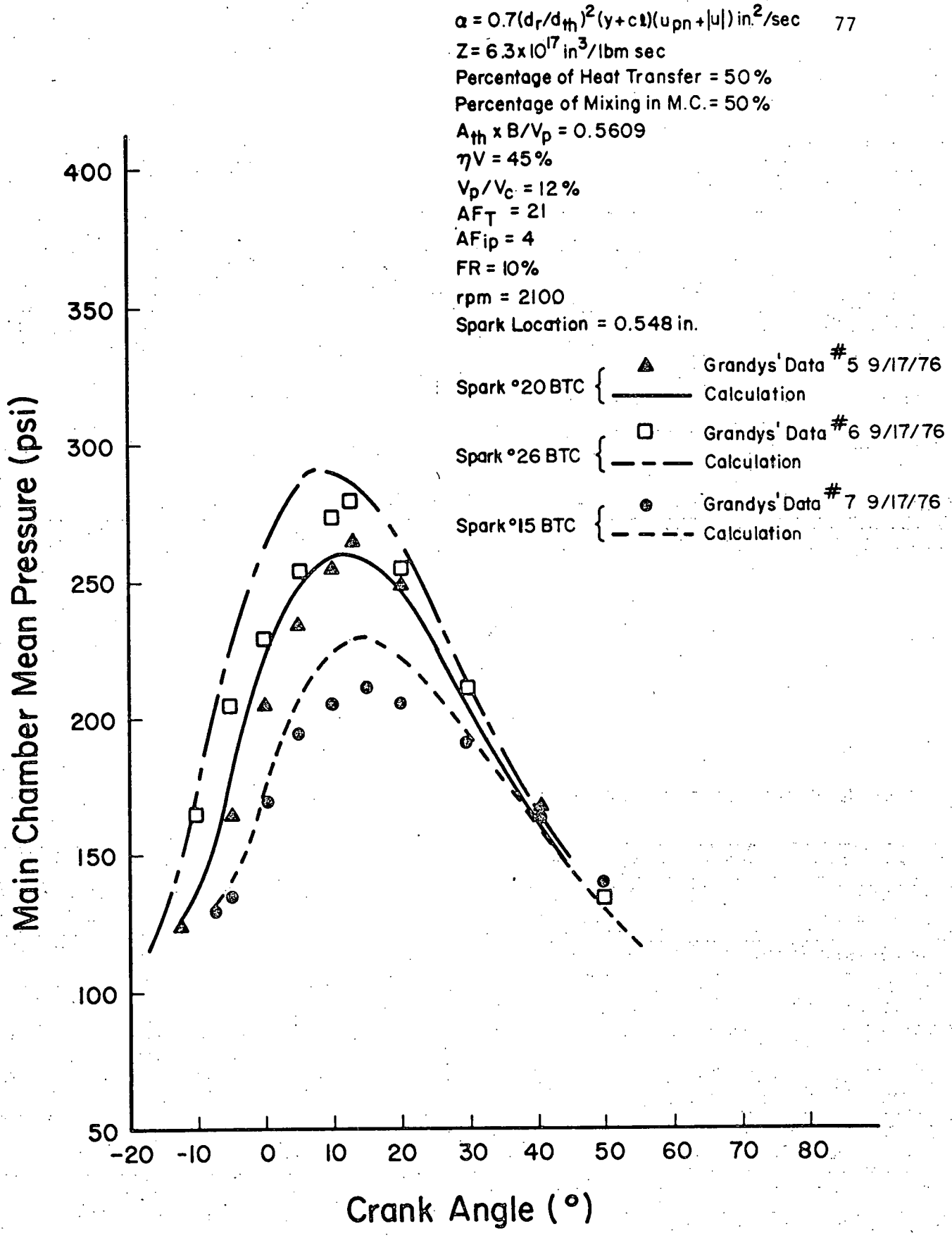

Figure 38. Effect Of Spark Timing On Pressure Time History

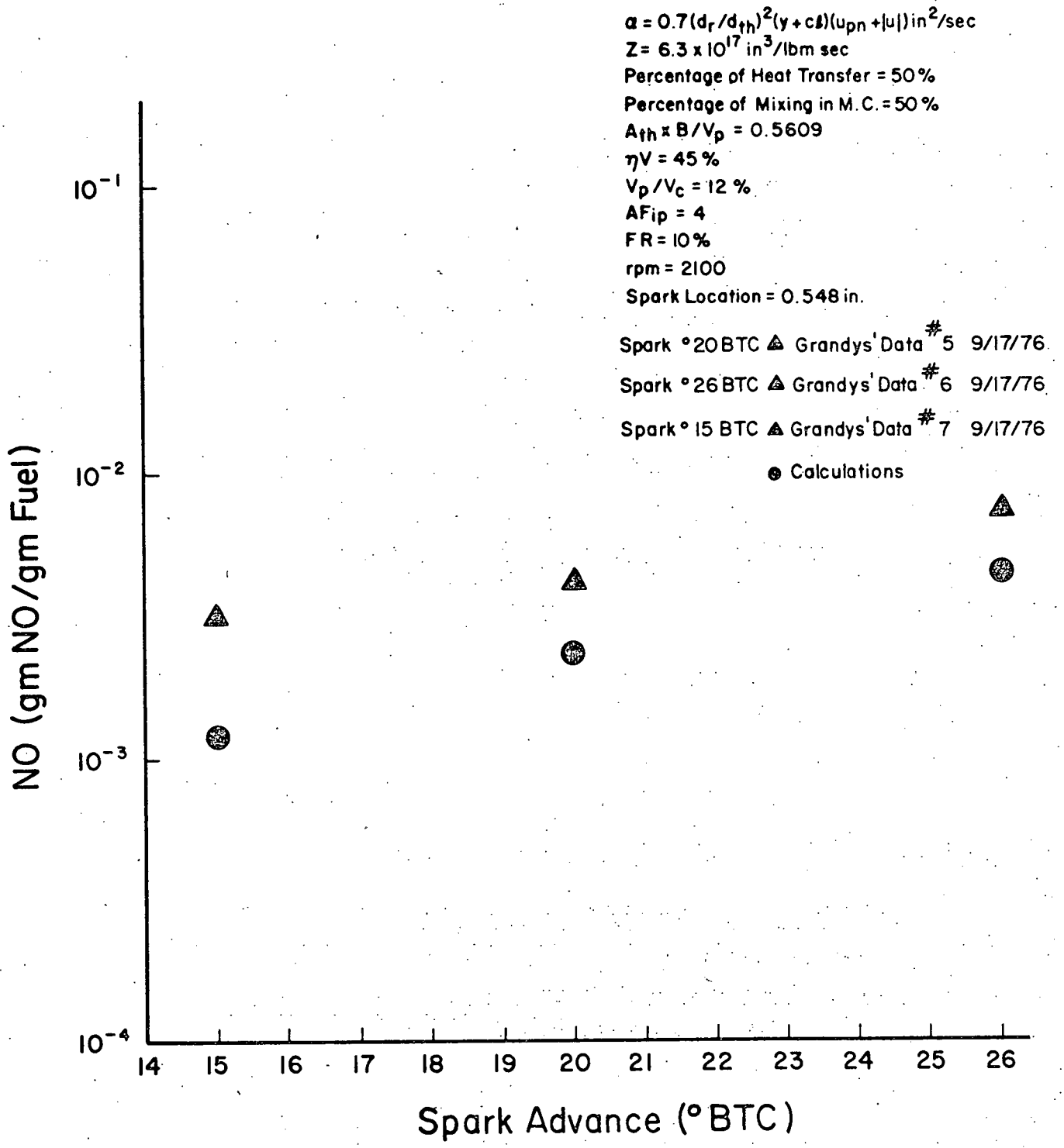

Figure 39. Effect Of Spark Timing On NO Production

temperature, it reduces the NO production. Figure 40 and Figure 41 also give the correlation between the calculation and the data for the pressure time history and the NO production at another set of conditions. One is the baseline run, the other has the spark retarded 2 crank angle degrees from the baseline. Table 3 gives the ignition delay estimated for the calculations.

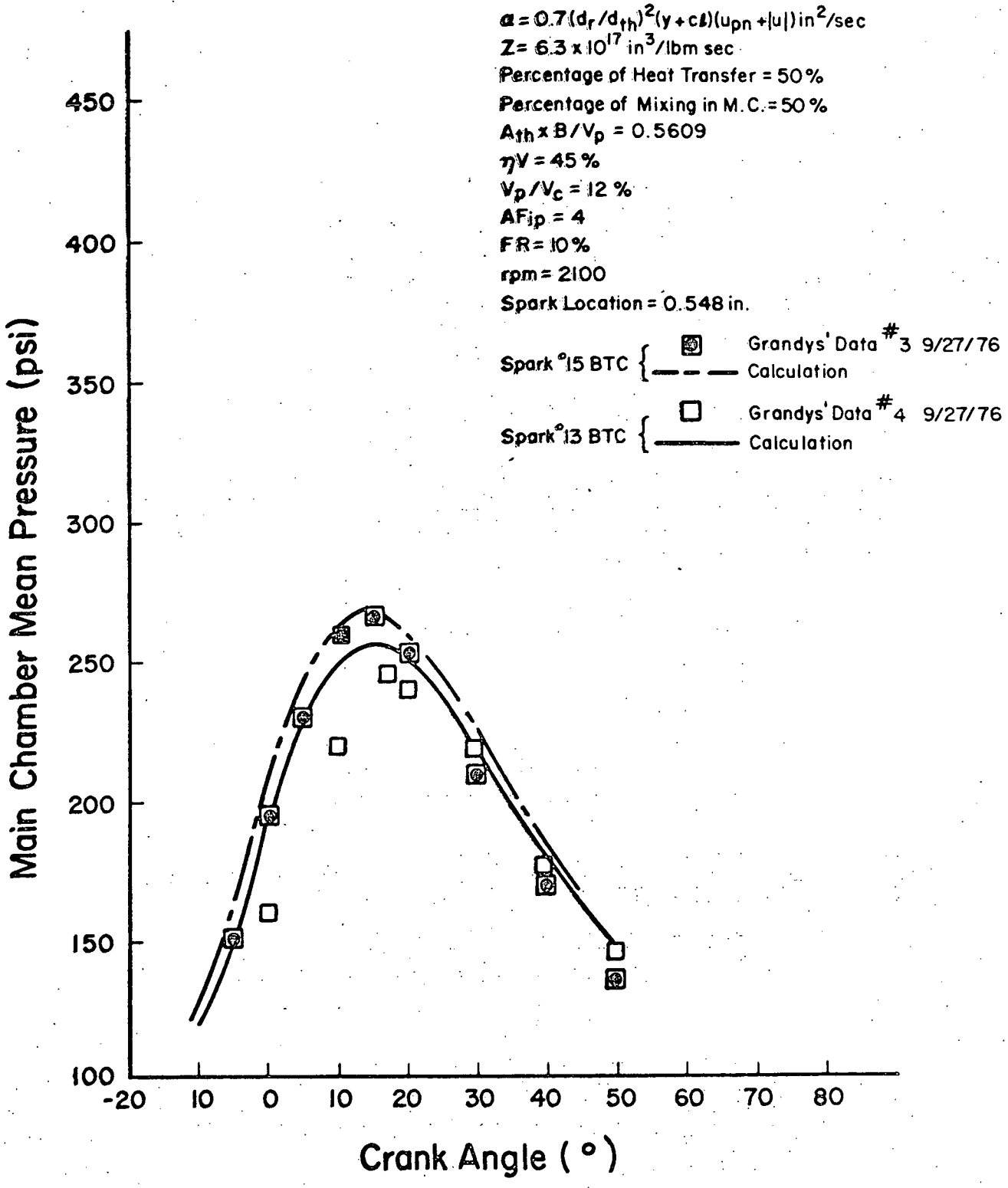

Figure 40. Effect Of Spark Timing On Pressure Time History

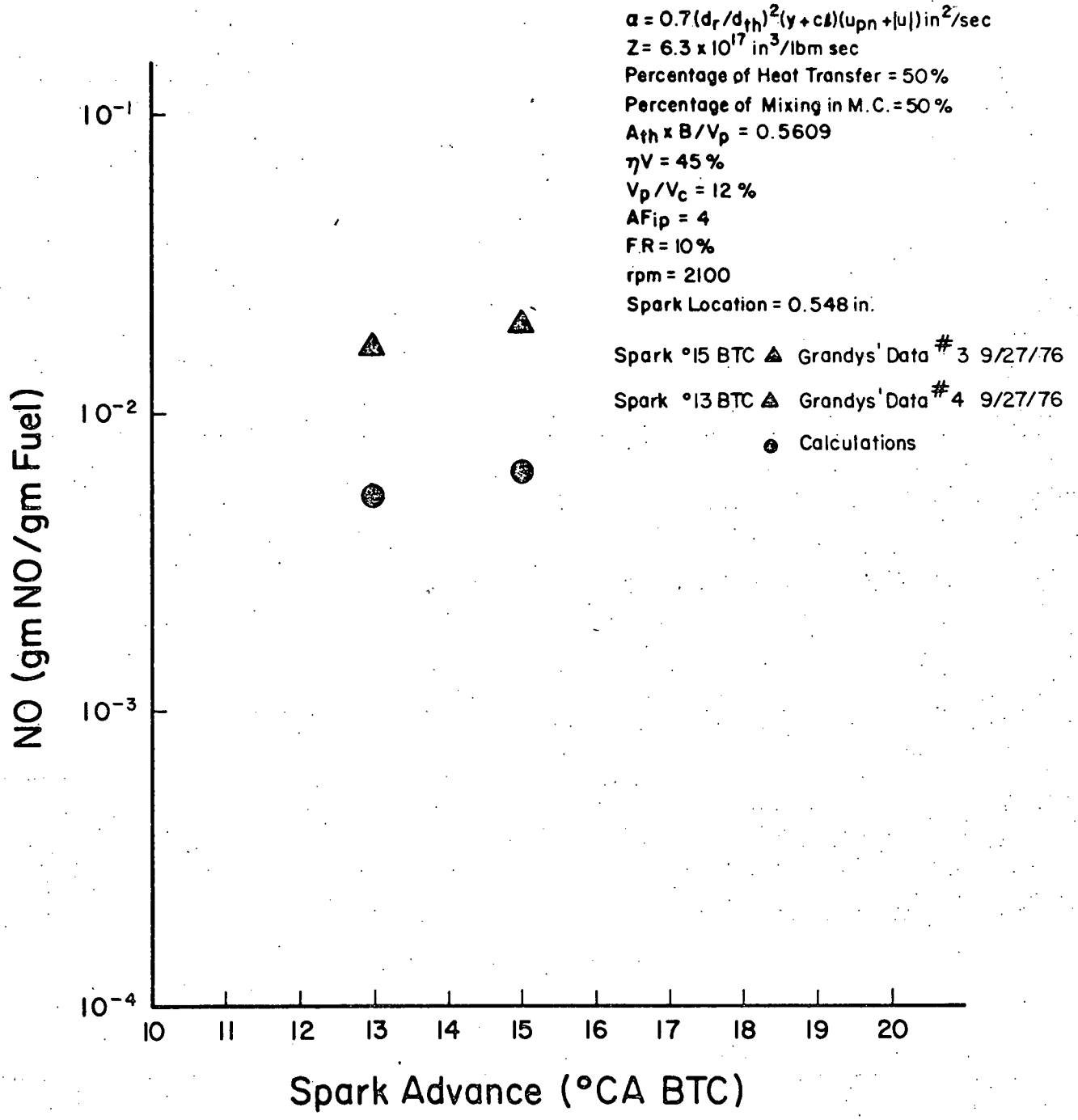

Figure 41. Effect Of Spark Timing On NO Production

CHAPTER VI

DISCUSSION, CONCLUSION AND RECOMMENDATION

A. Discussion

1. Assumptions

a) One-dimensional system

The combustion process is a three-dimensional phenomena. For simplification, a one-dimensional model was used for the simulation. The cross section area was used as the flame area while the true flame area should somewhat be like a spherical one. From the photograph study, a jet structure was observed at the orifice outlet for the small orifice (Hull and Sorenson 1978). This jet structure can not be described by the one-dimensional model, although the turbulence level has been correlated for the effect of throat diameter. Constant properties were assumed on the cross sectional plan. In the real case, there should be some gradients in temperature, velocity, and species concentration. Especially at the orifice outlet, there is a large velocity gradient due to the sudden area expansion.

General speaking, the one-dimensional model is adequate to describe the pressure level, the flame propagation rate, nitric oxide formation trends and the stratification phenomena. The mixing effect and the turbulent effect will be better simulated by the higher dimensional model.

b) The mixing model

The mixing process plays an important role in the DCSC simulation work. From the parameter study, the percentage of mixing affects the power output, the combustion rate and the NO emission level. It was believed that there should be an intermediate mixing zone in the DCSC system, as was called either mixture cloud (Date et al., 1974), or jet plume (Krieger et al., 1976). Due to the stratification, this intermediate mixing zone covers the air-fuel ratio around the stochiometric region. The quantity of this region will affect the combustion rate, the peak temperature, the peak pressure, and the NO formation. These effects have been verified from the parameter study of the percentage mixing. A constant mixing percentage was assumed for the calculation in all the conditions. Actually more mixing may exist for the small orifice than the large orifice because of the higher turbulence level on the intake stroke.

From the photograph study (Krieger, et al., 1976 and Oppenheim, et al., 1978) the intermediate mixing zone has either the shape of a hemisphere for large orifice or a round jet for the small orifice. The intermediate mixing zone in the mixing model for this research was mechanically divided by the space coordinate. This simulation is certainly an approximation to the real case, and could deviate from the actual case. The higher dimensional model should be superior in this area.

c) The fuel chemistry

In the test engine, propane C_3H_8 was supplied to the prechamber and isooctane C_8H_{18} was supplied to the main chamber. For simplicity, ethylene C_2H_4 was used as the fuel for the simulation model. Obviously, there are some differences of the molecular weight, the C/H ratio, the stoichiometric air fuel ratio, the heating value, and the chemical kinetics for these fuels, although the initial intake air fuel ratios have been corrected from the engine data for the simulation model as discussed in Appendix H1. The deviation from this simplification would not be expected to have a large effect on the simulation.

d) Identical molecular weight

Again, for simplification, the average molecular weight was assumed for the combustion of the ethylene C_2H_4 system. This is certainly not the case for the combustion of the propane C_3H_8 or the isooctane system. The mole fraction is no longer the same as the mass fraction, although for most hydrocarbon fuels, species mass fractions have little dependence on the carbon number of the fuel.

e) The chemical kinetics

In the combustion rate equation the values for the preexponential constant Z, the activation energy E, the correction power of β for the pressure, the reaction order of a for the fuel, and the reaction order of b for the oxygen are either correlated with the data or taken from the references. This rate equation though not perfect, is fairly numerically stable throughout a wide range of calculation conditions.

However, it needs to be verified by more data in order to be used more generally. Other kinetics (Tiggelen 1957, Edelman 1971 and 1977) have been tried for the simulation model, but all exhibit numerical instability. It is known that the combustion rate is very much controlled by the chemical kinetics. This could affect the power output, the flame speed, the combustion duration, and the emission level.

f) Nitric oxide kinetics

In the engine combustion, some dissociation occurs at the high temperature range, for example:

$$H_2O \rightleftharpoons OH + O \qquad \text{(VI.1)}$$

$$CO_2 \rightleftharpoons CO + \tfrac{1}{2}O_2 \qquad \text{(VI.2)}$$

$$H_2 \rightleftharpoons 2H \qquad \text{(VI.3)}$$

$$N_2 \rightleftharpoons 2N \qquad \text{(VI.4)}$$

In the simple Zeldovich mechanism, the dissociation was neglected, which underestimates the oxygen concentration. In the simple Zeldovich mechanism, the rate of reaction IV.7 is decreased, and the calculation of the NO formation could be thus reduced from the true value.

g) Heat transfer

Woschni's heat transfer equation was developed from diesel engine data. In diesel engines, 30% to 40% heat transfer during combustion is by radiation (Ebersole, et al., 1963). It would over-estimate the heat

loss by using his equation in the spark ignition engine, since the radiation is negligible in the case (Obert, 1973).

In Woschni's equation, the mean gas temperature was used for the gas temperature throughout the whole chamber. In the real engine, we know that there is always a certain temperature gradient across the chamber. The gas temperature next to the boundaries is usually lower than that of the core combustion zone. Also, the mean gas temperature is lower than the local gas temperature in the burned region, and higher than the local gas temperature in the unburned region. By this analysis, the Woschni's model may over-estimate the heat loss at the boundaries and in the unburned region, but under-estimate the heat loss in the burned region.

The parameter study indicates that the heat transfer is very influential to the burning rate, the power output, and the NO emission level. A correct heat transfer estimation is essential to the correct results.

h) Turbulent diffusivity

The magnitude of the turbulent diffusivity calculated from the one-dimensional model is in the same order as Lancaster's shrouded value. However, the use of a square power on the throat diameter to simulate the effect on the turbulence level needs more verification. The two-dimensional model should be more accurate than the one-dimensional model. Nevertheless, the two-dimensional model also needs experimental data to estimate its parameters. The importance of the turbulent diffusivity is confirmed by the parameter study.

2. The Initial Conditions

The initial velocity at the spark time was assigned zero in the simulation model. In the real engine, there should be some reverse flow at the spark time due to the compression. This initial gas velocity could contribute to the initial turbulence level.

The initial pressures were read from the photographs. The magnitude of the initial pressure at the spark time is not exact. The deviation from the true value could reach up to ±10 psi. In one case of calculation, 25 psi difference of the peak pressure was induced by only 5 psi difference of the initial pressure.

The initial condition of the air-fuel ratio in both chambers was estimated from the mixing model. When the mixing percentage changes, the initial air-fuel ratios in both the rich zone of the prechamber and the intermediate zone of the main chamber change. The effect of this percentage change has already been discussed. However, there is no experimental information about the true percentage mixing in the DCSC engine. Fifty percent mixing at spark was arbitrarily used for the calculation in all the conditions.

In the ignition model a Gaussian temperature profile was superimposed to simulate an established flame. Ignition delay was not considered. Therefore, for the simulation calculation, there is an ignition delay time difference from the experimental ignition time. The exact ignition delay of different conditions is not known however. The starting time for the calculation is approximately chosen when the experimental pressure starts to rise rapidly. The error of this

approximation could be ±5 crank angle. The effect of the ignition timing has already been discussed in the parameter study.

Seven percent residual fraction was used for the full load, fifteen percent residual fraction was used for the part load (Sorenson, 1977). The error of the residual fraction could affect the calculation for the initial species concentration and the initial total intake mass.

3. Numerical Technique

a) The numerical stability

The CFL stability criterion plus the restricted time step control gives satisfactory stability in the simulation model.

b) The numerical convergency

For the simulation model, at least 80 to 100 internal grid points are needed to give convergent results. The mass conservation for 80 grid points is around 2%.

4. Error Analysis

There are three basic types of errors in a numerical computation: inherent, truncation, and roundoff (Dorn 1972).

The inherent errors are errors associated with data, caused by the uncertainty in measurements, or the approximate nature of representing the data. The uncertainty in measurements is not the topic in this research work. Here, we will concentrate on the approximate nature of representing the data. First, it is known that there is some cyclic variation about the data measurement in the engine. The

statistical average of the data measured over a number of engine cycles is the standard way to present the engine data. Due to the lack of adequate instrumentation at the time the experiments were done, only the data of a single cycle were collected. Second, as mentioned before, due to the lack of the information of exact ignition delay, the starting point was approximately read from the photographs for the simulation model. Errors inherent in the supplied data are very probable.

Regard to the truncation errors, the MacCormack predictor-corrector finite difference method has a third order of truncation errors for the partial differential equations. A better, more accurate numerical technique is the only way to improve the truncation errors. Also, the truncation errors are function of the spatial grid size. The smaller the grid size, the smaller the truncation errors.

The computation of this numerical calculation uses a double precision feature, which has the accuracy up to 16 decimal digits. This means that the roundoff errors only appear on the 16th digit number. Therefore, the roundoff errors should be the least possible source of errors in the calculation.

B. Conclusions

(1) A one-dimensional model has been developed for the simulation of combustion in a dual chamber stratified charge spark ignition engine.

(2) Through the use of empirical corrections for nozzle diameter and pressure dependence of fuel kinetics,

quantitative predictions of burning rates can be achieved over a range of engine conditions.

(3) Relative changes in nitric oxide emission can be predicted quantitatively over these conditions although the absolute magnitude is low by a factor of two to three for most conditions.

(4) The predicted effects of changes in total air-fuel ratio, prechamber air-fuel ratio and mass flow percentage, volumetric efficiency, nozzle diameter, and spark timing on pressure time history and relative changes in NO emission agree well with the experimental data.

(5) The effects of heat transfer model assumptions on burning rate and NO formation have been investigated with the model.

(6) The degree of mixing between prechamber intake gases and main chamber intake gases on the intake stroke in the main chamber has a strong effect on NO formation. The majority of the NO produced results from slightly lean mixture resulting from partial mixing of the prechamber and the main chamber intake gases.

(7) The model can be used for the improvement of the performance and the design of dual chamber stratified charge spark ignition engines.

C. Recommendations

(1) A two-dimensional model needs to be developed.

(2) More investigation and data are needed for the mixing model in a DCSC engine.

(3) More sophisticated fuel chemistry and its chemical kinetics are needed.

(4) Better heat transfer correlation and modeling technique is worthwhile for further investigation.

(5) More data are needed to verify the turbulent diffusivity model.

(6) The statistical averaging of the pressure data over the cycles is strongly suggested.

(7) An ignition delay correlation is needed.

(8) More accurate information is needed for the initial conditions of the gas velocity, the pressure, the ignition timing and the residuals at spark.

(9) A complete cycle analysis for the correlation of the mean effective pressure and the specific fuel consumption is recommended for the further study.

(10) The experimental work on the effect of engine speed, mixing percentage, turbulence, and heat transfer is suggested.

REFERENCES

1. Asanuma, T., M. K. Gajendra Babu, and S. Yagi, "Simulation of Thermodynamic Cycle of Three-Valve Stratified Charge Engine," SAE Paper 780319.

2. Boni, A. A., Workshop on the Numerical Simulation of Combustion For Application to Spark and Compression Ignition Engines, La Jolla, California, 23-25 April 1975.

3. Boni, A. A., M. Chapman, G. P. Schneyer, "A One-Dimensional Variable Area Computer Simulation of Combustion in a Divided Chamber, Stratified Charge Engine," ASME Paper 75-WA/DGP-1.

4. Boni, A. A., M. Chapman, and G. P. Schneyer, "Computer Simulation of Combustion Processes in a Stratified Charge Engine," Acta Astronautica, Vol. 3, pp. 293-307, Pergamon Press, 1976.

5. Bracco, F. V., "Introducing a New Generation of More Informative Combustion Models," SAE Paper 741174.

6. Bracco, F. V., "Modeling of Two Phase, Two Dimensional, Unsteady Combustion for Internal Combustion Engines," C 171/77, Stratified Charge Engines, pp. 167-187.

7. Bracco, F. V., "Theoretical Analysis of Stratified, Two-Phase Wankel Engine Combustion," Comb. Sci. Tech., 8, 69-84.

8. Bracco, F. V., and W. A. Sirignano, "Theoretical Analysis of Wankel Engine Combustion," Proc., 7th Intersociety Energy Conversion Engineering Conf., San Diego, California, 25-29 September 1972.

9. Brandsteller, W. R., G. Decker, and K. Reichel, "The Water-Cooled Volkswagen PCI-Stratified Charge Engine," SAE Paper 750869.

10. Brandstetter, W. R., "Experimental Results From Volkswagen's Pre Chamber Stratified Charge Engines," C 249/76, Stratified Charge Engines, pp. 71-79.

11. Date, T., S. Yagi, A. Ishizuya, and I. Fujii, "Research and Development of the Honda CVCC Engine," SAE Paper 740605.

12. Davis, G. C., R. B. Krieger, and R. J. Tabaczynski, "Analysis of the Flow and Combustion Processes of a Three-Valve Stratified Charge Engine with a Small Prechamber," SAE Paper 741170.

13. Dorn, W. S., and D. D. McCracken, Numerical Methods With Fortran IV Case Studies, John Wiley & Sons, Inc., 1972.

14. Dwyer, H. A., and B. R. Sanders, "Unsteady Flow and Flame Propagation In a Prechamber of a Stratified Charge Engine," C 248/76, Stratified Charge Engines, pp. 65-70.

15. Dwyer, H., R. Allen, M. Ward, D. Karnopp, and D. Margolis, "Shock Capturing Finite Difference Methods for Unsteady Gas Transfer," AIAA Paper 74-521.

16. Ebersole, G. D., P. S. Myers, and O. A. Uyehara, "The Radiant and Convective Components of Diesel Engine Heat Transfer," Paper 701C presented at SAE International Summer Meeting, Montreal, June 1963.

17. Edelman, R. B., personal communication with Professor H. Krier, University of Illinois at Urbana-Champaign, 1977.

18. Edelman, R. B., O. Fortune, and Weilerstein, "Some Observations on Flows Described by Coupled Mixing and Kinetics," Emission From Continuous Combustion Systems, Symposium at General Motors Corp. Research Laboratories, pp. 55-90, 1971.

19. Grandys, K. W., "Improving the Performance and Exhaust Emissions of Dual Chamber Stratified Charge Spark Ignition Engine," Master of Science thesis, Department of Mechanical and Industrial Engineering, University of Illinois at Urbana-Champaign, 1977.

20. Hires, S. D., "Performance and Emission Modeling of a Jet Ignition Stratified Charge Engine," Master of Science thesis, MIT, Cambridge, Massachusetts, January 1975.

21. Hull, W. L., and S. C. Sorenson, "Research on a Dual-Chamber Stratified Charge Engine," SAE 780488.

22. Krieger, R. B., and G. C. Davis, "The Influence of the Degree of Stratification on Jet-Ignition Engine Emissions and Fuel Consumption," C 254/76, Stratified Charge Engines, pp. 109-119.

23. Lancaster, David R., "Effects of Engine Variables on Turbulence in a Spark-Ignition Engine," 1976 Automotive Engineering Congress and Exposition, Detroit, Michigan, 23 February 1976.

24. Miller, G. H., O. A. Uyehara, and P. S. Myers, "Practical Application of Engine Flame Temperature Measurements," SAE Trans., 62, 514, 1954.

25. Newhall, H. K., and S. M. Shahed, "Kinetics of Nitric Oxide Formation in High-Pressure Flames," Air Pollution 1976, pp. 381-389.

26. Obert, E. F., Internal Combustion Engines and Air Pollution, Intext Educational Publishers, New York, 1973.

27. Oppenheim, A. K., K. Teichman, K. Hom, and H. E. Stewart, "Jet Ignition of an Ultra-Lean Mixture," SAE Paper 780637.

28. Overbye, V. K., J. E. Bennethum, O. A. Uyehara, and P. S. Meyers, "Unsteady Heat Transfer In Engines," SAE Trans., Vol. 69, pp. 461-494, 1961.

29. Purins, E. A., "Pre-Chamber Stratified Charge Engine Combustion Studies," SAE Paper 741159.

30. Roessler, W. U., and A. Muraszen, Evaluation of Prechamber Spark Ignition Engine Concepts, EPA-650/2-75-023, February 1975.

31. Rosentweig-Bellan, J. and W. A. Sirignano, "A Theory of Turbulent Flame Development In Stratified Charge Internal Combustion Engines," Comb. Sci. Tech., 8, 51-68.

32. Savage, Jr., L. D., "A Subprogram for the Calculation of Thermodynamics and Transport Properties of Common Gaseous Mixtures," 1977, University of Illinois at Urbana-Champaign, Urbana, Illinois.

33. Semenov, E. S., "Studies of Turbulent Gas Flow In Piston Engines," Combustion in Turbulent Flow, pp. 122-147, 1963.

34. Sirignano, W. A., "One-Dimensional Analysis of Combustion in a Spark-Ignition Engine," SAE Paper 719010.

35. Sorenson, S. C., "Modeling Turbulent Transient Combustion," SAE Paper 780639.

36. Tiggelen, A. V., and J. Decker, "Chain Branching and Flame Propagation," Proc., Sixth Symposium (International) on Combustion, Reinhold, N.Y., pp. 61-66, 1957.

37. Turkish, M. C., "3-Valve Stratified Charge Engines: Evolvement, Analysis and Progression," SAE Paper 741163.

38. Warming, R. F., P. Kutler, and H. Lomex, "Second and Third Order Noncentered Difference Schemes for Nonlinear Hyperbolic Equations," AIAA J., Vol. 11, No. 2, February 1973.

39. Woschni, G., "A Universal Applicable Equation for the Instantaneous Heat Transfer Coefficient in the Internal Combustion Engine," SAE Paper 670931.

40. Yagi, S., I. Fujii, M. Watanabe, and Shin Nanasaka, "On the Emission-Combustion Temperature Relationship in the CVCC Engine," SAE Paper 760109.

APPENDIX A

DERIVATION OF THE DIFFERENTIAL EQUATIONS

When applying the basic conservation laws to a differential control volume, a set of differential equations can be written. The dual chamber model is a one-dimensional, time dependent, and variable area system, and so is the differential control volume.

1. Conservation Of Mass

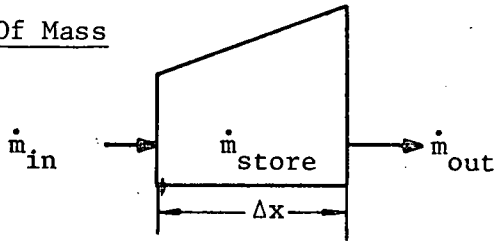

Applying the conservation of mass to the control volume, one can write,

$$\dot{m}_{store} = \dot{m}_{in} - \dot{m}_{out} \tag{A.1}$$

where $\dot{m}_{store} = \frac{\partial}{\partial t}(m) = \frac{\partial}{\partial t}(\rho A \Delta x)$

$\dot{m}_{in} = (\rho A u)\big|_x$

$\dot{m}_{out} = (\rho A u)\big|_{x+\Delta x}$.

Substituting back into the equation A.1, dividing by Δx, and taking the limit, $\Delta x \to 0$, one obtains the differential equation for the conservation of mass,

$$\frac{\partial}{\partial t}(\rho A) + \frac{\partial}{\partial x}(\rho A u) = 0 \ . \tag{A.2}$$

By differentiating, and manipulating, one obtains the time derivative for the density,

$$\frac{\partial \rho}{\partial t} = -\frac{\rho}{A}\frac{\partial A}{\partial t} - \rho\frac{\partial u}{\partial x} - \frac{\rho u}{A}\frac{\partial A}{\partial x} - u\frac{\partial \rho}{\partial x} \ . \qquad (A.3)$$

2. Conservation Of Momentum

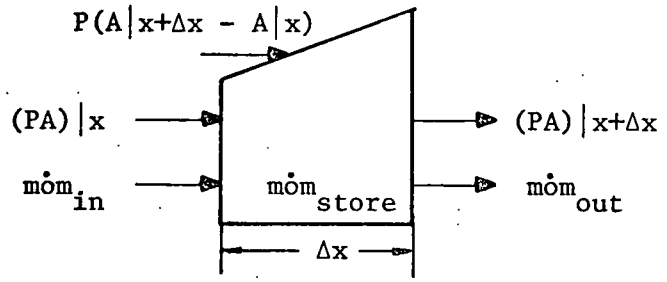

By Newton's second law, the momentum is balanced as,

$$\text{Total force} = \text{Time rate of momentum change} \qquad (A.4)$$

where total force $= (PA)|_x - (PA)|_{x+\Delta x} + P(A|_{x+\Delta x} - A|_x)$

time rate of momentum change $= \dot{mom}_{store} + \dot{mom}_{out} - \dot{mom}_{in}$

$$\dot{mom}_{store} = \frac{\partial}{\partial t}(mu) = \frac{\partial}{\partial t}(\rho A \Delta x u)$$

$$\dot{mom}_{out} = (\rho A u \cdot u)|_{x+\Delta x} - (\rho A \alpha \frac{\partial u}{\partial x})|_{x+\Delta x}$$

$$\dot{mom}_{in} = (\rho A u \cdot u)|_{x} - (\rho A \alpha \frac{\partial u}{\partial x})|_{x} \ .$$

The second terms in the $\dot{mom}_{out}$ and $\dot{mom}_{in}$ are the momentum contribution due to the diffusion effect. When substituting back to the balance equation A.4, dividing by Δx, and taking the limits, $\Delta x \to 0$, one obtains,

$$-\frac{\partial}{\partial x}(PA) + P\frac{\partial A}{\partial x} = \frac{\partial}{\partial t}(\rho A u) + \frac{\partial}{\partial x}(\rho A u^2) - \frac{\partial}{\partial x}(\rho A \alpha \frac{\partial u}{\partial x}) \ . \qquad (A.5)$$

By differentiating, manipulating, and applying the mass equation, one

obtains the differential equation for the conservation of momentum,

$$\frac{\partial u}{\partial t} + u \frac{\partial u}{\partial x} = - \frac{1}{\rho} \frac{\partial P}{\partial x} + \frac{1}{\rho A} \frac{\partial}{\partial x} (\rho A \alpha \frac{\partial u}{\partial x}). \qquad (A.6)$$

By further differentiating and manipulating, since $\alpha = f(u)$, one obtains the time derivative for the gas velocity,

$$\frac{\partial u}{\partial t} = - \frac{1}{\rho} \frac{\partial P}{\partial x} + \alpha \frac{\partial^2 u}{\partial x^2} + \frac{\partial u}{\partial x}[- u + \frac{\partial \alpha}{\partial u} \frac{\partial u}{\partial x} + \frac{\alpha}{A} \frac{\partial A}{\partial x} + \frac{\alpha}{\rho} \frac{\partial \rho}{\partial x}] . \qquad (A.7)$$

3. Conservation Of Energy

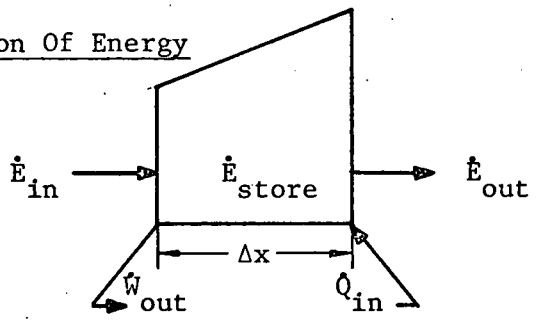

From first law of thermodynamics,

$$\dot{Q}_{in} - \dot{W}_{out} = \Delta \dot{E} \qquad (A.8)$$

where $\dot{Q}_{in} = \dot{Q}_{cond.} + \dot{Q}_{conv.} + \dot{Q}_{chem.}$

$$\dot{Q}_{cond.} = -[(\rho A C_p \alpha \frac{\partial T}{\partial x}) \Big| x - (\rho A C_p \alpha \frac{\partial T}{\partial x}) \Big| x+\Delta x]$$

$$\dot{Q}_{conv.} = -U\hat{P}\Delta x \ (T_g - T_W)$$

$$\dot{Q}_{chem.} = hr \ K2[A][B]A\Delta x$$

$$= hr \ ZP^{-\beta} \ e^{-E/RT} \frac{\varepsilon_1 \rho}{M} \frac{\varepsilon_2 \rho}{M} A\Delta x$$

$$= hr \ ZP^{-\beta} \ A\Delta x \frac{\varepsilon_1 \varepsilon_2 \rho^2}{M^2} \ e^{-E/RT}$$

$$\dot{W}_{out} = \bar{P} \frac{\partial v}{\partial t} = P\Delta x \frac{\partial A}{\partial t}$$

$$\Delta\dot{E} = \dot{E}_{store} + \dot{E}_{out} - \dot{E}_{in}$$

$$\dot{E}_{store} = \frac{\partial}{\partial t}(me) = \frac{\partial}{\partial t}\left[\rho A\Delta x\left(C_v T + \frac{u^2}{2}\right)\right]$$

$$\dot{E}_{out} = \rho A u\left(C_p \bar{T} + \frac{u^2}{2}\right)\Big|_{x+\Delta x}$$

$$\dot{E}_{in} = \rho A u\left(C_p \bar{T} + \frac{u^2}{2}\right)\Big|_{x} .$$

Where the heat conduction of the gas mixture is simulated by a turbulent diffusivity mechanism. By substituting all the terms back into the balance equation A.8, dividing by Δx, and taking the limit, $\Delta x \to 0$, one obtains,

$$\frac{\partial}{\partial x}\left(\rho A C_p \alpha \frac{\partial T}{\partial x}\right) - U\tilde{P}(T_g - \bar{T}_w) + hrZP^{-}\beta_A \frac{\varepsilon_1 \varepsilon_2 \rho^2}{M^2} e^{-E/RT} - P\frac{\partial A}{\partial t}$$

$$= \frac{\partial}{\partial t}\left[\rho A\left(C_v T + \frac{u^2}{2}\right)\right] + \frac{\partial}{\partial x}\left[\rho A u\left(C_p T + \frac{u^2}{2}\right)\right]. \qquad (A.9)$$

Since $h = u + Pv$, $C_p \bar{T} = C_v \bar{T} + P/\rho$, the second term on the right hand side becomes,

$$\frac{\partial}{\partial x}\left[\rho A u\left(C_p T + \frac{u^2}{2}\right)\right] = \frac{\partial}{\partial x}\left[\rho A u\left(C_v \bar{T} + \frac{u^2}{2}\right)\right] + \frac{\partial}{\partial x}(AuP) .$$

By further differentiating, substituting of the mass conservation equation, and substituting the momentum equation multiplied by the velocity, and upon further manipulating, one obtains,

$$\frac{\partial}{\partial t}(C_v T) + u\frac{\partial}{\partial x}(C_v T) + \frac{u}{\rho A}\frac{\partial}{\partial x}\left(\rho\alpha A\frac{\partial u}{\partial x}\right) + \frac{uP}{\rho A}\frac{\partial A}{\partial x} + \frac{P}{\rho}\frac{\partial u}{\partial x}$$

$$= \frac{1}{\rho A}\frac{\partial}{\partial x}\left[\rho A C_p \alpha \frac{\partial T}{\partial x}\right] - \frac{U\tilde{P}}{\rho A}(T_g - T_w) + hrZP^{-\beta}\frac{\epsilon_1\epsilon_2\rho}{M^2}\, e^{-E/RT} - \frac{P}{\rho A}\frac{\partial A}{\partial t} \quad (A.10)$$

By further differentiating and manipulating, using $C_v = f(T)$, and $\alpha = f(u)$, one obtains the differential equation for the conservation of energy,

$$\frac{\partial T}{\partial t}\left[C_v + T\frac{\partial C_v}{\partial T}\right] = -u\frac{\partial T}{\partial x}\left[C_v + T\frac{\partial C_v}{\partial T}\right]$$

$$- u\left[\alpha\frac{\partial^2 u}{\partial x^2} + \frac{\alpha}{A}\frac{\partial u}{\partial x}\frac{\partial A}{\partial x} + \frac{\partial u}{\partial x}\frac{\partial \alpha}{\partial u}\frac{\partial u}{\partial x} + \frac{\alpha}{\rho}\frac{\partial u}{\partial x}\frac{\partial \rho}{\partial x}\right]$$

$$- \frac{uP}{\rho A}\frac{\partial A}{\partial x} - \frac{P}{\rho}\frac{\partial u}{\partial x} + \left[C_p\alpha\frac{\partial^2 T}{\partial x^2} + C_p\frac{\partial T}{\partial x}\frac{\partial \alpha}{\partial u}\frac{\partial u}{\partial x} + \alpha\frac{\partial C_v}{\partial T}\left(\frac{\partial T}{\partial x}\right)^2\right.$$

$$\left. + \frac{\alpha}{A}C_p\frac{\partial T}{\partial x}\frac{\partial A}{\partial x} + \frac{\alpha}{\rho}C_p\frac{\partial T}{\partial x}\frac{\partial \rho}{\partial x}\right] - \frac{U\tilde{P}}{\rho A}(T_g - T_w)$$

$$+ hrZP^{-\beta}\frac{\epsilon_1\epsilon_2\rho}{M^2}\, e^{-E/RT} - \frac{P}{\rho A}\frac{\partial A}{\partial t}. \quad (A.11)$$

By defining $BB \equiv \dfrac{1}{C_v + T\dfrac{\partial C_v}{\partial T}}$, and solving for the time derivatives of the temperature, one obtains,

$$\frac{\partial T}{\partial t} = -u\frac{\partial T}{\partial x} + BB\left\{\left[C_p\frac{\partial T}{\partial x}\left(\frac{\partial \alpha}{\partial u}\frac{\partial u}{\partial x} + \frac{\alpha}{A}\frac{\partial A}{\partial x} + \frac{\alpha}{\rho}\frac{\partial \rho}{\partial x}\right)\right.\right.$$

$$\left. + \alpha\left(C_p\frac{\partial^2 T}{\partial x^2} + \frac{\partial C_v}{\partial T}\left(\frac{\partial T}{\partial x}\right)^2\right)\right]$$

$$+ \left[-\frac{P}{\rho}\left(\frac{u}{A}\frac{\partial A}{\partial x} + \frac{\partial u}{\partial x} + \frac{1}{A}\frac{\partial A}{\partial t}\right)\right]$$

$$+ \left[-\frac{U\tilde{P}}{\rho A}(T_g - T_w) + hrZP^{-\beta}\frac{\epsilon_1\epsilon_2\rho}{M^2}\, e^{-E/RT}\right]$$

$$\left. + \left[-u\alpha\frac{\partial^2 u}{\partial x^2} + u\frac{\partial u}{\partial x}\left(\frac{\partial \alpha}{\partial x}\frac{\partial u}{\partial x} + \frac{\alpha}{A}\frac{\partial A}{\partial x} + \frac{\alpha}{\rho}\frac{\partial \rho}{\partial x}\right)\right]\right\}. \quad (A.12)$$

4. Conservation Of Mass For Species

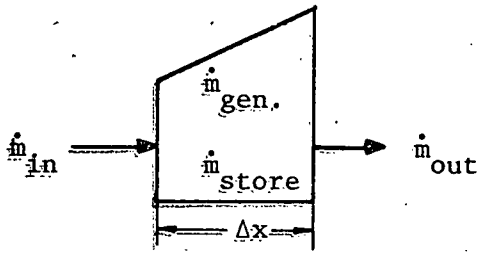

Applying conservation of mass to the control volume for the species, one can write,

$$\dot{m}_{store} = \dot{m}_{in} - \dot{m}_{out} + \dot{m}_{gen.} \tag{A.13}$$

where $\dot{m}_{store} = \frac{\partial}{\partial t}[m\epsilon_i] = \frac{\partial}{\partial t}[\rho A \Delta x \epsilon_i]$

$$\dot{m}_{in} = (\rho A u \epsilon_i)\big|x - (\rho A \alpha \frac{\partial \epsilon i}{\partial x})\big|x$$

$$\dot{m}_{out} = (\rho A u \epsilon_i)\big|x+\Delta x - (\rho A \alpha \frac{\partial \epsilon i}{\partial x})\big|x+\Delta x$$

$$\dot{m}_{gen.} = \nu_i Z P^{-\beta} e^{-E/RT} \frac{\epsilon_1 \epsilon_2 \rho^2}{M} A \Delta x .$$

The second terms of $\dot{m}_{in}$ and $\dot{m}_{out}$ are the mass contribution from the diffusion effect. Substituting all the terms back into the balance equation A.13, dividing by Δx, and taking the limit, $\Delta x \to 0$, one obtains,

$$\frac{\partial}{\partial t}[\rho A \epsilon_i] = -\frac{\partial}{\partial x}(\rho A u \epsilon_i) + \frac{\partial}{\partial x}(\rho A \alpha \frac{\partial \epsilon_i}{\partial x})$$

$$+ \nu_i Z P^{-\beta} A \frac{\epsilon_1 \epsilon_2 \rho^2}{M} e^{-E/RT}. \tag{A.14}$$

By differentiating, substituting the mass conservation equation, and manipulating, one obtains the differential equation for the conservation

of species,

$$\frac{\partial \varepsilon_i}{\partial t} + u \frac{\partial \varepsilon_i}{\partial x} = \frac{1}{\rho A} \frac{\partial}{\partial x} \left(\rho A \alpha \frac{\partial \varepsilon_i}{\partial x}\right) + \nu_i Z P^{-\beta} \frac{\varepsilon_1 \varepsilon_2 \rho}{M} e^{-E/RT}. \qquad (A.15)$$

By further differentiating, and manipulating, one obtains the time derivative for the species concentration,

$$\frac{\partial \varepsilon_i}{\partial t} = \alpha \frac{\partial^2 \varepsilon_i}{\partial x^2} + \frac{\partial \varepsilon_i}{\partial x} \left[-u + \frac{\partial \alpha}{\partial u} \frac{\partial u}{\partial x} + \frac{\alpha}{A} \frac{\partial A}{\partial x} + \frac{\alpha}{\rho} \frac{\partial \rho}{\partial x}\right] + \nu_i Z P^{-\beta} \frac{\varepsilon_1 \varepsilon_2 \rho}{M} e^{-E/RT} \qquad (A.16)$$

where ν_i = stoichiometric mole fraction for the species

$\nu_1 = -1$ for the fuel

$\nu_2 = -3$ for the oxygen

$\nu_3 = +4$ for the product.

APPENDIX B

FINITE DIFFERENCE EQUATIONS FOR THE PREDICTOR-CORRECTOR TECHNIQUE

All the time derivatives of the dependent variables are written in finite difference forms and solved by the MacCormack predictor-corrector technique. The subscript i represents the spatial grid points, and the superscript n the temporal steps.

1. Mass Equation

a) Predictor

$$\left(\overline{\frac{\partial \rho}{\partial t}}\right)_i^n = -\frac{\rho_i^n}{A_i^n}\left(\frac{\partial A}{\partial t}\right)_i^n - \rho_i^n \frac{u_{i+1}^n - u_i^n}{\Delta x} - \frac{\rho_i^n u_i^n}{A_i^n}\left(\frac{\partial A}{\partial x}\right)_i^n - u_i^n \frac{\rho_{i+1}^n - \rho_i^n}{\Delta x} \tag{B.1}$$

$$\rho_i^{n+1} = \rho_i^n + \left[\left(\overline{\frac{\partial \rho}{\partial t}}\right)_i^n\right]\Delta t \tag{B.2}$$

b) Corrector

$$\left(\frac{\partial \rho}{\partial t}\right)_i^{n+1} = -\frac{\rho_i^{n+1}}{A_i^{n+1}}\left(\frac{\partial A}{\partial t}\right)_i^{n+1} - \rho_i^{n+1} \frac{u_i^{n+1} - u_{i-1}^{n+1}}{\Delta x}$$

$$- \frac{\rho_i^{n+1} u_i^{n+1}}{A_i^{n+1}}\left(\frac{\partial A}{\partial x}\right)_i^{n+1} - u_i^{n+1} \frac{\rho_i^{n+1} - \rho_{i-1}^{n+1}}{\Delta x} \tag{B.3}$$

$$\rho_i^{n+1} = \tfrac{1}{2}\left[\rho_i^n + \overline{\rho_i^{n+1}} + \left(\overline{\frac{\partial \rho}{\partial t}}\right)_i^{n+1}\Delta t\right] \tag{B.4}$$

2. Momentum Equation

a) Predictor

$$\left(\overline{\frac{\partial u}{\partial t}}\right)_i^n = -\frac{1}{\rho_i^n}\frac{P_{i+1}^n - P_i^n}{\Delta x} + \alpha_i^n \frac{u_{i+1}^n - 2u_i^n + u_{i-1}^n}{\Delta x^2}$$

$$+ \frac{u_{i+1}^n - u_i^n}{\Delta x}\left[-u_i^n + \left(\frac{\partial \alpha}{\partial u}\right)_i^n \left(\frac{u_{i+1}^n - u_i^n}{\Delta x}\right) + \frac{\alpha_i^n}{A_i^n}\left(\frac{\partial A}{\partial x}\right)_i^n\right.$$

$$\left. + \frac{\alpha_i^n}{\rho_i^n}\frac{\rho_{i+1}^n - \rho_i^n}{\Delta x}\right] \qquad \text{(B.5)}$$

$$\overline{u_i^{n+1}} = u_i^n + \left[\left(\overline{\frac{\partial u}{\partial t}}\right)_i^n\right]\Delta t \qquad \text{(B.6)}$$

b) Corrector

$$\left(\frac{\partial u}{\partial t}\right)_i^{n+1} = -\frac{1}{\rho_i^{n+1}}\frac{P_i^{n+1} - P_{i-1}^{n+1}}{\Delta x} + \alpha_i^{n+1}\frac{u_{i+1}^{n+1} - 2u_i^{n+1} + u_{i-1}^{n+1}}{\Delta x^2}$$

$$+ \frac{u_i^{n+1} - u_{i-1}^{n+1}}{\Delta x}\left[-u_i^{n+1} + \left(\frac{\partial \alpha}{\partial u}\right)_i^{n+1}\left(\frac{u_i^{n+1} - u_{i-1}^{n+1}}{\Delta x}\right)\right.$$

$$\left. + \frac{\alpha_i^{n+1}}{A_i^{n+1}}\left(\frac{\partial A}{\partial x}\right)_i^{n+1} + \frac{\alpha_i^{n+1}}{\rho_i^{n+1}}\frac{\rho_i^{n+1} - \rho_{i-1}^{n+1}}{\Delta x}\right] \qquad \text{(B.7)}$$

$$u_i^{n+1} = \tfrac{1}{2}\left[u_i^n + \overline{u_i^{n+1}} + \left(\overline{\frac{\partial u}{\partial t}}\right)_i^{n+1}\Delta t\right] \qquad \text{(B.8)}$$

3. Energy Equation

a) Predictor

$$\left(\overline{\frac{\partial T}{\partial t}}\right)_i^n = -u_i^n \frac{T_{i+1}^n - T_i^n}{\Delta x} + BB_i^n \left\{\left[C_p \frac{T_{i+1}^n - T_i^n}{\Delta x}\left(\frac{\partial \alpha}{\partial u}\right)_i^n \frac{u_{i+1}^n - u_i^n}{\Delta x}\right.\right.$$

$$\left.\left. + \frac{\alpha_i^n}{A_i^n}\left(\frac{\partial A}{\partial x}\right)_i^n + \frac{\alpha_i^n}{\rho_i^n}\frac{\rho_{i+1}^n - \rho_i^n}{\Delta x}\right) + \alpha_i^n\left(C_p \frac{T_{i+1}^n - 2T_i^n + T_{i-1}^n}{\Delta x^2}\right.\right.$$

$$+ \left(\frac{\partial C_v}{\partial T}\right)_i^n \left(\frac{T_{i+1}^n - T_i^n}{\Delta x}\right)^2)] + [- \frac{P_i^n}{\rho_i^n} \frac{u_i^n}{A_i^n} \left(\frac{\partial A}{\partial x}\right)_i^n + \frac{u_{i+1}^n - u_i^n}{\Delta x}$$

$$+ \frac{1}{A_i^n} \left(\frac{\partial A}{\partial t}\right)_i^n)] + [- \frac{\tilde{UP}_i^n}{\rho_i^n A_i^n} (T_i^n - T_w) + hrZP^{-\beta} \rho_i^n \frac{\varepsilon 1_i^n \varepsilon 2_i^n}{M^2} e^{-E/RT_i^n}]$$

$$+ [- u_i^n \alpha_i^n \frac{u_{i+1}^n - 2u_i^n + u_{i-1}^n}{\Delta x^2} + u_i^n \frac{u_{i+1}^n - u_i^n}{\Delta x} \left(\left(\frac{\partial \alpha}{\partial u}\right)_i^n \frac{u_{i+1}^n - u_i^n}{\Delta x}\right.$$

$$\left. + \frac{\alpha_i^n}{A_i^n} \left(\frac{\partial A}{\partial x}\right)_i^n + \frac{\alpha_i^n}{\rho_i^n} \frac{\rho_{i+1}^n - \rho_i^n}{\Delta x}\right)]\} \qquad \text{(B.9)}$$

where $BB_i^n = \dfrac{1}{C_{v_i}^n + T_i^n \left(\frac{\partial C_v}{\partial T}\right)_i^n}$

$$\overline{T_i^{n+1}} = T_i^n + [\left(\frac{\overline{\partial T}}{\partial t}\right)_i^n] \Delta t \qquad \text{(B.10)}$$

b) Corrector

$$\left(\frac{\partial T}{\partial t}\right)_i^{n+1} = - u_i^{n+1} \frac{T_i^{n+1} - T_{i-1}^{n+1}}{\Delta x}$$

$$+ BB_i^{n+1} \{[C_p \frac{T_i^{n+1} - T_{i-1}^{n+1}}{\Delta x} \left(\left(\frac{\partial \alpha}{\partial u}\right)_i^{n+1} \frac{u_i^{n+1} - u_{i-1}^{n+1}}{\Delta x}\right.$$

$$\left. + \frac{\alpha_i^{n+1}}{A_i^{n+1}} \left(\frac{\partial A}{\partial x}\right)_i^{n+1} + \frac{\alpha_i^{n+1}}{\rho_i^{n+1}} \frac{\rho_i^{n+1} - \rho_{i-1}^{n+1}}{\Delta x}\right.$$

$$\left. + \alpha_i^{n+1} \left(C_p \frac{T_{i+1}^n - 2T_i^n + T_{i-1}^n}{\Delta x^2} + \left(\frac{\partial C_v}{\partial T}\right)_i^{n+1} \left(\frac{T_i^{n+1} - T_{i-1}^{n+1}}{\Delta x}\right)\right)\right]$$

$$+ [- \frac{P_i^{n+1}}{\rho_i^{n+1}} \frac{u_i^{n+1}}{A_i^{n+1}} \left(\frac{\partial A}{\partial x}\right)_i^{n+1} + \frac{u_i^{n+1} - u_{i-1}^{n+1}}{\Delta x} + \frac{1}{A^{n+1}} \left(\frac{\partial A}{\partial x}\right)_i^{n+1})]$$

$$+ \left[- \frac{\tilde{UP}_i^{n+1}}{\rho_i^{n+1} A_i^{n+1}} (T_i^{n+1} - T_w) + hrZP^{-\beta} \rho_i^{n+1} \frac{\varepsilon 1_i^{n+1} \varepsilon 2_i^{n+1}}{M^2} e^{-E/RT_i^{n+1}} \right]$$

$$+ \left[-u_i^{n+1} \alpha_i^{n+1} \frac{u_{i+1}^{n+1} - 2u_i^{n+1} + u_{i-1}^{n+1}}{\Delta x^2} \right.$$

$$+ u_i^{n+1} \frac{u_i^{n+1} - u_{i-1}^{n+1}}{\Delta x} \left(\left(\frac{\partial \alpha}{\partial u} \right)_i^{n+1} \frac{u_i^{n+1} - u_{i-1}^{n}}{\Delta x} + \frac{\alpha_i^{n+1}}{A_i^{n+1}} \left(\frac{\partial A}{\partial x} \right)_i^{n+1} \right.$$

$$\left. \left. + \frac{\alpha_i^{n+1}}{\rho_i^{n+1}} \frac{\rho_i^{n+1} - \rho_{i-1}^{n}}{\Delta x} \right) \right] \} \qquad \text{(B.11)}$$

where $$BB_i^{n+1} = \frac{1}{C_{v_i}^{n+1} + T_i^{n+1} \left(\frac{\partial C_v}{\partial T} \right)_i^{n+1}}$$

$$T_i^{n+1} = \tfrac{1}{2} \left[T_i^n + \overline{T_i^{n+1}} + \left(\overline{\frac{\partial T}{\partial t}} \right)_i^{n+1} \Delta t \right] \qquad \text{(B.12)}$$

4. Species Equation

a) Predictor

$$\left(\overline{\frac{\partial \varepsilon}{\partial t}} \right)_i^n = \alpha_i^n \frac{\varepsilon_{i+1}^n - 2\varepsilon_i^n + \varepsilon_{i-1}^n}{\Delta x^2}$$

$$+ \frac{\varepsilon_{i+1}^n - \varepsilon_i^n}{\Delta x} \left[-u_i^n + \left(\frac{\partial \alpha}{\partial u} \right)_i^n \frac{u_{i+1}^n - u_i^n}{\Delta x} + \frac{\alpha_i^n}{A_i^n} \left(\frac{\partial A}{\partial x} \right)_i^n \right.$$

$$\left. + \frac{\alpha_i^n}{\rho_i^n} \frac{\rho_{i+1}^n - \rho_i^n}{\Delta x} \right] + \nu_i ZP^{-\beta} \rho_i^n \frac{\varepsilon 1_i^n \varepsilon 2_i^n}{M} e^{-E/RT_i^n} \qquad \text{(B.13)}$$

where ν_i = the stoichiometric mole fractions for the species

$\nu_1 = -1$ for the fuel

$\nu_2 = -3$ for the oxygen

$\nu_3 = +4$ for the product

$$\overline{\varepsilon_i^{n+1}} = \varepsilon_i^n + [(\overline{\frac{\partial \varepsilon}{\partial x}})_i^n]\Delta t \tag{B.14}$$

b) Corrector

$$(\frac{\partial \varepsilon}{\partial t})_i^{n+1} = \alpha_i^{n+1} \frac{\varepsilon_{i+1}^{n+1} - 2\varepsilon_i^{n+1} + \varepsilon_{i-1}^{n+1}}{\Delta x^2}$$

$$+ \frac{\varepsilon_i^{n+1} - \varepsilon_{i-1}^{n+1}}{\Delta x}[-u_i^{n+1} + (\frac{\partial \alpha}{\partial u})_i^{n+1} \frac{u_i^{n+1} - u_{i-1}^{n+1}}{\Delta x} + \frac{\alpha_i^{n+1}}{A_i^{n+1}}(\frac{\partial A}{\partial x})_i^{n+1}$$

$$+ \frac{\alpha_i^{n+1}}{\rho_i^{n+1}} \frac{\rho_i^{n+1} - \rho_{i-1}^{n+1}}{\Delta x}] + \nu_i Z P^{-\beta} \rho_i^{n+1} \frac{\varepsilon 1_i^{n+1} \varepsilon 2_i^{n+1}}{M} e^{-E/RT} \tag{B.15}$$

$$\varepsilon_i^{n+1} = \tfrac{1}{2} [\varepsilon_i^n + \overline{\varepsilon_i^{n+1}} + (\overline{\frac{\partial \varepsilon}{\partial t}})_i^{n+1} \Delta t] \tag{B.16}$$

APPENDIX C

THE NITRIC OXIDE KINETICS

Newhall, H. K. and Shahed, S. M. (1967) used the simple Zeldovich mechanism to simulate the nitric oxide kinetics,

$$O + N_2 \underset{k4}{\overset{k1}{\rightleftharpoons}} NO + N \qquad (C.1)$$

$$N + O_2 \underset{k3}{\overset{k2}{\rightleftharpoons}} NO + O \; . \qquad (C.2)$$

The steady state for nitrogen atom concentration [N] and the equilibrium state for oxygen concentration $[O_2]$ and the oxygen atom concentration [O] were assumed; that is,

$$\frac{d[N]}{dt} = 0, \qquad (C.3)$$

and

$$k0 = \frac{[O]^2}{[O_2]} \; . \qquad (C.4)$$

By using the equations C.1 - C.4, the reaction rate for the nitric oxide was expressed as the following:

$$\frac{d[NO]}{dt} = 2k0^{\frac{1}{2}}k1[O_2]^{\frac{1}{2}}[N_2] \times B.C \qquad [\frac{gm\ moles}{cm^3\ sec}] \qquad (C.5)$$

where $$BC = \frac{1 - \frac{k3k4}{k1k2}\frac{[NO]^2}{[N_2][O_2]}}{1 + \frac{k4[NO]}{k2[O_2]}}$$

$k0 = 14.06 \exp(-115,600/RoT)$ $\left[\frac{\text{gm moles}}{\text{cm}^3}\right]$

$k1 = 7.14 \times 10^{13} \exp(-75,500/RoT)$ $\left[\frac{\text{cm}_3}{\text{gm mole sec}}\right]$

$k2 = 1.20 \times 10^{10} T \exp(-5,500/RoT)$ $\left[\frac{\text{cm}_3}{\text{gm mole sec}}\right]$

$k3 = 3.20 \times 10^{9} T \exp(-39,100/RoT)$ $\left[\frac{\text{cm}_3}{\text{gm mole sec}}\right]$

$k4 = 1.50 \times 10^{13}$ $\left[\frac{\text{cm}_3}{\text{gm mole sec}}\right]$

$[O_2] = \varepsilon_2 \rho$ $\left[\frac{\text{gm moles}}{\text{cm}^3}\right]$

$[N_2] = \varepsilon_5 \rho$ $\left[\frac{\text{gm moles}}{\text{cm}^3}\right]$

$[NO] = \varepsilon_4 \rho$ $\left[\frac{\text{gm moles}}{\text{cm}^3}\right]$

$Ro = 1.987$ [cal/gm mole °K]

$T = 1$ [°K]

$\rho = 1$ $\left[\frac{\text{gm mole}}{\text{cm}^3}\right]$.

By units conversion, and substituting into BC and C.5, and dividing by ρ, one obtains,

$$\left.\frac{\partial \varepsilon_{NO}}{\partial t}\right|_{\text{chem.}} = 5.24 \times 10^{14} \varepsilon_2^{\frac{1}{2}} \varepsilon_5 \rho^{\frac{1}{2}} \exp(-120754.90/T) \times BC \quad \left[\frac{1}{\text{sec}}\right] \qquad (C.6)$$

$$\text{where} \quad BC = \frac{1 - 5.60 \times 10^{-2} \frac{\varepsilon_4^2}{\varepsilon_5 \varepsilon_2} \exp(37956.72/T)}{1 + 2.25 \times 10^{3} \frac{\varepsilon_4}{T \varepsilon_3} \exp(4982.39/T)}$$

ε_2 = mass fraction of oxygen

ε_4 = mass fraction of nitric monoxide

ε_5 = mass fraction of nitrogen

T = gas temperature [°R]

ρ = gas density $\left[\frac{\text{lbm}}{\text{in}^3}\right]$.

APPENDIX D

GAUSSIAN DISTRIBUTION FOR THE IGNITION PROFILES

Assuming Gaussian distribution function for the ignition profile,

$$f(x) = \frac{1}{\sqrt{2\pi\delta^2}} \exp\left[-(x - \mu)^2/2\delta^2\right] \tag{D.1}$$

it gives,

$$\Delta T_i = \Delta T_s \exp[-(I - I_s)^2/2\delta^2] \quad [°R] \tag{D.2}$$

where $\Delta T_s = T_s - T_o$ [°R]

δ = standard deviation.

For the spark temperature calculation, three points are generated: the peak spark, middle spark, and the lower spark. It is assumed that 90.00% oxygen is consumed at peak spark, 12.18% middle spark, and 0.03% lower spark according to the Gaussian distribution function, i.e.,

$$\Delta\epsilon_{2H} = .9000\epsilon_{2s} \tag{D.3}$$

$$\Delta\epsilon_{2M} = .1218\epsilon_{2s} \tag{D.4}$$

$$\Delta\epsilon_{2L} = .0003\epsilon_{2s} \tag{D.5}$$

where $\Delta\epsilon_{2H}$ = the oxygen consumed at peak spark

$\Delta\epsilon_{2M}$ = the oxygen consumed at middle spark

$\Delta\epsilon_{2L}$ = the oxygen consumed at lower spark.

Through the stoichiometric relationship, the fuel consumed at three points can be obtained,

$$\Delta\epsilon_{1H} = 1/3\ \Delta\epsilon_{2H} \tag{D.6}$$

$$\Delta\epsilon_{1M} = 1/3\ \Delta\epsilon_{2M} \tag{D.7}$$

$$\Delta\epsilon_{1L} = 1/3\ \Delta\epsilon_{2L} \tag{D.8}$$

where $\Delta\epsilon_{1H}$ = the fuel consumed at peak spark

$\Delta\epsilon_{1M}$ = the fuel consumed at middle spark

$\Delta\epsilon_{1L}$ = the fuel consumed at lower spark.

The spark ignition temperatures are then estimated through the energy balance equation,

$$hr \times \frac{\Delta A}{A} = n_T \int_{T_o}^{T_f} C_p\, dT \tag{D.9}$$

where $hr = 1.71785 \times 10^8$ [lbf-in/lbm]

$$\frac{\Delta A}{A} = \begin{cases} \dfrac{\Delta\epsilon_{1H}}{\epsilon_{1s}} & \text{for peak spark} \\ \dfrac{\Delta\epsilon_{1M}}{\epsilon_{1s}} & \text{for middle spark} \\ \dfrac{\Delta\epsilon_{1L}}{\epsilon_{1s}} & \text{for lower spark} \end{cases}$$

$$n_T = \frac{1}{\epsilon_{1s}} \quad \text{[moles]}$$

T_f = flame temperature [°R]

$C_p = 2.257196 \times 10^3 - 1.858418 \times 10^5/T + 16.03333 \sqrt{T}$ [Btu/lbm°R].

The standard deviation is estimated by the following equation,

$$\delta = C\,K\left[\frac{1}{2\ln(\Delta T_H/\Delta T_M)}\right]^{\frac{1}{2}}$$

where C = dimensionless constant, 0.5

K = a constant for controlling the number of gride points

ΔT_H = temperature rise at peak spark [°R]

ΔT_M = temperature rise at middle spark [°R].

Since the standard deviation δ determines the steepness of the ignition profile, the constant c can be adjusted to simulate the proper flame thickness. The temperature profile in the vicinity of the spark is then calculated through,

$$T_i = T_o + \Delta T_i. \tag{D.11}$$

The ignition species profile is estimated from the ignition temperature profile accordingly,

$$\frac{\Delta\epsilon_{1i}}{\epsilon_{1o} - \epsilon_{1s}} = \frac{\Delta T_i}{T_s - T_o} \tag{D.12}$$

$$\Delta\epsilon_{1i} = \frac{\epsilon_{1o} - \epsilon_{1s}}{T_s - T_o}\,\Delta T_i \tag{D.13}$$

$$\epsilon_{1i} = \epsilon_{1o} - \Delta\epsilon_{1i}. \tag{D.14}$$

Using the stoichiometric relationship for the reaction,

$$\Delta\varepsilon_{2i} = 3\Delta\varepsilon_{1i} \tag{D.15}$$

$$\Delta\varepsilon_{3i} = -4\Delta\varepsilon_{1i} \tag{D.16}$$

one obtains,

$$\varepsilon_{2i} = \varepsilon_{3o} - \Delta\varepsilon_{2i} \tag{D.17}$$

$$\varepsilon_{3i} = \varepsilon_{3o} - \Delta\varepsilon_{3i} \; . \tag{d.18}$$

The ignition profile for any location can thus be established.

APPENDIX E

HEAT TRANSFER MODEL

For turbulent flow in pipes, the conventional heat transfer relationship is of the form,

$$Nu = f\ (Re,\ Pr,\ D/L). \tag{E.1}$$

By assuming,

(1) constant Prandtl number

(2) neglecting the influence of burned fuel on thermal conductivity of the gas

(3) piston diameter and mean piston speed being characteristic parameters,

Woschni (1967) obtained the correlation,

$$Nu = 0.035\ Re^{0.8}. \tag{E.2}$$

By substituting proper correlations for k, ρ, and μ, Woschni simplified the equation to,

$$h = 110 P^{0.8} W^{0.8} D^{-0.2} T^{-0.53} \qquad [Kcal/m^2 hr °K] \tag{E.3}$$

where P = gas pressure [atm]

W = Wn + Wc, gas velocity [m/sec]

Wn = 2.28 cm [m/sec]

cm = mean piston speed [m/sec]

$Wc = 0.00324\ Ts \frac{Vd}{Vs} \frac{Pf - Pm}{Ps}$ [m/sec]

Ts = gas temperature at spark [°K]

Vd =	engine displacement	[m^3]
Vs =	volume at spark	[m^3]
Pf =	peak firing pressure	[atm]
Pm =	peak motoring pressure	[atm]
Ps =	pressure at spark	[atm]
D =	bore size	[m]
T =	mean gas temperature	[°K] .

By units conversion, one obtains,

$$h = 7.1309 \times 10^{-3} P^{0.8} U^{0.8} D^{-0.2} T^{-0.53} \quad [\text{in-lbf/in}^2\text{sec°R}] \quad \text{(E.4)}$$

where P =	gas pressure	[psi]
U =	gas velocity	[in/sec]
D =	bore size	[in]
T =	mean gas temperature	[°R].

APPENDIX F

THE LEAST SQUARE FITTING OF SPECIFIC HEAT AS A FUNCTION OF TEMPERATURE

Assuming the following case,

$\Phi_p = 1.075$ $\Phi_m = 0.829$

$f_p = 0.081$ $f_m = 0.088$

$V_p = 0.08$ $V_m = 0.92$

and for the stoichiometric combustion reaction,

$$C_2H_4 + 3O_2 + 3 \times 3.764\ N_2 \rightarrow 2CO_2 + 2H_2O + 3 \times 3.764\ N_2 \qquad (F.1)$$

the initial mass fraction of the species were calculated:

Prechamber		Main Chamber
0.0644	C_2H_4	0.0500
0.1818	O_2	0.1836
0.0091	CO_2	0.00985
0.0091	H_2O	0.00985
0.7356	N_2	0.7467

Assuming all the oxygen in the prechamber and all the fuel in the main chamber being consumed at the end of combustion process, the final mass fraction of the species becomes:

Prechamber		Main Chamber
0.0038	C_2H_4	0
0	O_2	0.0336
0.1303	CO_2	0.10985
0.1303	H_2O	0.10985
0.7356	N_2	0.7467 .

Some data of the specific heat at constant pressures as a function of temperature were generated through a subprogram PROPSI (Savage 1977). The correlation for the specific heat at constant pressure of temperature dependence was then established through the least square fitting technique. Assuming the correlation is as following,

$$C_p = a0 + a1/T + a2\sqrt{T} \qquad [\text{lbf-in/lbm°R}]. \quad (F.2)$$

The least square fitting technique (Dorn and McCracken 1972) gives,

$$S = \sum_{i=1}^{m} (C_{pi} - a0 - a1T_i^{-1} - a2T_i^{\frac{1}{2}})^2$$

$$\frac{\partial S}{\partial a0} = \sum_{i=1}^{m} 2(C_{pi} - a0 - a1T_i^{-1} - a2T_i^{\frac{1}{2}})(-1) = 0$$

$$\frac{\partial S}{\partial a1} = \sum_{i=1}^{m} 2(C_{pi} - a0 - a1T_i^{-1} - a2T_i^{\frac{1}{2}})(-T_i^{-1}) = 0$$

$$\frac{\partial S}{\partial a2} = \sum_{i=1}^{m} 2(C_{pi} - a0 - a1T_i^{-1} - a2Ti^{\frac{1}{2}})(-T_i^{\frac{1}{2}}) = 0 .$$

Three equations with the three unknown coefficients can be written as,

$$ma0 + \Sigma T_i^{-1} a1 + \Sigma T_i^{\frac{1}{2}} a2 = \Sigma C_{pi}$$

$$\Sigma T_i^{-1} a0 + \Sigma (T_i^{-1})^2 \, a1 + \Sigma (T_i^{\frac{1}{2}})(T_i^{-1}) \, a2 = \Sigma C_{pi} T_i^{-1}$$

$$\Sigma T_i^{\frac{1}{2}} \, a0 + \Sigma (T_i^{-1})(T_i^{\frac{1}{2}}) \, a1 + \Sigma (T_i^{\frac{1}{2}})^2 \, a2 = \Sigma C_{pi} T_i^{\frac{1}{2}}$$

In matrix form, it appears,

$$\begin{bmatrix} m & \Sigma T_i^{-1} & \Sigma T_i^{\frac{1}{2}} \\ \Sigma T_i^{-1} & \Sigma T_i^{-2} & \Sigma T_i^{-\frac{1}{2}} \\ \Sigma T_i^{\frac{1}{2}} & \Sigma T_i^{-\frac{1}{2}} & \Sigma T_i \end{bmatrix} \begin{bmatrix} a0 \\ a1 \\ a2 \end{bmatrix} = \begin{bmatrix} \Sigma C_{pi} \\ \Sigma C_{pi} T_i^{-1} \\ \Sigma C_{pi} T_i^{\frac{1}{2}} \end{bmatrix}.$$

Through computer programming and calculation, the constant coefficients were obtained,

$$a0 = 2.257196 \times 10^{3}$$

$$a1 = -1.858418 \times 10^{5}$$

$$a2 = 1.603333 \times 10^{1}.$$

The least square fitting with the original data was plotted on Figure 42. The specific heat at constant volume was then calculated through the following relationship,

$$C_v = C_p - R \qquad [\text{lbf-in/lbm°R}] \qquad (F.3)$$

where R = 642.6343 [lbf-in/lbm°R].

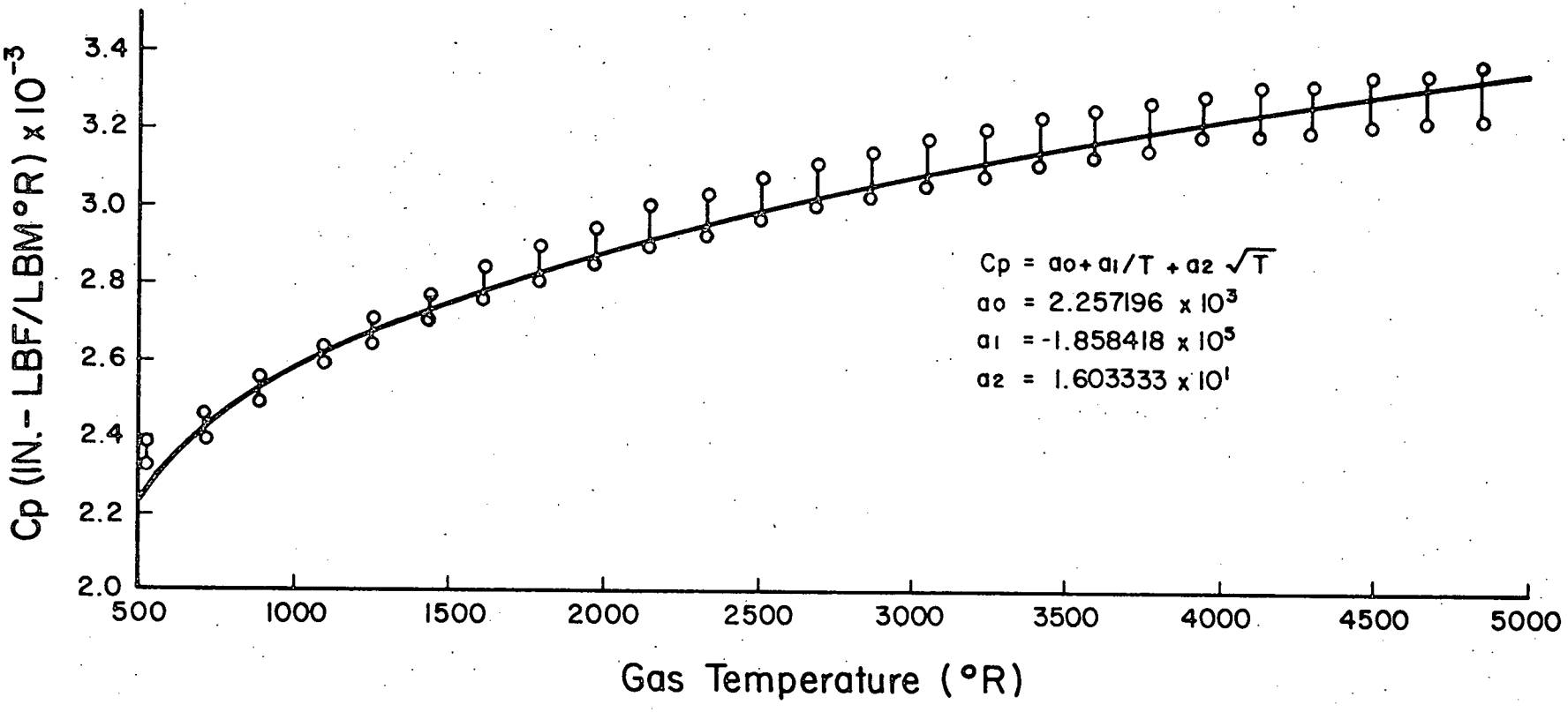

Figure 42. The Least Square Fitting Of Specific Heat Function

The temperature derivative of the specific heat was also calculated,

$$\frac{dC_v}{dT} = \frac{dC_p}{dT} = - a1/T^2 + a2/s\sqrt{T} \quad . \tag{F.4}$$

APPENDIX G

AVERAGE MOLECULAR WEIGHT

For the combustion of ethylene C_2H_4, the stoichiometric reaction is,

$$C_2H_4 + 3O_2 + 3 \times 3.764\ N_2 \longrightarrow 2CO_2 + 2H_2O + 3 \times 3.64\ N_2 \ .$$

The stoichiometric air-fuel ratio has the value of,

$$AF_{st} = \frac{3 \times 4.764 \times 28.96}{2 \times 12 + 4 \times 1.008} = 14.77 \ .$$

The total moles of reactants are,

$$n_R = 1 + 3 + 3 \times 3.764 = 15.29 \ .$$

The average molecular weight of the reactant mixture is thus,

$$M_R = \frac{1}{15.29} \times (2 \times 12 + 4 \times 1.008) + \frac{3 \times 4.764}{15.29} \times (28.96) = 28.90 \ .$$

The total moles of products are,

$$n_p = 2 + 2 + 3 \times 3.764 = 15.29 \ .$$

The average molecular weight of the product mixture is thus,

$$M_p = \frac{2}{15.29} \times (1 \times 12 + 2 \times 16) + \frac{2}{15.29}$$

$$\times (2 \times 1.008 + 1 \times 16) + \frac{3 \times 3.764}{15.29} \times (28) = 28.79 \ .$$

The average molecular weight of the gas mixture is then,

$$\overline{M} = \frac{28.90 + 28.79}{2} = 28.85.$$

Basing on the average molecular weight, the stoichiometric air-fuel ratio becomes,

$$AF_{st} = \frac{3 \times 4.764 \times 28.85}{1 \times 28.85} = 14.292 \ .$$

APPENDIX H

EQUIVALENCE RATIO

1. The Intake Equivalence Ratio Calculation

In the engine case, propane C_3H_8 was used in the prechamber, isooctane C_8H_{18} was used in the main chamber. However, ethylene C_2H_4 was used in the simulation model calculation for simplicity. For the consistency of the comparison, equivalence ratio has to be converted from the engine data. For the combustion of propane C_3H_8, the stoichiometric reaction gives,

$$C_3H_8 + 5O_2 + 5 \times 3.764\ N_2 \rightarrow 3CO_2 + 4H_2O + 5 \times 3.764\ N_2 \ . \qquad (H.1)$$

The stoichiometric air-fuel ratio for propane is,

$$AF_{stC_3H_8} = \frac{5 \times 4.764 \times 28.96}{3 \times 12 + 8 \times 1.008} = 15.66 \ .$$

For the combustion of isooctane C_8H_{18}, the stoichiometric reaction gives,

$$C_8H_{18} + 12.5O_2 + 12.5 \times 3.764\ N_2 \rightarrow 8CO_2 + 9H_2O + 12.5 \times 3.764\ N_2 . \qquad (H.2)$$

The stoichiometric air-fuel ratio for isooctane is,

$$AF_{stC_8H_{18}} = \frac{12.5 \times 4.764 \times 28.96}{8 \times 12 + 18 \times 1.008} = 15.11 \ .$$

The total stoichiometric air-fuel ratio can be calculated by,

$$AF_{Tst} = AF_{stC_3H_8} \times FR + AF_{stC_8H_{18}}(1 - FR) \ . \qquad (H.3)$$

The equivalence ratios of the prechamber, the main chamber, and the total at the intake condition are calculated through,

$$\Phi_{ip} = \frac{AF_{stC_3H_8}}{AF_{ip}} \tag{H.4}$$

$$\Phi_{im} = \frac{AF_{stC_8H_{18}}}{AF_{im}} \tag{H.5}$$

$$\Phi_T = \frac{AF_{Tst}}{AF_T} \quad . \tag{H.6}$$

The air-fuel ratios for the simulation model at the intake condition are then calculated through,

$$AF_{ip} = \frac{AF_{stC_2H_4}}{\Phi_{ip}} \tag{H.7}$$

$$AF_{im} = \frac{AF_{stC_2H_4}}{\Phi_{im}} \tag{H.8}$$

$$AF_T = \frac{AF_{stC_2H_4}}{\Phi_T} \quad . \tag{H.9}$$

2. The Instantaneous Local Equivalence Ratio

Knowing that the stoichiometric reaction has the following form,

$$A + 3B \rightarrow 4C \tag{H.10}$$

and assuming the same average molecular weight for all the substances, the instantaneous combustion reaction equation can be written as,

$$(a + \frac{c}{4})\ A + (b + \frac{3c}{4})\ B \rightarrow C \tag{H.11}$$

where $a = \varepsilon_1$

$b = \varepsilon_2$

$c = \varepsilon_3 - \varepsilon_{30}$.

The instantaneous local equivalence ratio is then obtained,

$$\Phi_i = \frac{AF_{st}}{AF_i} = \frac{3 \times 4.764/1}{(b + \frac{3c}{4})(4.764)/(a + \frac{c}{4})}$$

$$= 3 \left[\frac{a + c/4}{b + 3c/4}\right] \quad . \qquad \text{(H.12)}$$

APPENDIX I

GEOMETRY FUNCTIONS FOR DUAL CHAMBER SYSTEM

1. Prechamber

a) Cylindrical prechamber

$$x_i \leq x_{oi}$$

$$A_i = A_p \tag{I.1}$$

$$\Delta V_i = A_p \Delta x \tag{I.2}$$

$$\frac{\partial A_i}{\partial x} = 0 \tag{I.3}$$

$$\frac{\partial A_i}{\partial t} = 0 \tag{I.4}$$

b) Nozzle shaped orifice

(1) converging section

$$x_{oi} \leq x_i \leq x_{th}$$

$$A_i = A_p - B1\ (x_i - x_{oi}) \tag{I.5}$$

when $x_i = x_{th}$ $A_i = A_{th}$

thus $$B1 = \frac{A_p - A_{th}}{x_{th} - x_{oi}}$$

$$\Delta V_i = \int_{x_{i-\frac{1}{2}}}^{x_{i+\frac{1}{2}}} [A_p - B1(x_i - x_{oi})]dx$$

$$= \Delta x[B3 - B4(x_{i+\frac{1}{2}} + x_{i-\frac{1}{2}})] \tag{I.6}$$

$$A_i = B3 - B4(x_{i+\frac{1}{2}} + x_{i-\frac{1}{2}}) \tag{I.7}$$

where $B3 = A_p + B1\ x_{oi}$

$$B4 = \frac{B1}{2}$$

$$\frac{\partial A_i}{\partial x} = - B1 \tag{I.8}$$

$$\frac{\partial A_i}{\partial t} = 0 \tag{I.9}$$

(2) diverging section

$$x_{th} \leq x_i \leq x_{oo}$$

$$A_i = A_{th} \exp[B2(x_i - x_{th})] \tag{I.10}$$

when $x_i = x_{oo+\frac{1}{2}}$ $A = A_{oo+\frac{1}{2}}$

$$\text{thus } B2 = \frac{\ln(A_{oo+\frac{1}{2}}/A_{th})}{(x_{oo+\frac{1}{2}} - x_{th})}$$

$$\Delta V_i = \int_{x_{i-\frac{1}{2}}}^{x_{i+\frac{1}{2}}} A_{th} \exp[B2(x_i - x_{th})]dx$$

$$+ B5[\exp(B2x_{i+\frac{1}{2}}) - \exp(B2x_{i-\frac{1}{2}})] \tag{I.11}$$

$$\text{where } B5 = \frac{A_{th}}{B2} \exp(-B2\ x_{th})$$

$$A_i = \Delta V_i/\Delta x \tag{I.12}$$

$$\frac{\partial A_i}{\partial x} = A_{th} B2 \exp[B2(x_i - x_{th})] \tag{I.13}$$

$$\frac{\partial A_i}{\partial t} = 0 \tag{I.14}$$

(3) three connecting cells

(a) the orifice inlet

$$x_i = x_{oi}$$

$$A_{oi} = \tfrac{1}{2}[A_p + B3 - B4(x_{oi+\frac{1}{2}} + x_{oi})] \tag{I.15}$$

$$\Delta V_{oi} = A_{oi}\Delta x \tag{I.16}$$

$$\frac{\partial A}{\partial x}_{oi} = -\tfrac{1}{2}B1 \tag{I.17}$$

$$\frac{\partial A}{\partial t}_{oi} = 0 \tag{I.18}$$

(b) the throat

$$x_i = x_{th}$$

$$\Delta V_{th} = \tfrac{1}{2}\Delta x[B3 - B4(x_{th} + x_{th-\frac{1}{2}})] + B5[\exp(B2x_{th+\frac{1}{2}}) - \exp(B2x_{th})] \tag{I.19}$$

$$A_{th} = \Delta V_{th}/\Delta x \tag{I.20}$$

$$\left.\frac{\partial A}{\partial x}\right|_{th} = 0 \tag{I.21}$$

$$\left.\frac{\partial A}{\partial t}\right|_{th} = 0 \tag{I.22}$$

(c) the orifice outlet

$$x_i = x_{oo}$$

$$A_{oo-\frac{1}{2}} = B5[\exp(B2x_{oo}) - \exp(B2x_{oo-\frac{1}{2}})]/\tfrac{1}{2}\Delta x \tag{I.23}$$

$$A_{oo+\frac{1}{2}} = D_{oo+\frac{1}{2}}(H_{oo+\frac{1}{2}} + Y) \tag{I.24}$$

$$A_{oo} = \tfrac{1}{2}(A_{oo-\frac{1}{2}} + A_{oo+\frac{1}{2}}) \tag{I.25}$$

$$\Delta V_{oo} = A_{oo}\Delta x \tag{I.26}$$

$$\left.\frac{\partial A}{\partial x}\right|_{oo} = \frac{A_{oo+\frac{1}{2}} - A_{oo-\frac{1}{2}}}{\Delta x} \tag{I.27}$$

$$\left.\frac{\partial A}{\partial t}\right|_{oo} = \tfrac{1}{2} D_{oo+\frac{1}{2}} \frac{\partial Y}{\partial t} \qquad \text{(I.28)}$$

where $D_{oo+\frac{1}{2}} = D\ (x_{oo+\frac{1}{2}})$

$H_{oo+\frac{1}{2}} = H\ (x_{oo+\frac{1}{2}})$

2. Main Chamber

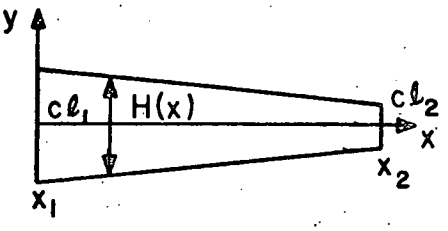

$x_i > x_{oo}$

$y = a + bx$

when $x = x_1$ $y = C\ell_1$ $C\ell_1 = a + bx_1$

when $x = x_2$ $y = C\ell_2$ $C\ell_2 = a + bx_2$

$$a = \frac{C\ell_1 x_2 - C\ell_2 x_1}{x_2 - x_1}$$

$$b = \frac{C\ell_1 - C\ell_2}{x_2 - x_1}$$

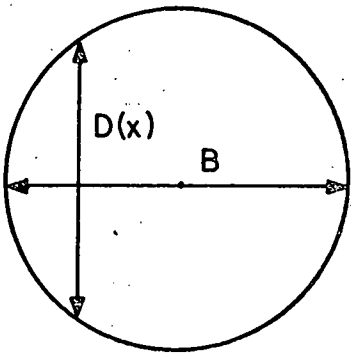

$$y = [(C\ell_1 x_2 - C\ell_2 x_1) - (C\ell_1 - C\ell_2)x]/(x_2 - x_1) \qquad \text{(I.29)}$$

$$H(x) = 2y = \frac{2}{(x_2 - x_1)} [(C\ell_1 x_2 - C\ell_2 x_1) - (C\ell_1 - C\ell_2)x] \qquad \text{(I.30)}$$

$$D(x) = 2\sqrt{(x - x_1)(x_2 - x)} \qquad \text{(I.31)}$$

$$y(t) = RC(1 - \cos\theta) + \frac{RC^2}{4L}(1 - \cos 2\theta) \qquad \text{(I.32)}$$

$$\frac{dH}{dx} = -\frac{2}{(x_2 - x_1)} (C\ell_1 - C\ell_2) \qquad \text{(I.33)}$$

$$\frac{dD}{dx} = \frac{(x_2 - 2x + x_1)}{\sqrt{(x - x_1)(x_2 - x)}} \qquad \text{(I.34)}$$

$$\frac{dy}{dt} = RC\omega\left(\sin\theta + \frac{RC}{2L}\sin 2\theta\right) \qquad \text{(I.35)}$$

$$A(x,t) = D(x)[H(x) + y(t)] \tag{I.36}$$

$$\frac{dA}{dx} = D(x)\,\frac{dH}{dx} + [H(x) + y(t)]\,\frac{dD}{dx} \tag{I.37}$$

$$\frac{dA}{dt} = D(x)\,\frac{dy}{dt} \tag{I.38}$$

APPENDIX J

MIXING MODEL

1. Definition And Assumption

a) General definitions

$$m_{tp} = m_{ap} + m_{fp}$$

$$m_{tm} = m_{am} + m_{fm}$$

$$m_{at} = m_{ap} + m_{am}$$

$$m_{ft} = m_{fp} + m_{fm}$$

$$m_t = m_{tp} + m_{tm} = m_{at} + m_{ft} = m_{ap} + m_{fp} + m_{am} + m_{fm}$$

$$\frac{m_{fp}}{m_{tp}} = \frac{m_{fp}}{m_{ap} + m_{fp}} = \frac{1}{1 + AF_p}$$

$$\frac{m_{fm}}{m_{tm}} = \frac{m_{fm}}{m_{am} + m_{fm}} = \frac{1}{1 + AF_m}$$

$$\frac{m_{ap}}{m_{tp}} = \frac{m_{ap}}{m_{ap} + m_{fp}} = \frac{AF_p}{1 + AF_p}$$

$$\frac{m_{am}}{m_{tm}} = \frac{m_{am}}{m_{am} + m_{fm}} = \frac{AF_m}{1 + AF_m}$$

$$FR = \frac{m_{tp}}{m_t} \qquad m_{tp} = m_t FR$$

$$1 - FR = \frac{m_{tm}}{m_t} \qquad m_{tm} = m_t(1 - FR)$$

b) Special definitions and assumptions

(1) assuming equal density in both chambers

mass through the P.C. intake value = m_t FR

mass to fill the P.C. = $\rho_o V_p = m_t \frac{V_p}{V_T}$

mass of the P.C. overflow into the M.C. = $m_t(FR - \frac{V_p}{V_T})$

percentage of the P.C. intake mass overflow into the M.C.,

$$X = \frac{m_t(FR - \frac{V_p}{V_T})}{m_t FR} = \frac{FR - \frac{V_p}{V_T}}{FR} \qquad (J.1)$$

(2) assuming two zones, ml and m2, in the M.C., where ml is the lean zone in which mixing never occurs, m2 is the intermediate zone which has perfect mixing effect with the overflow from the P.C. The mixing percentage is defined as,

$$PM2 = \frac{m2}{ml + m2} \quad . \qquad (J.2)$$

(3) assuming certain percentage mass of the M.C. flowing back into the P.C. during compression period. According to Hires' derivation (1975),

$$Y = (\frac{V_T - V_s}{V_T - V_p})\frac{V_p}{V_s} \quad . \qquad (J.3)$$

(4) assuming m2 being the portion that flows back into the P.C. during compression, ml stays constant, the mixing percentage changes.

$$m2\phi = m_t(1 - \frac{V_p}{V_T})P\phi M2$$

$$m2,3_s = m_t(1 - \frac{V_p}{V_T}) \sum_{\Theta_\phi}^{\Theta_s} \Delta Y$$

$$m2_s = m2_\phi - m2,3_s = m_t\left(1 - \frac{V_p}{V_T}\right)\left(P\phi M2 - \sum_{\Theta_\phi}^{\Theta_s} \Delta Y\right)$$

$$PsM2 = \frac{m2_s}{m_{ms}} = \left(P\phi M2 - \sum_{\Theta_\phi}^{\Theta_s} \Delta Y\right)\frac{1 - \frac{V_p}{V_T}}{1 - \frac{V_p}{V_{Ts}}} \qquad (J.4)$$

$$P\phi M2 = PsM2\,\frac{1 - \frac{V_p}{V_{Ts}}}{1 - \frac{V_p}{V_T}} + \sum_{\Theta_\phi}^{\Theta_s} \Delta Y \qquad (J.5)$$

2. Air-Fuel Ratio Estimation

a) Overall air-fuel ratio

$$m_{at} = m_{ap} + m_{am} = m_{tp}\frac{m_{ap}}{m_{tp}} + m_{tm}\frac{m_{am}}{m_{tm}} = m_t FR\,\frac{AF_{ip}}{1+AF_{ip}} + m_t(1-FR)\frac{AF_{im}}{1+AF_{im}}$$

$$m_{ft} = m_{fp} + m_{fm} = m_{tp}\frac{m_{fp}}{m_{tp}} + m_{tm}\frac{m_{fm}}{m_{tm}} = m_t FR\,\frac{1}{1+AF_{ip}} + m_t(1-FR)\frac{1}{1+AF_{im}}$$

$$AF_t = \frac{m_{at}}{m_{ft}} = \frac{FR\,\frac{AF_{ip}}{1+AF_{ip}} + (1-FR)\,\frac{AF_{im}}{1+AF_{im}}}{FR\,\frac{1}{1+AF_{ip}} + (1-FR)\frac{1}{1+AF_{im}}} \qquad (J.6)$$

By manipulation, solving for AF_{im}, one obtains,

$$AF_{im} = \frac{AF_{ip}FR(AF_t+1) - AF_t(1+AF_{ip})}{FR(AF_t+1) - (1+AF_{ip})} \qquad (J.7)$$

b) Air-fuel ratio at BDC

$$AF_{\phi mi} = AF_{im} \qquad (J.8)$$

$$m2_{a\phi} = m_t\left[(1-FR)\,\frac{AF_{im}}{1+AF_{im}}\,P\phi M2 + FR\,\frac{AF_{ip}}{1+AF_{ip}}\,X\right]$$

$$m2_{f\phi} = m_t[(1-FR)\ \frac{1}{1+AF_{im}}\ P\phi M2 + FR\ \frac{1}{1+AF_{ip}}\ X]$$

$$AF_{\phi m2} = \frac{m2_{a\phi}}{m2_{f\phi}} = \frac{[(1-FR)\ \frac{AF_{im}}{1+AF_{im}}\ P\phi M2 + FR\ \frac{AF_{ip}}{1+AF_{ip}}\ X]}{[(1-FR)\ \frac{1}{1+AF_{im}}\ P\phi M2 + FR\ \frac{1}{1+AF_{ip}}\ X]} \qquad (J.9)$$

$$AF_{\phi m} = AF_{\phi m1}\ (1-P\phi M2) + AF_{\phi m2}\ (P\phi M2) \qquad (J.10)$$

$$AF_{\phi p} = AF_{ip} \qquad (J.11)$$

c) Air-fuel ratio at spark

$$AF_{sm1} = AF_{\phi m1} = AF_{im} \qquad (J.12)$$

$$AF_{sm2} = AF_{\phi m2} \qquad (J.13)$$

$$\Delta m2,3_{as} = m_t\ (1 - \frac{V_p}{V_T})\ \frac{AF_{\phi m2}}{1+AF_{\phi m2}}\ \Delta Y$$

$$m_{asp} = m_{a\phi p} + \sum_{\Theta_\phi}^{\Theta_s} \Delta m2,3_{as}$$

$$= m_t\ \frac{V_p}{V_T}\ \frac{AF_{ip}}{1+AF_{ip}} + \sum_{\Theta_\phi}^{\Theta_s} m_t\ (1 - \frac{V_p}{V_T})\ \frac{AF_{\phi m2}}{1+AF_{\phi m2}}\ \Delta Y$$

$$= m_t\ [\frac{V_p}{V_T}\ \frac{AF_{ip}}{1+AF_{ip}} + (1- \frac{V_p}{V_T})\ \frac{AF_{\phi m2}}{1+AF_{\phi m2}}\ \sum_{\Theta_\phi}^{\Theta_s} \Delta Y]$$

$$m_{fsp} = m_t[\frac{V_p}{V_T}\ \frac{1}{1+AF_{ip}} + (1 - \frac{V_p}{V_T})\ \frac{1}{1+AF_{\phi m2}}\ \sum_{\Theta_\phi}^{\Theta_s} \Delta Y]$$

$$AF_{sp} = \frac{m_{asp}}{m_{fsp}} = \frac{[\frac{V_p}{V_T}\frac{AF_{ip}}{1+AF_{ip}} + (1-\frac{V_p}{V_T})\frac{AF_{\phi m2}}{1+AF_{\phi m2}} \sum_{\Theta_\phi}^{\Theta_s} \Delta Y]}{[\frac{V_p}{V_T}\frac{1}{1+AF_{ip}} + (1-\frac{V_p}{V_T})\frac{1}{1+AF_{\phi m2}} \sum_{\Theta_\phi}^{\Theta_s} \Delta Y]} \quad \text{(J.14)}$$

3. Residual Estimation

a) Overall products

$$A + \frac{3}{\Phi_T}(B + 3.764D) \rightarrow (\frac{3}{\Phi_T} - 3)\,B + 4C + \frac{3}{\Phi_T} \times 3.764D$$

$$n_p = (\frac{3}{\Phi_T} - 3) + 4 + \frac{3}{\Phi_T} \times 3.764$$

$$f_2 = \frac{(\frac{3}{\Phi_T} - 3)}{n_p}$$

$$f_3 = \frac{4}{n_p}$$

b) Mixing model

at TDC

$$f_p = f_T \frac{V_p}{V_c}$$

$$f_m = f_T - f_p$$

assuming the residual perfectly mixed with the intake fresh change in both the P.C. and the M.C.

$$m_T = m_t + m_R$$

$$\frac{m_{Rp}}{m_t + m_{Rp} + m_{Rm}} = f_p$$

$$\frac{m_{Rp}}{m_t + m_{Rp} + m_{Rm}} = f_m$$

By solving the equations, one obtains,

$$m_{Rp} = C1 m_t \tag{J.15}$$

$$m_{Rm} = C2 m_t \tag{J.16}$$

where $C1 = \frac{f_p}{1 - f_t}$

$$C2 = \frac{f_m}{1 - f_t} .$$

The total mass in the engine becomes,

$$m_T = m_t + m_{Rp} + m_{Rm} = (1 + C1 + C2)\, m_t \tag{J.17}$$

4. Mass Fraction Estimation

a) Mass fraction of residuals

(1) at TDC

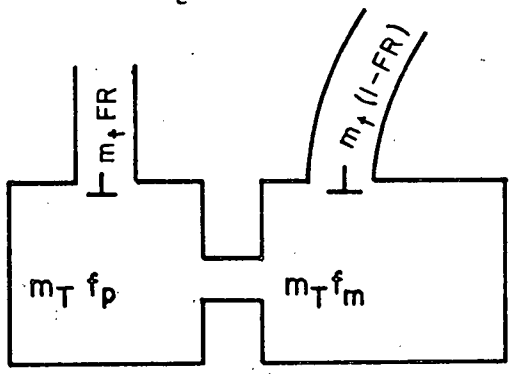

$$\varepsilon f_{ip} = \frac{m_T f_p}{m_t FR + m_T f_p}$$

$$= \frac{(1 + C1 + C2) f_p}{FR + (1 + C1 + C2) f_p} \tag{J.18}$$

$$\varepsilon f_{im} = \frac{m_T f_m}{m_t (1 - FR) + m_T f_m}$$

$$= \frac{(1 + C1 + C2) f_m}{(1 - FR) + (1 + C1 + C2) f_m} \tag{J.19}$$

(2) at BDC

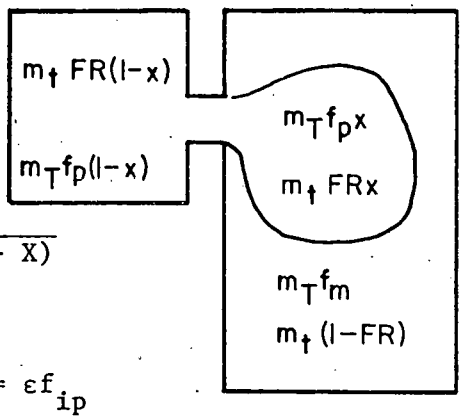

$$\varepsilon f_{\phi p} = \frac{m_T f_p (1 - X)}{m_t FR(1 - X) + m_T f_p (1 - X)}$$

$$= \frac{(1 + C1 + C2) f_p}{FR + (1 + C1 + C2) f_p} = \varepsilon f_{ip} \qquad \text{(J.20)}$$

$$\varepsilon f_{\phi m} = \frac{m_T f_p X + m_T f_m}{m_T f_m + m_T f_p X + m_t (1-FR) + m_t FRX}$$

$$= \frac{(1 + C1 + C2)(F_m + f_p X)}{(1 + C1 + C2)(f_m + f_p X) + (1 - FR + FRX)} \qquad \text{(J.21)}$$

Assuming the mass fraction of the residuals in both the P.C. and the M.C. are uniform at all the time i.e.,

$$\varepsilon f_{ip} = \varepsilon f_{im} \qquad \text{(J.22)}$$

$$\varepsilon f_{\phi p} = \varepsilon f_{\phi m} \qquad \text{(J.23)}$$

$$\varepsilon f_{sp} = \varepsilon f_{sm} \, . \qquad \text{(J.24)}$$

b) Mass fraction of species

(1) at BDC

$$m_{R\phi p} = m_{Rp} (1 - X) = C1(1 - X) m_t$$

$$m_{R\phi m} = m_{Rm} + m_{Rp} X = (C2 + C1X) m_t$$

$$m_{f\phi p} = \rho_o V_p \frac{m_{fp}}{m_{tp}} = m_t \frac{V_p}{V_T} \frac{1}{1+AF_{ip}}$$

$$m_{a\phi p} = \rho_o V_p \frac{m_{ap}}{m_{tp}} = m_t \frac{V_p}{V_T} \frac{AF_{ip}}{1+AF_{ip}}$$

$$m_{t\phi p} = m_t \frac{V_p}{V_T}$$

$$m_{T\phi p} = m_{t\phi p} + m_{R\phi p} = m_t [\frac{V_p}{V_T} + C1(1-X)]$$

$$m_{f\phi m} = m_t \frac{m_{tm}}{m_t} \frac{m_{fm}}{m_{tm}} + m_t \frac{m_{tp}}{m_t} \frac{m_{fp}}{m_{tp}} X$$

$$= m_t [(1-FR) \frac{1}{1+AF_{im}} + FR \frac{1}{1+AF_{ip}} X]$$

$$m_{a\phi m} = m_t \frac{m_{tm}}{m_t} \frac{m_{am}}{m_{tm}} + m_t \frac{m_{tp}}{m_t} \frac{m_{ap}}{m_{tp}} X$$

$$= m_t [(1-FR) \frac{AF_{im}}{1+AF_{im}} + FR \frac{AF_{ip}}{1+AF_{ip}} X]$$

$$m_{t\phi m} = m_{f\phi m} + m_{a\phi m} = m_t [1 - FR + FRX]$$

$$m_{T\phi m} = m_{t\phi m} + m_{R\phi m} = m_t [1 - FR + FRX + C2 + C1X]$$

Let $f_{\phi p} = C1 \ (1 - X)$

$f_{\phi m} = C2 + C1X$

$G_T = 1 + C1 + C2$

$$G_{T\phi p} = \frac{V_p}{V_T} + C1\ (1 - X)$$

$$G_{T\phi M} = 1 - FR + FRX + C2 + C1X$$

$$\varepsilon_{1\phi p} = \frac{m_{f\phi p}}{m_{T\phi p}} = \frac{V_p}{V_T} \frac{1}{1+AF_{ip}} /G_{T\phi p} \qquad (J.25)$$

$$\varepsilon_{2\phi p} = \frac{m_{a\phi p}/4.764 + m_{R\phi p} f_2}{m_{T\phi p}} = [\frac{V_p}{V_T} \frac{AF_{ip}}{1+AF_{ip}} /4.764 + f_{\phi p}\ f_2]/G_{T\phi p} \qquad (J.26)$$

$$\varepsilon_{3\phi p} = \frac{m_{R\phi p} f_3}{m_{T\phi p}} = f_{\phi p} f_3 / G_{T\phi p} \qquad (J.27)$$

$$\varepsilon_{5\phi p} = 1 - \varepsilon_{1\phi p} - \varepsilon_{2\phi p} - \varepsilon_{3\phi p} \qquad (J.28)$$

$$\varepsilon_{1\phi m2} = \frac{m_{f\phi m2}}{m_{T\phi m} P\phi M2} = [(1-FR) \frac{1}{1+AF_{im}}\ P\phi M2 + FR \frac{1}{1+AF_{ip}} X]/G_{T\phi m} P\phi M2 \qquad (J.29)$$

$$\varepsilon_{2\phi m2} = \frac{m_{a\phi m2}/4.764 + m_{R\phi m} f_2 P\phi M2}{m_{T\phi m} P\phi M2}$$

$$= \{[(1-FR) \frac{AF_{im}}{1+AF_{im}} P\phi M2 + FR \frac{AF_{ip}}{1+AF_{ip}} X]/4.764$$

$$+ f_{\phi m} f_2 P\phi M2\}/G_{T\phi m} P\phi M2 \qquad (J.30)$$

$$\varepsilon_{3\phi m2} = \frac{m_{R\phi m} f_3 P\phi M2}{M_{T\phi m} P\phi M2} = f_{\phi m} f_3 / G_{T\phi m} \qquad (J.31)$$

$$\varepsilon_{5\phi m2} = 1 - \varepsilon_{1\phi m2} - \varepsilon_{2\phi m2} - \varepsilon_{3\phi m2} \qquad (J.32)$$

$$m_{f\phi m1} = m_t \frac{m_{tm}}{m_t} \frac{m_{fm}}{m_{tm}} (1 - P\phi M2) = m_t (1 - FR) \frac{1}{1+AF_{im}} (1 - P\phi M2)$$

$$m_{a\phi m1} = m_t \frac{m_{tm}}{m_t} \frac{m_{am}}{m_{tm}} (1 - P\phi M2) = m_t (1 - FR) \frac{AF_{im}}{1+AF_{im}} (1 - P\phi M2)$$

$$\varepsilon_{1\phi m1} = \frac{m_{f\phi m1}}{m_{T\phi m}(1-P\phi M2)} = (1 - FR) \frac{1}{1+AF_{im}} / G_{T\phi m} \qquad (J.33)$$

$$\varepsilon_{2\phi m1} = \frac{m_{a\phi m1}/4.764 + m_{R\phi m} f_2 (1 - P\phi M2)}{m_{T\phi m} (1 - P\phi M2)}$$

$$= [(1 - FR) \frac{AF_{im}}{1+AF_{im}}/4.764 + f_{\phi m} f_2]/G_{T\phi m} \qquad (J.34)$$

$$\varepsilon_{3\phi m1} = \frac{m_{R\phi m} f_3 (1 - R\phi M2)}{M_{T\phi m}(1 - P\phi M2)} = f_{\phi m} f_3 / G_{T\phi m} \qquad (J.35)$$

$$\varepsilon_{5\phi m1} = 1 - \varepsilon_{1\phi m1} - \varepsilon_{2\phi m1} - \varepsilon_{3\phi m1} \qquad (J.36)$$

(2) at spark

$$\frac{m_{R\phi p}}{m_{T\phi p}} = \frac{f_{\phi p}}{G_{T\phi p}}$$

$$\frac{m_{R\phi m}}{m_{T\phi m}} = \frac{f_{\phi m}}{G_{T\phi m}}$$

$$m_{Rsm} = \rho_s (V_m + V_{ds}) \frac{m_{R\phi m}}{m_{T\phi m}} = m_t (1 - \frac{V_p}{V_{Ts}}) \frac{f_{\phi m}}{G_{T\phi m}}$$

$$m_{RT} = m_{Rp} + m_{Rm} = (C1 + C2) m_t$$

$$m_{Rsp} = m_{RT} - m_{Rsm} = [C1 + C2 - (1 - \frac{V_p}{V_{Ts}}) \frac{f_{\phi m}}{G_{T\phi m}}] \, m_t$$

$$m_{Tsp} = m_{fsp} + m_{asp} + m_{Rsp}$$

$$= m_t [\frac{V_p}{V_T} + (1 - \frac{V_p}{V_T}) \sum_{\Theta_\phi}^{\Theta_s} \Delta Y + C1 + C2 - (1 - \frac{V_p}{V_{Ts}}) \frac{f_{\phi m}}{G_{T\phi m}}]$$

$$m_{Tsm} = m_T - m_{Tsp} = m_t [(1 - \frac{V_p}{V_T})(1 - \sum_{\Theta_\phi}^{\Theta_s} \Delta Y) + (1 - \frac{V_p}{V_{Ts}}) \frac{f_{\phi m}}{G_{T\phi m}}]$$

Let $f_{sp} = C1 + C2 - (1 - \frac{V_p}{V_{Ts}}) \frac{f_{\phi m}}{G_{T\phi m}}$

$$f_{sm} = (1 - \frac{V_p}{V_{Ts}}) \frac{f_{\phi m}}{G_{T\phi m}}$$

$$G_{Tsp} = \frac{V_p}{V_T} + (1 - \frac{V_p}{V_T}) \sum_{\Theta_\phi}^{\Theta_s} \Delta Y + C1 + C2 - (1 - \frac{V_p}{V_{Ts}}) \frac{f_{\phi m}}{G_{T\phi m}}$$

$$G_{Tsm} = (1 - \frac{V_p}{V_T})(1 - \sum_{\Theta_\phi}^{\Theta_s} \Delta Y) + (1 - \frac{V_p}{V_{Ts}}) \frac{f_{\phi m}}{G_{T\phi m}}$$

$$\varepsilon_{1sp} = \frac{m_{fsp}}{m_{Tsp}} = [\frac{V_p}{V_T} \frac{1}{1+AF_{ip}} + (1 - \frac{V_p}{V_T}) \frac{1}{1+AF_{\phi m2}} \sum_{\Theta_\phi}^{\Theta_s} \Delta Y]/G_{Tsp} \qquad (J.37)$$

$$\varepsilon_{2sp} = \frac{m_{asp}/4.764 + m_{Rsp} f_2}{m_{Tsp}}$$

$$= \{[\frac{V_p}{V_T} \frac{AF_{ip}}{1+AF_{ip}} + (1 - \frac{V_p}{V_T}) \frac{AF_{\phi m2}}{1+AF_{\phi m2}} \sum_{\Theta_\phi}^{\Theta_s} \Delta Y]/4.764 + f_{sp} f_2\}/G_{Tsp} \qquad (J.38)$$

$$\varepsilon_{3sp} = \frac{m_{Rsp} f_3}{m_{Tsp}} = f_{sp} f_3 / G_{Tsp} \tag{J.39}$$

$$\varepsilon_{5sp} = 1 - \varepsilon_{1sp} - \varepsilon_{2sp} - \varepsilon_{3sp} \tag{J.40}$$

$$m_{f\phi m2} = m_t \left(1 - \frac{V_p}{V_T}\right) P\phi M2 \frac{1}{1+AF_{\phi m2}}$$

$$m_{a\phi m2} = m_t \left(1 - \frac{V_p}{V_T}\right) P\phi M2 \frac{AF_{\phi m2}}{1+AF_{\phi m2}}$$

$$m_{asm2} = m_{a\phi m2} - \sum_{\Theta_\phi}^{\Theta_s} \Delta m_{asm2,3}$$

$$= m_t \left(1 - \frac{V_p}{V_T}\right) \frac{AF_{\phi m2}}{1+AF_{\phi m2}} \left[P\phi M2 - \sum_{\Theta_\phi}^{\Theta_s} \Delta Y\right]$$

$$m_{fsm2} = m_t \left(1 - \frac{V_p}{V_T}\right) \frac{1}{1+AF_{\phi m2}} \left[P\phi M2 - \sum_{\Theta_\phi}^{\Theta_s} \Delta Y\right]$$

$$\varepsilon_{1sm2} = \frac{m_{fsm2}}{m_{Tsm} PsM2} = \left(1 - \frac{V_p}{V_T}\right) \frac{1}{1+AF_{\phi m2}} \left[P\phi M2 - \sum_{\Theta_\phi}^{\Theta_s} \Delta Y\right] / G_{Tsm} PsM2 \tag{J.41}$$

$$\varepsilon_{2sm2} = \frac{m_{asm2}/4.764 + m_{Rsm} f_2 PsM2}{M_{Tsm} PsM2}$$

$$= \left\{\left(1 - \frac{V_p}{V_T}\right) \frac{AF_{\phi m2}}{1+AF_{\phi m2}} \left[P\phi M2 - \sum_{\Theta_\phi}^{\Theta_s} \Delta Y\right]/4.764 + f_{sm} f_2 PsM2\right\} / G_{Tsm} PsM2 \tag{J.42}$$

$$\varepsilon_{3sm2} = \frac{m_{Rsm} f_3 PsM2}{m_{Tsm} PsM2} = f_{sm} f_3 / G_{Tsm} \tag{J.43}$$

$$\varepsilon_{5sm2} = 1 - \varepsilon_{1sm2} - \varepsilon_{2sm2} - \varepsilon_{3sm2} \tag{J.44}$$

$$m_{fsm1} = m_t \left(1 - \frac{V_p}{V_{Ts}}\right) \frac{1}{1+AF_{im}} (1 - PsM2)$$

$$m_{asm1} = m_t \left(1 - \frac{V_p}{V_{Ts}}\right) \frac{AF_{im}}{1+AF_{im}} (1 - PsM2)$$

$$\varepsilon_{1sm1} = \frac{m_{fsm1}}{m_{Tsm}(1 - PsM2)} = \left(1 - \frac{V_p}{V_{Ts}}\right) \frac{1}{1+AF_{im}} / G_{Tsm} \qquad (J.45)$$

$$\varepsilon_{2sm1} = \frac{m_{asm1}/4.764 + m_{Rsm} f_2 (1 - PsM2)}{m_{Tsm}(1 - PsM2)}$$

$$= \left[\left(1 - \frac{V_p}{V_{Ts}}\right) \frac{AF_{im}}{1+AF_{im}} /4.764 + f_{sm} f_2\right] / G_{Tsm} \qquad (J.46)$$

$$\varepsilon_{3sm1} = \frac{m_{Rsm} f_2 (1 - PsM2)}{m_{Tsm}(1 - PsM2)} = f_{sm} f_3 / G_{Tsm} \qquad (J.47)$$

$$\varepsilon_{5sm1} = 1 - \varepsilon_{1sm1} - \varepsilon_{2sm1} - \varepsilon_{3sm} \qquad (J.48)$$

APPENDIX K

DESCRIPTION AND LISTING OF COMPUTER PROGRAM

1. Main Program

Originally, there was a long main program. When the model became more complex, all the sections which have a specific routine task were programmed into subroutines. Then, the main program had a compact form and became more distinctive and understandable. The flow chart of the main program is illustrated on Figure 43.

2. Subroutines

a) INI

This is the initialization subroutine for the model. All the initial values are calculated and assigned. All the constant values are calculated in this subroutine.

b) MIX

This is the subroutine for the species mixing between the fresh charge and the residuals, the rich mixture in the prechamber and the lean mixture in the main chamber. All the air-fuel ratios and the concentration of the species of the three mixing zones are calculated for at the time of spark.

c) GOM

This is the geometry functions subroutine. The spatial locations, the cross section areas, the perimeters, the area derivatives, the individual cell volumes, and the total volume are all calculated in this subroutine.

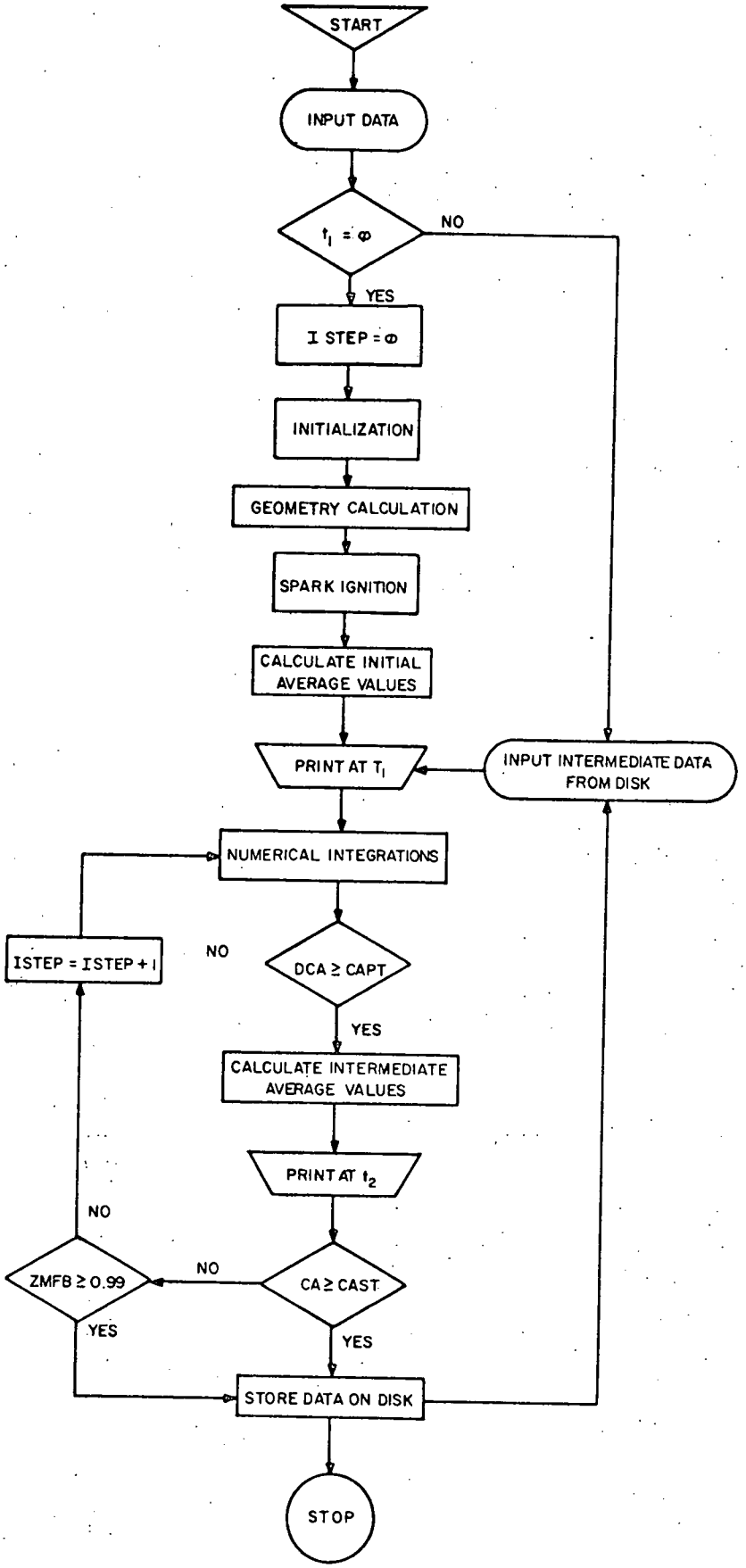

Figure 43. Simulation Model Main Computer Program Flow Chart

d) SPK

This is the subroutine simulating the spark ignition. The ignition temperature is estimated through energy balance equation. After the spark location is defined, A Gaussian temperature profile is assigned in the vicinity of the spark. The proper species concentration profiles are also estimated according to the temperature profile. The ignition is thus established. The detailed theory is given in Appendix D.

e) SUM

This is the subroutine for calculating the instantaneous mean values in the dual chamber system. First it sums up all the local numerical quantities of a specific variable in each chamber. The average value of that variable in each chamber is then calculated by dividing the summation over the number of grid points in each chamber. The mass fraction burned and the average values of the pressure, the equivalence ratio, and the species concentration can be obtained at any time when the subroutine is called. The detail of the local equivalence ratio calculation is given in Appendix H2. The detail of the mass fraction burned calculation appears in Appendix I.

f) PRC

This is the output subroutine for all the constant parameters. The constant parameters are classified as the geometrical parameters, the operating parameters, the thermal parameters, and the numerical

parameters. By this way, output formats can be separated from the main program.

g) PRV

This is the output subroutine for all the variable parameters. Any parameter which is a function of either space or time belongs to this category. The intermediate values of all the variables can be printed out at any time when this subroutine is called. The frequency of the output is controlled by an input parameter of crank angle interval. Since both PRC and PRV have the same structure and data block, two programs are combined into one single subroutine by a multiple entries feature. PRC is the main subprogram; PRV is associated to it by an entry point.

h) INT

This is the subroutine for numerical integration. The MacCormack predictor-corrector scheme is programed into this subroutine. It can be easily substituted by any other standard numerical integration technique.

i) DER

This is the subroutine for derivatives. All the spatial derivatives and the temporal derivatives are included in this subroutine. Again, it can be easily modified by changing the equations to simulate different systems.

j) TMP

This is the subroutine for thermal properties calculation. The mean gas temperature of the system, the specific heats, and the overall heat transfer coefficient are calculated through this subroutine.

k) TTD

This is the subroutine for the turbulent diffusivity model. The turbulent diffusivity is calculated by this subroutine.

l) TSC

This is the subroutine for restricted time step control. The feature and the purpose of the restricted time step control has been discussed in section C2b) of Chapter IV.

m) BOD

This is the subroutine for the boundary conditions. It is easily changed for any modification of the boundary conditions for different problems.

3. Subfunctions

a) FX(W)

This is the subfunction for spatial location calculation. Any integer grid point can be transferred into exact spatial location through this function.

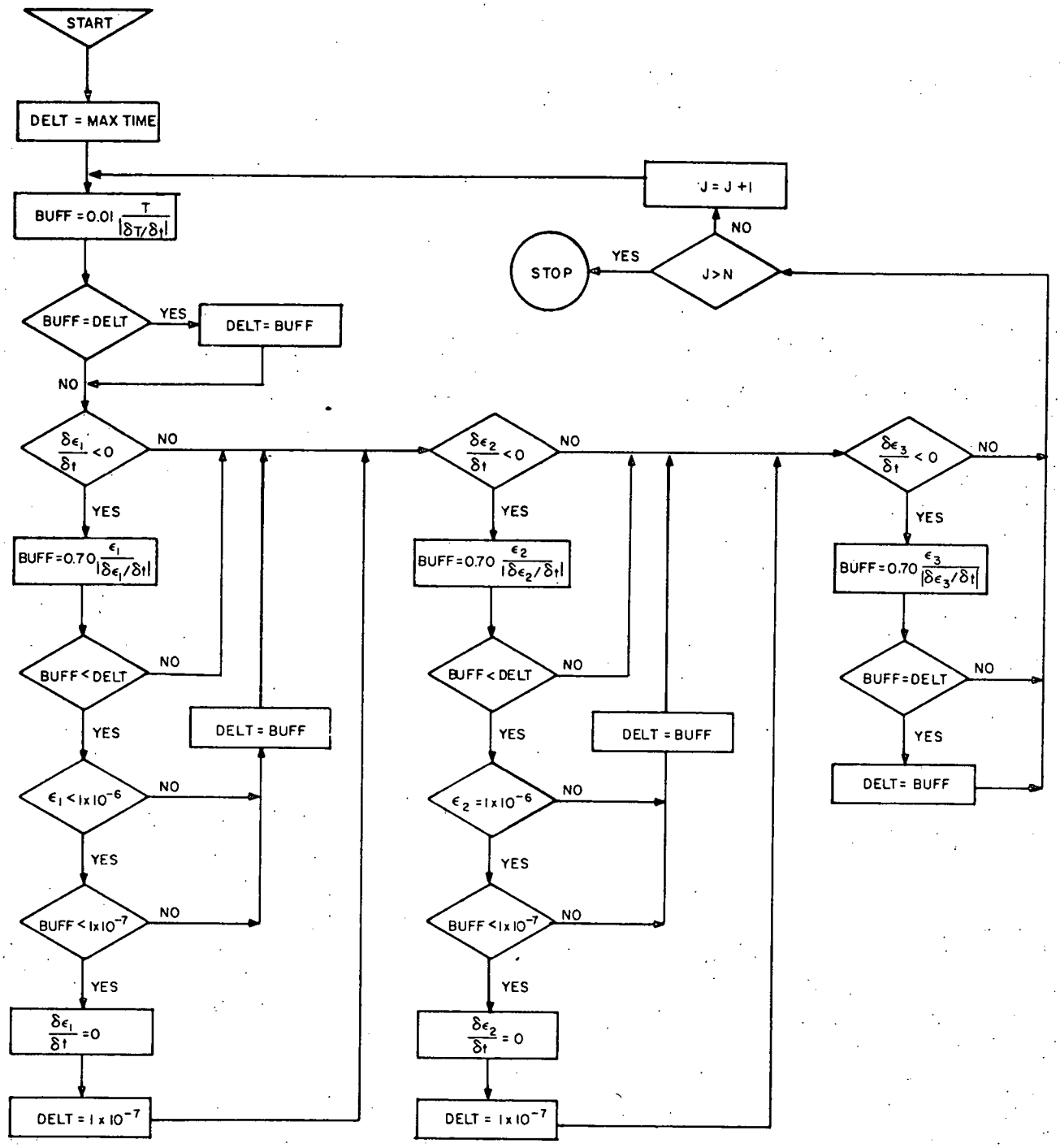

Figure 44. Restricted Time Step Size Control Program Flow Chart

b) FD(W)

This is the subfunction for the chord length calculation. The chord length of the main chamber at any location is calculated through this function.

c) FH(W)

This is the subfunction for the clearance height calculations. The clearance height at any location in the main chamber can be obtained through this function.

4. Common Data Block

Common blocks have been used for communicating the specific data between the main program and the subroutines or between the subroutines. Through the common blocks, not only it can share the memory space among the programs, but also eliminate the parameter list in the SUBROUTINE and the CALL statements. All the data which is in the common blocks can be initialized in this common data block.

5. Computer FORTRAN Names

A	area
AFIM	M.C. intake A/F
AFIP	P.C. intake A/F
AFIT	total intake A/F
AFSM1	A/F of M.C. lean zone at spark time
AFSM2	A/F of M.C. intermediate zone at spark time
AFSP	A/F of P.C. at spark time
AFST	total A/F at spark time
AFSTM	stoichiometric A/F for C_8H_{18} in M.C.
AFSTP	stoichiometric A/F for C_3H_8 in P.C.
AFSTT	overall stoichiometric A/F
AFΦM	M.C. A/F at BDC
AFΦMI	A/F of M.C. lean zone at BDC
AFΦM2	A/F of M.C. intermediate zone at BDC
AL	turbulent diffusivity
ALU	derivative of turbulent diffusivity with respect to the velocity, $\frac{\partial \alpha}{\partial u}$
ALO	initial turbulent diffusivity
AM	stoichiometric coefficient of fuel
AMW	average molecular weight
ANG	crank angle in radian
AOMR	stoichiometric mole fraction for air
AOOM	cross section area at $X_{oo-\frac{1}{2}}$
AOOP	cross section area at $X_{oo+\frac{1}{2}}$

AP	cross section area of P.C.
APS	piston area
AREN	chemical kinetics for the combustion
ARENO	chemical kinetics for NO
AT	time derivative of area function, $\frac{\partial A}{\partial t}$
ATDA	$\frac{1}{A}\frac{\partial A}{\partial t}$
ATDVP	ratio of throat area to P.C. volume, A_{th}/V_p
ATH	orifice throat area
AX	spatial derivative of area function, $\frac{\partial A}{\partial x}$
AXDA	$\frac{1}{A}\frac{\partial A}{\partial x}$
A0, A1, A2	constant coefficients for specific heat function
BA	variable in energy equation
BB	variable in energy equation
BBM	stoichiometric mole fraction of oxygen for C_8H_{18}
BBP	stoichiometric mole fraction of oxygen for C_3H_8
BC	variable in chemical kinetic equation
BD	variable in energy equation
BM	stoichiometric coefficient of oxygen
BOD	subroutine for boundary values
BORE	bore size
BSQ	square of the bore size
BSY	function of bore size
BUF	maximum time step size under control
B1, B2, B3, B4, B5	constant coefficients for geometry functions
CA	crank angle in degree

CAPT	crank angle duration for output
CAR	reference crank angle
CAST	crank angle for data storage
CL	average M.C. clearance
CLL	maximum M.C. clearance
CLR	minimum M.C. clearance
CM	stoichiometric coefficient of product
COI	node location of orifice inlet in real number
COO	node location of orifice outlet in real number
CP	specific heat at constant pressure
CR	compression ratio
CS	constant coefficient for turbulent model
CSP	node location of spark in real number
CT	derivative of specific heat with respect to temperature, $\frac{\partial C}{\partial T}$
CTH	node location of throat in real number
CV	specific heat at constant volume
C1,C2,C3	constant coefficients for residual fractions
D	M.C. chord
DAH	variable in spark temperature calculation
DAM	variable in spark temperature calculation
DCA	crank angle difference
DCL	clearance difference
DCX	clearance function
DEG	conversion factor from radian to degree
DELT	time step size

DELTA	standard deviation for Gaussian distribution function
DELX	spatial grid size
DER	Subroutine for the derivative equations
DE1	function of fuel consumption
DEIDT	proportional function for fuel in the ignition model
DE2	function of oxygen consumption
DE2DT	proportional function for oxygen in the ignition model
DE2H	mass fraction of oxygen consumed at peak spark temperature
DE2M	mass fraction of oxygen consumed at middle spark temperature
DE3	function of product formation
DIAP	diameter of P.C.
DIAT	diameter of throat
DLTMAX	maximum time step
DLTMIN	minimum time step
DLXHF	$\frac{1}{2}\Delta X$
DLXSQ	ΔX^2
DM	differential mass
DOOP	$D(X_{oo+\frac{1}{2}})$
DPP	peak pressure difference between firing and motoring
DT	Gaussian distribution function for temperature profile
DV	differential volume
DVP	differential volume in P.C.
DVR	VSR/VTR
DX	spatial derivative of D function, $\frac{dD}{dx}$
EDR	ratio of activation energy to universal gas constant, E/Ro

EMIN minimum value for the species mass fraction

ENER1, ENER2, ENER3, ENER4 lumped terms used in the energy equation

EPC maximum percentage of species consumption

E1 mass fraction of fuel

E1F predicted E1 at $t + \Delta t$

E1S E1 at spark time

E1SM1 E1 of M.C. lean zone at spark time

E1SM2 E1 of M.C. intermediate zone at spark time

E1SP E1 of P.C. at spark time

E1T time derivative of E1, $\frac{\partial \epsilon_1}{\partial t}$

E1X spatial derivative of E1, $\frac{\partial \epsilon 1}{\partial x}$

E1XX second spatial derivative of E1, $\frac{\partial^2 \epsilon 1}{\partial x^2}$

E1ΦM1 E1 of M.C. lean zone at BDC

E1ΦM2 E1 of M.C. intermediate zone at BDC

E1ΦP E1 of P.C. at BDC

E2 mass fraction of oxygen

E2F predicted E2 at $t + \Delta t$

E2S E2 at spark time

E2SM1 E2 of M.C. lean zone at spark time

E2SM2 E2 of M.C. intermediate zone at spark time

E2SP E2 of P.C. at spark time

E2T time derivative of E2, $\frac{\partial \epsilon 2}{\partial t}$

E2X spatial derivative of E2, $\frac{\partial \epsilon 2}{\partial x}$

E2XX second spatial derivative of E2, $\frac{\partial^2 \epsilon 2}{\partial x 2}$

E2ΦM1 E2 of M.C. lean zone at BDC

E2ΦM2	E2 of M.C. intermediate zone at BDC
E2ΦP	E2 of P.C. at BDC
E3	mass fraction of product
E3F	predicted E3 at $t + \Delta t$
E3SM1	E3 of M.C. lean zone at spark time
E3SM2	E3 of M.C. intermediate zone at spark time
E3SP	E3 of P.C. at spark time
E3T	time derivative of E3, $\frac{\partial \varepsilon 3}{\partial t}$
E3X	spatial derivative of E3, $\frac{\partial \varepsilon 3}{\partial x}$
E3XX	second spatial derivative of E3, $\frac{\partial^2 \varepsilon 3}{\partial x^2}$
E30	initial E3
E3ΦM1	E3 of M.C. lean zone at BDC
E3ΦM2	E3 of M.C. intermediate zone at BDC
E3ΦP	E3 of P.C. at BDC
E4	mass fraction of nitric monoxide
E4F	predicted E4 at $t + \Delta t$
E4T	time derivative of E4, $\frac{\partial \varepsilon 4}{\partial t}$
E4X	spatial derivative of E4, $\frac{\partial \varepsilon 4}{\partial x}$
E4XX	second spatial derivative of E4, $\frac{\partial^2 \varepsilon 4}{\partial x^2}$
E5	mass fraction of nitrogen
E5F	predicted E5 at $t + \Delta t$
E5SM1	E5 of M.C. lean zone
E5SM2	E5 of M.C. intermediate zone
E5SP	E5 of P.C. at spark time
E5ΦM1	E5 of M.C. lean zone at BDC

E5ΦM2	E5 of M.C. intermediate zone at BDC
E5ΦP	E5 of P.C. at BTC
FD(W)	function of M.C. chord
FH(W)	function of M.C. clearance
FM	M.C. residual fraction
FODPI	$4/\pi$
FOTPI	4π
FOUR	four
FM	M.C. residual fraction
FP	P.C. residual fraction
FR	P.C. intake mass flow ratio
FRMVPT	FR - VP/VTT
FRT	total intake mass flow rate
FSM	residual fraction in M.C. at spark time
FSP	residual fraction in P.C. at spark time
FT	total residual fraction
FTΦ	total residual fraction at BDC
FX(W)	function of spatial location
FΦM	residual fraction in M.C. at BDC
FΦP	residual fraction in P.C. at BDC
F2	residual fraction of oxygen
F3	residual fraction of product
GOM	subroutine of geometry function
GR	gravity constant, gc
GTSM	total mass fraction in M.C. at spark time

GTSP	total mass fraction in P.C. at spark time
CTΦ	total mass fraction at BDC
GTΦM	total mass fraction in M.C. at BDC
GTΦP	total mass fraction in P.C. at BDC
H	clearance in M.C.
HALF	one half
HOOP	$H(X_{oo+\frac{1}{2}})$
HPY	H + Y
HR	heat of reaction
HT	heat transfer coefficient
HX	spatial derivative of H function, $\frac{dH}{dx}$
I	internal grid point
INI	subroutine for initiatization
INT	subroutine for numerical integration
IP1	I + 1
ISTEP	counter for the integration steps
J	grid point
JB	K + 1
JBM1	JB - 1
JM1	J - 1
JP1	J + 1
JSPL	left side grid points from the spark
JSPR	right side grid points from the spark
K	code number for grid size control

K1	code with values of 1,2,3,4 to indicate the restrictive time step control due to fuel, oxygen, product and temperature respectively
K2	code to indicate grid point where the restricted time step applies
K3	code for transfer control
K4	percentage of heat transfer
MARM	mass fraction of air in main chamber
MARM1	mass fraction of air in M.C. lean zone
MARM2	mass fraction of air in M.C. intermediate zone
MARP	mass fraction of air in P.C.
MFRM	mass fraction of fuel in M.C.
MFRM1	mass fraction of fuel in M.C. lean zone
MFRM2	mass fraction of fuel in M.C. intermediate zone
MFRP	mass fraction of fuel in P.C.
MWA	molecular weight of air
MWFM	molecular weight of C_8H_{18}
MWFP	molecular weight of C_3H_8
M2	dividing node between intermediate zone and lean zone
M2P1	M2 + 1
N	number of grid points
NM	number of grid points in M.C.
NM1	N - 1
NM2	N - 2
NOI	node location of orifice inlet

NOO	node location of orifice outlet
NOOM1	NOO - 1
NOOP1	NOO + 1
NP	number of grid points in P.C.
NSP	node location of spark
NTH	node location of throat
OMEGA	angular frequency
ONE	one
ONEMFR	1 - FR
ONEMO	1 - O32
ONEMPS	1 - PSM2
ONEMPΦ	1 - PΦM2
OXBH	percentage of oxygen consumption at peak ignition temperature
OXBM	percentage of oxygen consumption at middle ignition temperature
O32	overflow form P.C. to M.C.
P	gas pressure
PER	perimeter of the cross section area
PERP	perimeter of P.C.
PERT	perimeter of throat
PF	predicted P at $t + \Delta t$
PH	equivalence ratio
PHIM	intake equivalence ratio of M.C.
PHIP	intake equivalence ratio of P.C.
PHIT	total intake equivalence ratio
PHM	equivalence ratio of M.C.

PHP	equivalence ratio of P.C.
PHSM	equivalence ratio of M.C. at spark time
PHSM1	equivalence ratio of M.C. lean zone
PHSM2	equivalence ratio of M.C. intermediate zone
PHSP	equivalence ratio of P.C. at spark time
PHT	total equivalence ratio
PHΦM	equivalence ratio of M.C. at BDC
PHΦM1	equivalence ratio of M.C. lean zone at BDC
PHΦM2	equivalence ratio of M.C. intermediate zone at BDC
PHΦP	equivalence ratio of P.C. at BDC
PI	π
PM	M.C. mean pressure
PP	P.C. mean pressure
PRC	subroutine for constant output
PRV	subroutine for variable output
PS	pressure at spark time
PSM2	percentage mixing at spark time
PSY	mean pressure of the system
PTT	total residuals
PX	spatial derivative of gas pressure
PΦM2	percentage mixing at BDC
P2T	residual of oxygen
P3T	residual of product
P5T	residual of nitrogen
RAD	conversion factor from angle to radian

RC	crank arm length
RO	gas density
ROF	predicted RO at $t + \Delta t$
ROS	RO at spark temperature
ROT	time derivative of RO, $\frac{\partial \rho}{\partial t}$
ROX	spatial derivative of RO, $\frac{\partial \rho}{\partial x}$
RPM	engine speed, rpm
RR	universal gas constant
R23	reverse-flow from M.C. to P.C.
S	stroke
SDE3	summation of E3
SDE3M	summation of E3 in M.C.
SDE3P	summation of E3 in P.C.
SE1	summation of E1
SE1M	summation of E1 in M.C.
SE1P	summation of E1 in P.C.
SE2	summation of E2
SE2M	summation of E2 in M.C.
SE2P	summation of E2 in P.C.
SM1	total mass of fuel
SM10	initial mass of fuel
SM2	total mass of oxygen
SM3	total mass of product
SM4	total mass of NO
SM5	total mass of nitrogen

SMT	total mass in the system
SMTM	total mass in M.C.
SMTP	total mass in P.C.
SMT0	initial total mass
SMT1	total mass in M.C. lean zone
SMT2	total mass in M.C. intermediate zone
SOO	slope at orifice outlet
SP	summation of pressure
SPK	subroutine for ignition
SPM	summation of pressure in M.C.
SPP	summation of pressure in P.C.
SRT	square root of mean temperature
SUM	subroutine for average value calculation
SUMA23	mass of air flows back into the P.C.
SUMF23	mass of fuel flows back into the P.C.
SUMM23	total mass flows back into the P.C.
S1	characteristic length for the turbulent model
T	gas temperature
TF	predicted T at $t + \Delta t$
TH	temperature difference of peak spark temperature from inital temperature
THREE	three
TIME	current time
TIMSC	spark time in crank angle
TIMSR	spark time in radian

TM	temperature difference of middle spark temperature from initial temperature
TMP	subroutine for thermal properties
TNP	total moles of the mixture
TPC	maximum percentage of temperature change
TS	temperature at spark time
TSC	subroutine for time step control
TSH	peak spark temperature
TSM	middle spark temperature
TSY	mean temperature in the system
TT	time derivative of T, $\frac{\partial T}{\partial t}$
TTD	subroutine for turbulent diffusivity
TW	wall temperature
TWO	two
TWOANG	2θ
TWODB	2/B
TWOD3	2/3
TX	spatial derivative of T, $\frac{\partial T}{\partial t}$
TXX	second spatial derivative of T, $\frac{\partial^2 T}{\partial x^2}$
U	gas velocity
UF	predicted U at $t + \Delta t$
UP	piston speed
UPN	normalized piston speed
UPR	reference piston speed
US	gas velocity at spark time

USY	mean velocity in the system
UT	time derivative of U, $\frac{\partial U}{\partial t}$
UX	spatial derivative of U, $\frac{\partial U}{\partial x}$
UXX	second spatial derivative of U, $\frac{\partial^2 U}{\partial x^2}$
V	volume
VC	combustion chamber volume
VD	engine displacement
VM	M.C. volume
VMT	summation of M.C. volume
VO	orifice volume
VP	P.C. volume
VPA	estimated P.C. volume
VPB	estimated P.C. volume
VPDVC	ratio of P.C. volume to total combustion chamber volume, VP/VC
VPDVTS	VP/VTS
VPDVTT	VP/VTT
VSR	1 - VP/VTS
VT	total volume
VTR	1 - VP/VTT
VTS	total volume at spark time
VTT	total volume
VTTMVP	VTT - VP
WC	function of gas velocity due to combustion
WN	function of engine speed
X	spatial location

XJM	$X_{J-\frac{1}{2}}$
XJP	$X_{J+\frac{1}{2}}$
XLC	total spatial length of the dual chamber system
XLO	spatial length of the orifice
XLR	connecting rod length
XOI	spatial location of orifice inlet
XOO	spatial location of orifice outlet
XOOM	Xoo - ½
XOOP	Xoo + ½
XPO	spatial variable in geometry function
XSP	spatial location of spark
XTH	spatial location of throat
Y	piston travel distance from TDC
YT	time derivative of Y, $\frac{\partial Y}{\partial t}$
Y1	specific heat of initial temperature
Y2	specific heat of spark temperature
Z	preexponential constant for chemical kinetics
ZERO	zero
ZMFB	mass fraction burned

6. List of Computer Programs

```
C*****************************************************************************
C COMBUSTION MODEL MAIN PROGRAM                                               *
C*****************************************************************************
      IMPLICIT REAL*8(A-H,O-Z)
      COMMON /BLCTL/ZERO,HALF,ONE,TWO,THREE,FOUR,PI,TIMSC,TIME,CA,
     1              RPM,CR,VD,TWODB,PHIP,PHIM,PHIT,PHT,FT,FP,FM,GR,FBT,
     2              FB,RR,HR,Z,EDR,APST,POM2,PSM2,ISTEP,M2,N,K4,
     3              NM1,NM2,NP,NM,NSP,NOI,NTH,NOO,NOOM1,NOOP1,K,K1,K2,K3
      COMMON /BLINI/US,TS,PS,PHOP,PHOM2,PHOM1,PHSP,PHSM2,PHSM1,PHSM,
     1              E1SP,E2SP,E3SP,E5SP,E1SM2,E2SM2,E3SM2,E5SM2,E1SM1,
     2              E2SM1,E3SM1,E5SM1,APIP,APIT
      COMMON /BLGOM/XLC,XOI,XOO,CL,DCL,CLL,CLR,S,RC,XLR,DIAT,DIAP,AP,
     1              ATH,APS,PERP,PERT,XPO,XLO,VP,VM,VC,DVP,VPDVC,ATDVP,
     2              B1,B2,B3,B4,B5,DLXHF,XTH,DOOP,HOOP,SOO,AOOM,DCX,HX,
     3              XSP,OMEGA,TIMSR,FOTPI,DEG,VT,VTS,BORE
      COMMON /BLSPK/TSH,TSM,E1S,E2S,DAH,DAM,TNP
      COMMON /BLSUM/PP,PM,SMT,SM1,SM2,SM3,SM4,SM5,SMTO,SM10,ZMFB,PHP,PHM
      COMMON /BLDER/AMW,PSY,TW,USY,BSY,UPN,CS,S1,DELX,DLXSQ,HT,TSY
      COMMON /BLTSC/TPC,EPC,EMIN,DELT,DLTMIN,DLTMAX
      DIMENSION RO(101),U(101),T(101),P(101),E1(101),E2(101),E3(101),
     1          E4(101),E5(101),PH(101),E30(101),ROF(101),UF(101),
     2          TF(101),PF(101),E1F(101),E2F(101),E3F(101),E4F(101),
     3          E5F(101),ROT(101),UT(101),TT(101),E1T(101),E2T(101),
     4          E3T(101),E4T(101),X(101),D(101),H(101),PER(101),A(101),
     5          V(101),AX(101),DX(101),AT(101),AL(101)
   10 FORMAT(8D10.2)
   20 FORMAT(615)
      CALL UNDERZ('OFF')
C               ***  DATA INPUT  ***
      READ(5,10)TIME,CAPT,CAST
C               ***  CHECK IF TIME = ZERO  ***
      IF(TIME.NE.ZERO)GOTO 30
      READ(5,10)TIMSC,PS,ATDVP,DIAT
      READ(5,10)APIP,APIT,FR,FBT,FT
      READ(5,20)K,M2,K4
C               ***  INITIALIZE VARIABLES AT TIME = ZERO  ***
      ISTEP=0
      N=K*20+1
      CALL INI(RO,U,T,P,E1,E2,E3,E4,E5,PH,E30,X,D,H,PER,A,V,AX,DX,AT,AL)
      GOTO 40
C               ***  READ INTERMEDIATE DATA FROM THE DISK IF TIME > ZERO  ***
   30 READ(11)N,(RO(J),U(J),T(J),P(J),E1(J),E2(J),E3(J),E4(J),E5(J),
     1    PH(J),E30(J),X(J),D(J),H(J),PER(J),A(J),V(J),AX(J),DX(J),AT(J),
     2    AL(J),J=1,N),TIME,CA,OMEGA,TIMSR,FOTPI,DEG,DOOP,HOOP,RC,HX,
     3    AOOM,SOO,S1,TSY,VT,VP,PP,PM,SMT,SM1,SM2,SM3,SM4,SM5,SMTO,SM10,
     4    PHP,PHM,PHT,ZMFB,RR,HR,UPN,DELX,DLXSQ,DELT,HT,USY,BSY,PSY,
     5    DLTMAX,ISTEP,NM1,NP,NM,NOI,NTH,NOO,NOOM1,NOOP1,K1,K2,K3,K4
C               ***  PRINT INITIAL VARIABLES  ***
   40 CALL PRV(RO,U,T,P,E1,E2,E3,E4,E5,X,PH,AL)
      CAR=CA
C               ***  NUMERICAL INTEGRATION  ***
   50 ISTEP=ISTEP+1
      CALL INT(RO,U,T,P,E1,E2,E3,E4,E5,ROF,UF,TF,PF,E1F,E2F,E3F,E4F,E5F,
     1         ROT,UT,TT,E1T,E2T,E3T,E4T,X,D,H,PER,A,V,AX,DX,AT,AL)
      DCA=CA-CAR
C               ***  CHECK IF DCA = CAP FOR PRINTOUT  ***
      IF(DCA.LT.CAPT)GOTO 50
      CALL SUM(RO,P,E1,E2,E3,E4,E5,V,E30,PH)
C               ***  PRINT VARIABLES EVERY CAP ANGLES  ***
```

```
      CALL PRV(RO,U,T,P,E1,E2,E3,E4,E5,X,PH,AL)
      CAR=CA
C               ***  CHECK IF CA = CAS FOR DISK STORAGE  ***
      IF(CA.GE.CAST)GOTO 60
C               ***  CHECK IF COMB TIME HAS FINISHED  ***
      IF(ZMFB-LT-0.99D0)GOTO 50
C               ***  DISK STORAGE  ***
   60 REWIND 11
      WRITE(11)N,(RO(J),U(J),T(J),P(J),E1(J),E2(J),E3(J),E4(J),E5(J),
     1    PH(J),E30(J),X(J),D(J),H(J),PER(J),A(J),V(J),AX(J),DX(J),AT(J),
     2    AL(J),J=1,N),TIME,CA,OMEGA,TIMSR,FCTPI,DEG,DOOP,HOOP,RC,HX,
     3    AOOM,SOO,S1,TSY,VT,VP,PP,PM,SMT,SM1,SM2,SM3,SM4,SM5,SMTO,SM10,
     4    PHP,PHM,PHT,ZMFB,RR,HR,UPN,DELX,DLXSQ,DELT,HT,USY,BSY,PSY,
     5    DLTMAX,ISTEP,NM1,NP,NM,NOI,NTH,NOO,NOOM1,NOOP1,K1,K2,K3,K4
   70 STOP
      END
```

```
C*****************************************************************************
C INITIALIZATION SUBPROGRAM                                                    *
C*****************************************************************************
      SUBROUTINE INI(RO,U,T,P,E1,E2,E3,E4,E5,PH,E30,X,D,H,PER,A,V,AX,
     1               DX,AT,AL)
      IMPLICIT REAL*8(A-H,O-Z)
      COMMON /BLCTL/ZERO,HALF,ONE,TWO,THREE,FOUR,PI,TIMSC,TIME,CA,
     1              RPM,CR,VD,TWODD,PHIP,PHIM,PHIT,PHT,FT,FP,FM,GR,FRT,
     2              FR,RH,HR,Z,EDR,APST,POM2,PSM2,ISTEP,M2,N,K4,
     3              NM1,NM2,NP,NM,NSP,NOI,NTH,NOO,NOOM1,NOOP1,K,K1,K2,K3
      COMMON /BLINI/US,TS,PS,PHOP,PHOM2,PHOM1,PHSP,PHSM2,PHSM1,PHSM,
     1              E1SP,E2SP,E3SP,E5SP,E1SM2,E2SM2,E3SM2,E5SM2,E1SM1,
     2              E2SM1,E3SM1,E5SM1,APIP,APIT
      COMMON /BLGOM/XLC,XOI,XOO,CL,DCL,CLL,CLR,S,RC,XLR,DIAT,DIAP,AP,
     1              ATH,APS,PERP,PERT,XPO,XLO,VP,VM,VC,DVP,VPDVC,AIDVP,
     2              B1,B2,B3,B4,B5,DLXHF,XTH,DOOP,HOOP,SOO,AOOM,DCX,HX,
     3              XSP,OMEGA,TIMSR,FOTPI,DEG,VT,VTS,BORE
      COMMON /BLSPK/TSH,TSM,E1S,E2S,DAH,DAM,TNP
      COMMON /BLSUM/PP,PM,SMT,SM1,SM2,SM3,SM4,SM5,SMTO,SM10,ZMFB,PHP,PHM
      COMMON /BLDER/AMW,PSY,TW,USY,BSY,UPN,CS,S1,DELX,DLXSQ,HT,TSY
      COMMON /BLTSC/TPC,EPC,EMIN,DELT,DLTMIN,DLTMAX
      DIMENSION RO(N),U(N),T(N),P(N),E1(N),E2(N),E3(N),E4(N),E5(N),
     1          PH(N),E30(N),X(N),D(N),H(N),PER(N),A(N),V(N),AX(N),
     2          DX(N),AT(N),AL(N)
      K1=0
      K3=0
      NSP=(NSP-1)*K+1
      NOI=5*K+1
      NTH=6*K+1
      NOO=7*K+1
      M2=M2*K+1+K/2
      IF(M2.GT.N)M2=N
      DLTMAX=DLTMAX/K
      NM1=N-1
      NM2=N-2
      DELX=XLC/NM1
      DLXHF=HALF*DELX
      DLXSQ=DELX**2
      DELT=DLTMAX
      NOOP1=NOO+1
      NOOM1=NOO-1
      M2P1=M2+1
      NP=NOO
      NM=N-NP
      CSP=NSP
      COI=NOI
      CTH=NTH
      COO=NOO
      XSP=FX(CSP)
      XOI=FX(COI)
      XTH=FX(CTH)
      XOO=FX(COO)
      XOOP=FX(COO+HALF)
      XOOM=FX(COO-HALF)
      RAD=PI/180.D0
      DEG=ONE/RAD
      TIMSR=TIMSC*RAD
      OMEGA=RPM*TWO*PI/60.D0
      RR=RR/AMW
```

```
      HR=HR/AMW
      XLO=XOO-XOI
      XPO=XLC+XOO
      BORE=XLC-XOO
      TWODB=TWO/BORE
      FOTPI=FOUR*PI
      FODPI=FOUR/PI
      BSQ=BORE**2
      APS=BSQ/FODPI
      ATH=PI/FOUR*DIAT**2
      VP=ATH/ATDVP
      ATDVP=ATDVP*BORE
      VM=APS*CL
      VC=VP+VM
      VPDVC=VP/VC
      CR=ONE+VD/VC
      AP=VP/XOO
      DIAP=DSQRT(FODPI*AP)
      PERP=PI*DIAP
      PERT=PI*DIAT
      CS=0.7D0*(.332D0/DIAT)**2
      CLR=CL-CLL
      DCL=CLL-CLR
      HX=-TWODB*DCL
      DCX=CLL*XLC-CLR*XOO
      S=FODPI*VD/BSQ
      RC=S/TWO
      UPR=2100.D0*TWO*S/60.D0
      UP=RPM*TWO*S/60.D0
      UPN=UP**2/UPR
      DOOP=FD(XOOP)
      HOOP=FH(XOOP)
      AOOP=DOOP*HOOP
      B2=DLOG(AOOP/ATH)/(XOOP-XTH)
   10 B1=(AP-ATH)/(XTH-XOI)
      B3=AP+XOI*B1
      B4=B1/TWO
      B5=ATH/B2*DEXP(-B2*XTH)
      VO=B3*(XTH-XOI)-B4*(XTH**2-XOI**2)
     1   +B5*(DEXP(B2*XOO)-DEXP(B2*XTH))
      VPA=VP-VO
      VPB=AP*XOI
      DV=DABS(VPB-VPA)
      IF(DV.LE.1.D-6)GOTO 20
      AP=VPA/XOI
      GOTO 10
   20 DVP=AP*DELX
      DIAP=DSQRT(FODPI*AP)
      PERP=PI*DIAP
      AOOM=BS*(DEXP(B2*XOO)-DEXP(B2*XOOM))/DLXHP
            DO 30 J=NOOP1,N
      XJ=J
      X(J)=FX(XJ)
      D(J)=FD(X(J))
      H(J)=FH(X(J))
      DX(J)=TWO*(XPO-TWO*X(J))/D(J)
   30          CONTINUE
      CALL GOH(X,D,H,PER,A,V,AX,DX,AT)
      ALO=S1*UPN
```

```
      SMT=TWO*FRT/((ONE-FT)*RPM*60.D0)
      VTS=VT
      TS=PS*VTS/(SMT*RR)
      ROS=SMT/VTS
      SMT2=ZERO
                DO 40 J=NOOP1,M2
      DM=ROS*V(J)
      SMT2=SMT2+DM
   40           CONTINUE
      SMT1=ZERO
      IF(M2.EQ.N)GOTO 60
                DO 50 J=M2P1,N
      DM=ROS*V(J)
      SMT1=SMT1+DM
   50           CONTINUE
   60 SMTM=SMT1+SMT2
      PSM2=SMT2/SMTM
      CALL MIX
      SMTP=ZERO
      SM10=ZERO
                DO 70 J=1,NOO
      XJ=J
      X(J)=FX(XJ)
      U(J)=US
      T(J)=TS
      P(J)=PS
      RO(J)=ROS
      E1(J)=E1SP
      E2(J)=E2SP
      E3(J)=E3SP
      E4(J)=ZERO
      E5(J)=E5SP
      PH(J)=PHSP
      E30(J)=E3SP
      AL(J)=ALO
      DM=ROS*V(J)
      SMTP=SMTP+DM
      SM10=SM10+DM*E1SP
   70           CONTINUE
                DO 80 J=NOOP1,M2
      U(J)=US
      T(J)=TS
      P(J)=PS
      RO(J)=ROS
      E1(J)=E1SM2
      E2(J)=E2SM2
      E3(J)=E3SM2
      E4(J)=ZERO
      E5(J)=E5SM2
      PH(J)=PHSM2
      E30(J)=E3SM2
      AL(J)=ALO
      DM=ROS*V(J)
      SM10=SM10+DM*E1SM2
   80           CONTINUE
      IF(M2.EQ.N)GOTO 100
                DO 90 J=M2P1,N
      U(J)=US
      T(J)=TS
```

```
      P(J)=PS
      RO(J)=ROS
      E1(J)=E1SM1
      E2(J)=E2SM1
      E3(J)=E3SM1
      E4(J)=ZERO
      E5(J)=E5SM1
      PH(J)=PHSM1
      E30(J)=E3SM1
      AL(J)=ALO
      DM=ROS*V(J)
      SM10=SM10+DM*E1SM1
   90          CONTINUE
  100 SMTO=SMTP+SMTM
      CALL SPK(RO,T,E1,E2,E3)
      CALL SUM(RO,P,E1,E2,E3,E4,E5,V,E30,PH)
      DPP=250.D0
      PSY=PS
      WN=2.28D0*.0254D0*UP
      WC=.00324D0*TSH/1.8D0*VD/VT*(DPP/PSY)
      USY=((WN+WC)/.0254D0)**.8D0
      BSY=BORE**.2D0
      CALL TMP(CP,CV,CT)
      CALL PRC(RO,U,T,P,E1,E2,E3,E4,E5,X,PH,AL)
      RETURN
      END
```

```
C*************************************************************************
C INITIAL MASS MIXING SUBPROGRAM                                         *
C*************************************************************************
      SUBROUTINE MIX
      IMPLICIT REAL*8(A-H,O-Z)
      REAL*8 MFRP,MFRM,MARP,MARM,MFRM1,MARM1,MFRM2,MARM2,MWFP,MWFM,MWA
      COMMON /BLCTL/ZERO,HALF,ONE,TWO,THREE,FOUR,PI,TIMSC,TIME,CA,
     1              RPM,CR,VD,TWODB,PHIP,PHIM,PHIT,PHT,FT,FP,FM,GR,FRT,
     2              FR,RR,HR,Z,EDR,AFST,POM2,PSM2,ISTEP,M2,N,K4,
     3              NM1,NM2,NP,NM,NSP,NOI,NTH,NOO,NOOM1,NOOP1,K,K1,K2,K3
      COMMON /BLINI/US,TS,PS,PHOP,PHOM2,PHOM1,PHSP,PHSM2,PHSM1,PHSM,
     1              E1SP,E2SP,E3SP,E5SP,E1SM2,E2SM2,E3SM2,E5SM2,E1SM1,
     2              E2SM1,E3SM1,E5SM1,AFIP,AFIT
      COMMON /BLGOM/XLC,XOI,XOO,CL,DCL,CLL,CLR,S,RC,XLR,DIAT,DIAP,AP,
     1              ATH,APS,PERP,PERT,XPO,XLO,VP,VM,VC,DVP,VPDVC,ATDVP,
     2              B1,B2,B3,B4,B5,DLXHP,XTH,DOOP,HOOP,SOO,AOOM,DCX,HX,
     3              XSP,OMEGA,TIMSR,FOTPI,DEG,VT,VTS,BORE
      COMMON /BLSPK/TSH,TSM,E1S,E2S,DAH,DAM,TNP
      DATA AM/1.D0/,BM/3.D0/,CM/4.D0/,OXBM/.9D0/,OXBM/.1218D0/,
     1     BBP/5.D0/,BBM/12.5D0/,MWFP/44.064D0/,MWFM/114.144D0/,
     2     MWA/28.96D0/,AOMR/4.764D0/
      DM=BM*3.764D0
      ONEMFR=ONE-FR
      ANG=PI
      TWOANG=TWO*ANG
      Y=RC*(ONE-DCOS(ANG)+RC*(ONE-DCOS(TWOANG))/(FOUR*XLR))
      VTT=VC+APS*Y
      VTTMVP=VTT-VP
      VPDVTT=VP/VTT
      VTR=ONE-VPDVTT
      ANG=-TIMSR
      TWOANG=TWO*ANG
      Y=RC*(ONE-DCOS(ANG)+RC*(ONE-DCOS(TWOANG))/(FOUR*XLR))
      VTS=VC+APS*Y
      VPDVTS=VP/VTS
      VSR=ONE-VPDVTS
      DVR=VSR/VTR
      FRMVPT=FR-VPDVTT
      O32=FRMVPT/FR
      ONEMO=ONE-O32
      R23=VPDVTS*(VTT-VTS)/VTTMVP
      SUMM23=R23
      ONEMPS=ONE-PSM2
      POM2=PSM2*DVR+SUMM23
      ONEMPO=ONE-POM2
      AFIM=(AFIP*FR*(AFIT+ONE)-AFIT*(AFIP+ONE))/
     1     (FR*(AFIT+ONE)-(AFIP+ONE))
      AFST=BM*AOMR/AM
      AFSTP=(BBP*AOMR*MWA)/(AM*MWFP)
      AFSTM=(BBM*AOMR*MWA)/(AM*MWFM)
      AFSTT=AFSTP*FR+AFSTM*ONEMFR
      PHIP=AFSTP/AFIP
      PHIM=AFSTM/AFIM
      PHIT=AFSTT/AFIT
      AFIP=AFST/PHIP
      AFIM=AFST/PHIM
      AFIT=AFST/PHIT
      MFRP=ONE/(AFIP+ONE)
      MARP=AFIP/(AFIP+ONE)
```

```
      MFRM=ONE/(AFIM+ONE)
      MARM=AFIM/(AFIM+ONE)
      PHOP=PHIP
      AFOM2=(ONEMFR*MARM*POM2+FR*MARP*O32)/
     1       (ONEMFR*MFRM*POM2+FR*MFRP*O32)
      PHOM2=AFST/AFOM2
      AFOM1=AFIM
      PHOM1=PHIM
      AFOM=AFOM2*POM2+AFOM1*ONEMPO
      PHOM=AFST/AFOM
      MARM2=AFOM2/(AFOM2+ONE)
      MFRM2=ONE/(AFOM2+ONE)
      MARM1=MARM
      MFRM1=MFRM
      SUMA23=SUMM23*MARM2
      SUMF23=SUMM23*MFRM2
      AFSP=(VPDVTT*MARP+VTR*SUMA23)/(VPDVTT*MFRP+VTR*SUMF23)
      PHSP=AFST/AFSP
      AFSM2=AFOM2
      PHSM2=PHOM2
      AFSM1=AFOM1
      PHSM1=PHOM1
      PHSM2=AFST/AFSM2
      PHSM=PHSM2*PSM2+PHSM1*ONEMPS
      P2T=BM/PHIT-BM
      P3T=CM
      P5T=DM/PHIT
      PTT=P2T+P3T+P5T
      F2=P2T/PTT
      F3=P3T/PTT
      FP=FT*VPDVC
      FM=FT-FP
      C1=FP/(ONE-FT)
      C2=FM/(ONE-FT)
      FTO=C1+C2
      GTO=ONE+FTO
      FOP=C1*ONEMO
      FOM=C2+C1*O32
      GTOP=VPDVTT+FOP
      GTOM=ONEMFR+FR*O32+FOM
      E10P=VPDVTT*MFRP/GTOP
      E20P=(VPDVTT*MARP/AOMR+FOP*F2)/GTOP
      E30P=FOP*F3/GTOP
      E50P=ONE-E10P-E20P-E30P
      E10M2=(ONEMFR*MFRM*POM2+FR*O32*MFRP)/GTOM/POM2
      E20M2=((ONEMFR*MARM*POM2+FR*O32*MARP)/AOMR+FOM*F2*POM2)/GTOM/POM2
      E30M2=FOM*F3/GTOM
      E50M2=ONE-E10M2-E20M2-E30M2
      E10M1=ONEMFR*MFRM/GTOM
      E20M1=(ONEMFR*MARM/AOMR+FOM*F2)/GTOM
      E30M1=FOM*F3/GTOM
      E50M1=ONE-E10M1-E20M1-E30M1
      C3=FOM/GTOM
      FSM=VSR*C3
      FSP=FTO-FSM
      GTSM=VTR*(ONE-SUMM23)+FSM
      GTSP=GTO-GTSM
      E1SP=(VPDVTT*MFRP+VTR*SUMF23)/GTSP
      E2SP=((VPDVTT*MARP+VTR*SUMA23)/AOMR+FSP*F2)/GTSP
```

```
E3SP=FSP*P3/GTSP
E5SP=ONE-E1SP-E2SP-E3SP
E1SM2=VTR*(PCM2*MFRM2-SUMP23)/GTSM/PSM2
E2SM2=(VTR*(PCM2*MARM2-SUMA23)/AOMR+FSM*P2*PSM2)/GTSM/PSM2
E3SM2=FSM*P3/GTSM
E5SM2=ONE-E1SM2-E2SM2-E3SM2
E1SM1=MFRM1*VTR/GTSM
E2SM1=(MARM1*VTR/AOMR+FSM*P2)/GTSM
E3SM1=FSM*P3/GTSM
E5SM1=ONE-E1SM1-E2SM1-E3SM1
DE2H=E2SP*OXBH
DE2M=E2SP*OXBM
DAH=DE2H/BM/E1SP
DAM=DE2M/BM/E1SP
E1S=E1SP-DE2H/BM
E2S=E2SP-DE2H
TNP=ONE/E1SP
RETURN
END
```

```
C*****************************************************************************
C GEOMETRY SUBPROGRAM                                                         *
C*****************************************************************************
      SUBROUTINE GOM(X,D,H,PER,A,V,AX,DX,AT)
      IMPLICIT REAL*8(A-H,O-Z)
      COMMON /BLCTL/ZERO,HALF,ONE,TWO,THREE,FOUR,PI,TIMSC,TIME,CA,
     1               RPM,CR,VD,TWODB,PHIP,PHIM,PHIT,PHT,FT,PP,PM,GR,PRT,
     2               FR,RR,HR,Z,EDR,APST,POM2,PSM2,ISTEP,M2,N,K4,
     3               NM1,NM2,NP,NM,NSP,NOI,NTH,NOO,NOOM1,NOOP1,K,K1,K2,K3
      COMMON /BLGOM/XLC,XOI,XOO,CL,DCL,CLL,CLR,S,RC,XLR,DIAT,DIAP,AP,
     1               ATH,APS,PERP,PERT,XPO,XLO,VP,VM,VC,DVP,VPDVC,ATDVP,
     2               B1,B2,B3,B4,B5,DLXHF,XTH,DCOP,HOCP,SOO,AOOM,DCX,HX,
     3               XSP,OMEGA,TIMSR,POTPI,DEG,VT,VTS,BORE
      COMMON /BLDER/AMW,PSY,TW,USY,BSY,UPN,CS,S1,DELX,DLXSQ,HT,TSY
      DIMENSION X(N),D(N),H(N),PER(N),A(N),V(N),AX(N),DX(N),AT(N)
      ANG=OMEGA*TIME-TIMSR
      TWOANG=TWO*ANG
      Y=RC*(ONE-DCOS(ANG)+RC*(ONE-DCOS(TWOANG))/(FOUR*XLR))
      S1=CS*(Y+CL)
      CA=ANG*DEG
      YT=OMEGA*RC*(DSIN(ANG)+RC*DSIN(TWOANG)/(TWO*XLR))
      IF(K3.EQ.1)GOTO 70
C               ***  PRECHAMBER VALUES  ***
      DO 60 J=1,NOOM1
      XJ=J
      XJP=FX(XJ+HALF)
      XJM=FX(XJ-HALF)
      IF(J.GT.NOI)GOTO 20
      IF(J.EQ.NOI)GOTO 10
      A(J)=AP
      PER(J)=PERP
      AX(J)=ZERO
      AT(J)=ZERO
      V(J)=DVP
      IF(J.EQ.1)V(J)=HALF*DVP
      GOTO 60
   10 A(J)=HALF*(AP+B3-B4*(XJP+XOI))
      V(J)=A(J)*DELX
      AX(J)=-HALF*B1
      GO TO 50
C               ***  ORIFICE VALUES  ***
   20 IF(J.GT.NTH)GOTO 40
      IF(J.EQ.NTH)GOTO 30
      A(J)=B3-B4*(XJP+XJM)
      V(J)=A(J)*DELX
      AX(J)=-B1
      GOTO 50
   30 V(J)=DLXHF*(B3-B4*(XTH+XJM))+B5*(DEXP(B2*XJP)-DEXP(B2*XTH))
      A(J)=V(J)/DELX
      AX(J)=ZERO
      GOTO 50
   40 V(J)=B5*(DEXP(B2*XJP)-DEXP(B2*XJM))
      AX(J)=ATH*B2*DEXP(B2*(FX(XJ)-XTH))
      A(J)=V(J)/DELX
   50 PER(J)=DSQRT(POTPI*A(J))
      AT(J)=ZERO
   60 CONTINUE
      K3=1
C               ***  MAIN CHAMBER VALUES  ***
```

```
 70 VMT=ZERO
          DO 100 J=NOO,N
    IF(J.NE.NOO)GOTO 80
    AOOP=DOOP*(HOOP+Y)
    A(J)=HALF*(AOOM+AOOP)
    V(J)=A(J)*DELX
    PER(J)=DSQRT(FOTPI*A(J))
    AX(J)=(AOOP-AOOM)/DELX
    AT(J)=HALF*DOOP*YT
    GOTO 90
 80 HPY=H(J)+Y
    A(J)=D(J)*HPY
    PER(J)=TWO*(D(J)+HPY)
    AX(J)=D(J)*HX+HPY*DX(J)
    AT(J)=D(J)*YT
    V(J)=A(J)*DELX
    IF(J.EQ.N)V(J)=HALF*V(J)
 90 VMT=VMT+V(J)
100 CONTINUE
    VT=VP+VMT
    RETURN
    END
```

```
C*******************************************************************************
C IGNITION SUBPROGRAM                                                          *
C*******************************************************************************
      SUBROUTINE SPK(RO,T,E1,E2,E3)
      IMPLICIT REAL*8(A-H,O-Z)
      COMMON /BLCTL/ZERO,HALF,ONE,TWO,THREE,FOUR,PI,TIMSC,TIME,CA,
     1               RPM,CR,VD,TWODB,PHIP,PHIM,PHIT,PHT,PT,PP,PM,GR,PRT,
     2               PR,RR,HR,Z,EDR,AFST,POM2,PSM2,ISTEP,M2,N,K4,
     3               NM1,NM2,NP,NM,NSP,NOI,NTH,NOO,NOOM1,NOOP1,K,K1,K2,K3
      COMMON /BLINI/US,TS,PS,PHOP,PHOM2,PHOM1,PHSP,PHSM2,PHSM1,PHSN,
     1               E1SP,E2SP,E3SP,E5SP,E1SM2,E2SM2,E3SM2,E5SM2,E1SM1,
     2               E2SM1,E3SM1,E5SM1,APIP,APIT
      COMMON /BLSPK/TSH,TSM,E1S,E2S,DAH,DAM,TNP
      DIMENSION RO(N),T(N),E1(N),E2(N),E3(N)
      DATA A0/2.257196D3/,A1/-1.858418D5/,A2/1.603333D1/
      DT(L)=TH*DEXP(-(L-NSP)**2/(TWO*DELTA**2))
      TWOD3=TWO/THREE
      DO 30 I=1,2
      IF(I.EQ.1)DA=DAH
      IF(I.EQ.2)DA=DAM
      X=TS
      Y1=TNP*(A0*X+A1*DLOG(X)+TWOD3*A2*X**(1.5D0))
   10 Y2=TNP*(A0*X+A1*DLOG(X)+TWOD3*A2*X**(1.5D0))
      Y=Y2-Y1-HR*DA
      DY=DABS(Y)
      IF(DY.LE.1.D-3)GOTO 20
      YD=TNP*(A0+A1/X+A2*DSQRT(X))
      X=X-Y/YD
      GOTO 10
   20 IF(I.EQ.1)TSH=X
      IF(I.EQ.2)TSM=X
   30 CONTINUE
      TH=TSH-TS
      TM=TSM-TS
      DELTA=K*HALF*DSQRT(-HALF/DLOG(TM/TH))
      JB=K+1
      JSPR=NSP+3*K
      JSPL=NSP-3*K
      IF(JSPL.LT.JB)JSPL=JB
      JBM1=JB-1
      DE1DT=(E1SP-E1S)/TH
      DE2DT=(E2SP-E2S)/TH
            DO 40 J=JSPL,JSPR
      DTJ=DT(J)
      DE1=DE1DT*DTJ
      DE2=DE2DT*DTJ
      DE3=-FOUR*DE1
      T(J)=TS+DTJ
      RO(J)=PS/(RR*T(J))
      E1(J)=E1SP-DE1
      E2(J)=E2SP-DE2
      E3(J)=E3SP-DE3
      IF(J.NE.JB)GOTO 40
      TJB=T(JB)
      ROJB=RO(JB)
      E1JB=E1(JB)
      E2JB=E2(JB)
      E3JB=E3(JB)
   40       CONTINUE
```

```
      IF(JSPL.NE.JB)GOTO 60
                  DO 50 J=2,JB-1
      T(J)=TJB
      RO(J)=ROJB
      E1(J)=E1JB
      E2(J)=E2JB
      E3(J)=E3JB
50                CONTINUE
60    T(1)=T(2)
      RO(1)=RO(2)
      E1(1)=E1(2)
      E2(1)=E2(2)
      E3(1)=E3(2)
      RETURN
      END
```

```
C*******************************************************************************
C SUMMATION SUBPROGRAM                                                          *
C*******************************************************************************
      SUBROUTINE SUM(RO,P,E1,E2,E3,E4,E5,V,E30,PH)
      IMPLICIT REAL*8(A-H,O-Z)
      COMMON /BLCTL/ZERO,HALF,ONE,TWO,THREE,FOUR,PI,TIMSC,TIME,CA,
     1              RPM,CR,VD,TWODB,PHIP,PHIM,PHIT,PHT,FT,FP,FM,GR,FRT,
     2              FR,RR,HR,Z,EDR,APST,POM2,PSM2,ISTEP,M2,N,K4,
     3              NM1,NM2,NP,NM,NSP,NOI,NTH,NOO,NOOM1,NOOP1,K,K1,K2,K3
      COMMON /BLSUM/PP,PM,SMT,SM1,SM2,SM3,SM4,SM5,SMT0,SM10,ZMFB,PHP,PHM
      DIMENSION RO(N),P(N),E1(N),E2(N),E3(N),E4(N),E5(N),PH(N),E30(N),
     1          V(N)
      SPP=ZERO
      SPM=ZERO
      SMT=ZERO
      SE1P=ZERO
      SE1M=ZERO
      SE2P=ZERO
      SE2M=ZERO
      SDE3P=ZERO
      SDE3M=ZERO
      SM1=ZERO
      SM2=ZERO
      SM3=ZERO
      SM4=ZERO
      SM5=ZERO
            DO 10 J=1,NOO
      E1J=E1(J)
      E2J=E2(J)
      E3J=E3(J)
      E4J=E4(J)
      E5J=E5(J)
      E30J=E30(J)
      DE3J=E3J-E30J
      PH(J)=THREE*(E1J+.25D0*DE3J)/(E2J+.75D0*DE3J)
      SPP=SPP+P(J)
      SE1P=SE1P+E1J
      SE2P=SE2P+E2J
      SDE3P=SDE3P+DE3J
      DM=RO(J)*V(J)
      SMT=SMT+DM
      SM1=SM1+DM*E1J
      SM2=SM2+DM*E2J
      SM3=SM3+DM*E3J
      SM4=SM4+DM*E4J
      SM5=SM5+DM*E5J
   10 CONTINUE
      PP=SPP/NP
      PHP=THREE*(SE1P+.25D0*SDE3P)/(SE2P+.75D0*SDE3P)
            DO 20 J=NOOP1,N
      E1J=E1(J)
      E2J=E2(J)
      E3J=E3(J)
      E4J=E4(J)
      E5J=E5(J)
      E30J=E30(J)
      DE3J=E3J-E30J
      PH(J)=THREE*(E1J+.25D0*DE3J)/(E2J+.75D0*DE3J)
      SPM=SPM+P(J)
```

```
      SE1M=SE1M+E1J
      SE2M=SE2M+E2J
      SDE3M=SDE3M+DE3J
      DM=RO(J)*V(J)
      SMT=SMT+DM
      SM1=SM1+DM*E1J
      SM2=SM2+DM*E2J
      SM3=SM3+DM*E3J
      SM4=SM4+DM*E4J
      SM5=SM5+DM*E5J
   20       CONTINUE
      PM=SPM/NM
      PHM=THREE*(SE1M+.25D0*SDE3M)/(SE2M+.75D0*SDE3M)
      SE1=SE1P+SE1M
      SE2=SE2P+SE2M
      SDE3=SDE3P+SDE3M
      PHT=THREE*(SE1+.25D0*SDE3)/(SE2+.75D0*SDE3)
      ZMFB=(SM10-SM1)/SM10
      RETURN
      END
```

```
C*****************************************************************************
C OUTPUT SUBPROGRAM                                                           *
C*****************************************************************************
      SUBROUTINE PRC(RO,U,T,P,E1,E2,E3,E4,E5,X,PH,AL)
      IMPLICIT REAL*8(A-H,O-Z)
      COMMON /BLCTL/ZERO,HALP,ONE,TWO,THREE,FOUR,PI,TIMSC,TIME,CA,
     1              RPM,CR,VD,TWODB,PHIP,PHIM,PHIT,PHT,FT,PP,PM,GR,PRT,
     2              PR,RR,HR,Z,EDR,APST,POM2,PSM2,ISTEP,M2,N,K4,
     3              NM1,NM2,NP,NM,NSP,NOI,NTH,NOO,NOOM1,NOOP1,K,K1,K2,K3
      COMMON /BLINI/US,TS,PS,PHOP,PHOM2,PHOM1,PHSP,PHSM2,PHSM1,PHSM,
     1              E1SP,E2SP,E3SP,E5SP,E1SM2,E2SM2,E3SM2,E5SM2,E1SM1,
     2              E2SM1,E3SM1,E5SM1,AFIP,AFIT
      COMMON /BLGOM/XLC,XOI,XOO,CL,DCL,CLL,CLR,S,RC,XLR,DIAT,DIAP,AP,
     1              ATH,APS,PERP,PERT,XPO,XLO,VP,VM,VC,DVP,VPDVC,ATDVP,
     2              B1,B2,B3,B4,B5,DLXHP,XTH,DOOP,HOOP,SOO,AOOM,DCX,HX,
     3              XSP,OMEGA,TIMSR,FOTPI,DEG,VT,VTS,BORE
      COMMON /BLSPK/TSH,TSM,E1S,E2S,DAH,DAM,TNP
      COMMON /BLSUM/PP,PM,SMT,SM1,SM2,SM3,SM4,SM5,SMT0,SM10,ZMPB,PHP,PHM
      COMMON /BLDER/AMW,PSY,TW,USY,BSY,UPN,CS,S1,DELX,DLXSQ,HT,TSY
      COMMON /BLTSC/TPC,EPC,EMIN,DELT,DLTMIN,DLTMAX
      DIMENSION RO(N),U(N),T(N),P(N),E1(N),E2(N),E3(N),E4(N),E5(N),
     1          X(N),PH(N),AL(N)
   10 FORMAT('1'/30X,'*****  DUAL CHAMBER COMBUSTION MODEL PARAMETERS  *
     1*****'////40X,'*****  GEOMETRICAL PARAMETERS  *****'//
     2       ' VPDVC =',T17,2PF12.4,T30,'%',T40,'ATH*BORE/VP =',T57,
     3       0PF12.4,T80,'VD =',T97,F12.4,T110,'CBIN'/
     4       ' VP =',T17,F12.4,T30,'CBIN',T40,'VM =',T57,F12.4,T70,
     5       'CBIN',T80,'VC =',T97,F12.4,T110,'CBIN'/
     6       ' AP =',T17,F12.4,T30,'SQIN',T40,'ATH =',T57,F12.4,T70,
     7       'SQIN',T80,'APS =',T97,F12.4,T110,'SQIN'/
     8       ' DIAP =',T17,F12.4,T30,'IN',T40,'DIAT =',T57,F12.4,
     9       T70,'IN',T80,'BORE =',T97,F12.4,T110,'IN'/
     A       ' XLC =',T17,F12.4,T30,'IN',T40,'XLR =',
     B       T57,F12.4,T70,'IN',T80,'S =',T97,F12.4,T110,'IN'/
     C       ' XOI =',T17,F12.4,T30,'IN',T40,'XLO =',T57,
     D       F12.4,T70,'IN',T80,'XOO =',T97,F12.4,T110,'IN'/
     E       ' CLL =',T17,F12.4,T30,'IN',T40,'CLR =',T57,
     F       F12.4,T70,'IN',T80,'CL =',T97,F12.4,T110,'IN'/
     G       ' CR =',T17,F12.4)
   20 FORMAT('-'/40X,'*****  OPERATIONAL PARAMETERS  *****'//
     1       ' FR =',T17,2PF12.4,T30,'%',T40,'TIMSC =',T57,
     2       0PF12.4,T70,'BTC',T80,'RPM =',T97,F12.4/
     3       ' XSP =',T17,F12.4,T30,'IN',T40,'AF ST =',T57,
     4       F12.4,T80,'SM10 =',T97,1PE12.5,T110,'LBM'/
     5       ' TSH =',T17,0PF12.4,T30,'R',T40,'TW =',T57,
     6       F12.4,T70,'R',T80,'SMT0 =',T97,1PE12.5,T110,'LBM'/
     7       ' PP =',T17,0PF12.4,T40,'PM =',T57,F12.4,
     8       T80,'FT =',T97,F12.4/' PHIP =',T17,F12.4,T40,
     9       'PHIM =',T57,F12.4,T80,'PHIT =',T97,F12.4/
     A       ' PHOP =',T17,F12.4,T40,'PHOM2 =',T57,F12.4,T80,
     B       'PHOM1 ',T97,F12.4/' PHSP =',T17,F12.4,T40,
     C       'PHSM2 =',T57,F12.4,T80,'PHSM1 =',T97,F12.4/
     D       ' US P.C. =',T17,F12.4,T30,'IN/SEC',T40,
     E       'US M.C. =',T57,F12.4,T70,'IN/SEC'/
     F       ' PS P.C. =',T17,F12.4,T30,'PSI',T40,
     G       'PS M.C. =',T57,F12.4,T70,'PSI'/
     H       ' TS P.C. =',T17,0PF12.4,T30,'R',T40,
     I       'TS M.C. =',T57,F12.4,T70,'R')
   30 FORMAT('-'/40X,'*****  COMBUSTION PARAMETERS  *****'//
```

```
     1       ' RR =',T21,F12.2,T34,'LBF-IN/LBM-R',T70,
     2       'EDR =',T97,F12.2,T110,'R'/
     3       ' Z =',T21,1PE12.5,T34,'CBIN/LBM-SEC',T70,
     4       'GR =',T97,0PF12.2,T110,'LBM-IN/LBF-SQSEC'/
     5       ' HR =',T21,1PE12.5,T34,'LBF-IN/LBM',T70,
     6       'AMW =',T97,0PF12.2,T110,'LBM/LBMCLE'/
     7       ' K4 =',T21,I12,T34,'%',T70,'CS =',T97,1PE12.4)
    40 FORMAT('-'/40X,'*****  NUMERICAL PARAMETERS  *****',//
     1       ' N =',T17,I12,T40,'NP =',T57,
     2       I12,T80,'NM =',T97,I12/
     3       ' NOI =',T17,I12,T40,'NTH =',T57,I12,
     4       T80,'NOO =',T97,I12/
     5       ' M2 =',T17,I12,T40,'P0M2 =',T57,2PF12.4,T70,
     6       '%',T80,'PSM2 =',T97,F12.4,T110,'%'/
     7       ' EPC =',T17,F12.2,T30,'%',T40,
     8       'EMIN =',T57,1PE12.5,T80,
     9       'TPC =',T97,2PF12.2,T110,'%'/
     A       ' DLTMAX =',T17,1PE12.5,T30,'SEC',T40,
     B       'DLTMIN =',T57,E12.5,T70,'SEC',T80,
     D       'DELX =',T97,E12.5,T110,'IN')
    50 FORMAT('1','TIME   =',T15,1PE13.5,T30,'SEC',T40,'CA     =',
     1       T51,0PF13.2,T66,'ATC',T80,'ZMFB   =',T95,2PF13.5,T110,
     2       '%'///' ISTEP  =',T15,0PI13,T40,
     3       'TSY    =',T51,F13.2,T66,'R',T80,'HT     =',T95,
     4       F13.2,T110,'IN-LBF/S-R-SQIN'/' PP     =',T18,F10.2,T30,
     5       'PSI',T40,'PM     =',T54,F10.2,T66,'PSI',T80,
     6       'VT     =',T95,F13.5,T110,'CBIN'/
     7       ' SMT    =',T15,1PE13.5,T30,'LBM',T40,'SM1    =',T51,
     8       E13.5,T66,'LBM',T80,'SM2    =',T95,E13.5,T110,'LBM'/
     9       ' SM3    =',T15,E13.5,T30,'LBM',T40,'SM4    =',T51,
     A       E13.5,T66,'LBM',T80,'SM5    =',T95,E13.5,T110,'LBM'/
     B       ' PHP    =',T15,0PF13.4,T40,'PHM    =',T51,F13.4,T80,
     C       'PHT    =',T95,F13.4)
    60 FORMAT(' DELT   =',T15,1PE13.5,T30,'SEC',7X,'NO TIME CONTROL')
    70 FORMAT(' DELT   =',T15,1PE13.5,T30,'SEC',7X,'FUEL CONTROL AT',I9)
    80 FORMAT(' DELT   =',T15,1PE13.5,T30,'SEC',7X,'OXYG CONTROL AT',I9)
    90 FORMAT(' DELT   =',T15,1PE13.5,T30,'SEC',7X,'PROD CONTROL AT',I9)
   100 FORMAT(' DELT   =',T15,1PE13.5,T30,'SEC',7X,'TEMP CONTROL AT',I9)
   110 FORMAT(' /'   J      X        RO          U        AL       T     P
     1     E1           E2          E3          E4          E5
     2  PH '/'         IN     LBM/CBIN     IN/SEC   SQIN/SEC    R    PSI'/)
   120 FORMAT(1X,I3,F7.2,1P2E12.3,0PF7.2,F7.0,F6.0,1P5E13.5,0PF8.4)
       WRITE(6,10) VPDVC,ATDVP,VD,VP,VM,VC,AP,ATH,APS,DIAP,DIAT,BORE,XLC,
     1             XLR,S,XOI,XLO,XOO,CLL,CLR,CL,CR
       WRITE(6,20) PR,TIMSC,RPM,XSP,AFST,SM10,TSH,TW,SMT0,FP,FM,FT,PHIP,
     1             PHIM,PHIT,PH0P,PH0M2,PH0M1,PHSP,PHSM2,
     2             PHSM1,US,US,PS,PS,TS,TS
       WRITE(6,30) RR,EDR,Z,GR,HR,AMW,K4,CS
       WRITE(6,40) N,NP,NM,NOI,NTH,NOO,M2,P0M2,PSM2,EPC,EMIN,TPC,DLTMAX,
     1             DLTMIN,DELX
       RETURN
       ENTRY PRV(RO,U,T,P,E1,E2,E3,E4,E5,X,PH,AL)
       WRITE(6,50) TIME,CA,ZMFB,ISTEP,TSY,HT,PP,PM,VT,SMT,SM1,SM2,SM3,SM4,
     1             SM5,PHP,PHM,PHT
       IF(K1.EQ.0) WRITE(6,60) DELT
       IF(K1.EQ.1) WRITE(6,70) DELT,K2
       IF(K1.EQ.2) WRITE(6,80) DELT,K2
       IF(K1.EQ.3) WRITE(6,90) DELT,K2
       IF(K1.EQ.4) WRITE(6,100) DELT,K2
```

```
      WRITE(6,110)
      WRITE(6,120) (J,X(J),RO(J),U(J),AL(J),T(J),P(J),E1(J),E2(J),
     1              E3(J),E4(J),E5(J),PH(J),J=1,N)
      RETURN
      END
```

```
C*************************************************************************
C NUMERICAL INTEGRATION SUBPROGRAM                                       *
C*************************************************************************
      SUBROUTINE INT(RO,U,T,P,E1,E2,E3,E4,E5,ROF,UF,TF,PF,E1F,E2F,E3F,
     1          E4F,E5F,ROT,UT,TT,E1T,E2T,E3T,E4T,X,D,H,PER,A,V,AX,DX,AT,
     2          AL)
      IMPLICIT REAL*8(A-H,O-Z)
      COMMON /BLCTL/ZERO,HALF,ONE,TWO,THREE,FOUR,PI,TIMSC,TIME,CA,
     1               RPM,CR,VD,TWODB,PHIP,PHIM,PHIT,PHT,PT,PP,PM,GR,PRT,
     2               PR,RR,HR,Z,EDR,AFST,POM2,PSM2,ISTEP,M2,N,K4,
     3               NM1,NM2,NP,NM,NSP,NOI,NTH,NOO,NOOM1,NOOP1,K,K1,K2,K3
      COMMON /BLGOM/XLC,XOI,XOO,CL,DCL,CLL,CLR,S,RC,XLR,DIAT,DIAP,AP,
     1               ATH,APS,PERP,PERT,XPO,XLO,VP,VM,VC,DVP,VPDVC,ATDVP,
     2               B1,B2,B3,B4,B5,DLXHP,XTH,DOOP,HOOP,SOO,AOOM,DCX,HX,
     3               XSP,OMEGA,TIMSR,FOTPI,DEG,VT,VTS,BORE
      COMMON /BLDER/AMW,PSY,TW,USY,BSY,UPN,CS,S1,DELX,DLXSQ,HT,TSY
      COMMON /BLTSC/TPC,EPC,EMIN,DELT,DLTMIN,DLTMAX
      DIMENSION RO(N),U(N),T(N),P(N),E1(N),E2(N),E3(N),E4(N),E5(N),
     1          ROF(N),UF(N),TF(N),PF(N),E1F(N),E2F(N),E3F(N),E4F(N),
     2          E5F(N),ROT(N),UT(N),TT(N),E1T(N),E2T(N),E3T(N),E4T(N),
     3          X(N),D(N),H(N),PER(N),A(N),V(N),AX(N),DX(N),AT(N),AL(N)
      DELT=DLTMAX
C             ***  PREDICTOR CALCULATIONS  ***
      CALL GOM(X,D,H,PER,A,V,AX,DX,AT)
      CALL TMP(CP,CV,CT)
      K1=0
      K2=0
         DO 10 J=2,NM1
      I=J
      CALL DER(I,J,RO,U,T,P,E1,E2,E3,E4,E5,ROT,UT,TT,E1T,E2T,E3T,
     1          E4T,PER,A,AX,AT,AL,CP,CV,CT)
      CALL TSC(J,T,E1,E2,E3,TT,E1T,E2T,E3T)
   10         CONTINUE
      SP=ZERO
             DO 20 J=2,NM1
      ROF(J)=RO(J)+ROT(J)*DELT
      UF(J)=U(J)+UT(J)*DELT
      TF(J)=T(J)+TT(J)*DELT
      PF(J)=ROF(J)*TF(J)*RR
      E1F(J)=E1(J)+E1T(J)*DELT
      E2F(J)=E2(J)+E2T(J)*DELT
      E3F(J)=E3(J)+E3T(J)*DELT
      E4F(J)=E4(J)+E4T(J)*DELT
      E5F(J)=ONE-E1F(J)-E2F(J)-E3F(J)-E4F(J)
      SP=SP+PF(J)
   20         CONTINUE
C             ***  PREDICTOR BOUNDARY VALUES  ***
      CALL BOD(ROF,UF,TF,PF,E1F,E2F,E3F,E4F)
      PSY=(SP+PF(1)+PF(N))/N
C             ***  CORRECTOR CALCULATIONS  ***
      TIME=TIME+DELT
      CALL GOM(X,D,H,PER,A,V,AX,DX,AT)
      CALL TMP(CP,CV,CT)
      SP=ZERO
             DO 30 J=2,NM1
      I=J-1
      CALL DER(I,J,ROF,UF,TF,PF,E1F,E2F,E3F,E4F,E5F,ROT,UT,TT,E1T,E2T,
     1          E3T,E4T,PER,A,AX,AT,AL,CP,CV,CT)
      RO(J)=HALF*(RO(J)+ROF(J)+DELT*ROT(J))
```

```
      U(J)=HALF*(U(J)+UP(J)+DELT*UT(J))
      T(J)=HALF*(T(J)+TP(J)+DELT*TT(J))
      P(J)=RO(J)*T(J)*RR
      E1(J)=HALF*(E1(J)+E1P(J)+DELT*E1T(J))
      E2(J)=HALF*(E2(J)+E2P(J)+DELT*E2T(J))
      E3(J)=HALF*(E3(J)+E3P(J)+DELT*E3T(J))
      E4(J)=HALF*(E4(J)+E4P(J)+DELT*E4T(J))
      E5(J)=ONE-E1(J)-E2(J)-E3(J)-E4(J)
      SP=SP+P(J)
   30 CONTINUE
C                *** CORRECTOR BOUNDARY VALUES ***
      CALL BOD(RO,U,T,P,E1,E2,E3,E4)
      PSY=(SP+P(1)+P(N))/N
      RETURN
      END
```

```
C*******************************************************************************
C DIFFERENTIAL EQUATIONS SUBPROGRAM                                            *
C*******************************************************************************
      SUBROUTINE DER(I,J,RO,U,T,P,E1,E2,E3,E4,E5,ROT,UT,TT,E1T,E2T,E3T,
     1          E4T,PER,A,AX,AT,AL,CP,CV,CT)
      IMPLICIT REAL*8(A-H,O-Z)
      COMMON /BLCTL/ZERO,HALF,ONE,TWO,THREE,FOUR,PI,TIMSC,TIME,CA,
     1               RPM,CR,VD,TWODB,PHIP,PHIM,PHIT,PHT,FT,FP,FM,GR,FRT,
     2               FR,RR,HR,Z,EDR,AFST,POM2,PSM2,ISTEP,M2,N,K4,
     3               NM1,NM2,NP,NM,NSP,NOI,NTH,NOO,NOOM1,NOOP1,K,K1,K2,K3
      COMMON /BLGOM/XLC,XOI,XOO,CL,DCL,CLL,CLR,S,RC,XLR,DIAT,DIAP,AP,
     1               ATH,APS,PERP,PERT,XPO,XLO,VP,VM,VC,DVP,VPDVC,ATDVP,
     2               B1,B2,B3,B4,B5,DLXHP,XTH,DOOP,HOOP,SOO,AOOM,DCX,HX,
     3               XSP,OMEGA,TIMSR,POTPI,DEG,VT,VTS,DORE
      COMMON /BLDER/AMW,PSY,TW,USY,BSY,UPN,CS,S1,DELX,DLXSQ,HT,TSY
      DIMENSION RO(N),U(N),T(N),P(N),E1(N),E2(N),E3(N),E4(N),E5(N),
     1          ROT(N),UT(N),TT(N),E1T(N),E2T(N),E3T(N),E4T(N),PER(N),
     2          A(N),AX(N),AT(N),AL(N)
      IP1=I+1
      JP1=J+1
      JM1=J-1
      ROJ=RO(J)
      UJ=U(J)
      TJ=T(J)
      PJ=P(J)
      E1J=E1(J)
      E2J=E2(J)
      E3J=E3(J)
      E4J=E4(J)
      E5J=E5(J)
      AJ=A(J)
      PERJ=PER(J)
      ROX=(RO(IP1)-RO(I))/DELX
      UX=(U(IP1)-U(I))/DELX
      TX=(T(IP1)-T(I))/DELX
      PX=(P(IP1)-P(I))/DELX
      E1X=(E1(IP1)-E1(I))/DELX
      E2X=(E2(IP1)-E2(I))/DELX
      E3X=(E3(IP1)-E3(I))/DELX
      E4X=(E4(IP1)-E4(I))/DELX
      AXDA=AX(J)/AJ
      ATDA=AT(J)/AJ
      UXX=(U(JP1)-TWO*UJ+U(JM1))/DLXSQ
      TXX=(T(JP1)-TWO*TJ+T(JM1))/DLXSQ
      E1XX=(E1(JP1)-TWO*E1J+E1(JM1))/DLXSQ
      E2XX=(E2(JP1)-TWO*E2J+E2(JM1))/DLXSQ
      E3XX=(E3(JP1)-TWO*E3J+E3(JM1))/DLXSQ
      E4XX=(E4(JP1)-TWO*E4J+E4(JM1))/DLXSQ
      CALL TTD(UJ,ALJ,ALU)
      AL(J)=ALJ
      BA=-UJ+ALU*UX+ALJ*(AXDA+ROX/ROJ)
      BB=ONE/(CV+TJ*CT)
      BC=(ONE-5.60D-2*E4J**2/(E5J*E2J)*DEXP(37956.72D0/TJ))
     1   /(ONE+2.25D3*E4J/(TJ*E2J)*DEXP(4982.39D0/TJ))
      BD=ATDA+UX+UJ*AXDA
      AREN=Z*PJ**(-2.D0)*E1J*E2J*ROJ*DEXP(-EDR/TJ)
      ARENO=5.45D14*E2J**.5D0*E5J*ROJ**.5D0*DEXP(-120754.91D0/TJ)*BC
      ENER1=CP*TX*(BA+UJ)+ALJ*(CP*TXX+CT*TX*TX)
      ENER2=-PJ/ROJ*BD
```

```
ENER3=-HT*PERJ/(ROJ*AJ)*(TSY-TW)+HR*AREN
ENER4=-UJ/GR*(ALJ*UXX+UX*(BA+UJ))
ROT(J)=-HJ*ROX-ROJ*DD
UT(J)=-GR/ROJ*PX+ALJ*UXX+UX*BA
TT(J)=-UJ*TX+BB*(ENER1+ENER2+ENER3+ENER4)
E1T(J)=ALJ*E1XX+E1X*BA-AREN
E2T(J)=ALJ*E2XX+E2X*BA-THREE*AREN-HALF*ARENO
E3T(J)=ALJ*E3XX+E3X*BA+FOUR*AREN
E4T(J)=ALJ*E4XX+E4X*BA+ARENO
RETURN
END
```

```
C*************************************************************************
C THERMAL PROPERTIES SUBPROGRAM                                          *
C*************************************************************************
      SUBROUTINE TMP(CP,CV,CT)
      IMPLICIT REAL*8(A-H,O-Z)
      COMMON /BLCTL/ZERO,HALP,ONE,TWO,THREE,FOUR,PI,TIMSC,TIME,CA,
     1               RPM,CR,VD,TWODB,PHIP,PHIM,PHIT,PHT,PT,PP,PM,GR,PRT,
     2               PR,RR,HR,Z,EDR,APST,PSM2,PSM2,ISIEP,M2,N,K4,
     3               NM1,NM2,NP,NM,NSP,NOI,NTH,NOO,NOOM1,NOOP1,K,K1,K2,K3
      COMMON /BLGOM/XLC,XOI,XOO,CL,DCL,CLL,CLR,S,RC,XLR,DIAT,DIAP,AP,
     1               ATH,APS,PERP,PERT,XPO,XLO,VP,VM,VC,DVP,VPDVC,ATDVP,
     2               B1,B2,B3,B4,B5,DLXHF,XTH,DOOP,HOOP,SOO,AOOM,DCX,HX,
     3               XSP,OMEGA,TIMSH,POTPI,DEG,VT,VTS,BORE
      COMMON /BLSUM/PP,PM,SMT,SM1,SM2,SM3,SM4,SM5,SMTO,SM10,ZMFB,PHP,PHM
      COMMON /BLDER/AMW,PSY,TH,USY,BSY,UPM,CS,S1,DELX,DLXSQ,HT,TSY
      DATA A0/2.257196D3/,A1/-1.858418D5/,A2/1.603333D1/
      TSY=(PSY*VT)/(SMTO*RR)
      SRT=DSQRT(TSY)
      CP=A0+A1/TSY+A2*SRT
      CV=CP-RR
      CT=-A1/TSY**2+A2/(TWO*SRT)
      HT=K4/100.D0*(7.1309D-3*PSY**.8D0*USY/BSY/TSY**.53D0)
      RETURN
      END
```

```
C*************************************************************************
C TURBULENT DIFFUSIVITY SUBPROGRAM                                       *
C*************************************************************************
      SUBROUTINE TTD(U,AL,ALU)
      IMPLICIT REAL*8(A-H,O-Z)
      COMMON /BLDER/ANW,PSY,TW,USY,BSY,UPN,CS,S1,DELX,DLXSQ,HT,TSY
      AL=S1*(UPN+DABS(U))
      ALU=S1
      RETURN
      END
```

```
C*************************************************************************************
C TIME STEP CONTROL SUBPROGRAM                                                       *
C*************************************************************************************
      SUBROUTINE TSC(J,T,E1,E2,E3,TT,E1T,E2T,E3T)
      IMPLICIT REAL*8(A-H,O-Z)
      COMMON /BLCTL/ZERO,HALF,ONE,TWO,THREE,FOUR,PI,TIMSC,TIME,CA,
     1               RPM,CR,VD,TWODB,PHIP,PHIM,PHIT,PHT,FT,FP,FM,GB,FRT,
     2               FR,RR,HR,Z,EDR,APST,POM2,PSM2,ISTEP,M2,N,K4,
     3               NM1,NM2,NP,NM,NSP,NOI,NTH,NOO,NOOM1,NOOP1,K,K1,K2,K3
      COMMON /BLTSC/TPC,EPC,EMIN,DELT,DLTMIN,DLTMAX
      DIMENSION T(N),E1(N),E2(N),E3(N),TT(N),E1T(N),E2T(N),E3T(N)
    5 FORMAT('-'/5X,'TIME STEP IS TOO SMALL',5X,'ISTEP =',I5,5X,'K1 =',
     1       I3,5X,'K2 =',I3,5X,'DELT =',1PE12.5)
      TTJ=TT(J)
      TJ=T(J)
      BUF=TPC*DABS(TJ/TTJ)
      IF(BUF.GE.DELT)GOTO 10
      DELT=BUF
      K1=4
      K2=J
   10 E1TJ=E1T(J)
      E1J=E1(J)
      IF(E1TJ.GE.ZERO)GOTO 40
      BUF=EPC*DABS(E1J/E1TJ)
      IF(BUF.GE.DELT)GOTO 40
      IF(E1J.GE.EMIN)GOTO 20
      IF(BUF.GE.DLTMIN)GOTO 20
      E1T(J)=ZERO
      DELT=DLTMIN
                GOTO 30
   20 DELT=BUF
   30 K1=1
      K2=J
   40 E2TJ=E2T(J)
      E2J=E2(J)
      IF(E2TJ.GE.ZERO)GOTO 70
      BUF=EPC*DABS(E2J/E2TJ)
      IF(BUF.GE.DELT)GOTO 70
      IF(E2J.GE.EMIN)GOTO 50
      IF(BUF.GE.DLTMIN)GOTO 50
      E2T(J)=ZERO
      DELT=DLTMIN
                GOTO 60
   50 DELT=BUF
   60 K1=2
      K2=J
   70 E3TJ=E3T(J)
      E3J=E3(J)
      IF(E3TJ.GE.ZERO)GOTO 80
      BUF=EPC*DABS(E3J/E3TJ)
      IF(BUF.GE.DELT)GOTO 80
      DELT=BUF
      K1=3
      K2=J
   80 IF(DELT.LT.1.D-10)GOTO 90
      RETURN
   90 WRITE(6,5)ISTEP,K1,K2,DELT
      STOP
      END
```

```
C*************************************************************************
C BOUNDARY VALUE SUBPROGRAM                                              *
C*************************************************************************
      SUBROUTINE BOD(RO,U,T,P,E1,E2,E3,E4)
      IMPLICIT REAL*8(A-H,O-Z)
      COMMON /BLCTL/ZERO,HALF,ONE,TWO,THREE,FOUR,PI,TIMSC,TIME,CA,
     1               RPM,CR,VD,TWODB,PHIP,PHIM,PHIT,PHT,PT,PP,PM,GR,PRT,
     2               PR,RE,HR,Z,EDR,APST,POM2,PSM2,ISTEP,M2,N,K4,
     3               NM1,NM2,NP,NM,NSP,NOI,NTH,NOO,NOOM1,NOOP1,K,K1,K2,K3
      DIMENSION RO(N),U(N),T(N),P(N),E1(N),E2(N),E3(N),E4(N)
      RO(1)=RO(2)
      U(1)=ZERO
      T(1)=T(2)
      P(1)=P(2)
      E1(1)=E1(2)
      E2(1)=E2(2)
      E3(1)=E3(2)
      E4(1)=E4(2)
      RO(N)=RO(NM1)
      U(N)=ZERO
      T(N)=T(NM1)
      P(N)=P(NM1)
      E1(N)=E1(NM1)
      E2(N)=E2(NM1)
      E3(N)=E3(NM1)
      E4(N)=E4(NM1)
      RETURN
      END
```

```
C*************************************************************************************
C FUNCTION SUBPROGRAM                                                                 *
C*************************************************************************************
      FUNCTION FX(W)
      IMPLICIT REAL*8(A-H,O-Z)
       COMMON /BLCTL/ZERO,HALF,ONE,TWO,THREE,FOUR,PI,TIMSC,TIME,CA,
     1               RPM,CR,VD,TWODB,PHIP,PHIM,PHIT,PHT,FT,FP,FM,GR,PRT,
     2               FR,RR,HR,Z,EDR,APST,PSM2,PSM2,ISTEP,M2,N,K4,
     3               NM1,NM2,NP,NM,NSP,NOI,NIH,NOO,NOOM1,NOOP1,K,K1,K2,K3
       COMMON /BLGOM/XLC,XOI,XOO,CL,DCL,CLL,CLR,S,RC,XLR,DIAT,DIAP,AP,
     1               ATH,APS,PERP,PERT,XPO,XLO,VP,VM,VC,DVP,VPDVC,ATDVP,
     2               B1,B2,B3,B4,B5,DLXHF,XTH,DOOP,HOOP,SOO,AOOM,DCX,HX,
     3               XSP,OMEGA,TIMSR,POTPI,DEG,VT,VTS,BORE
       COMMON /BLDER/AMW,PSY,TW,USY,BSY,UPN,CS,S1,DELX,DLXSQ,HT,TSY
       FX=(W-ONE)*DELX
       RETURN
       ENTRY FD(W)
       FD=TWO*DSQRT((W-XOO)*(XLC-W))
       RETURN
       ENTRY FH(W)
       FH=TWODB*(DCX-DCL*W)
       RETURN
       END
```

```
C*******************************************************************************
C COMMON DATA BLOCK                                                            *
C*******************************************************************************
      BLOCK DATA
      IMPLICIT REAL*8(A-H,O-Z)
       COMMON /BLCTL/ZERO,HALF,ONE,TWO,THREE,FOUR,PI,TIMSC,TIME,CA,
     1               RPM,CR,VD,TWODB,PHIP,PHIM,PHIT,PHT,FT,FP,FM,GR,PRT,
     2               FR,RR,HR,Z,EDR,AFST,POM2,PSM2,ISTEP,M2,N,K4,
     3               NM1,NM2,NP,NM,NSP,NOI,NTH,NOO,NOOM1,NOOP1,K,K1,K2,K3
       COMMON /BLINI/US,TS,PS,PHCP,PHCM2,PHCM1,PHSP,PHSM2,PHSM1,PHSM,
     1               E1SP,E2SP,E3SP,E5SP,E1SM2,E2SM2,E3SM2,E5SM2,E1SM1,
     2               E2SM1,E3SM1,E5SM1,AFIP,AFIT
       COMMON /BLGOM/XLC,XOI,XOO,CL,DCL,CLL,CLR,S,RC,XLR,DIAT,DIAP,AP,
     1               ATH,APS,PERP,PERT,XPO,XLO,VP,VM,VC,DVP,VPDVC,ATDVP,
     2               B1,B2,B3,B4,B5,DLXHF,XTH,DOOP,HOOP,SOO,AOOM,DCX,HX,
     3               XSP,OMEGA,TIMSR,POTPI,DEG,VT,VTS,BORE
       COMMON /BLSPK/TSH,TSM,E1S,E2S,DAH,DAM,TNP
       COMMON /BLSUM/PP,PM,SMT,SM1,SM2,SM3,SM4,SM5,SMT0,SM10,ZMFB,PHP,PHM
       COMMON /BLDER/AMW,PSY,TW,USY,BSY,UPN,CS,S1,DELX,DLXSQ,HT,TSY
       COMMON /BLTSC/TPC,EPC,EMIN,DELT,DLTMIN,DLTMAX
       DATA HALF/.5D0/,ONE/1.D0/,TWO/2.D0/,THREE/3.D0/,FOUR/4.D0/,NSP/3/,
     1      XLC/5.48D0/,XLR/6.44D0/,VD/32.4D0/,CL/.4104D0/,CLL/.4037D0/,
     2      RPM/2100.D0/,PI/3.1415927D0/,DLTMAX/6.0D-6/,AMW/28.85D0/,
     3      GR/386.D0/,RR/1.854D4/,HR/4.956D9/,EDR/27193.D0/,TW/900.D0/,
     4      Z/6.30D17/,EMIN/1.D-6/,ZERO,US/2*0.D0/,TPC/-.01D0/,EPC/-.70D0/,
     5      DLTMIN/1.D-7/
       END
```

SECTION II

Section II is based on the Master of Science thesis entitled "Investigating the Performance and Exhaust Emissions of a Fuel Injected, Dual Chamber Stratified Charge Spark Ignition Engine," by James J. Bruckbauer, Department of Mechanical and Industrial Engineering, University of Illinois at Urbana-Champaign, May 1979.

INVESTIGATING THE PERFORMANCE AND EXHAUST EMISSIONS OF A FUEL INJECTED, DUAL CHAMBER STRATIFIED CHARGE ENGINE

BY

JAMES JOSEPH BRUCKBAUER

B.S., University of Illinois, 1977

THESIS

Submitted in partial fulfillment of the requirements
for the degree of Master of Science in Mechanical Engineering
in the Graduate College of the
University of Illinois at Urbana-Champaign, 1979

Urbana, Illinois

ACKNOWLEDGEMENTS

This investigation was made possible by grants from the National Science Foundation and U. S. Department of Energy. The actual experimental data was taken by the author with fellow graduate assistants Glenn Gehrke and Mike White. The project was carried out under the supervision of Prof. Spencer C. Sorenson at the University of Illinois. Professors William L. Hull and Ronald D. Matthews also gave invaluable assistance during the study. Many thanks are given to these three for their time and insights. The continued help of Mr. William Morfey in producing the experimental setup is also greatly appreciated. Mr. Joe Link is acknowledged for assistance in the electrical circuit for the fuel injection used in this project.

TABLE OF CONTENTS

TABLE OF SYMBOLS

A/Fa	Auxiliary chamber input air/fuel ratio.
F/Fm	Main chamber input air/fuel ratio.
A/Ft	Overall input air/fuel ratio to engine.
bmep, imep	Brake and indicated mean effective pressure.
bsfc, isfc	Brake and indicated specific fuel consumption.
CVCC	Compound vortex controlled combustion.
CO	Carbon monoxide.
HC	Unburned hydrocarbons.
NOx	Nitric oxides.
Ga	Mass of fuel and air to auxiliary chamber.
Gt	Total mass of fuel and air to engine.
GFa	Mass of fuel to auxiliary chamber.
GFt	Total mass of fuel to engine.
EGR	Exhaust gas recirculation.
A/Fai	Auxiliary chaber air/fuel ratio at ignition.
A/Fmi	Main chamber air/fuel ratio at ignition.
Va	Auxiliary chamber clearance volume.
Vc	Engine clearance volume.
Ft	Torch area.
MBT	Minimum spark advance for best torque.
FID	Flame ionization detector.
NDIR	Non-dispersive infrared detector.
ppm	Parts per million.
ATC, BTC	After and before top dead center for piston.
VOLF	Volumetric efficiency.
A/F	Air to fuel ratio.

S.I.	Spark ignition.
TDC	Top dead center.
SFC	Specific fuel consumption.
MEP	Mean effective pressure.

I. INTRODUCTION

Recent government regulations on the automotive engine have made it necessary to improve fuel economy while decreasing HC, CO, and NOx emissions. As of now, these three combustion products are the only tailpipe discharges controlled under the Clean Air Act. The primary theory of smog formation is that reactive hydrocarbons and nitrogen oxides in a particular mixture react photochemically to form many products [1]. The complex set of reactions involved receive energy from the ultraviolet end of the solar spectrum. This is why pollution is often worst on hot, dry summer days. The powerful irritant ozone is one of the products of the hydrocarbon-nitrogen oxide reactions. Air pollution and smog can be reduced by decreasing the number of reactive hydrocarbons at one particular concentration of NOx. Therefore decreasing NOx should also improve air quality. Carbon monoxide can impair nerves and heart of man by reducing the oxygen-carrying capability of the blood. It has a life of five years before being destroyed by oxidation reactions.

While the environmentalists are attempting to rid our air of pollution, projected oil supply deficiencies may rid the country of its large automobile. By 1985 an auto company must field a fleet of cars that average 27.5 mpg. The search is on in the technical community for either alternate powerplants, fuels, or the desired modifications to existing engines which will comply with the laws. If this is not accomplished, cars will have to be downsized and the large auto will disappear.

Current industry solutions to the problems are far from being final. The use of catalysts means lead free fuel must be used. Exhaust gas recirculation (EGR) and air pumps with all their controls are making the auto engine into a very intricate piece of machinery. Electronic controls make the future look even more complex. Diesel engines may have difficulty with future emission laws because of high NOx and particulates. Three way catalysts to reduce HC, CO, and NOx create problems of exact fuel metering needs which cannot be accomplished with conventional carburetors.

One engine concept that has received a great deal of attention in the past decade is the stratified charge engine. This engine allows an air/fuel mixture to burn more perfectly at relatively low peak temperatures. This paper will be dealing with a three-value, divided chamber stratified charge engine.

II. THE THREE-VALVE, DIVIDED CHAMBER STRATIFIED CHARGE ENGINE

The conventional S.I. engine has several weaknesses that a stratified charge engine can overcome. The homogeneous mixtures of conventional engines within the air/fuel limits that allow flame propagation yield low combustion efficiency. Operation also occurs in air/fuel ranges which correspond to that of maximum NOx and high HC emissions. Also, with these mixtures, end gases can self-ignite and octane requirements are higher than what would be needed for a leaner mixture.

The stratified charge concept in engines can overcome many of the pollution problems of the S.I. engine with as good or better fuel economy. Lean ignitability is possible by introducing a small, rich charge around the spark which can ignite the bulk of the mixture, which is lean. Operating with lean equivalence ratios means lower octane requirements, higher thermal efficiencies and combustion in the region of low NOx and CO formation with low HC emissions. Open chamber stratified charge engines inject fuel into an air swirl to achieve the regions of rich and lean mixture. These types show great promise, but also have particulate emissions like diesels. The 3-valve stratified charge engine uses a supplementary chamber and extra valve to supply the rich charge about the spark plug. This prechamber serves as the place for flame initiation and physically creates charge stratification when a lean mixture is supplied to the main chamber.

Since the rich auxiliary mixture is only a small portion of the total mixture supplied to the engine, leaner overall air/fuel ratios can give better economy or at least as good as a conventional engine. By operating rich, the prechamber is in a

region of low NOx formation. The orifice between the auxiliary and main chambers adds turbulence to the escaping prechamber gases which aids in ignition of the lean main chamber. This orifice is refered to as the torch opening.

Prechamber studies of this type make interesting studies since mixture formation is rather complex. During the intake stroke both auxiliary and main intake valves open with rich charge delivered to the prechamber and a lean charge to the main chamber. The rich prechamber mixture combines with any residual left in the prechamber. A portion of this mixture overflows through the torch opening into the main chamber and mixes to some degree with the lean charge. Upon compression, some of the mixture formed in the main chamber is pushed back into the auxiliary chamber and dilutes the prechamber mixture. This helps insure good ignitability. The degree of stratification is an important part of the mixture formation. If the overflow does not perfectly mix, then an intermediate mixture is formed near the torch opening. Two or possibly more layers of stratification would then exist in the main chamber alone. However, if the prechamber overflow did mix completely with the lean main chamber mixture, then only the stratification between the rich prechamber and lean main chamber would exist. Figure 1 illustrates the intermediate zone. This is what Honda refers to as their mixture cloud [2].

The question of degree of mixing is one that this investigation attempted to answer. Most past studies by Honda, Ford, GM and others have involved main chamber carburetion. In order to gain added insight into mixture formation and optimum operating

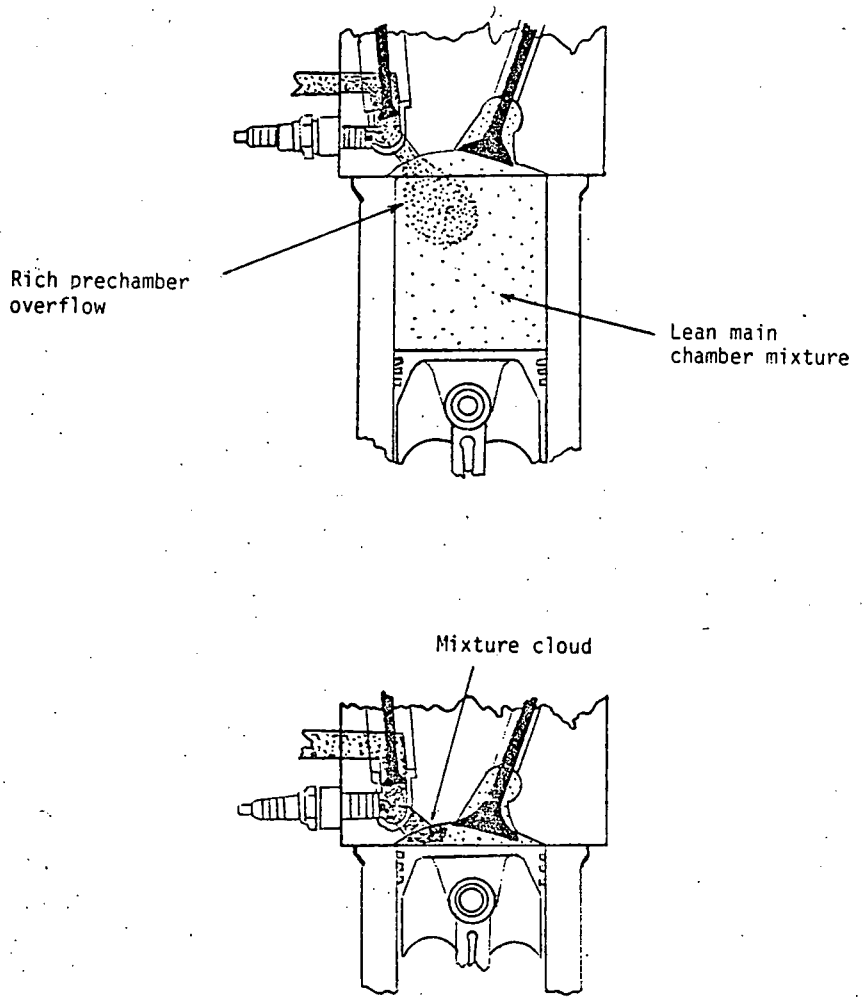

Figure 1. Three-valve stratified charge mixture formation.

conditions, the main chamber was fuel injected in this study. It was reasoned that the added flexibility of variable injection timing and more precise fuel metering would aid in the understanding of the engine operating conditions.

III. EXPERIMENTAL SETUP AND PROGRAM

A. The Stratified Charge Engine

The base for the engine in this experiment was a modified 32.4 cubic inch, single cylinder, flathead, utility engine by Briggs and Stratton. The three-valve prechamber head was designed in a graduate project by Glenn Miller. The head was then built at the University of Illinois with fabricated and purchased components. Honda's CVCC engine, the only stratified charge type in current production vehicles, formed the basis for the head design.

The head was machined out of a steel block and contains the three valves and prechamber. It was built in a wedge configuration much like Honda's design. The engine could also be run as an overhead valve, conventional version if a spark plug was screwed into the orifice outlet and the prechamber intake valve was disconnected. The orifice itself was removable and three sizes were initially built and tested. Prechamber volume (V_a) was also made adjustable. Data taken by Grandys [3] was available for the engine run in the conventional S.I. version.

The overhead valves of the main chamber ran off of the original Briggs and Stratton cam with lengthened push rods. The third valve, acting as an intake valve for the auxiliary chamber, was operated by a separate cam and follower. The cam ran at half of crank speed by a belt drive off the crankshaft. Both auxiliary and main chamber intake valves opened at approximately the same time. The camshaft operating the third valve also

had a lobe which operated a set of points that were adjustable for variable ignition timing. A conventional automotive ignition system with coil, points and condenser was used. An adaptation of a Kistler pressure transducer to the Champion spark plug was made to monitor prechamber pressure. Crank angle pulses every ten degrees from magnetic pickups were displayed along with the pressure traces on an oscilloscope. Pictures taken with a polaroid scope camera recorded the display, with triggering off the ignition points.

Two separate fuel metering systems supplied main and auxiliary combustion chambers. Air and propane from compressed tank sources were used to supply the prechamber to avoid vaporization problems pointed out by Purins [4]. The use of Matheson dual-float rotameters equipped with a 605 tube for air and 603 tube for propane allowed good control over the rich mixtures. The air and propane mixed in a surge tank before entering the prechamber.

During initial investigations of this engine, the original Briggs and Stratton updraft carburetor was used to supply main chamber charge. In this study the main chamber was supplied with fuel by port fuel injection. The fuel injector used was a Volkswagen type 3 injector mounted at a 30 degree angle to the air flow. The original updraft carburetor was retained for use in throttling the air flow. The fuel line system was a common rail with only one rail used (since it was a one cylinder engine). A Bosch fuel pump was utilized in conjunction with a Volvo pressure regulator. These gave an injection pressure of 25 psi. Air consumption was measured by a laminar flow meter which was

upstream of a surge tank. Iso octane was supplied as fuel to the main chamber and its consumption measured by an electric timer and burette.

In order to fire and close the fuel injector a combination mechanical-electrical unit was built. The diagram of the system is shown in Figure 2. Mechanical points ran off another lobe on the same camshaft that operated the prechamber intake valve. Injection timing was adjusted by rotating the points around the lobe. When the points closed, the injector opened, since the righthand portion of the circuit was closed between injector coil, battery and bulb. The zener diode kept a constant voltage in the circuit. Meanwhile in the lefthand portion of the circuit, the RC circuit, consisting of a capacitor and adjustable resistance, began to charge. When the required voltage was reached, the unijunction fired and current passed through resistors 1 and 2. Current then flowed to the SRC and fired it. This opened a one way gate. A short circuit occured and current flowed through EBC instead of EAD, and the fuel injection closed since no current passed through the injector coil.

When the points open, all voltages in the circuit went back to zero and the process started over again. Varying the value of the resistance varied the time the injector was held open, and fuel metering was controlled in this way. Changing resistance changed the amount of fuel added to the air stream flowing through the port, and thus changed the A/Fm. Two 12 volt batteries were used, one for the ignition system and fuel pump and one for the fuel injection circuit. Figures 3 and 4 show these circuits.

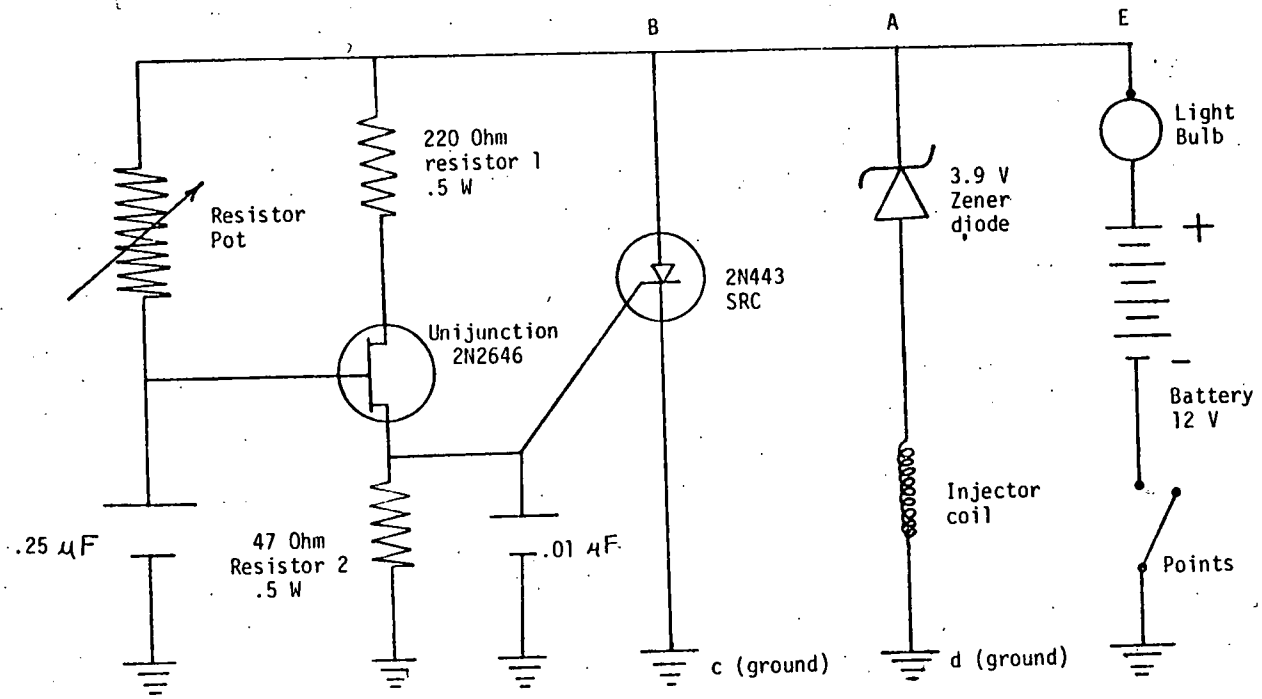

Figure 2. Fuel injection electrical-mechanical circuit.

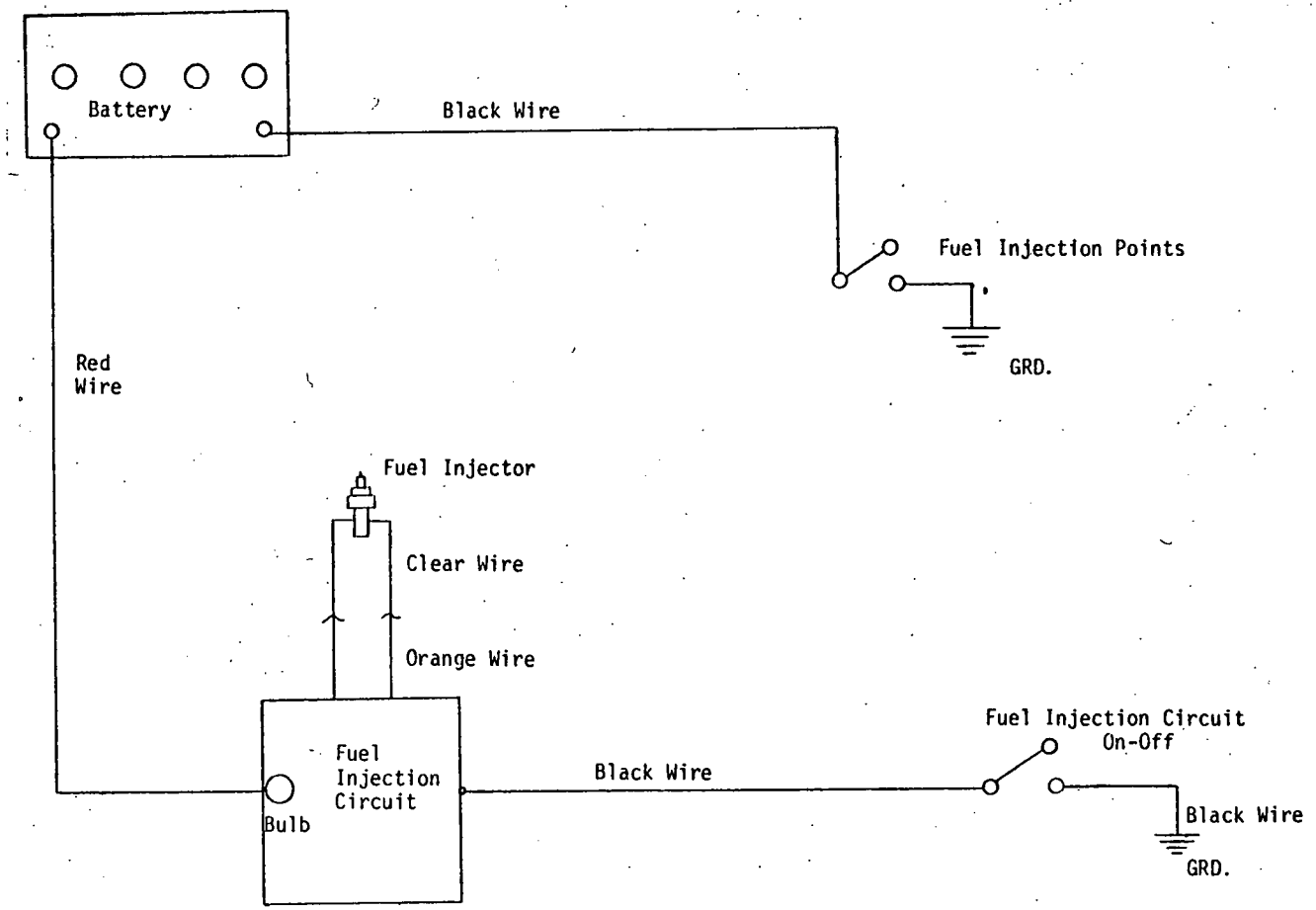

Figure 3 . Fuel injection circuit.

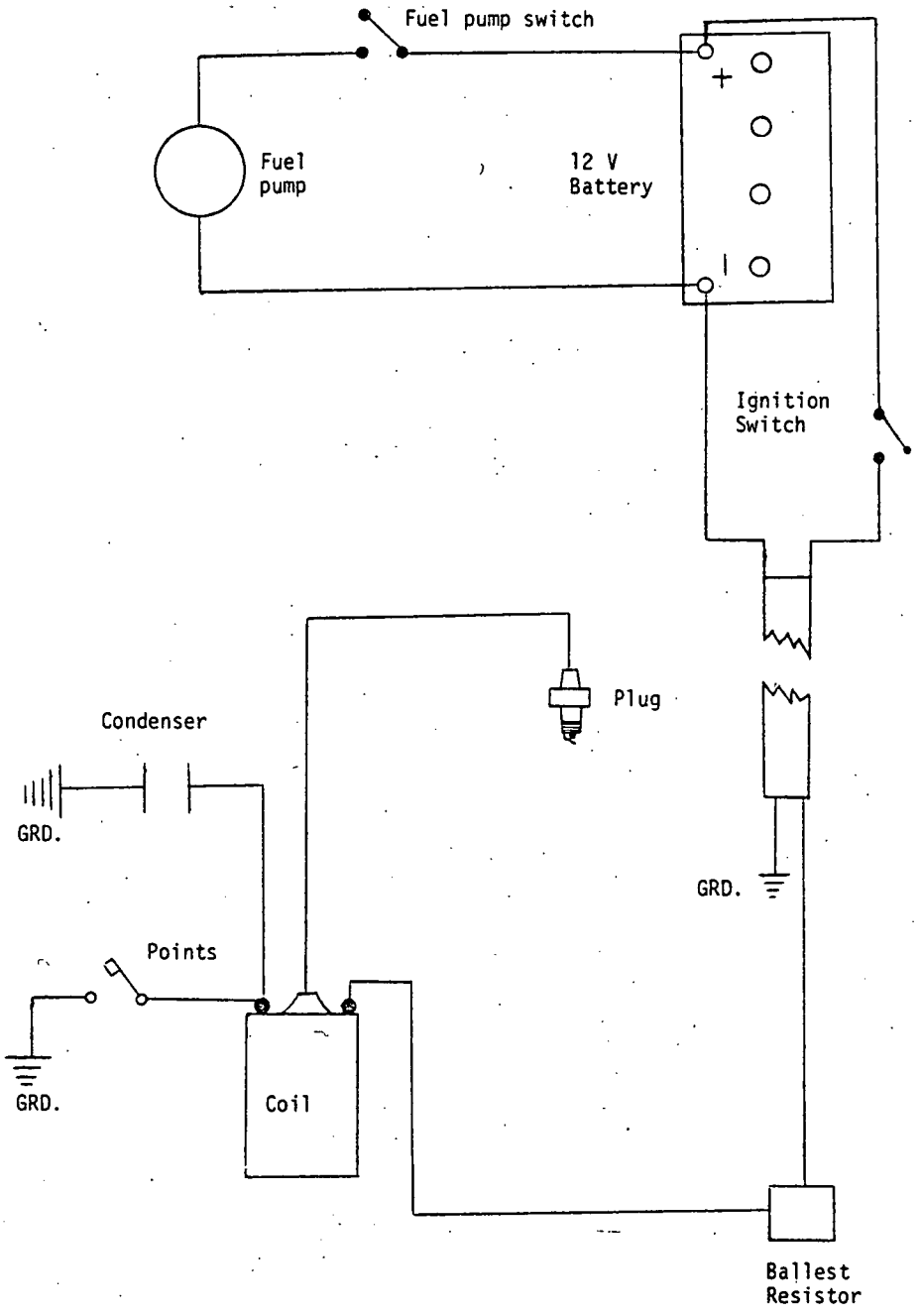

Figure 4. Ignition and Fuel pump circuits.

The head temperature was controlled by circulating coolant around the ports and controlling the amount of cooling water through the counterflow heat exchanger through which the coolant passed. A chromel-alumel thermocouple just downstream from the exhaust valve monitored exhaust temperature. Engine output was absorbed by a D-C motor-generator coupled to the output shaft.

B. Exhaust Testing System

An exhaust monitoring system was constructed which complied with standard SAE practices as stated in the 1976 handbook [5]. Hot gases from the engine entered a mixing tank with water cooled coils which removed some water vapor and froze exhaust reactions. Figure 5 shows the system used. The sample from the tank was used to test for HC, CO, and CO_2. Further water vapor was removed by a water trap. The portion of the sample to be tested for CO-CO_2 was run through a dessicant also, to remove all remaining water vapor. This protected the NDIR windows from water vapor damage. The sample to the FID was not run through the dessicant because of HC absorbtion problems. The first filter removed soot from the sample, the second removed dessicant particles.

Beckman 400 and 402 flame ionization detectors were used to give HC concentration in parts per million of methane (CH_4). CO was detected by a Beckman 315-A nondispersive infrared detector. Two ranges could be run with this unit, 0 - .65% and 0 - 10%. A Beckman 315-B NDIR gave CO_2 concentrations in a 0 - 15% range which could be used to help set air/fuel ratio.

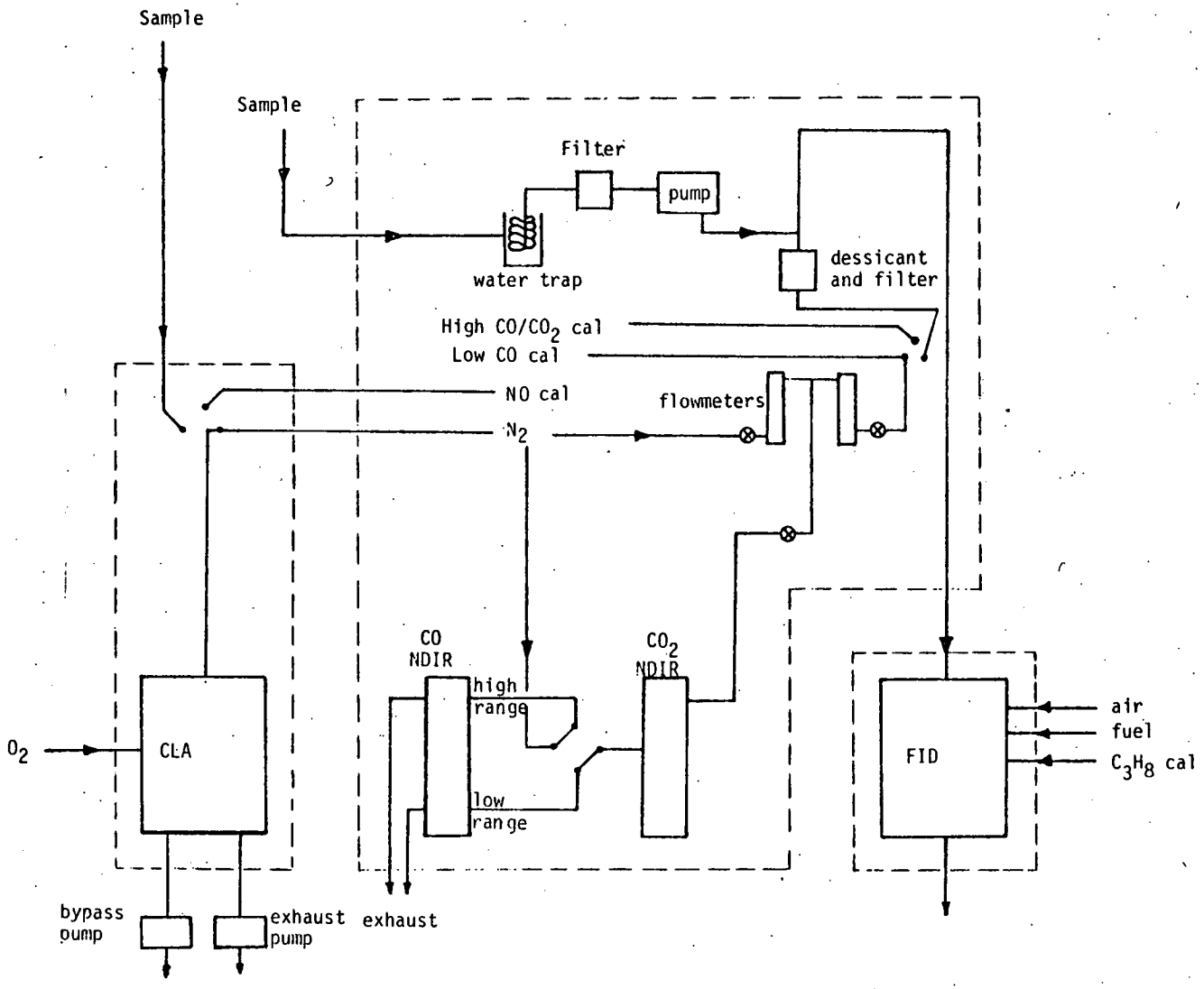

Figure 5. Exhaust analysis system.

In monitoring NOx, a chemiluminescent analyzer (CLA) was used. The unit used was a Thermal Electron 12A modified to sample at under one half atmosphere pressure to avoid condensation in the sampling line. Both NO and NOx readings could be taken with this instrument. The readout was in ppm NOx and NO. All emissions equipment output was recorded on Texas Instrument strip chart recorders. Nitric oxide readings were corrected according to the technique by Matthews, Sawyer and Schefer [6]. After startup and a warmup period emissions were sampled continuously.

C. Test Procedure

A program was decided upon which would try to determine the conditions of minimum NOx levels, since this is one of the main objectives of stratified combustion. Information on the mixing of the two charges was also one of the primary purposes of the investigation. The results of the fuel injection of the main chamber would be compared to the carbureted version tested by Grandys.

The important parameters of the prechamber stratified charge engine have been pointed out by Ford [4], Honda [2], GM [7] and others. They include prechamber volume (Va), the air/fuel ratio to the prechamber (A/Fa), the air/fuel ratio to the main chamber (A/Fm), total overall air/fuel ratio (A/Ft), ratio of auxiliary mass flow to total mass flow (Ga/Gt), and ratio of auxiliary fuel mass flow to total fuel mass flow (GFa/GFt). Dimensionless parameters of importance are the ratio of torch opening area to auxiliary chamber volume (Ft/Fa), and auxiliary volume to clearance volume (Va/Vc). The prechamber volume includes the volume within the .548 inch long removable nozzle.

Three nozzle sizes with diameters of .201, .332 and .437 inches were originally studied in the carbureted engine. However because of combustion knock, the smallest nozzle was discarded. The .332 diameter orifice was found to cause higher NOx emissions than the large .437 inch nozzle [3, 8]. Therefore the investigation was performed using only the large orifice (.437 inch diameter) which had a Ft/Va ratio of .1 cm^{-1}. All tests were performed at a constant speed of 2100 rpm. Prechamber volume (Va) was also kept constant during all tests.

In order to compare fuel injection with carburetion of the main chamber, the Grandy's experiment of running three prechamber fueling groups over a range of air/fuel ratios was repeated. Group A had an A/Fa=7, and Ga/Ft=10%. Group B had A/Fa=4 and Ga/Ft=5%, and Group C had A/Fa=4 and Ga/Ft=5%. These were all nominal values, with all full throttle values within 13%, and part throttle within 5%. These groups were run at full throttle (defined as 77% VOLF, within 3%) for fuel injection timings of 0^{o} and 110^{o} ATDC on the intake stroke. Spark timings were fixed to duplicate Grandy's runs from 25^{o} BTC to 36^{o} BTC over an air/fuel range of 15 to 22. Group A was also run at part throttle (44% VOLF, within 1%) for a fuel injection timing of 110^{o} ATC. Spark timings were fixed from 20^{o} BTC to 30^{o} BTC, over an A/F range of 15 to 21.

In order to investigate injection timing effects, Group A was run at full throttle for four injection timings over a range of A/F ratios. The fuel injection timings were 0, 60, 110 and 180 degrees ATC of the intake stroke. Runs were made at MBT timing that ranged from 28^{o} BTC to 30^{o} BTC.

The final experiment was to run at prechamber equivalence ratios of 1, 2, 3, 4 and 5. Total A/F ratio was kept at approximately 18. Each five equivalence ratios of the prechamber were run with Ga/Gt= 5% and Ga/Gt= 10%. Spark timing was kept constant at 25^{o} BTC to insure constant mixing of the prechamber overflow for all 5 equivalence ratios, even though the air/fuel ratios of the overflow would all have been different. This meant that since percentage of overflow was the same for all five runs, main chamber degree of mixing should have been the same for all runs.

Next these runs were repeated with all conditions the same except for a block being placed in the main chamber intake port to direct the incoming charge. This would cause swirl in the chamber, it was theorized. Figure 6 shows placement of the block in the intake port and theoretical swirl direction. It was hoped that the swirl would cause the prechamber overflow to mix more completely with the main chamber mixture. Therefore if there was a large difference between runs with and without swirl, information concerning degree of mixing without swirl might be found. The head design has very little built-in swirl, if any. Even with an offset valve, the intake port comes in at a 90^{o} angle to the valve, and thus there is no directing of the intake in a circular direction which would produce a swirl.

In all runs, the emission data was taken on the strip charts. Other data recorded was: exhaust temperature, fuel time, pot setting, burette fuel constant, dyno load, main chamber air flow-meter pressure differential, air and propane pressures and float levels, head temperature, injection timing, and spark timing.

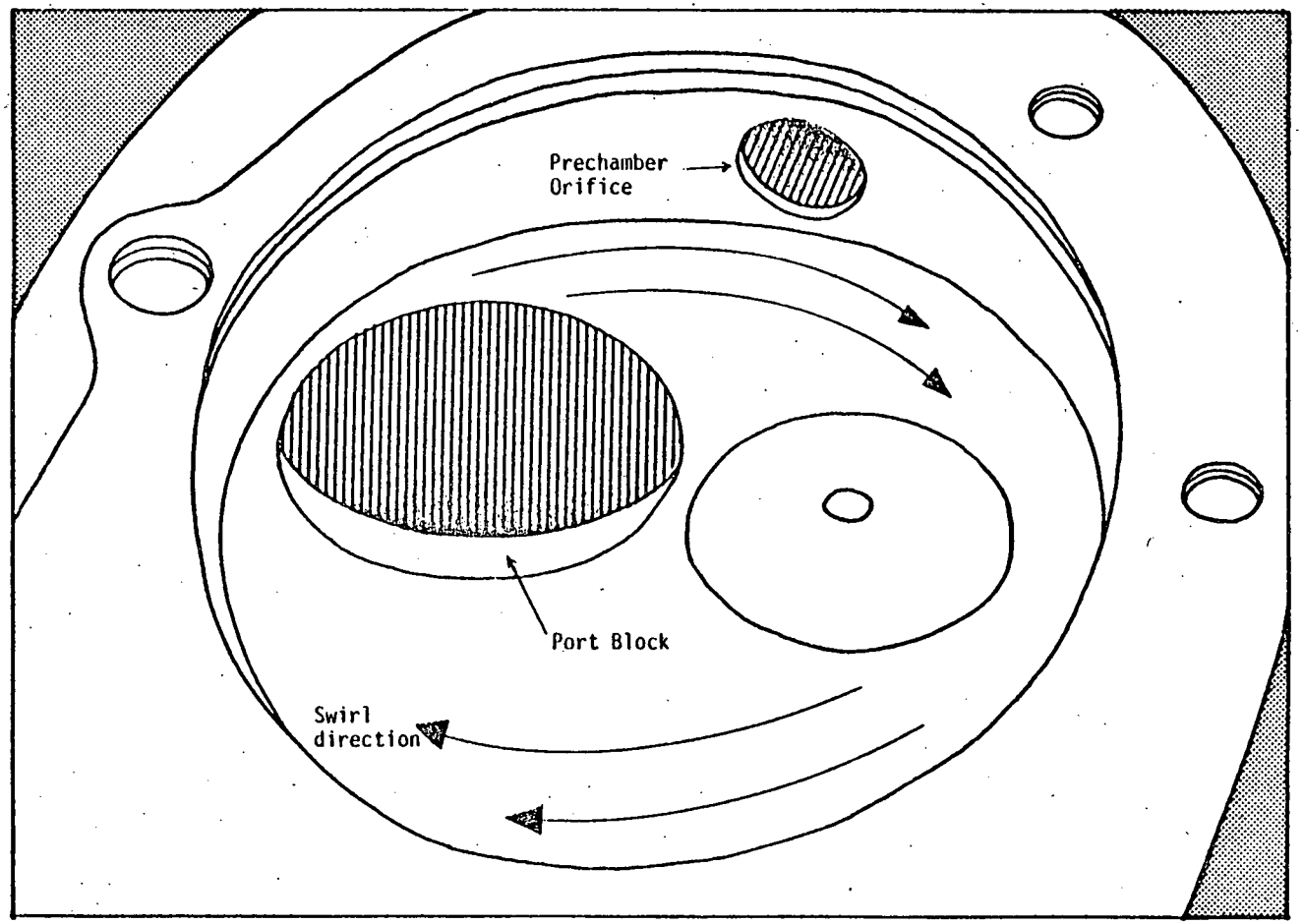

Figure 6. Diagram of three-valve head with block in intake port to produce swirl.

Friction loads were also taken after runs. A summary of engine conditions is shown in Table 1.

D. Combustion Photography with Carbureted Version

A second Briggs and Stratton block with an extended piston bolted to the original was set up to enable the main combusion chamber to be viewed from the bottom. A quartz window was used as the piston face, with the piston slotted front and back to allow it to move about a mirror, and the mirror to be viewed by a high speed camera. Thus high speed films of the combustion process could be taken, with the same head bolted to the extension. Iso octane was again used as fuel. Copper oleate was added (2% by weight) to try to get the lean combustion in the main chamber to burn more visibly. Both color and black and white pictures were taken. Spark timing was 20^{o} BTC. Engine speed was approximately 1700 rpm, but since the total running time for this setup was only five to ten seconds, exact operating conditions weren't known. This was especially true for the A/Fm, since it could not be determined in such a short time for carburetion.

TABLE 1

Engine Operating Conditions

Engine		
Speed	Constant	2100 rpm
Displacement		32.4 in^3.
Compression ratio		7.98
Coolant temperature		110^o-140^o F.
Spark timing	Fixed and MBT	20^o-49^o BTDC
Ft/Va	Large nozzle	.1 cm^{-1}.
Orifice diameter	Large nozzle	.437 in.
Va/Vc	With large nozzle	12.7%
Fuel injection timing	Variable	0^o, 60^o, 110^o, 180^o ATC
Volumetric Efficiency	Part throttle	44% ($\pm$ 1%)
	Full throttle	77% ($\pm$ 3%)
Main chamber fuel		Iso Octane
Prechamber fuel		Propane
Fuel line injection pressure		25 psi
Overall air/fuel range		15-24

Prechamber Fueling Groups	A/Fa	Ga/Gt (%)
A	7	10
B	4	10
C	4	5

IV. RESULTS AND DISCUSSION

A. Prechamber Fueling Groups

As stated before, the three prechamber groups run by Grandys were run in this study with similar spark timings for TDC fuel injection. The groups were as follows: Group A - A/Fa= 7, Ga/Gt=10%, Group B - A/Fa=4, Ga/Gt=10%, and Group C - A/Fa=4, Ga/Gt=5%. Figure 7 shows the results of mean effective pressure and specific fuel consumption plotted as a function of air/fuel ratio. All groups were run at full throttle (77% VOLF) and bmep, imep, and bsfc were corrected for changes in atmospheric humidity and temperature. These results show Group C has poorest fuel economy and lowest power. At ratios of under 18, Groups A and B show almost identical power and fuel consumption. Over 18, there is a slight advantage to Group B. The fuel consumption curves for B do not turn up at lean A/Ft as the ones for A and C do.

It is suggested that these results and the engine emission trends shown later can be explained using a concept presented by GM [9]. This is, that if both a lean and a rich region exist together, there will be a transition zone that exists which contains a mixture at or near the stoichiometric value. Honda's mixture cloud theory states that a region with an intermediate air/fuel ratio forms in the main chamber near the torch opening. This mixture cloud is the product of partial mixing of the rich prechamber overflow with lean A/Fm. The "correct" mixture cloud formation results in a cloud that is rich enough to promote good

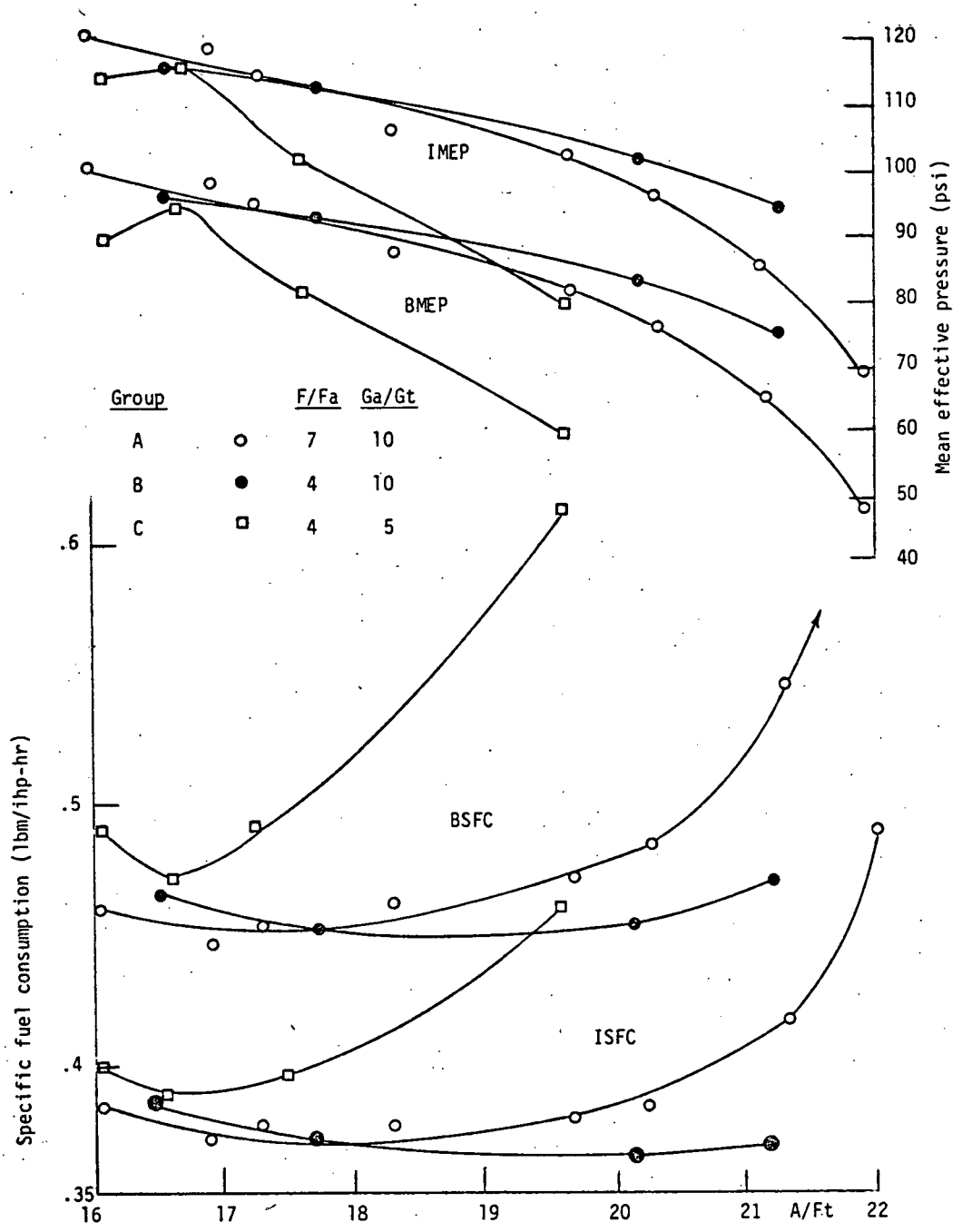

Figure 7. Mean effective pressure and specific fuel consumption - TDC Injection.

transitional burning from the prechamber to the lean A/Fm mixture. Thus, HC and CO oxidation will be good and these emissions will be low. Too rich of a cloud would cause rapid temperature and pressure rise in the main chamber, which would cause large NOx formation. Therefore, the correct size intermediate zone must be formed to give reduction in all three emissions.

It is believed that this mixture cloud theory is the best means of explaining the operation of this test engine. It has been shown in Figure 7 that there exists differences in power and fuel consumption between the three groups. Referring ahead to the emission curves, Figures 8, 9 and 10, it can be seen that even greater differences exist between emission values for the three groups. These differences cannot be explained with the perfect mixing assumption as Grandy's postulated. A computer simulation reported by Sorenson [8] used the assumption of perfect mixing of prechamber overflow to calculate air/fuel ratios in the prechamber and main chamber at ignition. The results are shown in Table 2 for A/Ft=20.2, full throttle and 20^{o} BTC spark timing.

TABLE 2

Caluclated A/Fmi and A/Fai Values for A/Ft=20

Group	A	B	C
A/Fmi	21	21.4	21.1
A/Fai	14.7	11.5	12.5

The calculated data shows that at ignition, Groups B and C would have almost the same prechamber and main chamber air/fuels. Therefore, experimental emission and performance for these two groups should have been almost identical. This was not found in test results as pointed out, which tends to disprove the perfect mixing, two zone combustion assumption.

Pan performed a three zone mixing model [9] with a prechamber perfectly mixed region, a main chamber intermediate zone, and the main chamber lean mixture. The intermediate zone only mixed with the prechamber gases. A 50% mixing percentage was assumed for all three groups. This model was able to predict NOx values fairly accurately and give the orders of the groups as far as NOx production found experimentally. Figure 8 shows the results of the NOx formation. Group C has the lowest production, with Group A second and Group B giving the highest values over the A/F range. It is believed that NOx production is a function of the intermediate zone A/F ratio, with the group having the most mixture near slightly leaner than stoichiometric ratio producing the most NOx. Table 3 shows representative calculations by Pan at full throttle, A/Ft=20.8 and the three zone equivalence ratios found. The intermediate zone equivalence ratio represents a point just outside the torch opening in the main chamber.

The calculated intermediate zone equivalence ratios show that Group B is richest, A second richest, and C leanest. This order corresponds to the order of experimental NOx curves. Group B was highest over the entire air/fuel tested, A second highest and C lowest as shown in Figure 8. The rich prechamber is a

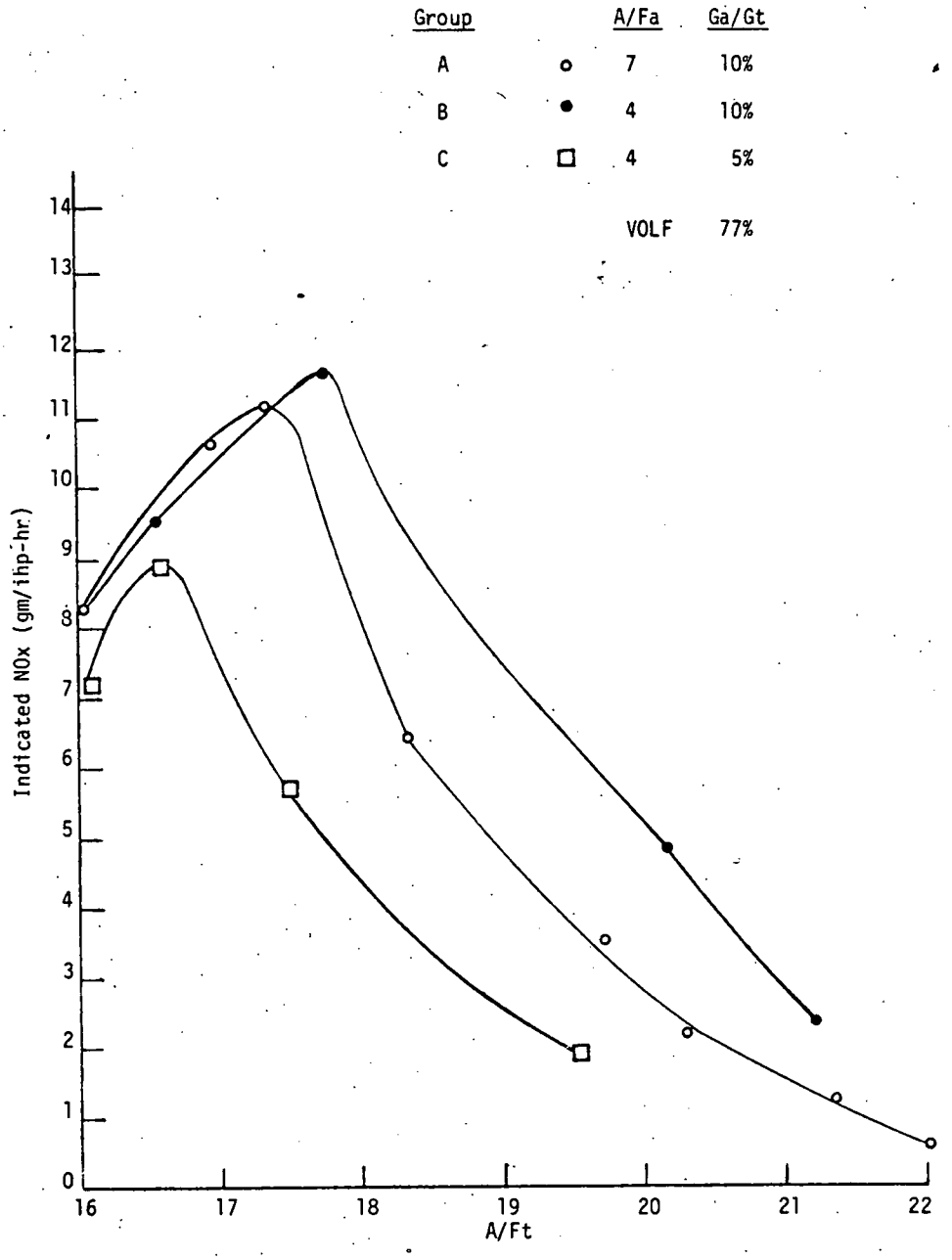

Figure 8. Indicated NOx - TDC injection.

TABLE 3

Calculated Equivalence Ratios for the Three Zones of Combustion Model, VOLF=77%, A/Ft=20

Group	Spark Time	Prechamber	Intermediate Zone	Main Chamber
A	10^{o} BTC	.993	.833	.63
B	10^{o} BTC	1.162	.872	.524
C	5^{o} BTC	1.065	.781	.639

TABLE 4

Calculated Equivalence Ratios for the Three Zones of Combustion Model, VOLF=44%, A/Ft=20.8

Group	Spark Time	Prechamber	Intermediate Zone	Main Chamber
A	2.5 BTC	.89	.79	.60
B	12.5 BTC	1.1	.85	.495
C	15.0 BTC	1.0	.76	.61

small quantity and does not produce much NOx, and the A/Fm is lean enough so that it will have low NOx production from slow combustion. It is the intermediate zone that controls NOx production, with the slightly richer Group B having more mixture slightly lean than the other groups. Thus it has the most NOx production. Table 4 shows the calculations for part throttle data.

Table 4 shows the same trends with part as full throttle. However, here Group B is richest in the intermediate zone, but C and A are almost identical. Part throttle runs by Grandy's with carburetion showed Group B produced highest NOx, but Groups C and A were almost the same in NOx emissions. The part throttle runs were not made with the fuel injected version for all three groups.

Figures 9 and 10 show indicated HC and CO emissions for the A/F range. The HC curves show that at A/Ft=16.5, Group C gives lowest hydrocarbon emissions. At higher A/F ratios, the Group C HC emissions are highest. Group A and B have similar HC emissions over the air/fuels tested. Group A was run lean enough to see the turn up of hydrocarbons. At an A/Ft=16.5, the Group C conditions must have a high enough intermediate zone A/F and A/Fm to give fast combustion that gave low HC. At higher ratios, the lean A/Fm and leaner intermediate zone than A or B gave slow combustion which resulted in unburned hydrocarbons being high. The lower power and higher fuel consumption shown in Figure 7 shows poor combustion at leaner mixtures than 16.5. Groups A and B appear to have favorable conditions for HC oxidation with the richer intermediate zones. This shows a trade-off between low HC and high NOx, with Group A giving the best combination of the three groups.

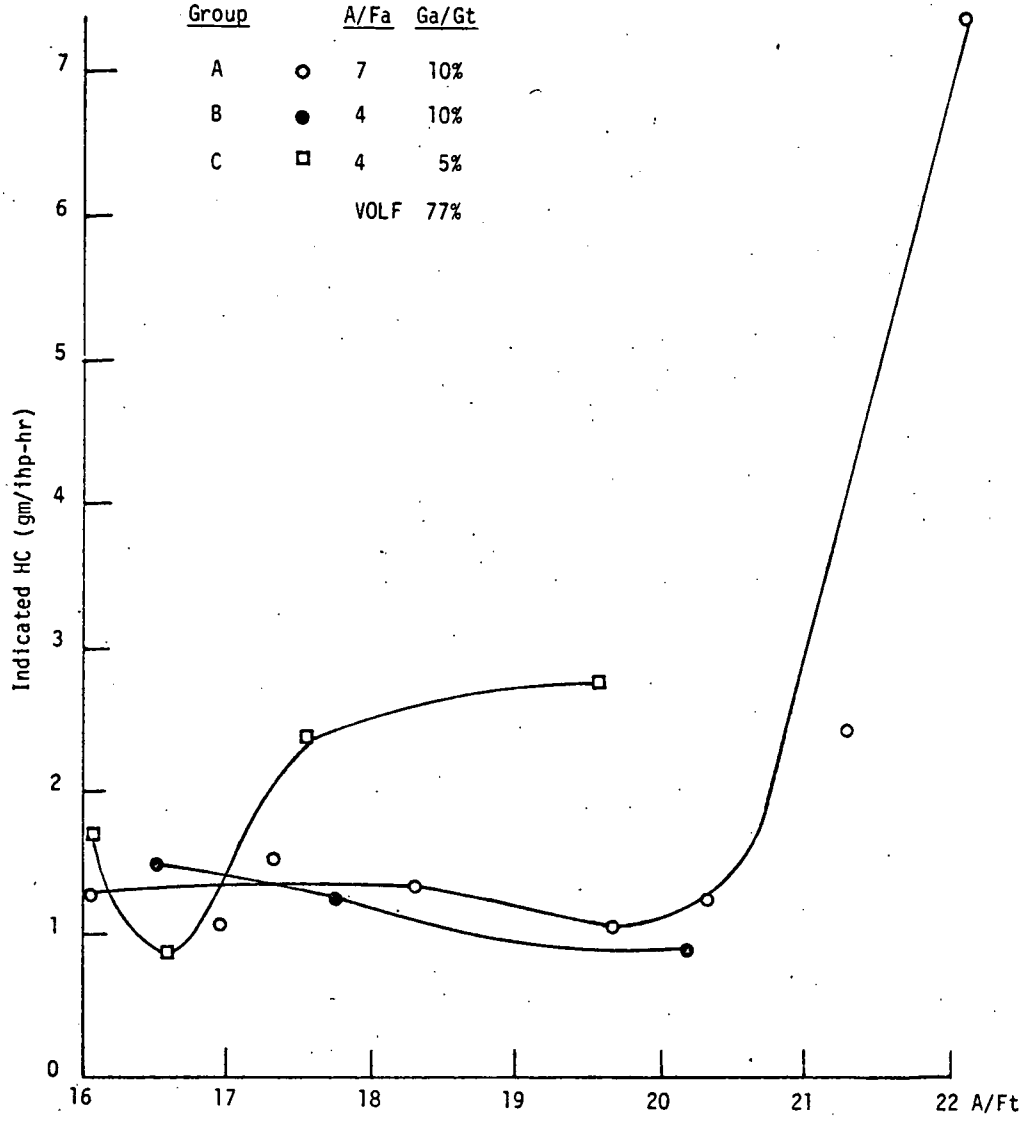

Figure 9. HC emissions - TDC injection.

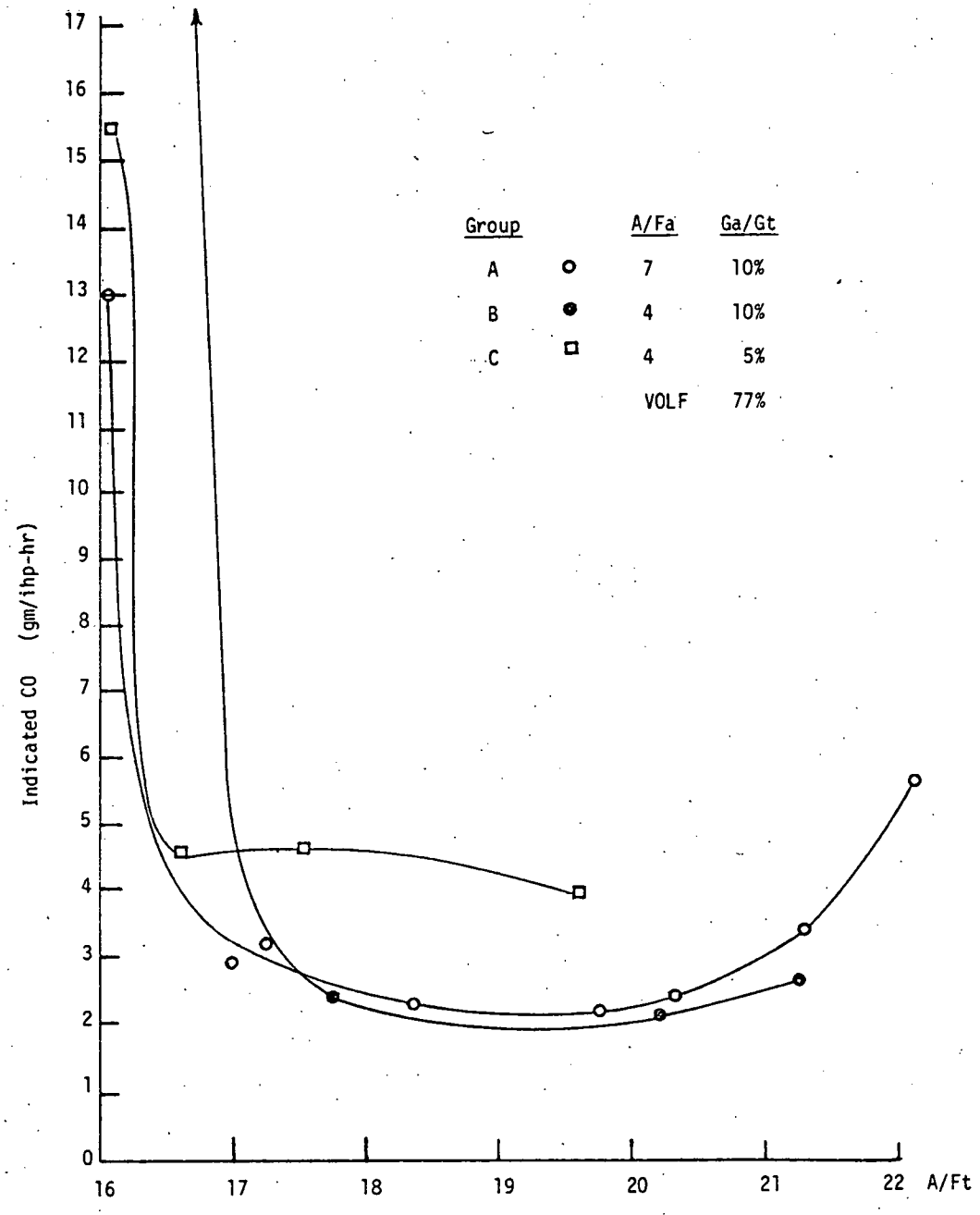

Figure 10. Indicated CO emissions - TDC injection.

The CO trends of Figure 10 agree with arguments presented so far. The poor combustion seen with Group C conditions shows up in higher CO. Group C showed higher exhaust temperatures in tests, indicating slower combustion in the cylinder with oxidation continuing during exhaust. The excess HC burns in post reactions, but CO is not oxidized to CO_2 because exhaust temperatures were not above the 1400°F needed to give good CO oxidation. Groups A and B show similar values for CO above an A/Ft of 17.5. The faster burning of these two because of the richer intermediate zones than for Group C gives the lower CO and showed up as cooler exhaust temperatures. Below 17.5 CO for Group B goes up faster than for Group A, probably because the intermediate zone becomes quite rich and more CO is produced than can be oxidized. Group A intermediate zone won't become as rich until a lower A/F is reached, so CO goes up at a lower A/Ft than for Group B. Figure 11 shows a comparison of spark timings for the three groups, and it is seen that all were very similar for any A/Ft to justify the comparison made.

B. Varying Prechamber Equivalence Ratio With and Without Swirl

In order to find basis for the mixture formation theory, the effects of varying stratification with constant Ga/Gt were probed. In Pan's model discussed before, a 50% mixing percentage was assumed for all fueling groups. This meant that half the A/Fm mixed with the prechamber overflow, no matter what Ga/Gt was. This assumed degree of mixing was not a function of Ga/Gt only, but rather could be related to engine geometry and charge flow

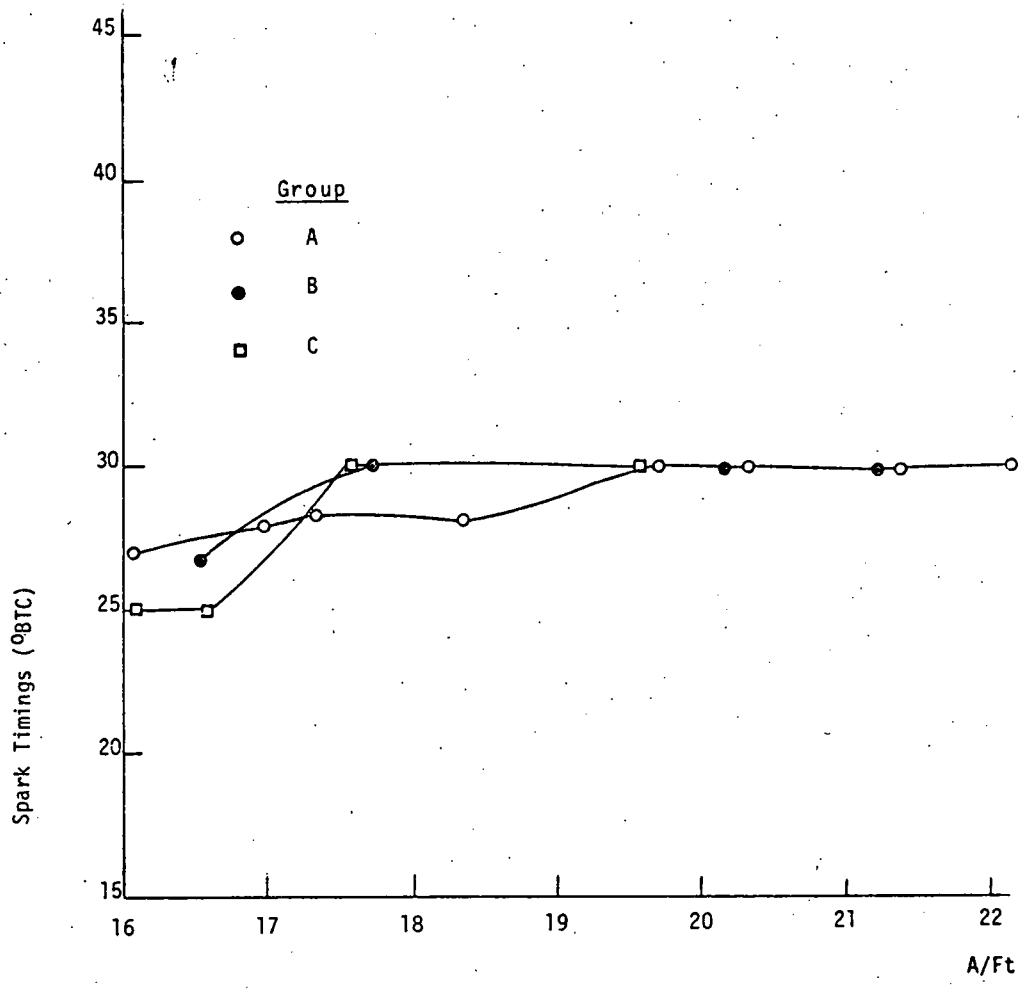

Figure 11. Spark Timings - TDC injection Groups A, B, C.

into the cylinder. It is not known whether this is a correct assumption. However in this test all the stratification was varied at constant Ga/Gt, so mixing should have been constant for each value of A/Fa no matter which mixing is related to. Ignition timing was held at 25° BTC to help insure constant mixing also.

The prechamber equivalence ratio was varied at ratios of 1, 2, 3, 4 and 5 while A/Ft was kept at a nominal value of 18. As prechamber equivalence ratio was increased, stratification increased because A/Fm was also being leaned to keep A/Ft constant. The test was run first with Ga/Gt equal to 5%, then repeated for Ga/Gt equal to 10%.

In-cylinder sampling of mixtures on the compression stroke at Nissan [10] showed pockets of rich mixture about the torch opening and main chamber at the end of intake. These pockets were found to disappear by the end of compression. It was found to occur because swirl existing in the main chamber. By ignition time, A/Fmi consists of a basically homogeneous mixture. This condition of one mixture, the A/Fmi, in the main chamber corresponds to the perfect mixing case for the prechamber overflow. Therefore the test, described above was repeated with swirl added to the main chamber. Figure 12 shows the NOx and IMEP values found with both cases versus prechamber equivalence ratio.

The effects of increasing equivalence ratio and thus increasing stratification showed that for the no swirl case, NOx went up as stratification was increased. Power also went up. The hydrocarbons and CO were found to decrease during the same process.

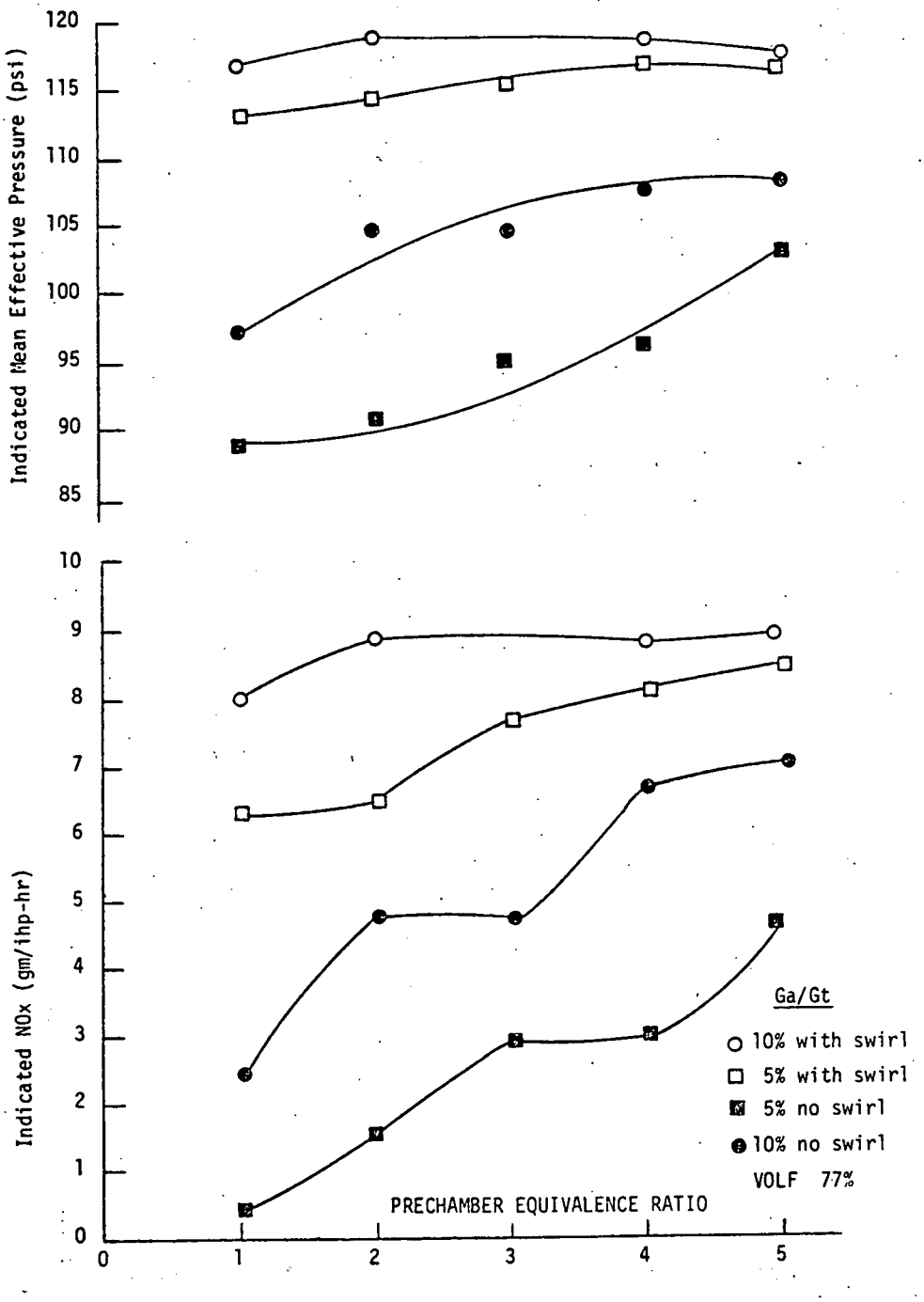

Figure 12. Indicated MEP and NOx versus p.c. equivalence ratio.

This seems to show better combustion as stratification was increased. It was stated that mixing should have been constant during the tests with the same Ga/Gt, the intermediate zone should have been the same size for each run. However A/F should have been increasing for each increase in equivalence ratio. This would explain the increase in NOx as the intermediate zone became richer and more mixture approached the slightly lean state.

The 10% Ga/Gt test showed higher NOx and power than the 5% case. This tends to show that Ga/Gt does effect mixing degree of prechamber overflow. No definite conclusions can be made about how much more mixing there is with a larger Ga/Gt. However, if a larger mixing zone was formed in the main chamber and contained more of the slightly lean mixture it would explain the higher NOx production and power. Higher power would also be influenced by greater torch strength as A/Fa was increased.

The same experiment of varying stratification was performed by GM [1] and gave somewhat different results. They found that NOx did not keep increasing for each increase in A/Fa. Rather, it peaked at some equivalence ratio and dropped off after that. This could be caused by different geometry factors that influence the mixing in the GM engine differently. Repeating the experiment on the U. of I. engine at a different A/Ft would give a better comparison to the GM data. For this experiment, a leveling off of NOx occured between equivalence ratios of 2 and 3 for the prechamber and 10% case, and 3 and 4 for the 5% case. However NOx increased again after these ratios. GM did have a similar conclusion that an intermediate air/fuel zone was formed that leads to high NOx formation.

Looking at the swirl curves in Figure 12 shows much flatter power curves and NOx curves. HC and CO were not found to decrease significantly with increased stratification. This would appear to be because the swirl mixed the chamber into a homogeneous mixture which had about the same A/Fm for all values of prechamber equivalence ratios. Only the added prechamber torch strength would increase power. With a homogeneous mixture, the combustion transition from prechamber to main chamber should have been slower without an intermediate zone. Therefore temperature and pressure rises would have been smaller and should have given lower NOx production, but this was not found.

Instead of lower NOx and lower power with the homogeneous mixture, Figure 12 showed higher power and higher NOx than the no swirl case. The cause of this is most likely the added main chamber turbulence from the swirl. If a comparison of NOx could be made at similar power levels for the no swirl and swirl case, it would be possible to find if NOx was less for the homogeneous case. Figure 13 has IMEP plotted versus NOx for the swirl and no swirl cases. By extending the curves slightly, NOx can be compared at the same IMEP for both. If 110 psi is selected, it is seen that NOx will be lower for the swirl case. This gives evidence to show that the homogeneous main chamber case would have lower NOx, and the no swirl case must have a non-homogeneous main chamber.

Figure 14 shows a block diagram with equivalence ratios that may be set up in the stratified charge engine. The dashed line represents the imperfectly mixed main chamber with an intermediate zone formed. Perfect mixing is represented by the solid line,

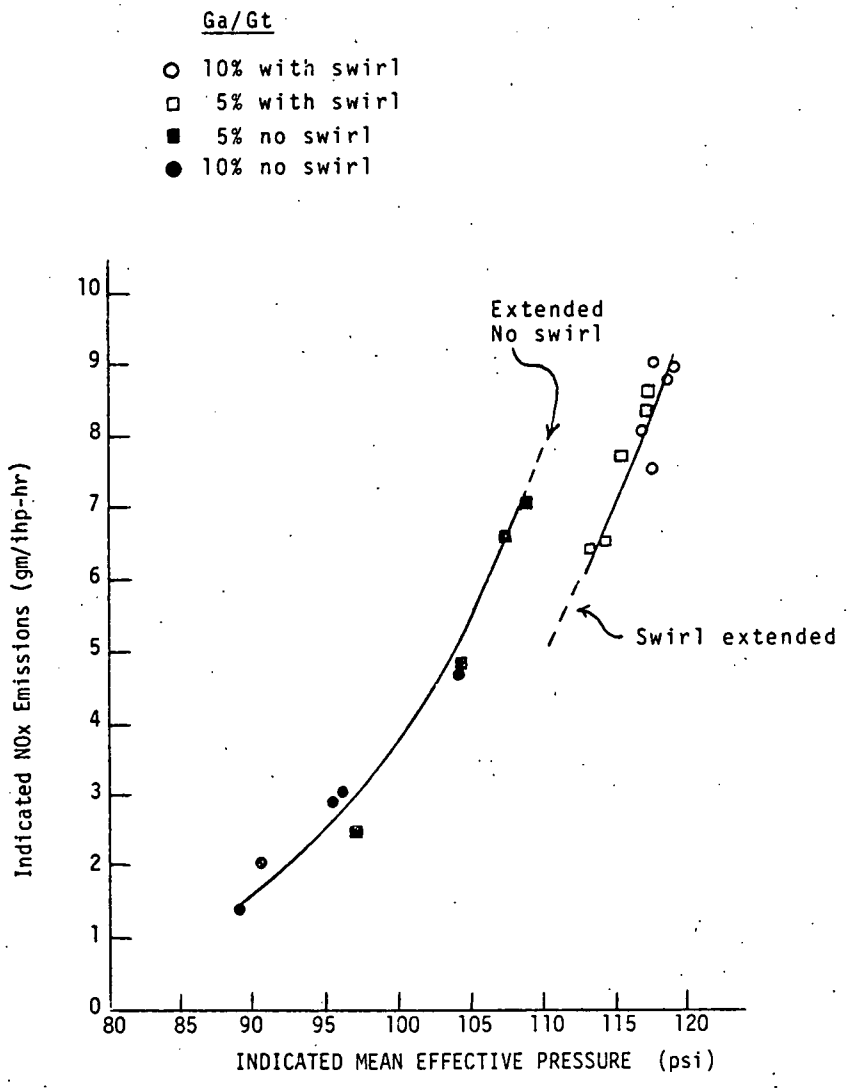

Figure 13. Indicated NOx versus IMEP - swirl and no swirl.

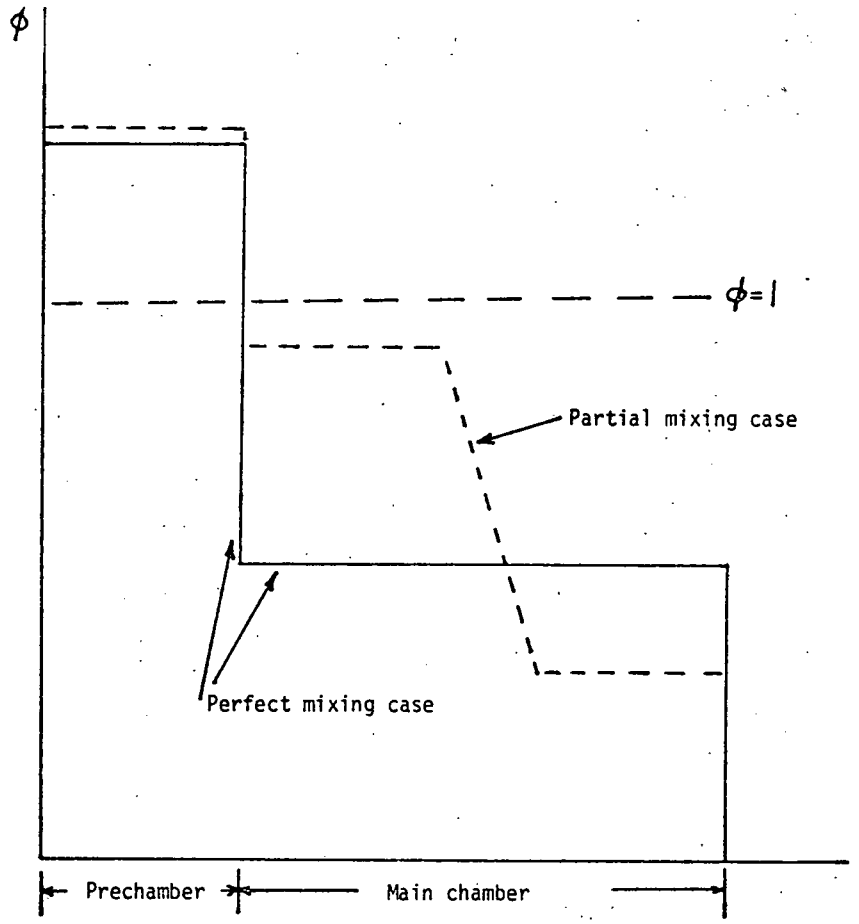

Figure 14. Block diagram showing possible equivalence ratios formed in the prechamber and main chamber.

where there are just two mixtures present, A/Fai and A/Fmi. It is illustrated by this diagram that the imperfect mix will have more regions near slightly leaner than stoichiometric. This would give higher NOx, but faster transitional burning between prechamber and main chamber which increases power and reduces HC and CO.

C. Comparison of Fuel Injection to Carburetion

Data taken by Grandys [3] for the carbureted version of this test engine will be compared to the fuel injected version for the three fueling groups. Two injection times 0 and 110 degrees ATC will be used for the comparison. Also, Group A at 110 ATC injection and part throttle will be compared to carbureted Group A data at part throttle.

Figures 15 and 16 show the emission and performance comparison for fueling Group A and TDC injection. Spark timings were similar for the comparison. Mean effective pressure is slightly higher and economy slightly better for the injected version. However the improvement is so small that it can be said that performance is similar for carburetion and injection. Emissions are not similar, as Figure 16 points out. CO is slightly higher over the A/F range and HC about twice as high for the curb version. NOx is higher for the injected version, however for any level of NOx picked, if HC and CO are compared at the NOx level for both, the injected version would still show a large advantage in lower emissions.

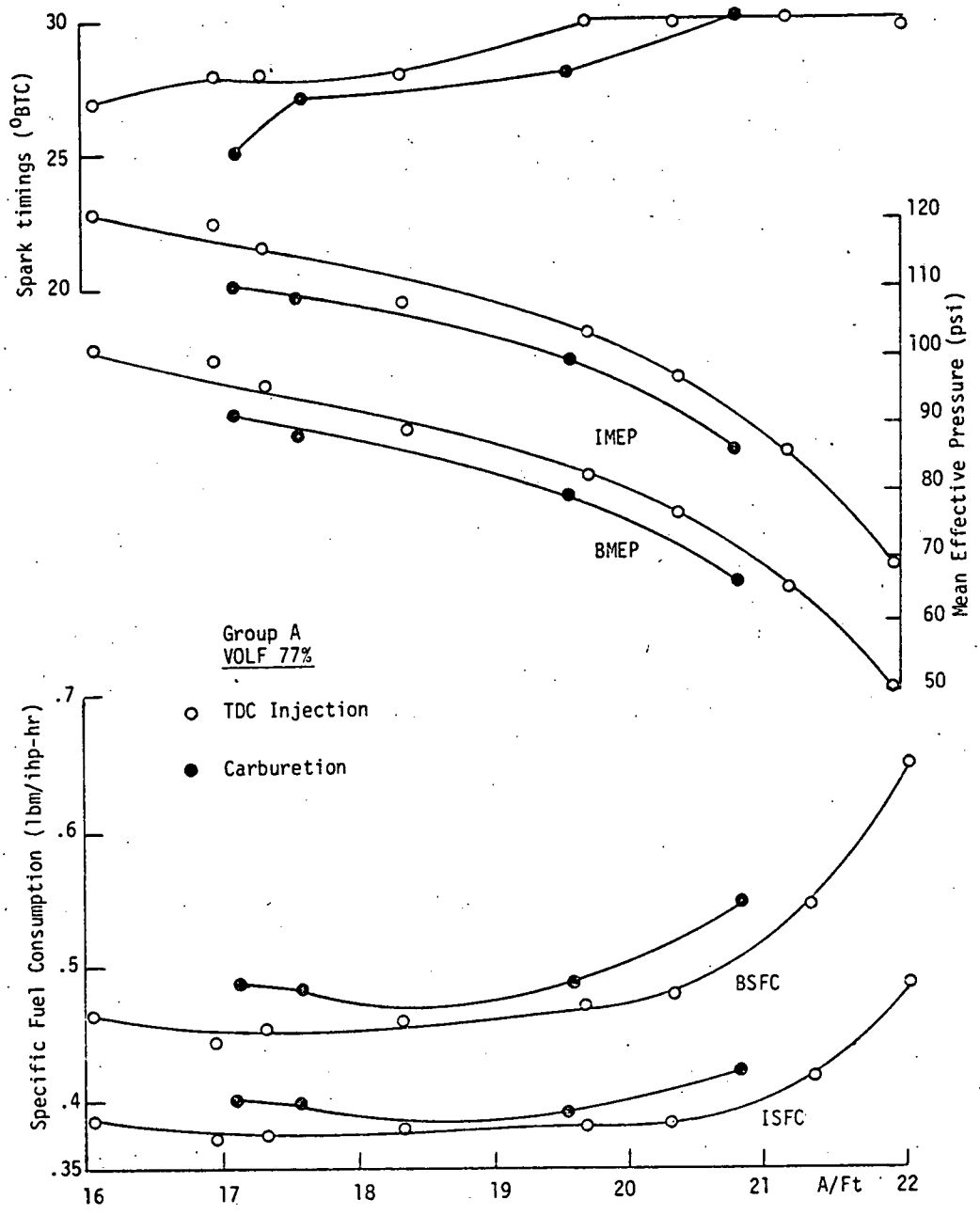

Figure 15. MEP, SFC and spark timings for carb and TDC injection.

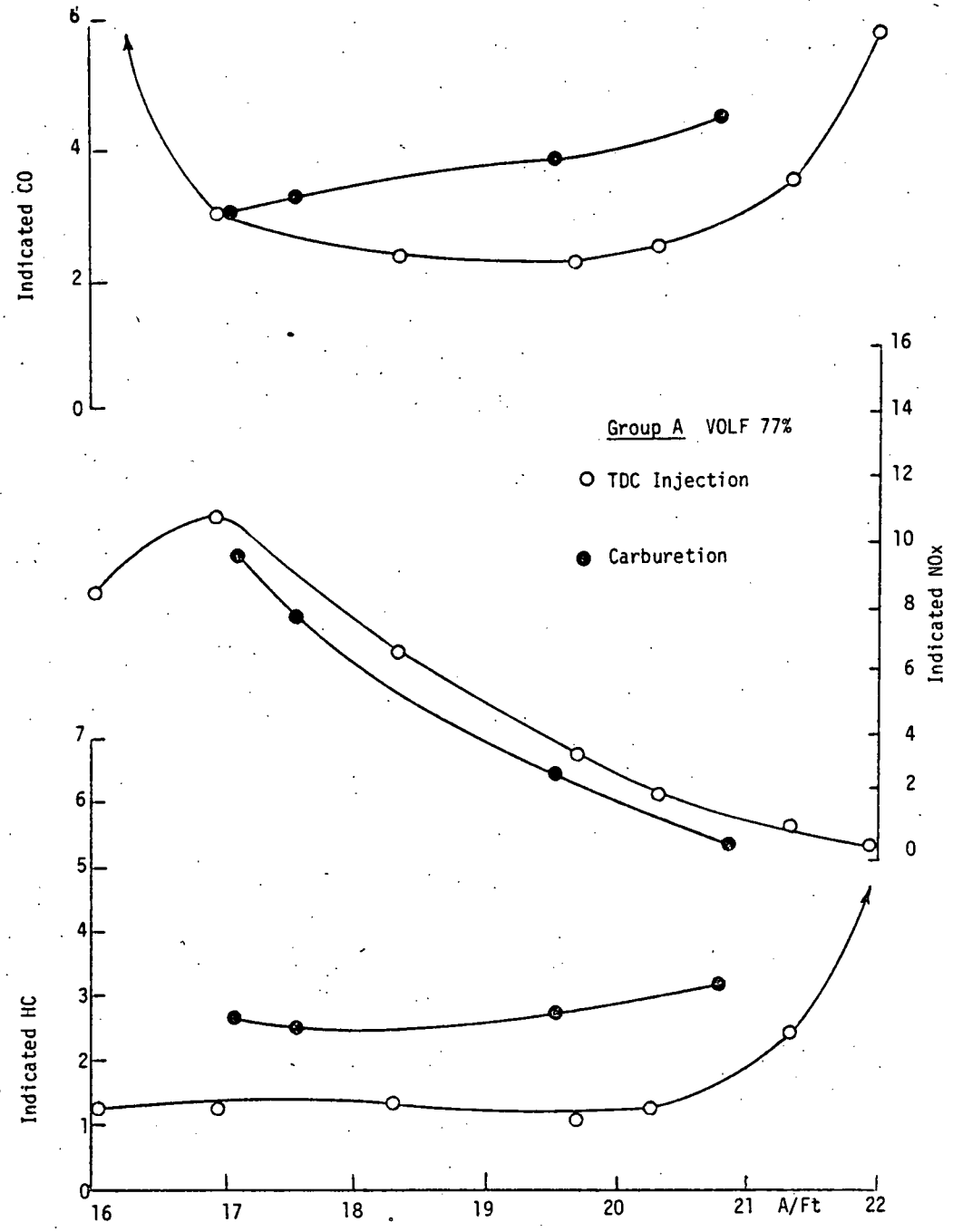

Figure 16. GM/ihp-hr emissions for carb and TDC injection.

The trends for Group A, TDC injection hold for the other groups and injection time as well. Figures 17 and 18 show the Group B, TDC injection comparison. Again spark times are shown to be similar for the comparison. There is a slight power and economy advantage to the injected version, but nothing significant. CO is higher for the carb version, and HC is again about twice as high as for the injected engine. NOx is up with injection, as was seen with Group A.

Figures 19 and 20 for Group C, TDC injection versus carburetion do show one different trend. Here is can be seen that the carbureted engine has a slight power advantage and lower fuel economy with similar spark times. CO is lower for the carb version, and HC emissions are the same for both here. The NOx results are reversed with the injected version having lower NOx. These different trends for Group C can be attributed to the poor running of the injection version under Group C conditions. The fact that the injected engine would run only out to an A/Ft of about 19.6 as opposed to 20.5 for the carb version illustrates the difficulty in operating the engine with injection and Group C fueling conditions.

Figures 21 and 22 show the Group A comparison, only with 110 ATC injection. The same trends appear as for the TDC-carb comparison. A slight power and fuel economy, with lower CO, lower HC and higher NOx for the injected engine.

Figures 23 and 24 show the same trends for Group B, 110 ATC injection. This is the same result seen for the TDC injection.

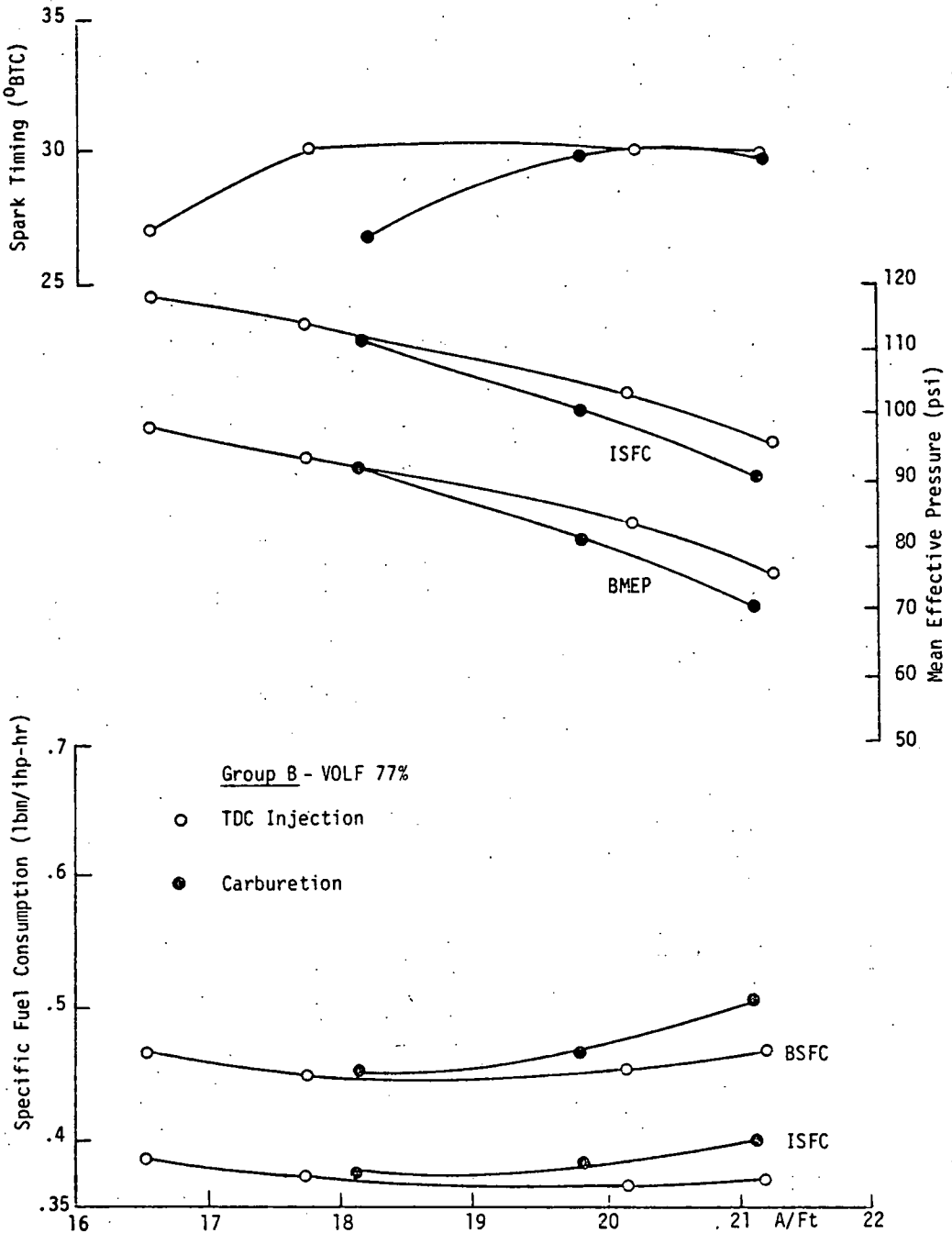

Figure 17. MEP, SFC and spark timings for carb and TDC injection.

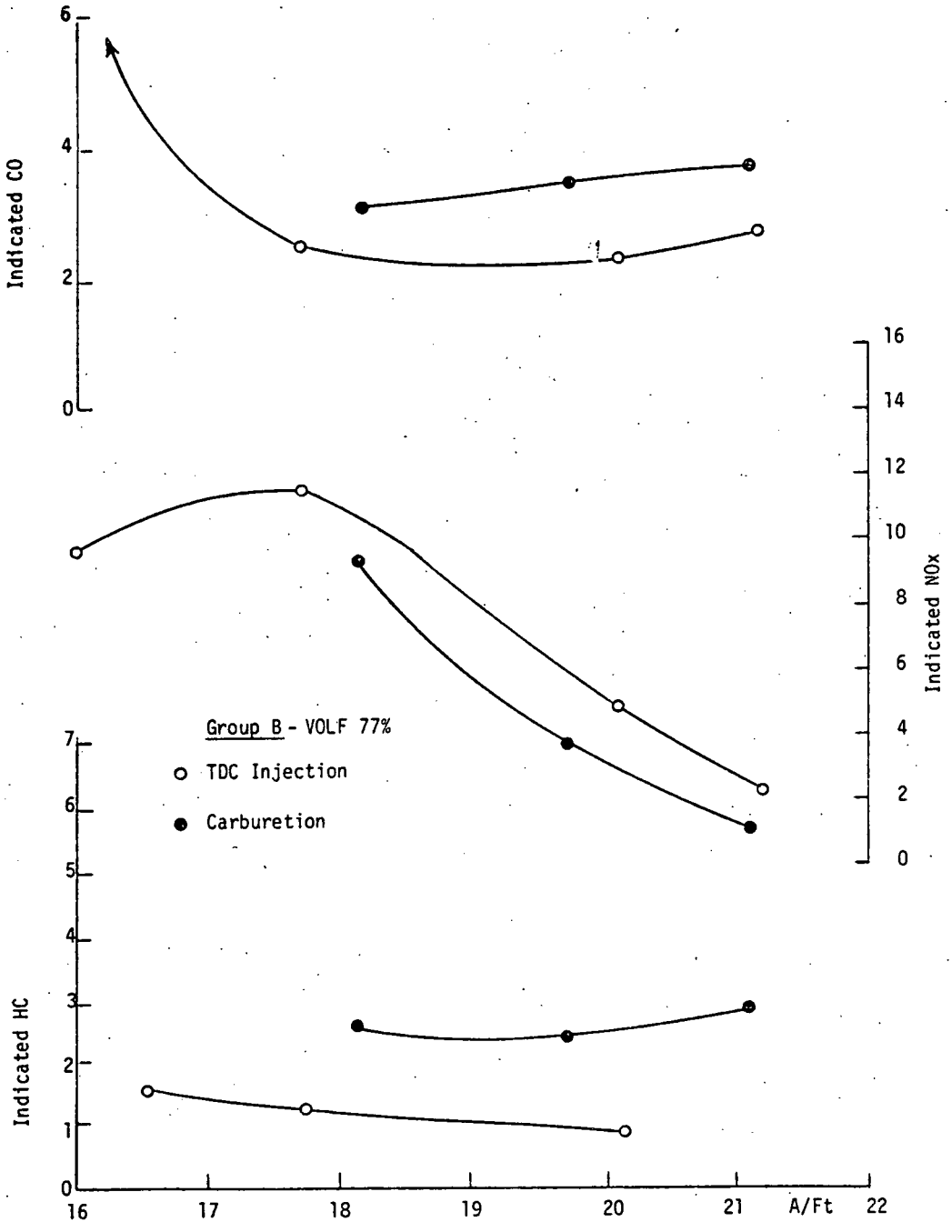

Figure 18. GM/ihp-hr Emissions for carb and TDC injection.

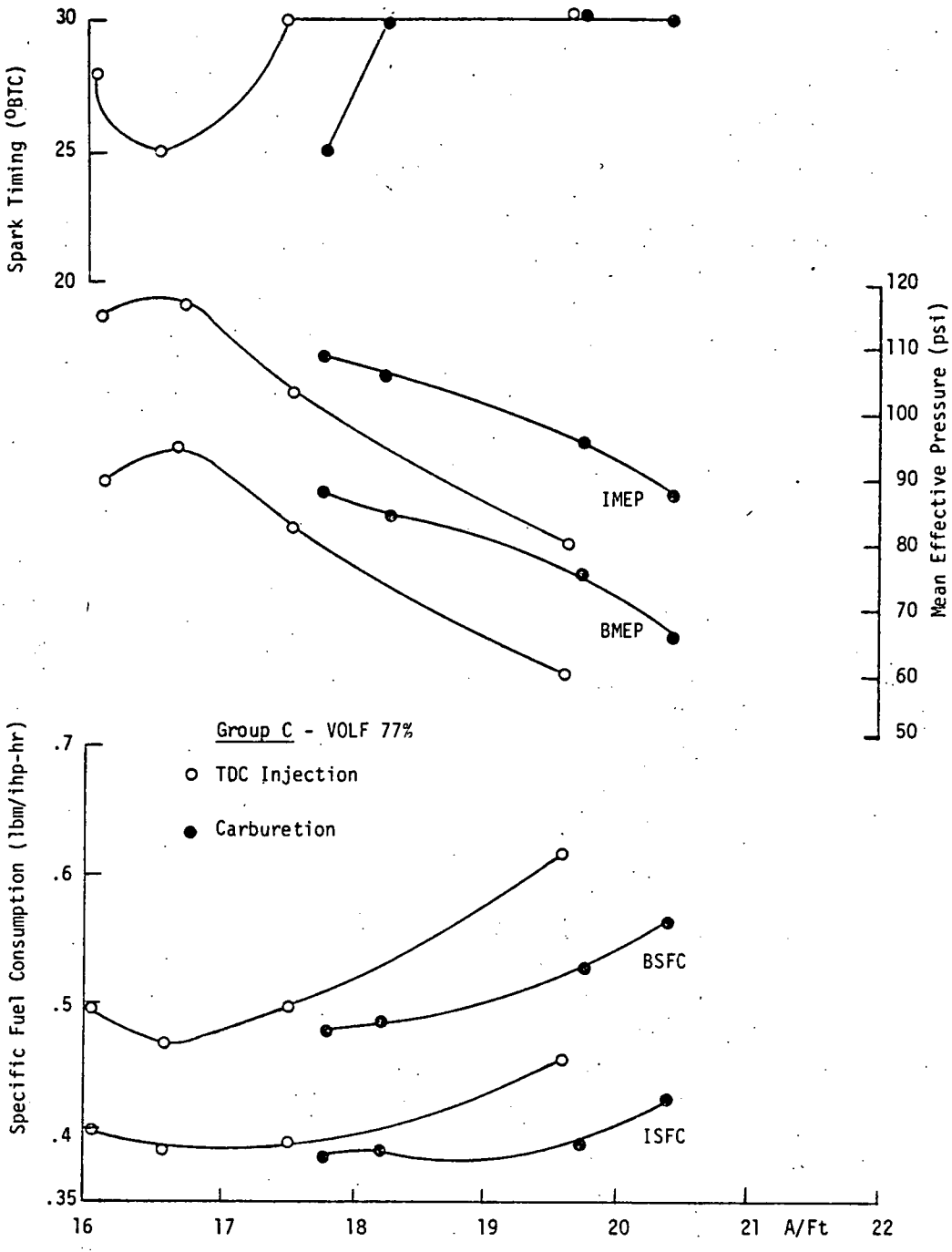

Figure 19. MEP, SFC, and Spark timings for carb and TDC injection.

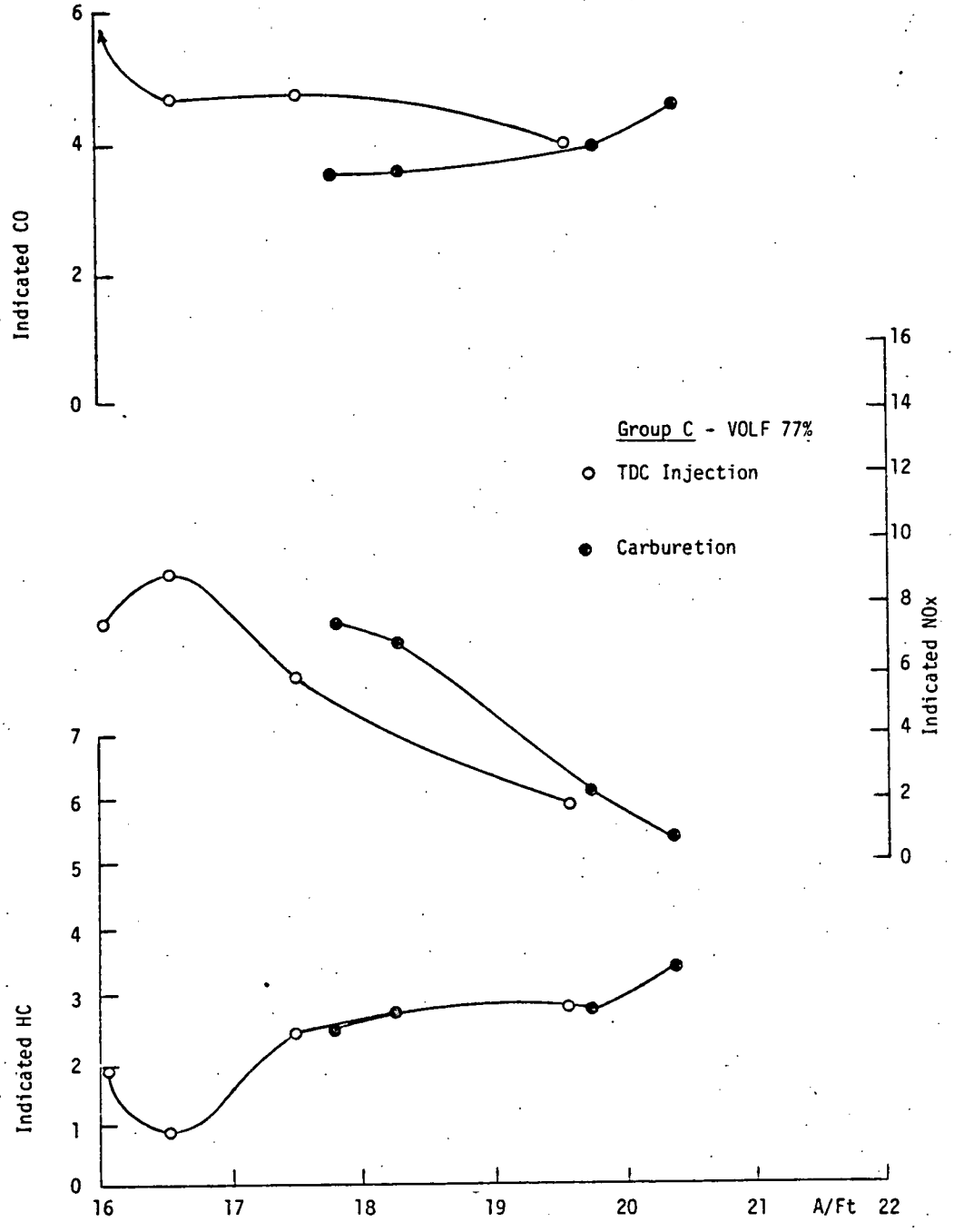

Figure 20. GM/ihp-hr Emissions for carb and TDC injection.

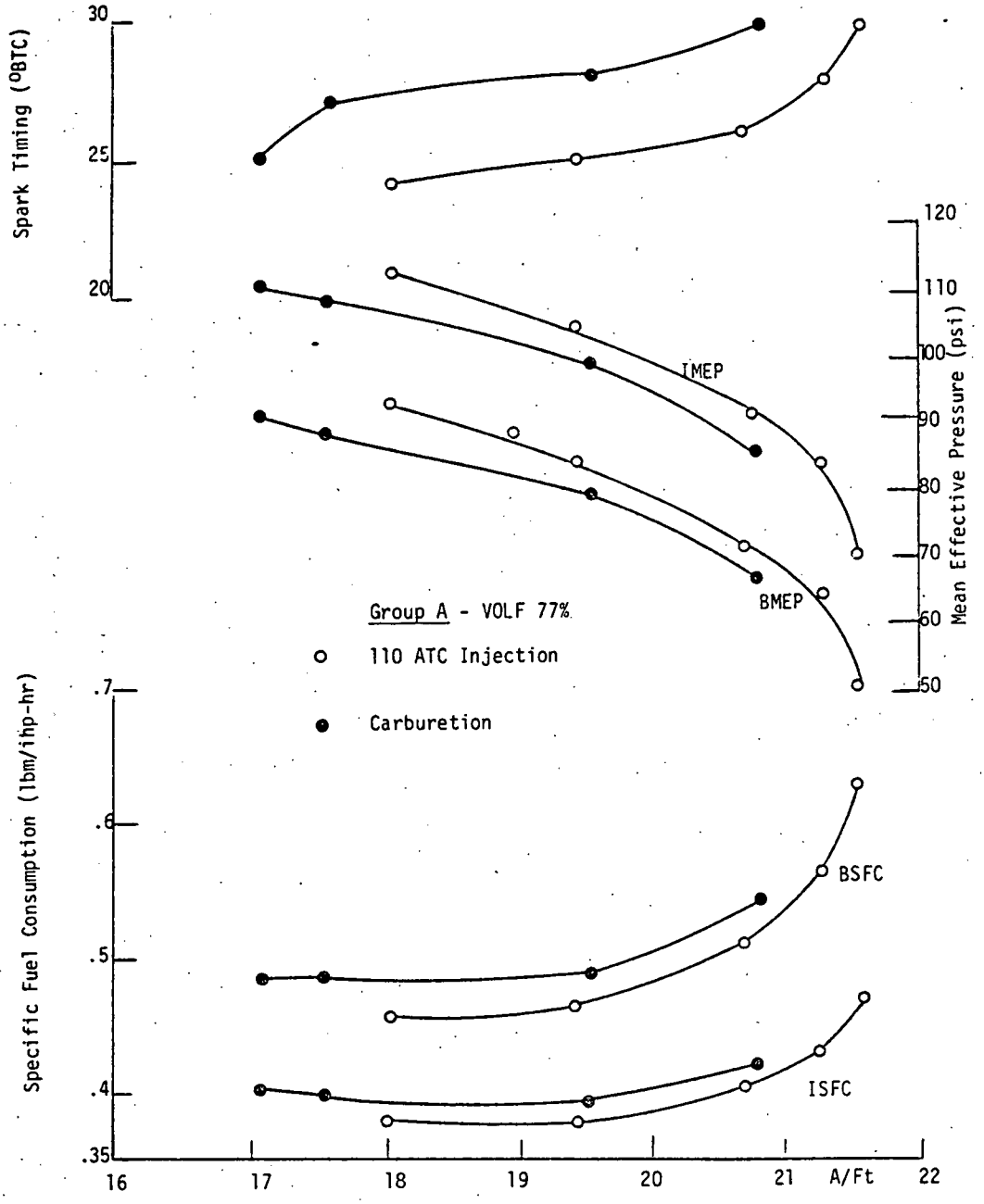

Figure 21. MEP, SFC, and Spark timings for carb and 110° injection.

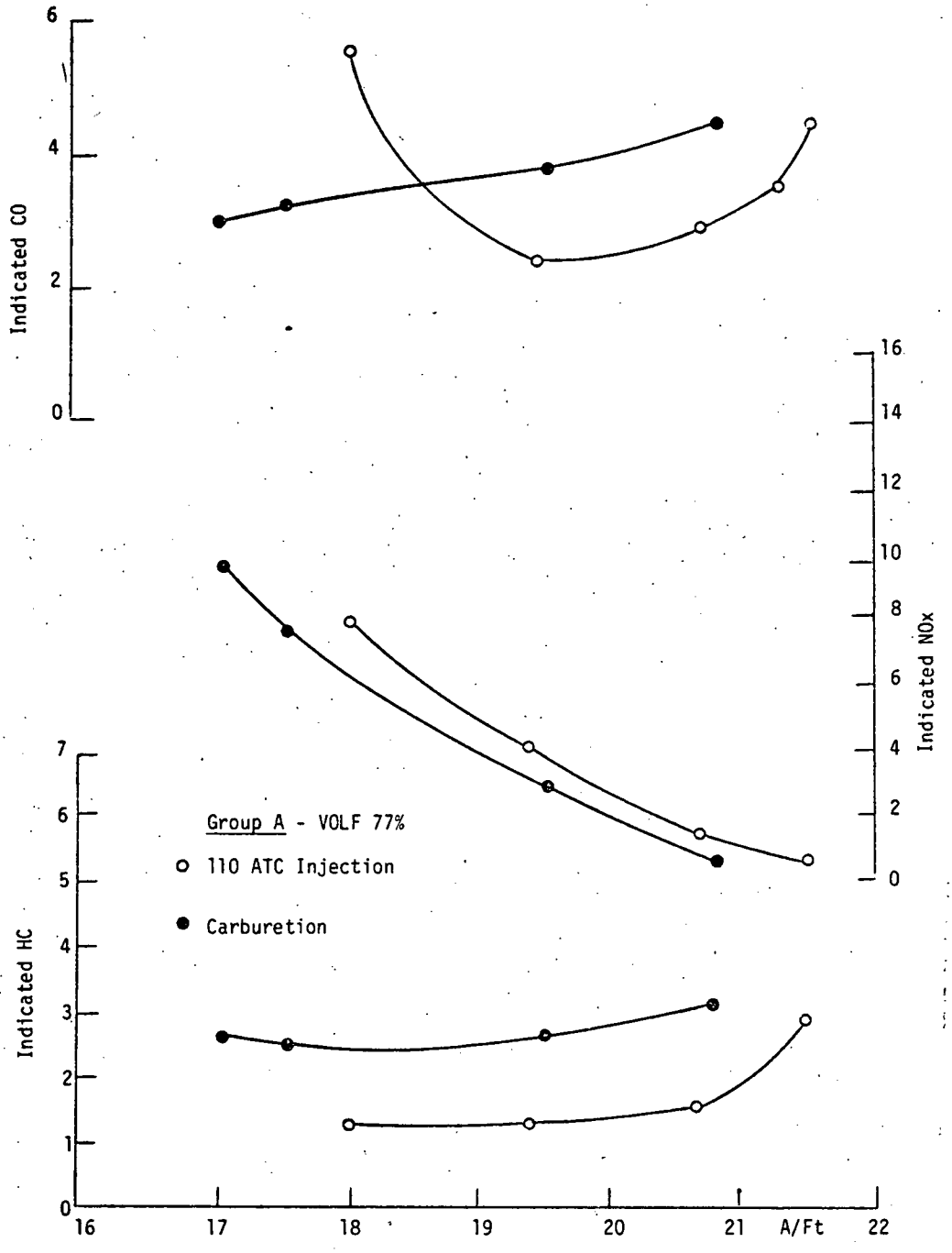

Figure 22. GM/ihp-hr Emissions for Group A, carb and 110° injection.

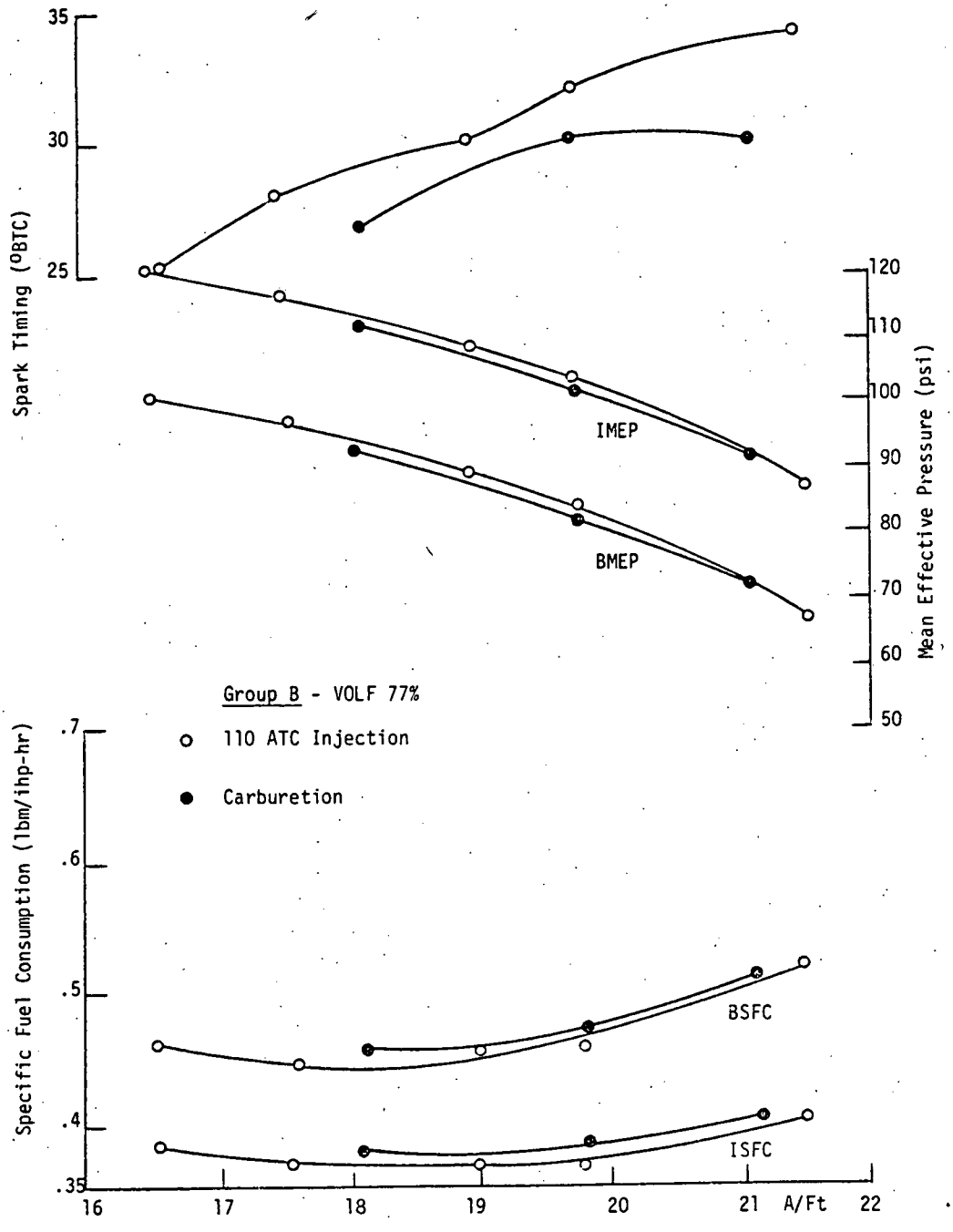

Figure 23. MEP, SFC and Spark times for carb and 110° injection.

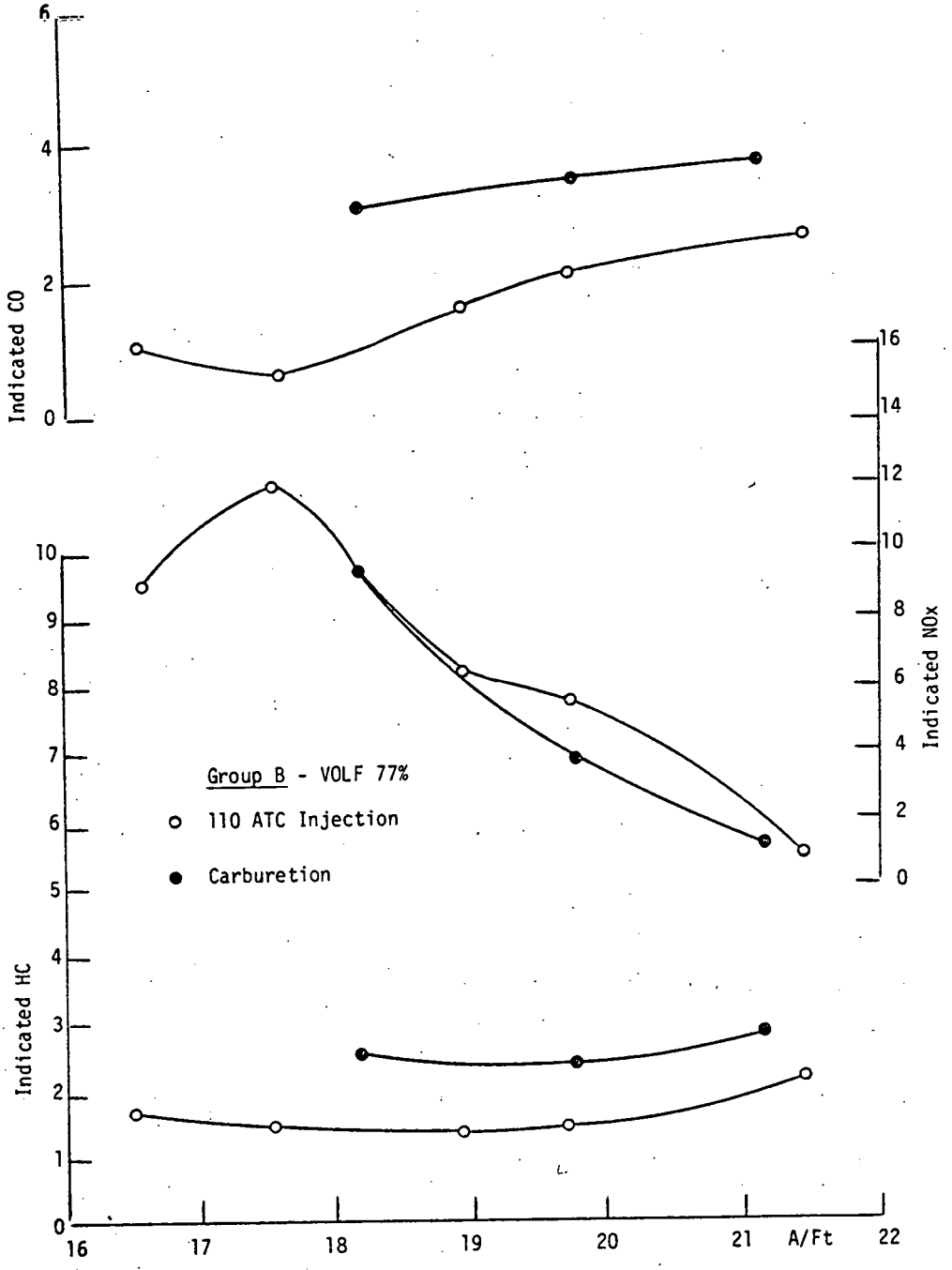

Figure 24. GM/ihp-hr Emissions for carb and 110° injection.

with the carb engine having higher specific fuel consumption, lower power, higher HC and CO, and lower NOx. Spark times are shown to be slightly retarded for the carb engine, which would make the comparison of emissions biased towards the carb engine. So it is seen that the NOx curves would be closer and the HC advantage better for the injected engine if sparks were more similar.

Fugures 25 and 26 have Group C comparisons to the 110 ATC injection. The spark for the injected version is slightly retarded, which should give the edge to the injected engine as far as lower HC and NOx. However HC is still so much lower for the injected version that it could not be from the spark timing differences. CO is much lower with injection, and NOx is slightly lower. Power is similar for both, with a slight advantage to the carb version, as is the case with fuel economy. The engine ran better for Group C fueling conditions with the 110 ATC injection timing. This is pointed by lower HC and CO emissions than the carb engine, which was reversed at TDC injection for CO. HC was the same as the carb engine.

Figures 27, 28 and 29 show a comparison at part throttle, Group A and 110 ATC injection timing. Figure 27 shows that power and fuel economy are similar for both versions. The HC advantage in lower emissions is smaller for part throttle with injection. The NOx curves also show much less difference, with the carburetion having a very small advantage with lower emissions. CO is less for the injection, although more points would be needed with the same A/Ft to make a better comparison. Basically, the trends are the same for part throttle Group A as full throttle,

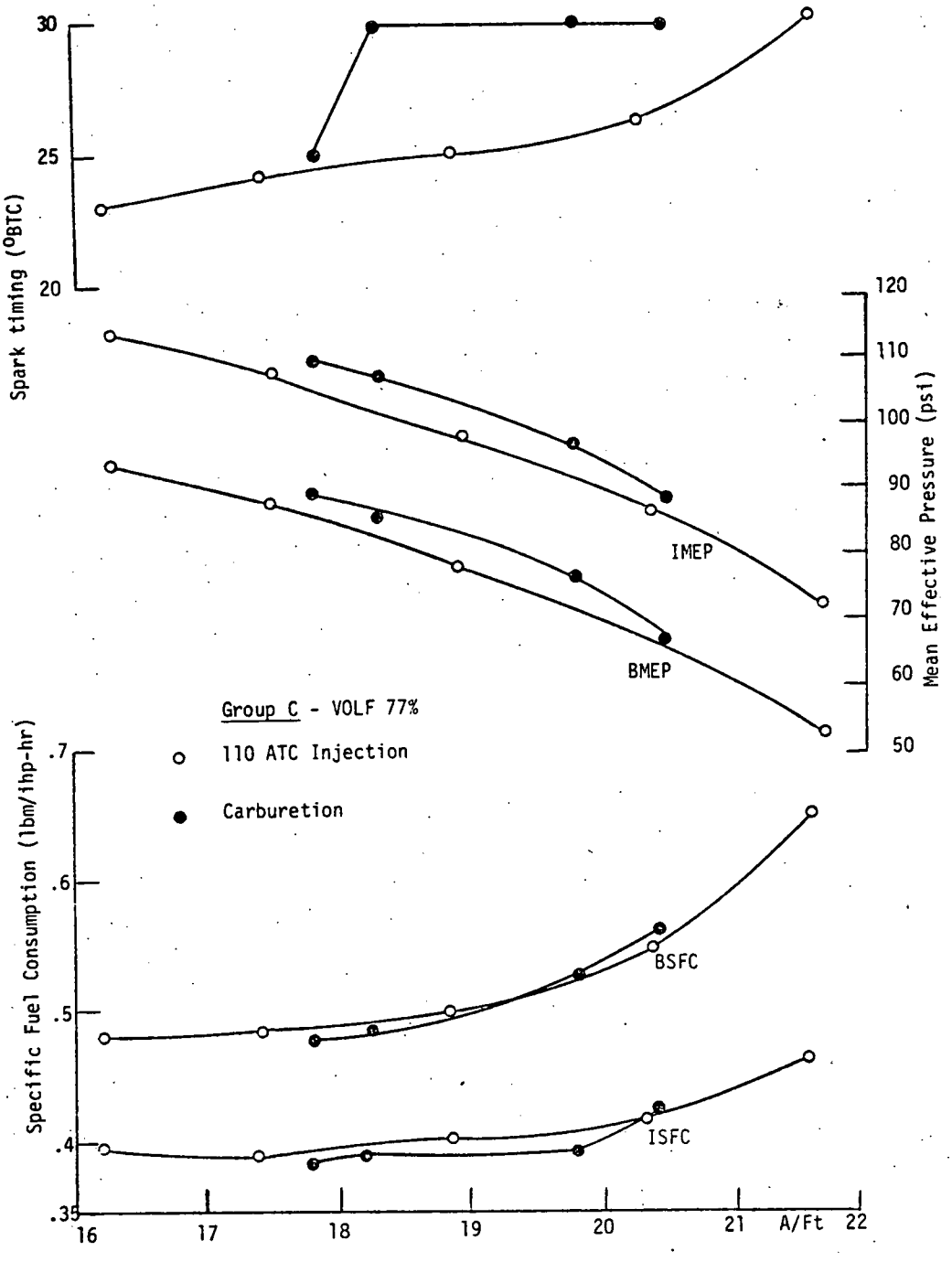

Figure 25. MEP, SFC and Spark times for carb and 110° injection.

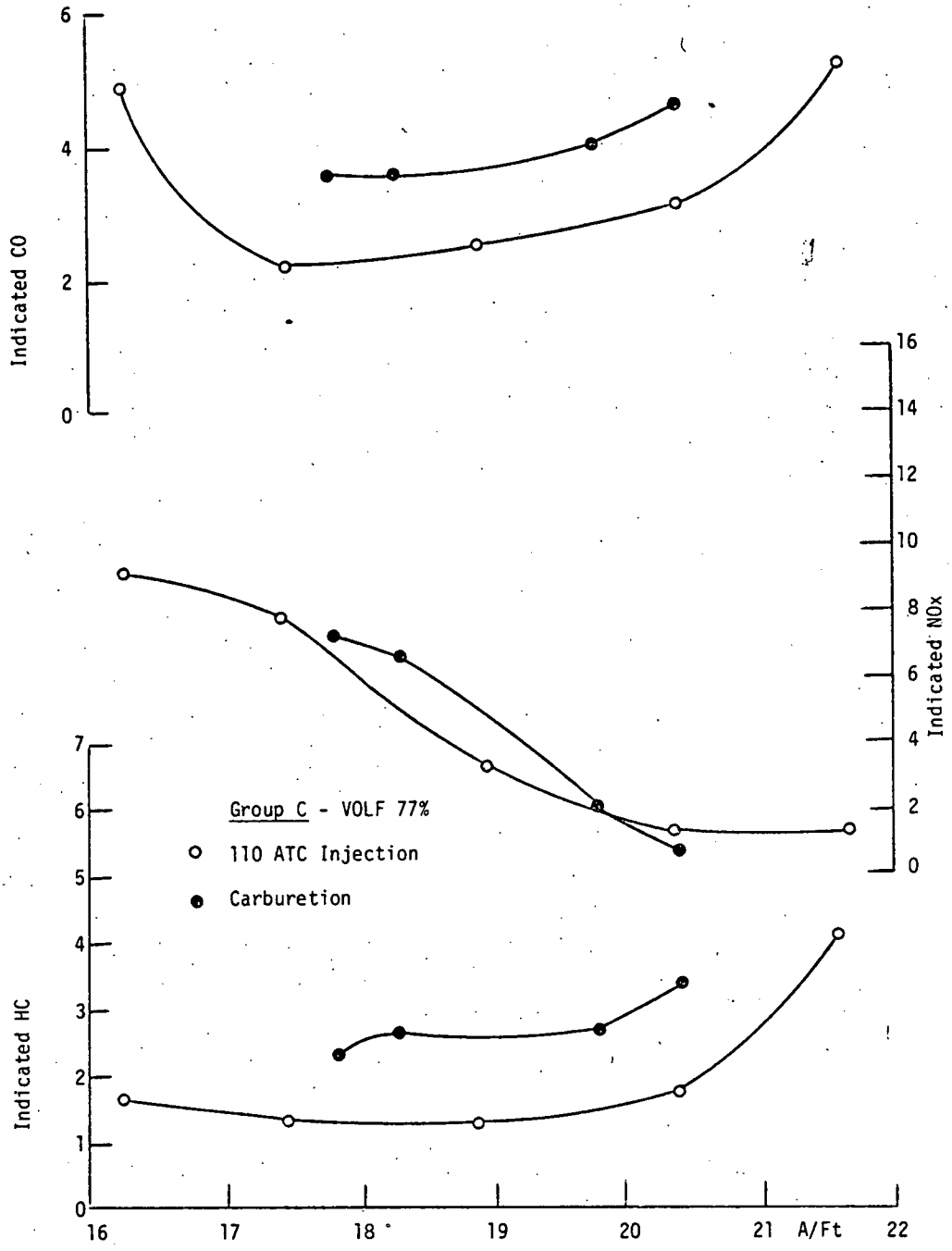

Figure 26. GM/ihp-hr Emissions for Group C, carb and 110° injection.

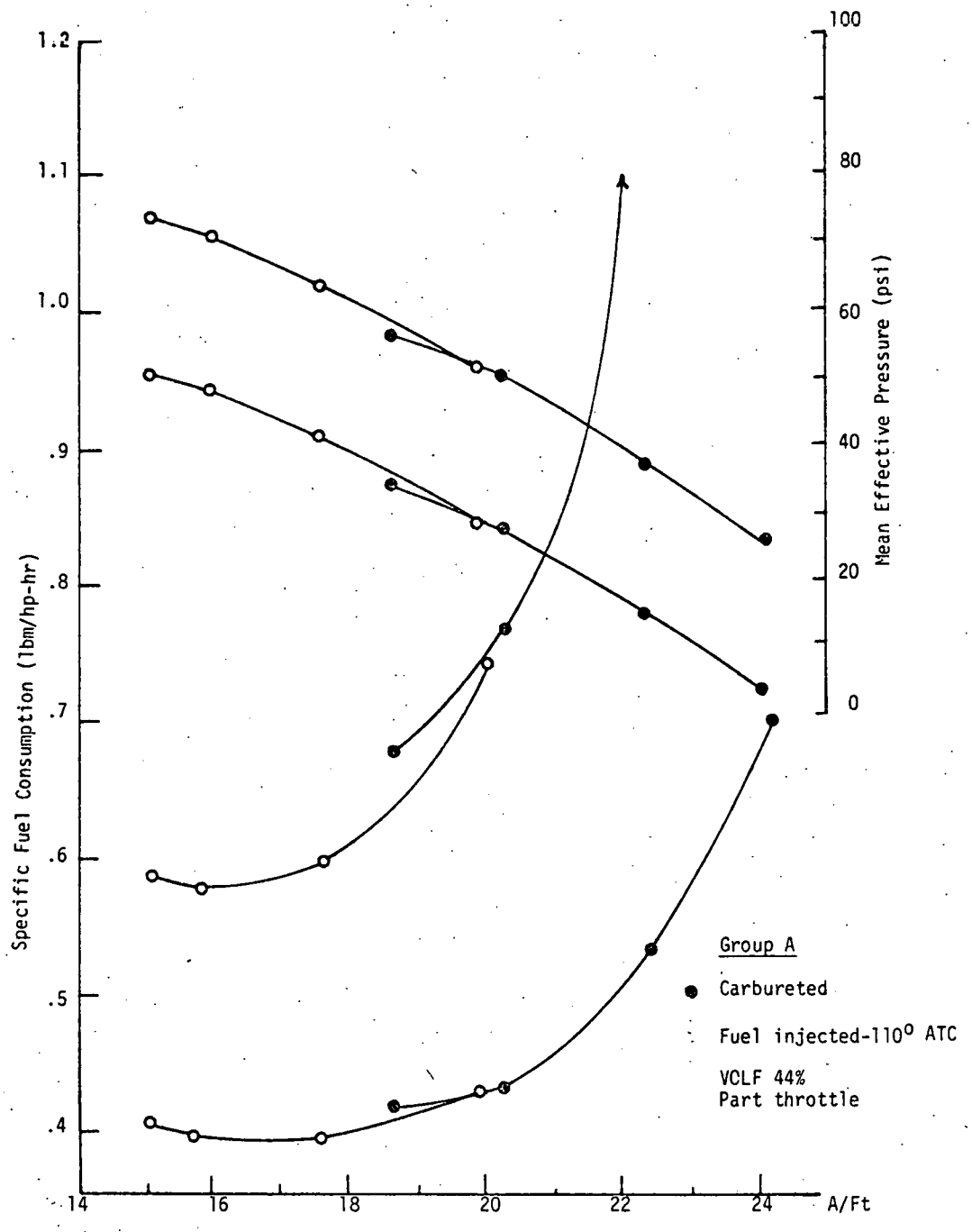

Figure 27. MEP and SFC for carburetion and 110° ATC injection.

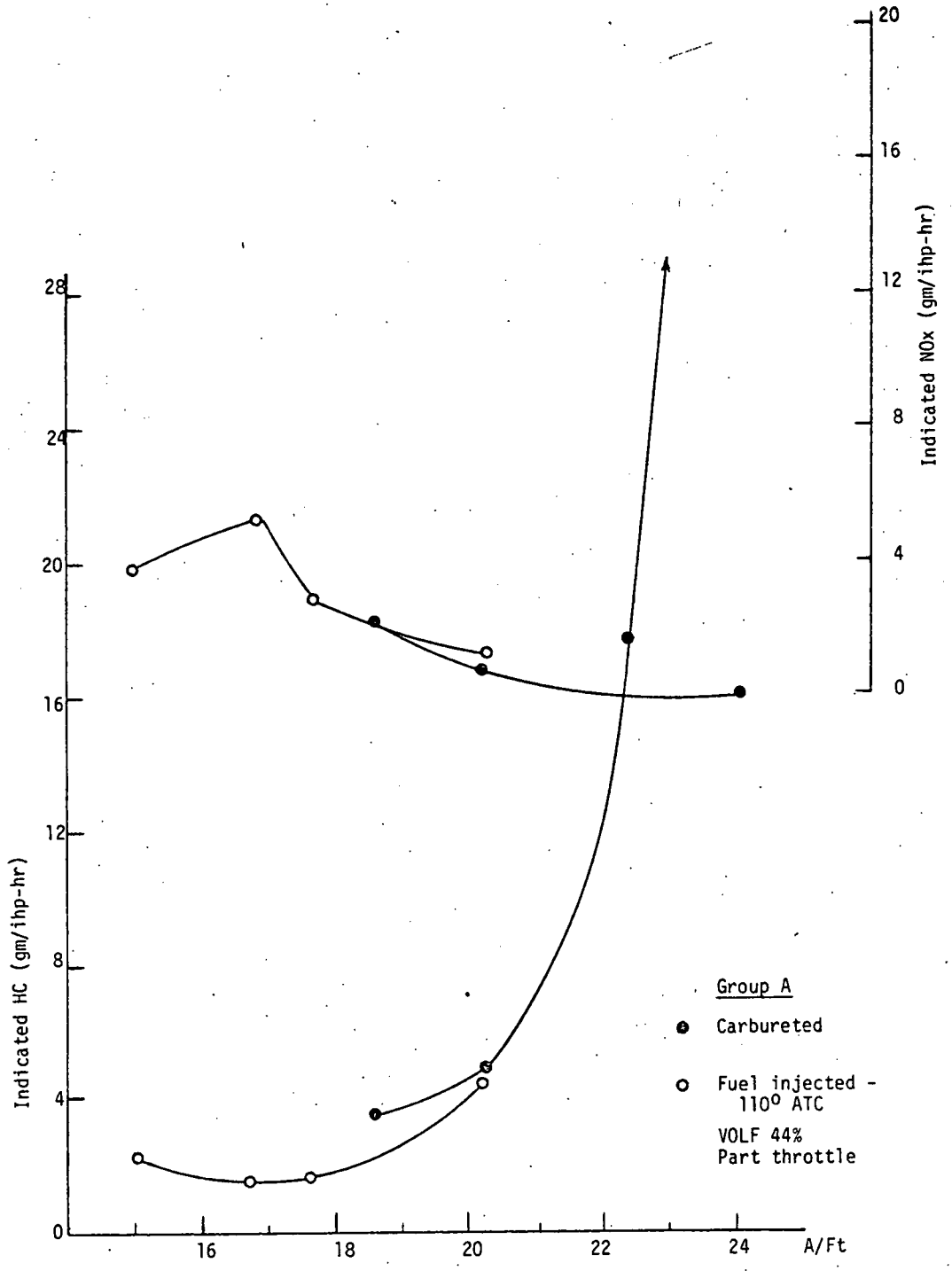

Figure 28. Indicated NOx and HC for carburetion and 110° ATC injection.

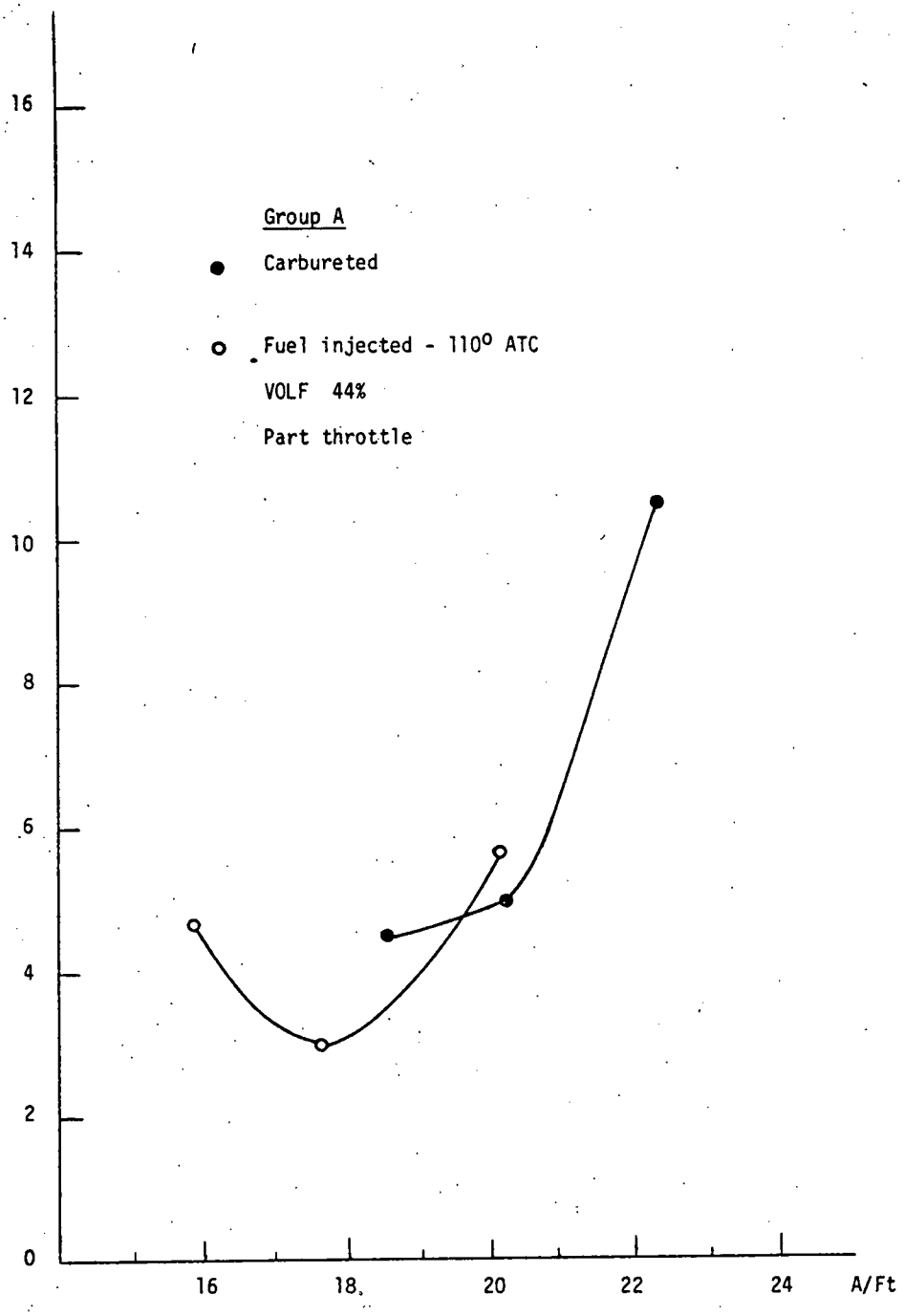

Figure 29. Indicated CO for carburetion and 110° ATC injection.

the differences between the carb and injected version are just not as great.

D. Varying Injection Timing for Fixed and MBT Spark Timings

In order to investigate injection timing effects, fuel Group A was run over an A/Ft range with injection times of 0, 60, 110, and 180 degrees ATC. Group A was run since it gave the best trade between low HC and low NOx of the three fueling groups. Initially fixed spark times were used. Then the experiments were repeated using MBT spark. Figures 30 and 31 show the times used for each A/Ft run for fixed and MBT times respectively.

Mean effective pressures and specific fuel consumptions for fixed and MBT runs are shown in Figures 32 and 33. These curves show power is essentially the same over the varied spark times, with the MBT power and economy curves almost the same as the fixed timing curves. This shows a very flat power curve over a spark range for this engine. Only the 180 ATC injection shows any significant power loss and SFC rise from the other three injection timings. This holds for both fixed and MBT runs. The basic conclusion from these curves is that fuel injection time has little effect on power and economy characteristics of this engine. However, as will be seen, the same is not true for emissions.

Figures 34 and 35 show NOx emissions for fixed and MBT times. For fixed timings, the four NOx curves are essentially the same curve. However for the MBT advanced times, there is a separate curve for each injection time. NOx values are higher for the

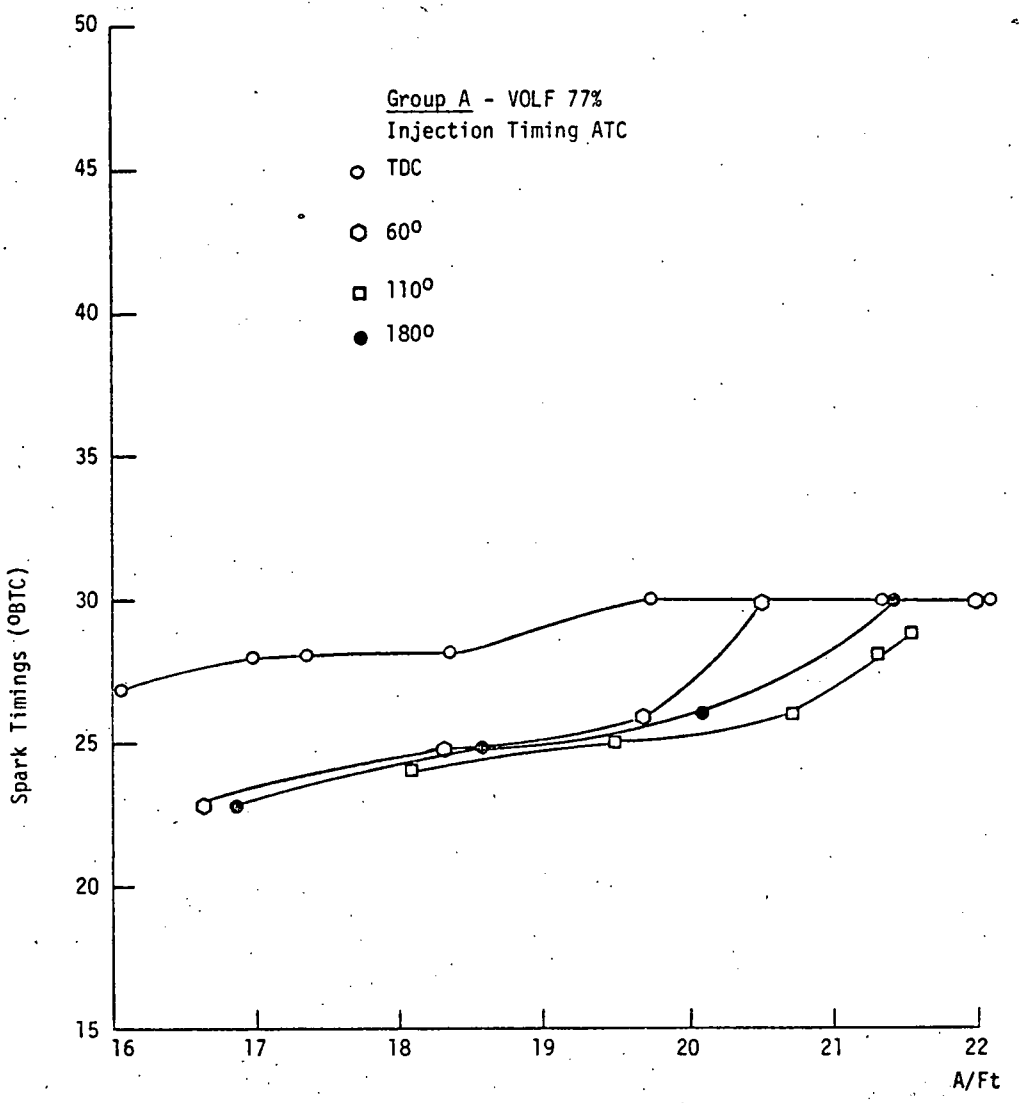

Figure 30. Fixed spark times for four injection timings.

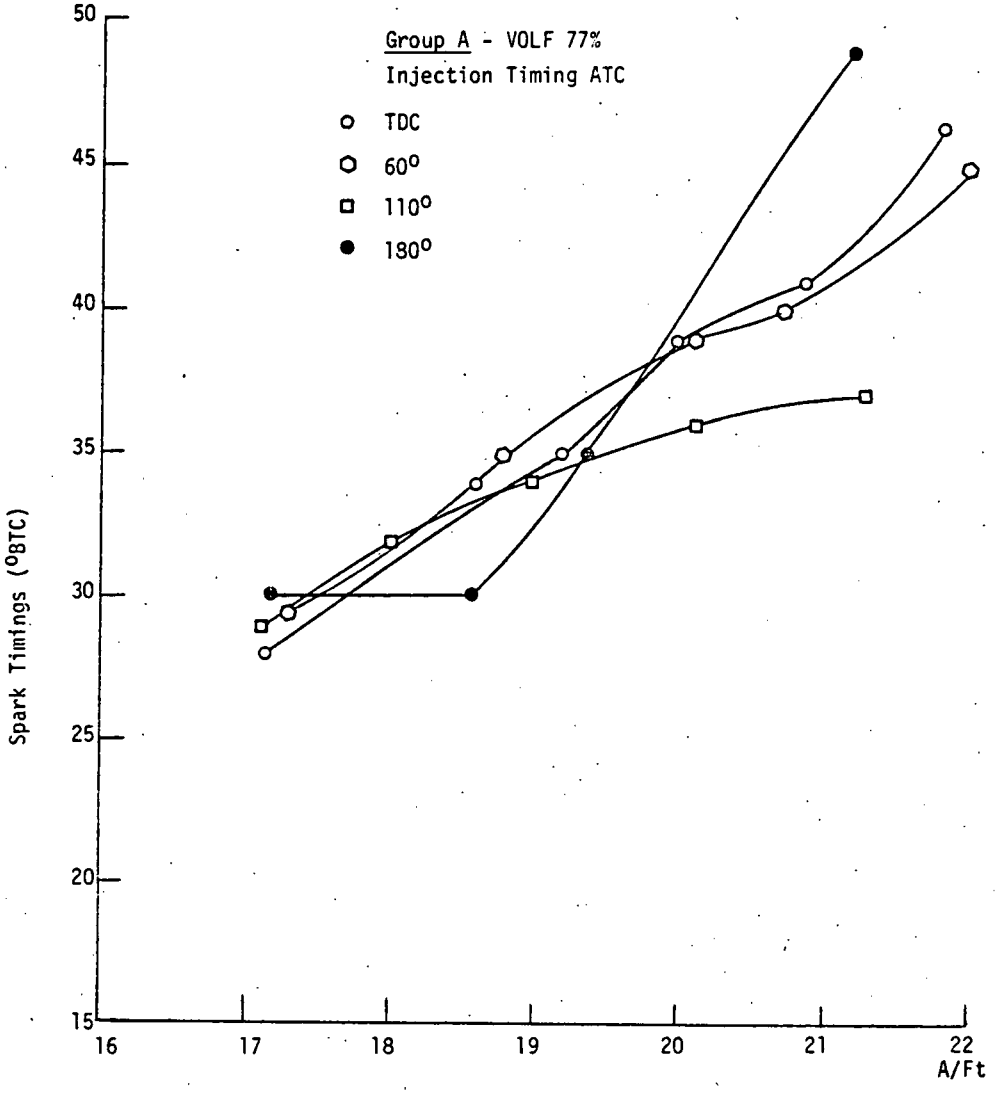

Figure 31. MBT Spark timings for four injection times.

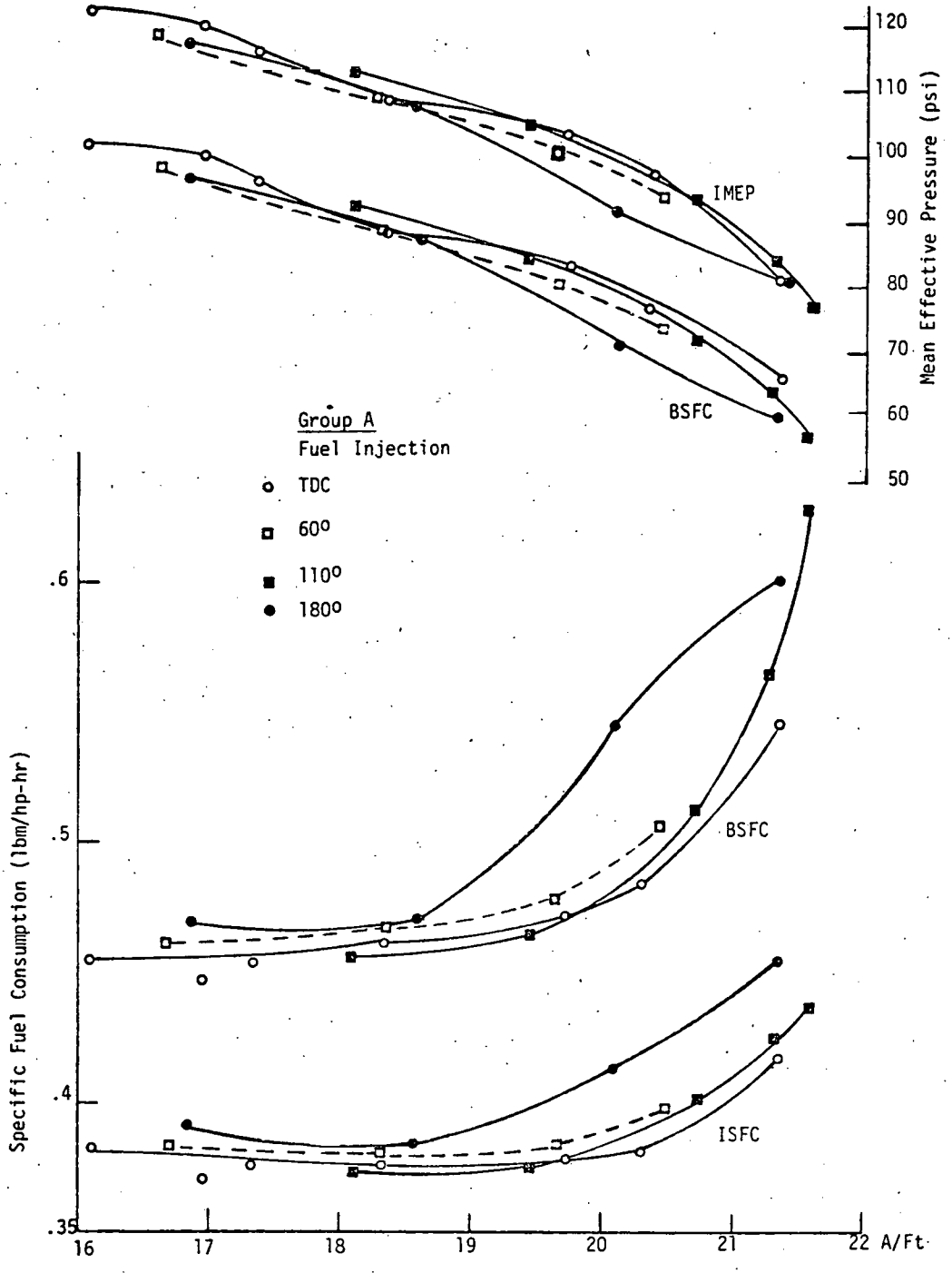

Figure 32. MEP and SFC for fixed spark timings - varied injection.

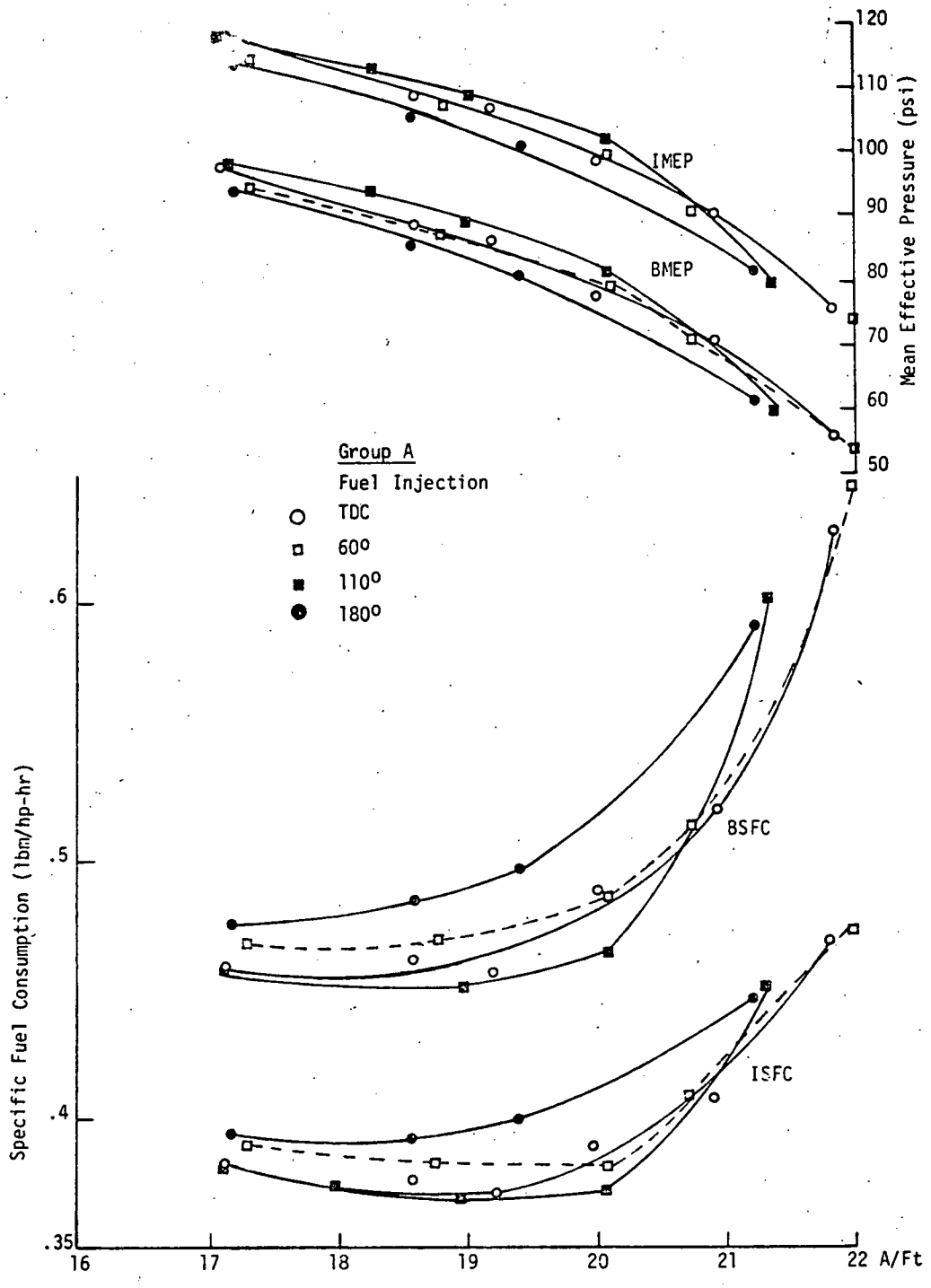

Figure 33. MEP and SFC for MBT spark timings - varied injection.

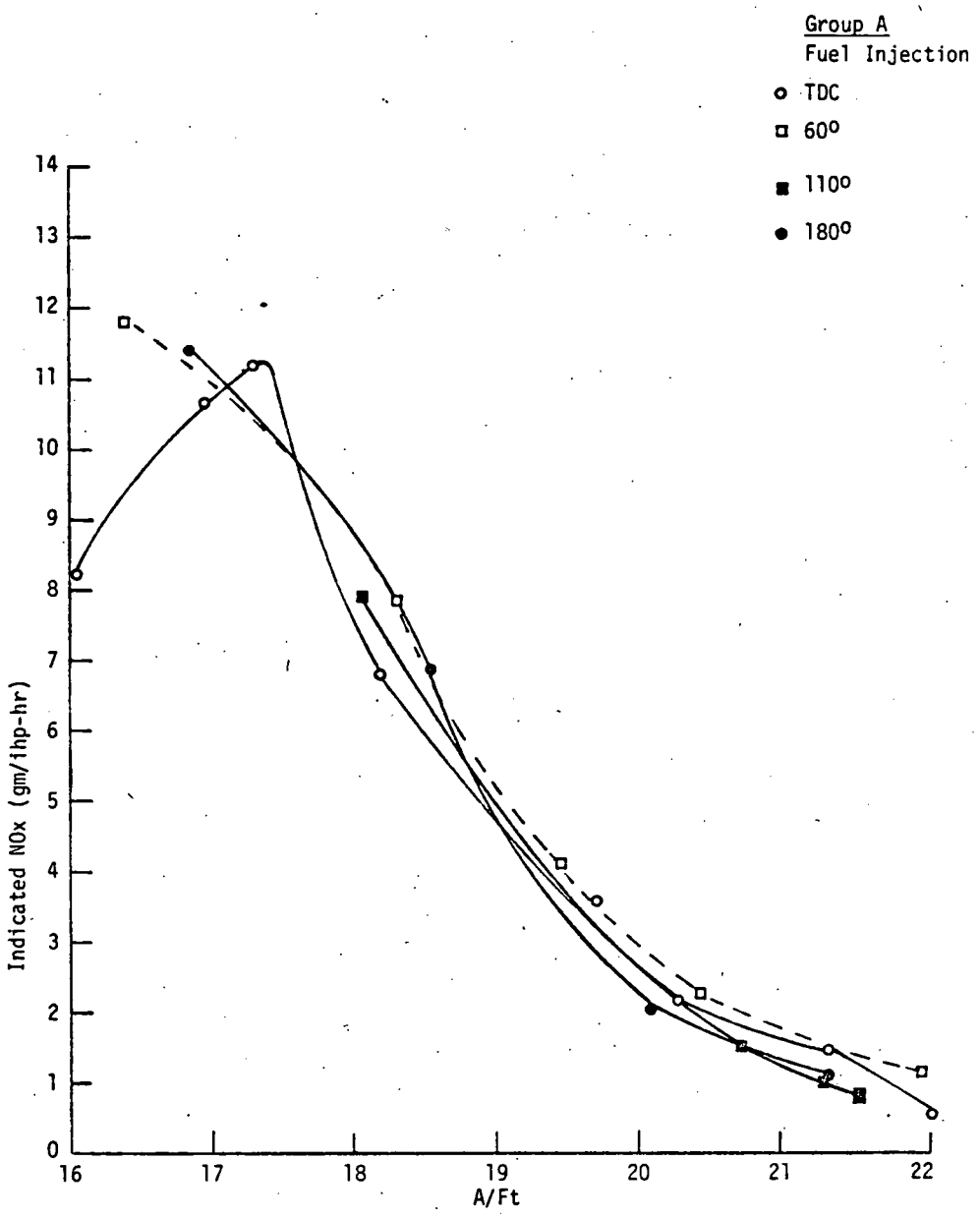

Figure 34. Indicated NOx for fixed spark timings - Varied injection.

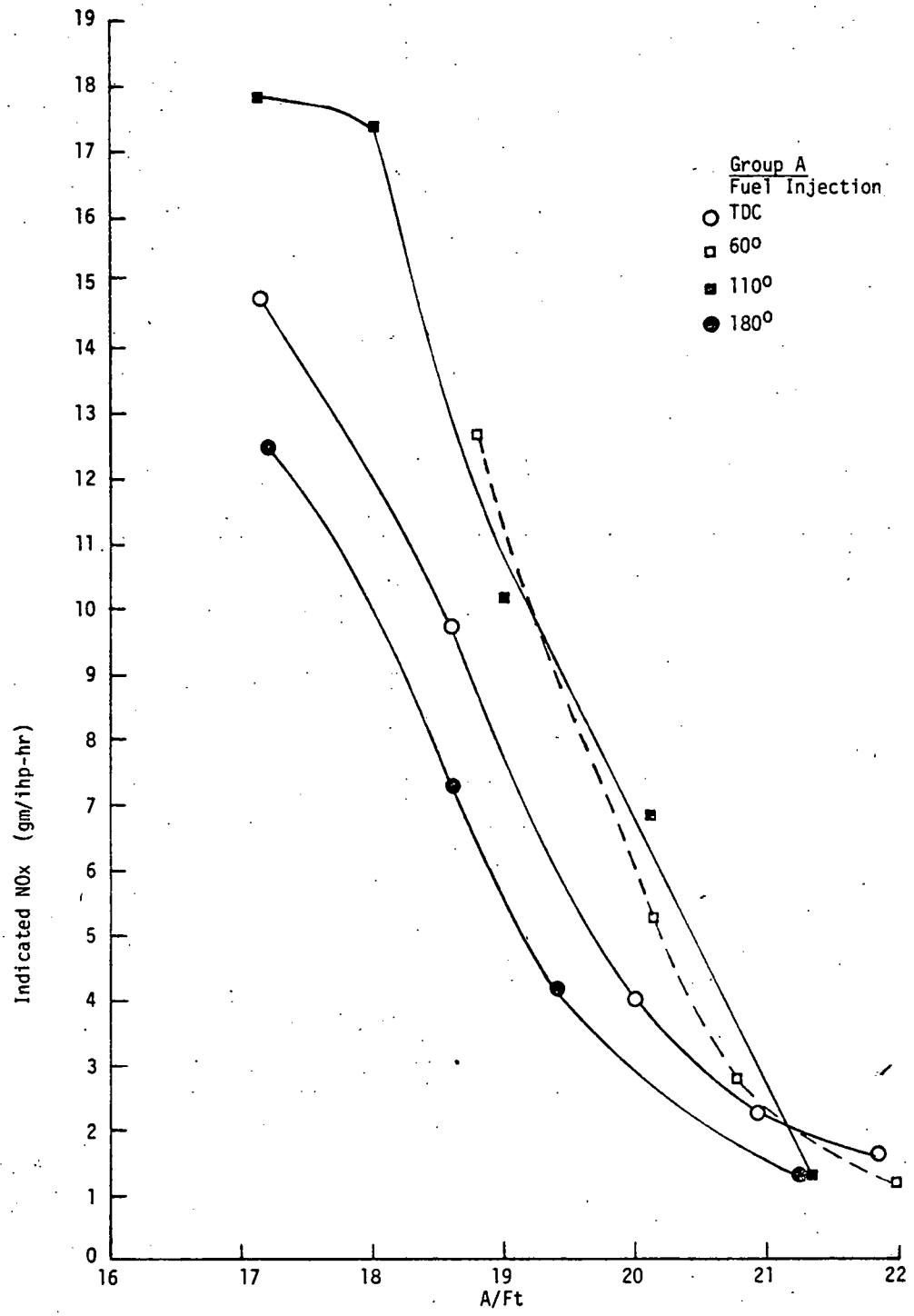

Figure 35. Indicated NOx for MBT spark timings - Varied injection.

advanced times of spark and that is expected as pointed out by Purins [4] in a Ford study. The 180 ATC case gives only slightly higher NOx values for MBT than the 180 at fixed spark. The HC and CO results shown later also have this bunching of the four curves at fixed times, and a spread in the curves at MBT, advanced times. This would tend to show that conditions existing in the engine at advanced times, disappear with further compression. It is possible that since this engine is injecting fuel into the air stream being drawn into the engine, varying when the fuel is injected can set up areas in the main chamber that have different air/fuel ratios. One section of the cylinder may contain the fuel and another may just have air that was taken in, and thus pockets of rich or lean mixture forms. It is impossible to determine how the mixture would be formed or where in the cylinder, but at MBT, the 180 injection gave lowest NOx, 110 second lowest, 60 third and TDC injection highest. At the more retarded timings of spark these pockets could disappear from more mixing caused by compression or some other turbulence in the cylinder.

This explanation can be supported further by the fact that the 180 ATC case showed the least difference between fixed and MBT cases, and gave lowest NOx emissions at MBT. The injection duration in this system was not known, but it was assumed that with injection at 180 ATC, the bulk of injection was with the value either partially or totally closed. In this engine, intake valve opening takes place at 29° BTC and closes at 233° ATC. Therefore in the 180 ATC case, fuel would not be injected into the air stream.

In fact with injection after the valve closed, the fuel would not be drawn in until the next intake stroke when incoming air would vaporize fuel off the valve and port. Therefore no pockets would be set up where some of the air had fuel mixed with it and some did not. Thus the MBT and fixed cases could be expected to have about the same mixture conditions and give NOx emissions which varied only because of spark timing differences. This was seen in the results, with the MBT NOx case being only slightly higher than fixed case. It was stated before that a more homogeneous mixture in the main chamber gives lower NOx, and it is possible that this is why the 180 ATC injection gave lower NOx at MBT. The mixture being vaporized off the intake valve and port could tend to give a more homogeneous mixture than if pockets of fuel were delivered to the engine in the airflow.

Another possible explanation for the results of the NOx curves is vaporization differences as pointed out by Peters and Quader [12]. They did tests with fuel injection timing using port injection and found it influenced emissions and performance. They theorize that the air/fuel mixture formed by injecting at peak valve opening contains many fuel droplets. The one formed by injection after valve closing would be a mixture somewhere between the one with many droplets and a prevaporized one. Peters and Quader conclude that the droplets cause an increase in flame speed and ignitability if optimum droplet size is present. One reason for this could be that stratification on a microscale could form around each droplet. Thus NOx could go up higher for the case with droplets, and go lower for the case where injection occurs after the valve closed

because of slower combustion. With TDC, 60° and 110° ATC injection, fuel is being injected into the air stream, and droplets could exist in the mixture formed. These three injection timing curves for NOx showed higher values than the 180 ATC case, which fits this explanation's prediction of NOx production. At more retarded spark times, the droplets could be atomized by further compression and the effects cancelled out, which would give the same emissions for all four injection timings. At MBT, there are differences in the NOx curves for each injection time. This could be because of differences in droplet formation because of injection time.

Beale [13] states that aerodynamic breakup of a fuel droplet is an important part of mixture formation. This is when dynamic forces on the droplet exceed surface tension. Beale states that as the valve first opens during intake, valve seat flow velocity is high and this is what causes atomization. After the valve opens, port velocities are high, and atomization of droplets occurs here instead of around the valve seat. Thus injection time could affect droplet size according to how open the valve was at injection. This would cause the differences seen at MBT in the NOx curves.

Figures 36 and 37 show HC results for fixed and MBT times. The small spread in curves is seen at fixed times, with about a 1 gm/ihp-hr difference in all four. At MBT, there is a 3 gm/ihp-hr spread. HC decreases at retarded timings because of increases in exhaust temperatures and more post reactions resulting. The 180 ATC gives highest HC emission for fixed and MBT curves, with 60 ATC injection second highest. The 110 ATC and TDC times

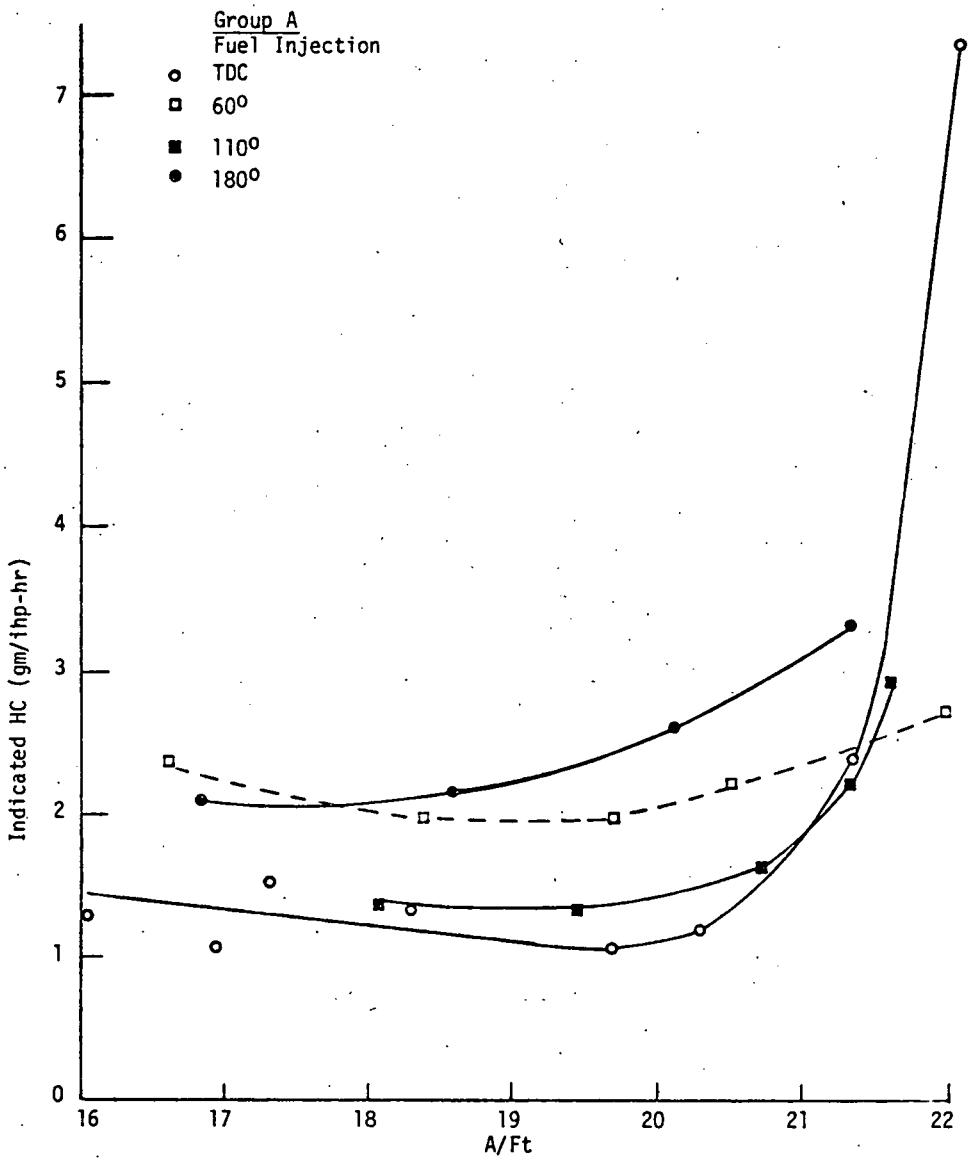

Figure 36. Indicated HC for fixed spark - varied injection.

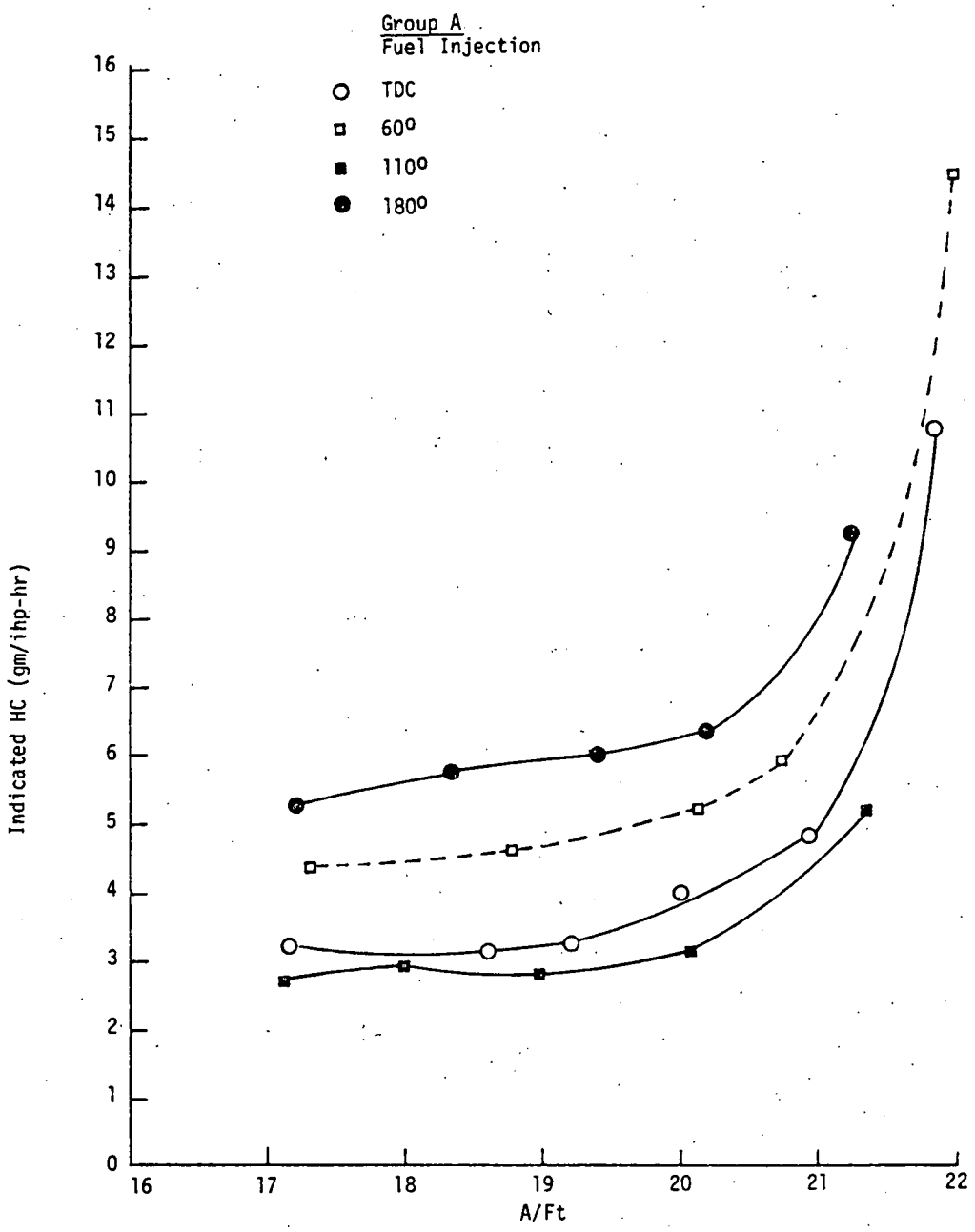

Figure 37. Indicated HC for MBT spark-varied injection.

gave similar emissions with these being the lowest. The TDC injection also gave second lowest NOx at MBT, showing that this injection time gives a good combination of low NOx and lowest HC.

Figures 38 and 39 show fixed and MBT CO emissions. The 180 ATC gave highest CO for both spark timings. The 60 ATC injection gave the lowest CO emissions. This could be because of the high HC for this case. In this engine the exhaust temperature range was between 1110-1250^{o}F, HC may oxidize to CO, but the CO does not oxidize. Thus reducing HC increases CO 4 .
The 110 ATC and TDC curves show higher CO and lower HC. Again, spread for fixed spark between the curves was small, while it was significant for the MBT spark.

E. Comparison of Injection Timings

In making the comparison of injection timings the NOx levels of 2 and 4 gm/ihp-hr were selected. Table 4 shows the comparison for MBT timings.

Table 4 tabulation shows the 180 ATC injection is least desirable. The poorer combustion is pointed out by high HC and CO and fuel consumption. The 60 ATC injection also gives high HC, but better fuel consumption. The 110 ATC injection gives the best HC values, but much higher CO than the TDC injection. The TDC gives the best timing, with good power, low fuel consumption and favorable HC and CO emissions. Table 5 shows the same comparison for fixed spark timings.

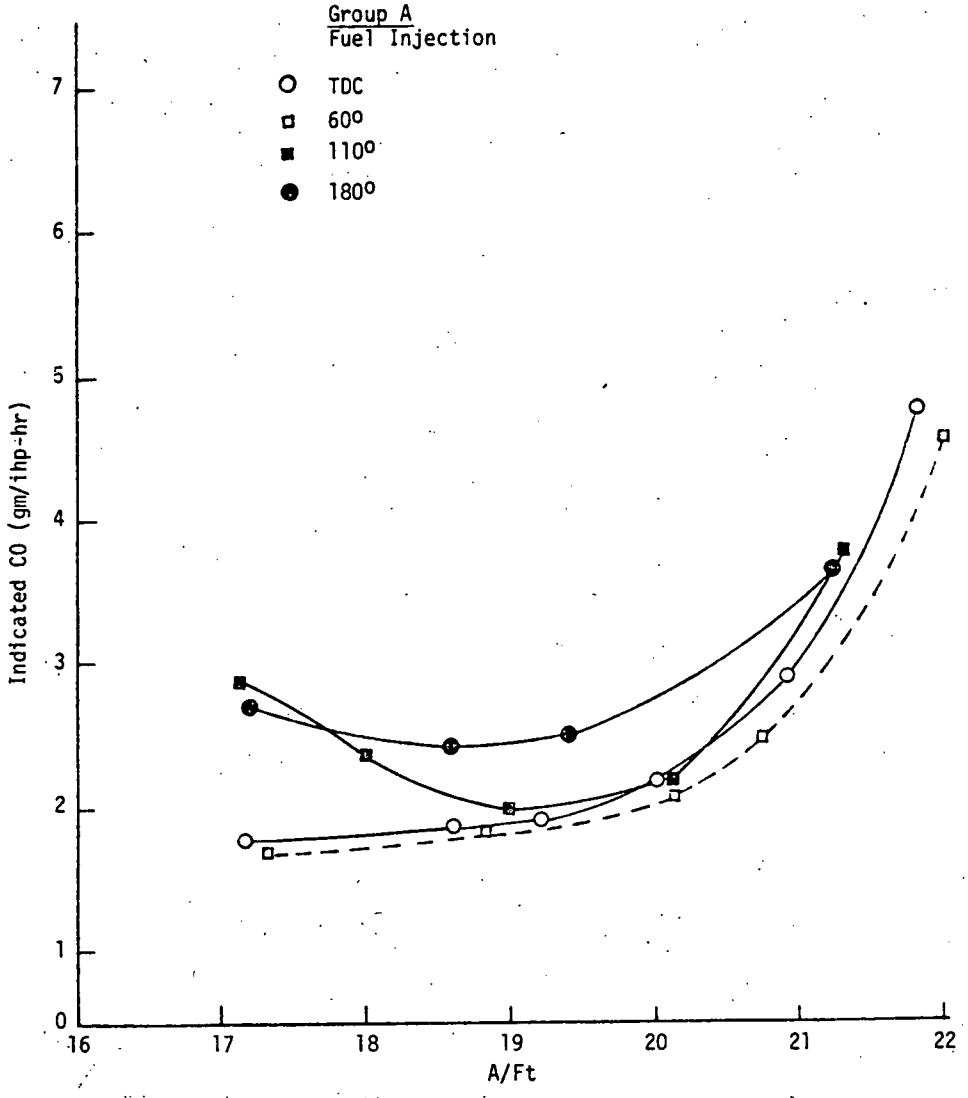

Figure 38. Indicated CO for MBT spark-varied injection.

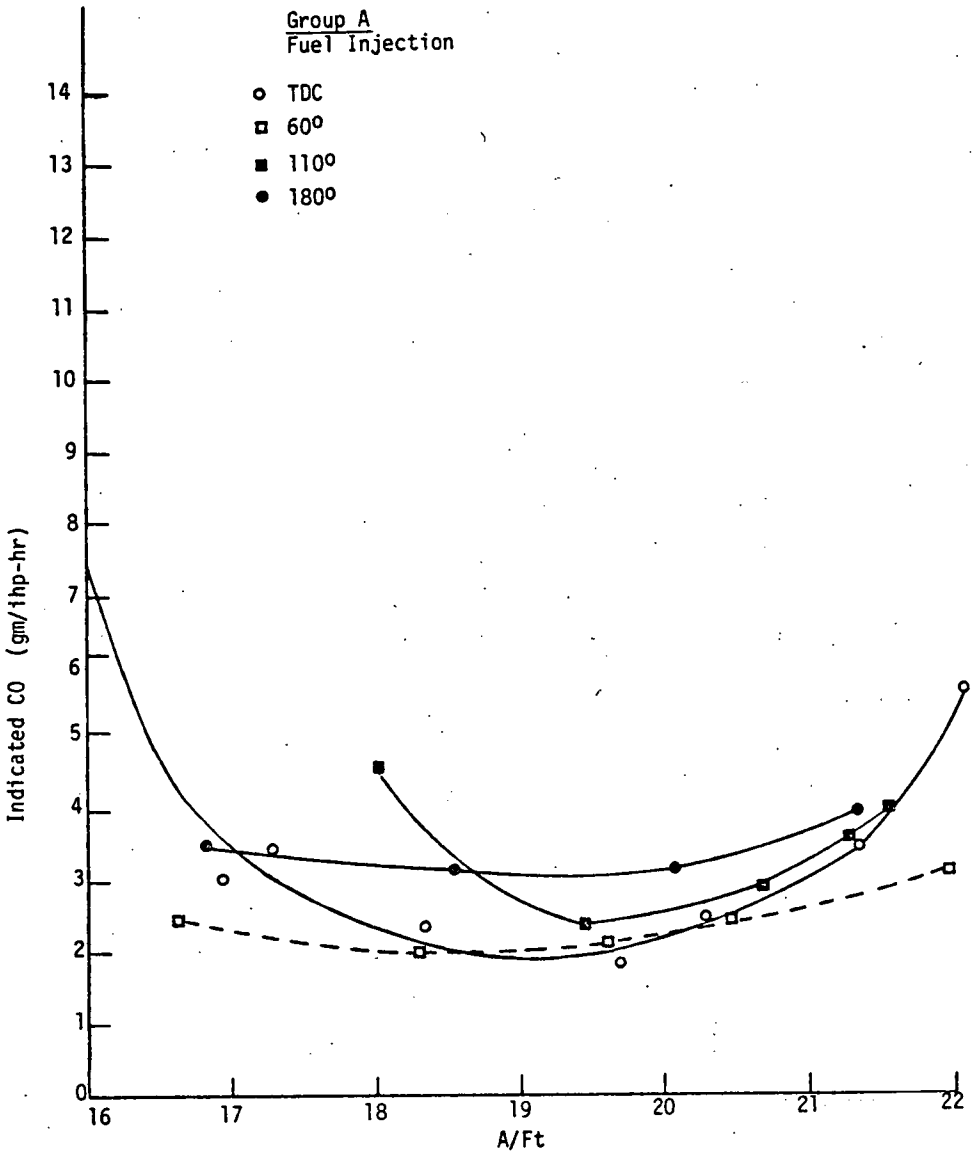

Figure 39. Indicated CO for fixed spark - varied injection.

TABLE 4

Comparison of Injection Timings for MBT Spark

NOx	Injection	HC	CO	A/Ft	IMEP	ISFC
4	TDC	3.9	2.18	20	98.6	.385
4	60	5.5	2.3	20.35	96	.39
4	110	3.8	2.7	20.6	93	.39
4	180	6.05	2.55	19.5	99	.403
4	Carb	2.7	3.8	19.25	100	.39
2	TDC	5.5	3.3	21.15	88	.427
2	60	7.2	2.95	21.15	88	.425
2	110	4.7	3.5	21.15	85	.435
2	180	7.0	3.15	20.6	88	.427
2	Carb	2.5	4.25	20.4	92.5	.41

TABLE 5

Comparison of Injection Timings for Fixed Spark

NOx	Injection	HC	CO	A/Ft	IMEP	ISFC
4	TDC	1.07	1.9	19.45	105.5	.375
4	60	2.0	2	19.3	104	.383
4	110	1.35	2.2	19.45	105	.375
4	180	2.25	3.1	19.25	101	.395
4	Carb	2.7	3.8	19.25	100	.39
2	TDC	1.65	2.8	20.8	91	.397
2	60	2.2	2.5	20.6	91	.4
2	110	1.6	2.8	20.45	96	.395
2	180	2.6	3.2	20.15	92	.415
2	Carb	2.5	4.25	20.4	92.5	.41

Again, Table 5 TDC injection shows a slight edge over the 110 ATC for most cases, with 60 ATC third best and 180 ATC worst. The 110 ATC shows some advantage at 2 gm/ihp-hr with better ISFC, HC and power levels. However this advantage is very marginal and is not seen at 4 gm/ihp-hr.

F. High Speed Photographic Studies

The high speed movies of the main chamber combustion were taken with the carbureted version as described before. Even though six runs were made, it is felt that this portion of the research was still in the initial stages. The photography shows no dramatic proof of the presence of the mixture cloud. The problem was trying to see the lean mixtures burning, since they burn a faint blue. Much of the visible flame seen from the film was believed to be the rich prechamber torch. Since rich mixtures burn bright yellow, this was photographed easier at high speeds.

The color pictures taken with copper oleate added do have some evidence to back up the theory of zones with rich mixture existing in the main chamber. This copper additive shows up in dark green regions in the main chamber. These regions were only visible in part of the main chamber. This tends to show that other regions were too lean to produce a dark enough color to be photographed.

V. CONCLUSIONS

The results of this investigation show that during the mixture formation process in the three-valve stratified charge engine, perfect mixing of the prechamber overflow does not occur. Instead, there is some degree of mixing with the main chamber mixture and an intermediate zone or zones form just outside the torch opening. This zone will be made up of mixture that is slightly lean or close to being slightly lean. Therefore this zone size controls NOx production, since slightly lean mixtures produce maximum nitric oxides. Too lean of an intermediate zone gives poor transitional burning from the rich prechamber to the lean main chamber, and high HC and CO can result along with low NOx from slow combustion. Too rich of an intermediate zone can give low HC and CO emissions from faster combustion, but will also create large NOx emissions. Therefore the optimum mixture cloud which gives both low HC and CO and low NOx must be produced in the engine for an emission advantage over the conventional S.I. engine.

It was found that with the engine geometry used, Group A fueling group gave the most desirable mixture formation. The values of A/Fa=7, Ga/Gt=10% gave a sufficiently large but also lean enough mixture zone with good torch strength to burn the lean A/Fm in the main chamber. This gave low HC and CO emissions and low NOx levels. Computer simulation showed that prechamber mixture percentage may be fixed for any prechamber overflow and not necessarily depend on amount of mass percentage delivered through the prechamber. Therefore it would be the intermediate zone A/F that controlled emissions and not zone size, since the size would

be about the same for all three fueling groups. Power and fuel economy is similar for Groups A and B and only slightly less desirable for Group C. However emissions vary much with changing fueling groups.

In general, the fuel injection produced a mixture which gave slightly higher NOx, but significantly less HC and CO over the carbureted engine when run over an A/Ft range. HC and CO could be reduced even more with a thermal reactor or insulated exhaust port. Exhaust temperatures were found to be from 1100-1200°F. This is much lower than the 1400°F needed to give complete HC-CO oxidation. Low head temperatures and thin exhaust port walls are the main reasons for lower temperatures than found in other stratified charge engines such as Honda's and Ford's. Power and economy were not significantly changed with fuel injection.

TDC injection gave the most favorable mixture formation for low NOx, CO and HC emissions. The 110 ATC injection also gave low HC and NOx but slightly higher CO emissions than the TDC case. The 60 ATC injection and 180 ATC injection gave much worse HC and CO emissions for a given NOx level. This was believed to have been caused by differences in mixture formation caused by different placement of rich zones in the cylinder because of the different injection time. It is possible also that droplet formation from the injection spray could have played a part in different mixture formation from changing atomization characteristics with changed injection time.

VI. RECOMMENDATIONS

In order to find further evidence to explain the stratified charge mixture formation, more experiments performed in this report could be run again using the swirl inducing port block. The fuel injection timing variation at fixed and MBT times could be run with the swirl in the main chamber. Then results of this swirl and no swirl data could be compared. Fuel injection variation could also be done using a premixed air and fuel charge. Then any droplet effects would be canceled out and pockets of mixture formed by injection into an air stream in the port would also not be present. This could help to find what causes emission changes with injection timing changes. Any of these tests could be run at part throttle also to see if the theories presented hold.

The experiment of varying prechamber equivalence ratio should be repeated at other A/Ft ratios. Also, the attempt should be made to find experimental points for the swirl and no swirl case of imep versus NOx that could be directly compared, so the curves would not have to be extended.

Much more work can be done with the photographic engine. A means must be found to enable crank angle to be photographed along with the combustion process. It is also suggested that a sodium compound such as sodium ethelate be used to dope the fuel instead of copper oleate. This should help the main chamber lean mixtures burn a brighter color so it can be filmed. Also the port block could be left in the head and pictures taken for comparison to the no swirl combustion. Then possibly exact degree of swirl could be determined. The fuel injection in the main chamber should

also give the approximate A/Ft and A/Fm in the engine. Fuel injection films should also be interesting to compare to the carbureted version photography.

APPENDIX

Formulas to figure specific mass emissions were taken from the SAE handbook [5]. For the experimental procedures used, the following equations were used to find emissions in gm/hr. The molecular weight of air was taken as 29 to reduce the SAE equations to those below.

HC, gm/hr = 0.000217 * (airflow + fuel flow) lbm/hr
* HC, ppm dry * K

CO, gm/hr = 4.38 * (airflow + fuel flow) lbm/hr
* CO, % dry * K

NOx, gm/hr = .00072 * (airflow + fuel flow) lbm/hr
* NOx, ppm wet * KH

K was a correction factor to convert dry measurements to wet basis.

$$K = 1. - (1.21 * F/A + 0.0407)$$

KH is a factor for correction NOx for the effect of humidity.

$$KH = 0.634 + .00654 * H - 0.0000222 * H^2$$

where $H = 7000 * W$

with W being the humidity ratio in lbm water/lbm air.

REFERENCES

1. E. Obert, Internal Combustion Engines and Air Pollution, Intext Educational Publishers, New York, N.Y., 1973.

2. T. Date, S. Yagi, A. Ishizuya, and I. Fujii, "Research and Development of the Honda CVCC Engine," SAE 740605, Aug. 1974.

3. K. Grandys, "Improving the Performance and Exhaust Emissions of Dual Chamber Stratified Charge Spark Ignition Engines," University of Illinois Master's Thesis, 1977.

4. E. Purins, "Pre-Chamber Stratified Charge Engine Combustion Studies," SAE 741159, Oct. 1974.

5. "Test Procedure for Measurement of Small Utility Engine Exhaust Emission - SAE J1088," SAE Handbook 1976, pp. 26.89-26.93.

6. R. Matthews, R. Sawyer, R. Schefer, "Interferences in Chemiluminescent Measurement of NO and NO_2 Emissions from Combustion Studies," Environmental Science and Technology, Vol. 11, p. 1092, Nov. 1977.

7. G. Davis, R. Krieger, R. Tabaczynski, "Analysis of the Flow and Combustion Processes of a Three-Valve Stratified Charge Engine with a Small Prechamber," SAE 741170, 1974.

8. S. Sorenson, "Improving the Performance and Fuel Consumption of Dual Chamber Stratified Charge Spark Ignition Engines," University of Illinois Research Report, May 1977.

9. S. Pan, "Combustion Simulation of a Dual Chamber Stratified Charge Engine," University of Illinois Research Report, May, 1979.

10. Y. Sakai, K. Kunii, M. Susaki, N. Kakuta, H. Alhara, "Combustion Characteristics of a Torch Ignited Engines - Analytical Measurements of Gas Temperature and Mixture Formation," Stratified Charge Engines, P. 55, Mechanical Engineering Publications Limited, London and New York, 1976.

11. R. Krieger, G. Davis, "The Influence of the Degree of Stratification on Jet-Ignition Engine Emissions and Fuel Consumption," Stratified Charge Engines, p. 109, Mechanical Engineering Publication Limited, London and New York, 1976.

12. B. Peters, A. Quader, "Wetting the Appetite of Spark Ignition Engines for Lean Combustion," SAE 780234, 1978.

13. W. Beale, "A Study of Fuel Atomization in the Induction Trace of a Fuel Injection Spark Ignition Engine," Thesis for Cranfield Institute of Technology, Beford, England, May 1965.